



Universitat
de les Illes Balears

DOCTORAL THESIS

2018

**DEVELOPMENT OF DEVICES TO INTEGRATE IN
AUTOMATIC METHODOLOGIES FOR
DETERMINING RADIONUCLIDES IN RESIDUES
AND ENVIRONMENTAL SAMPLES**

Melisa Rodas Ceballos



Universitat
de les Illes Balears

DOCTORAL THESIS

2018

**Doctoral Programme of Chemical Science and
Technology**

**DEVELOPMENT OF DEVICES TO INTEGRATE IN
AUTOMATIC METHODOLOGIES FOR
DETERMINING RADIONUCLIDES IN RESIDUES
AND ENVIRONMENTAL SAMPLES**

Melisa Rodas Ceballos

Thesis Supervisor: Laura Ferrer Trovato

Thesis Supervisor and Tutor: José Manuel Estela Ripoll

Doctor by the Universitat de les Illes Balears



Universitat
de les Illes Balears

Environmental
Radioactivity
Laboratory

Dr. Laura Ferrer Trovato and Dr. José Manuel Estela Ripoll, professors of the Chemistry Department of the University of the Balearic Islands (UIB), Spain

DECLARE

That the doctoral thesis, entitled "*Development of devices to integrate in automatic methodologies for determining radionuclides in residues and environmental samples*" presented by Melisa Rodas Ceballos was carried out at the Laboratory of Environmental Radioactivity (LaboRA) of UIB under our supervision, and meets all the requirements necessary to qualify for the International Doctoral degree.

And for this to be registered, we sign this document

Laura Ferrer Trovato

José Manuel Estela Ripoll

Palma de Mallorca, Spain 7th of September 2018

ACKNOWLEDGEMENTS

I would like to thank to Ministry of Economy and Competitiveness (MINECO) for the allowance of an Industrial PhD fellowship (DI-14-06961). Also, to SCWARE SYSTEMS for the co-funding of the Industrial PhD fellowship, and give me the opportunity to develop my thesis.

I would also like to thank the financial support from the Spanish State Agency for Research (AEI), MINECO co-financed by European Regional Development's funds (FEDER), through the project RAD SENSOR Ref. CTM2013-42401-R, and from the Government of the Balearic Islands co-financed by FEDER funds, through the project PROCOE/7/2017.

I would also like to extend my thanks to the University of the Balearic Islands for give me the opportunity to develop my thesis, and the Jožef Stefan Institute for give me the opportunity to make my PhD stay, especially to the department of Environmental Sciences.

Finally, I wish to thank Dra. Laura Ferrer, Dr. Víctor Cerdà and Dr. José Manuel Estela Ripoll, for give me the opportunity to performance my PhD. Especially, to Laura Ferrer for being my support throughout all this time, for being patient with me, for her optimistic and for always making me laugh.

DEDICATORIA

A lo largo de estos cuatro años he pasado por momentos muy difíciles y quisiera agradecerles a todas esas personas que me han apoyado y han hecho posible que hoy pueda decir misión cumplida.

Esta tesis se la quiero dedicar a toda mi familia de Guatemala, a mis tíos, primos y sobrinos. A mis hermanos Gustavo y Rita porque siempre han estado allí para mí y sé que siempre puedo contar con ustedes y por siempre cuidar de su hermana pequeña. A mi nueva hermana Jacquie Paz que fue una bendición tenerla en la familia y gracias por siempre estar allí para mí y mis hermanos, y darnos tu amor incondicional.

A mis sobrinos, Isabella, Juan Diego, Santiago y Ana Belén por ser siempre mi alegría.

A mi esposo Fernando Maya porque siempre ha estado conmigo en los buenos y no tan buenos momentos, por siempre hacerme sentir mejor con sus consejos y sus bromas constantes. Por su paciencia y ser siempre mi hombro de apoyo. Te amo guapito.

A mi familia política, porque siempre me ayudaron en todo lo que necesite y por siempre apoyarme y abrirme la puerta de su casa y hacerme sentir como una hija más.

Esta tesis se la quiero dedicar especialmente a mis padres, porque para mi madre Lilian Maritza era un sueño que yo alcanzaré el grado de doctor en química, ella siempre me inspiró a luchar por mis metas, nunca dejarme caer y siempre terminar lo que empecé. A mi padre Adolfo, por hacerme una persona fuerte, independiente y enseñarme que la vida no siempre es un camino de rosas, pero siempre debo seguir luchando por mis objetivos y nunca rendirme.

También, se la quiero dedicar a mis compañeros de laboratorio, especialmente a Donagi porque como siempre le dije a ella fue mi ángel, vino a Mallorca en el momento en que yo más necesitaba de una amiga. A Carlos Calderilla, porque siempre estuvo allí para mí y gracias por ser siempre tan sincero conmigo. A mi asesora Laura Ferrer por siempre ser comprensiva conmigo, paciente y ser positiva en toda circunstancia.

ABBREVIATIONS

AAS	Atomic Absorption Spectroscopy
AM	Additive Manufacturing
ANOVA	Analysis Of Variance
BI	Bead Injection
CPM	Counts per Minute
D	Depth
DLL	Dynamic Link Library
EDS	Energy-dispersive X-ray spectroscopy
FDM	Fused Deposition Modelling
FIA	Flow Injection Analysis
H	Height
HC	Holding Coil
HPLC	High Performance Liquid Chromatography
ICP-MS	Inductively Coupled Plasma Mass Spectrometry
ICP-OES	Inductively Coupled Plasma Optical Emission Spectrometry
IPA	Isopropyl Alcohol
L	Length
LBPC	Low Background Proportional Counter
LLE	Liquid-Liquid Extraction
LOD	Limit of Detection
LOV	Lab-On-Valve
LSC	Liquid Scintillation Counter
MBD	Macroporous Bead Cellulose
MDA	Minimum Detectable Activity
MSA	Magnetic-Stirring Assisted
MSFIA	Multisyringe Flow Injection Analysis
NORM	Naturally Occurring Radioactive Materials
PEEK	PolyEther Ether Ketone
PERALS	Photon/Electron- Rejecting Alpha Liquid Scintillation System
PG	PhosphoGypsum
PLC	Phosphogypsum Leaching Column
PMT	PhotoMultiplier Tube
PTFE	PolyTetraFluoroEthylene
PVDF	PolyVinylidene Fluoride
RF	Radio Frequency

RP	Rapid Prototyping
RSM	Response Surface Methodology
SEM	Scanning Electron Microscopy
SFF	Solid-Free-Form
SIA	Sequential Injection Analysis
SLA	StereoLithography
SLS	Selective Laser Sintering
SPE	Solid Phase Extraction
Sr-resin®	Resin for strontium extraction
TENORM	Technologically Enhanced Naturally Occurring Radioactive Materials
TEVA	TetraValent Actinides and technetium resin
UTEVA	Uranium and TEtraValents Actinides resin
UV	UltraViolet
W	Width
WHO	World Health Organization

INDEX

TABLE INDEX	1
FIGURE INDEX	2
ABSTRACT	7
RESUMEN	9
RESUM	11
CHAPTER 1. GENERAL INTRODUCTION	13
1.1. Natural radioactivity	15
1.1.1. NORM	15
1.1.2. TENORM.....	16
1.2. Artificial radioactivity	17
1.3. Radionuclides studied	18
1.3.1. Radium	18
1.3.2. Uranium.....	18
1.3.3. Thorium	19
1.3.4. Strontium	20
1.4. Flow analysis techniques	22
1.5. Extraction techniques	23
1.5.1. Extraction by selective resin	23
1.5.2. Extraction by co-precipitation.....	24
1.6. Detection techniques	25
1.7. 3D printing technology	25
CHAPTER 2. TECHNIQUES USED	27
2.1. Flow analysis techniques	29
2.1.1. Sequential injection analysis.....	29
2.1.2. Multisyringe flow injection analysis	29
2.1.3. Lab-On-Valve	30
2.2. Extraction techniques	31
2.2.1. UTEVA resin.....	31
2.2.2. TEVA resin	32
2.2.3. Sr-resin.....	32
2.2.4. Cellulose beads	33
2.3. Detection techniques	33
2.3.1. Inductively coupled plasma mass spectrometry	33
2.3.2. Low background proportional counter.....	35
2.3.3. Prototype sensor based on liquid scintillation counting	36

2.4. 3D printing technology: stereolithography.....	38
CHAPTER 3. OBJECTIVES AND WORK METHODOLOGY	41
3.1. General objective.....	43
3.1.1. Specific objectives	43
3.1.2. Work methodology.....	43
CHAPTER 4. MATERIALS AND METHODS.....	45
4.1. Flow systems configuration.....	47
4.1.1. Multisyringe burette	47
4.1.2. Solenoid valve	48
4.1.3. Selection valve and Lab-on-Valve.....	49
4.1.4. Pipes, connectors and lixiviation column.....	50
4.1.5. AutoAnalysis software	50
4.2. Components of the liquid scintillation prototype detector	52
4.3. 3D printing technology.....	54
4.3.1. Rhinoceros software	54
4.3.2. 3D printers.....	55
4.3.3. Photopolymeric resins	56
4.3.4. PreForm software	57
4.3.5. Ultraviolet crosslinker.....	57
4.4. Multivariate optimization.....	58
4.4.1. Screening of variables	58
4.5. Calculations	59
4.5.1. Total alpha measurements	60
4.5.2. Total beta measurements	61
4.5.3. Z-score value.....	62
CHAPTER 5. ²²⁶Ra DYNAMIC LIXIVIATION FROM PHOSPHOGYPSUM SAMPLES BY AN AUTOMATIC FLOW-THROUGH SYSTEM WITH INTEGRATED RENEWABLE SOLID-PHASE EXTRACTION.....	63
5.1. Introduction.....	65
5.2. Experimental.....	66
5.2.1. Reagents and solutions	66
5.2.2. Phosphogypsum samples.....	67
5.2.3. Analytical procedure	68
5.3. Results and discussion.....	71
5.3.1. Optimization of experimental conditions.....	71
5.3.2. Validation.....	73
5.3.3. ²²⁶ Ra dynamic lixiviation	74

5.4. Conclusions	78
CHAPTER 6. AN INTEGRATED AUTOMATIC SYSTEM TO EVALUATE U AND Th DYNAMIC LIXIVIATION FROM SOLID MATRICES, AND TO EXTRACT/ PRECONCENTRATE LEACHED ANALYTES PREVIOUS TO ICP-MS DETECTION	79
6.1. Introduction.....	81
6.2. Experimental	82
6.2.1. Reagents and solutions	82
6.2.2. Environmental solid samples	83
6.2.3. Sample treatment	83
6.2.4. Analytical procedure	84
6.3. Results and discussion.....	87
6.3.1. Optimization of experimental conditions.....	87
6.3.2. Validation of the automatic system	89
6.3.3. Dynamic lixiviation of U and Th from solid environmental samples	90
6.4. Conclusions	94
CHAPTER 7. 3D PRINTED DEVICE FOR URANIUM(VI) EXTRACTION AND ITS INTEGRATION IN AN AUTOMATIC FLOW-THROUGH SYSTEM.....	97
7.1. Introduction.....	99
Section A) 3D printed device for selective uranium extraction	100
7.2. Experimental	100
7.2.1. Reagents and solutions.....	100
7.2.2. Instrumentation and software.....	100
7.2.3. Immobilization of TEVA resin on the 3D printed device.....	101
7.2.4. Immobilization of the Aliquat®336 on the 3D printed device	101
7.2.5. Characterization and detection	101
7.2.6. Sample preparation	102
7.2.7. Analytical procedure	102
7.3. Results and discussion.....	102
Section B) 3D printed SPE device integrated in an automatic system	109
7.4. Experimental	109
7.4.1. Reagents and solutions	109
7.4.2. Sample preparation	109
7.4.3. 3D printed device.....	109
7.4.4. Automatic system set-up	111
7.4.5. Analytical procedure	112
7.5. Results and discussion.....	113

7.5.1. Optimization of experimental conditions.....	113
7.5.2. Analytical features	117
7.5.3. Application to water matrices	118
7.6. Conclusions.....	119
CHAPTER 8. FULLY AUTOMATED SYSTEM WITH INTEGRATED LIQUID SCINTILLATION DETECTOR FOR THE FAST DETECTION OF RADIOSTRONTIUM	121
8.1. Introduction.....	123
8.2. Experimental.....	124
8.2.1. Reagents and solutions	124
8.2.2. 3D printed devices	124
8.2.3. On-line radioactivity detection.....	127
8.2.4. Automatic system set-up	127
8.2.5. Analytical procedure	129
8.3. Results and discussion.....	131
8.3.1. Optimization of the mix between the cocktail and eluate.....	131
8.3.2. Optimization of experimental conditions.....	131
8.3.3. Cleaning procedure	132
8.3.4. Background	132
8.4. Conclusions.....	133
CHAPTER 9. FINAL CONCLUSIONS.....	135
REFERENCES	139
ANNEX.....	155

TABLE INDEX

Table 5.1 General procedure for lixiviation, extraction and preconcentration of ^{226}Ra from PG samples by a MSFIA-LOV system.	70
Table 5.2 Variables, levels and experimental matrix of the full factorial design for the PG lixiviation process.....	72
Table 5.3 Validation results of reference PG material (MatControl CSN-CIEMAT 2008).	74
Table 5.4 Activity concentration of ^{226}Ra in the leached fractions and the residual fraction in samples of phosphogypsum, using artificial rainwater as extracting agent at pH 5.4 and 2.0.....	75
Table 5.5 Comparison between static (24 h) and dynamic lixiviation of ^{226}Ra from PG samples with rainwater at pH 5.4 and 2.0.	77
Table 6.1 General procedure for lixiviation, extraction and preconcentration of U and Th from solid matrices by a MSFIA-LOV system.....	86
Table 6.2 Variables, levels and experimental matrix of the full factorial design for lixiviation process from soil and sediment samples.	88
Table 6.3 U and Th in leached fractions and residual fraction analyzed by the MSFIA-LOV system for lixiviation, extraction and preconcentration steps previous to ICP-MS detection, from reference materials.....	90
Table 7.1 Analysis of the reference materials using the 3D printed device coated with TEVA resin, for uranium(VI) extraction and ICP-MS detection.	108
Table 7.2 Variables, levels and experimental matrix of the full factorial design for U retention. U: $10\ \mu\text{g L}^{-1}$	113
Table 7.3 Variables, levels and experimental matrix of the full factorial design for U elution. U: $10\ \mu\text{g L}^{-1}$	115
Table 7.4 Figures of merit.....	117
Table 7.5 Analysis of the different type of water samples.	119
Table 8.1 General procedure for the extraction and detection of ^{90}Sr	130

FIGURE INDEX

Figure 2.1 UTEVA resin component and equilibrium extraction, E= extractant. Dipentyl phentylphosphate DP[PP], also called Diamyl amyolphosphate (DAAP).....	31
Figure 2.2 TEVA resin component, a quaternary ammonium salt (Aliquat®336).	32
Figure 2.3 Sr-resin and equilibrium extraction, E= 4,4'(5')-di-t-butylcyclohexano-18-crown-6 (2).	33
Figure 2.4 Coincidence circuit. PMT: photomultiplier tube, cpm: counts per minute. ..	37
Figure 2.5 Right-side up SLA. Reproduced from the ultimate guide to stereolithography (SLA) 3D printing [77].	38
Figure 2.6 Upside-down (inverted) SLA. Reproduced from the ultimate guide to stereolithography (SLA) 3D printing [77].	39
Figure 4.1 (I) Multisyringe burette, Multi-Burette 4S-D. Reproduced from the website of Crison [110]. (II) Diagram of the operation of a solenoid valve located on the top of each syringe. a) Solenoid valve activated in the On position and, b) solenoid valve deactivated in the Off position.....	48
Figure 4.2 External solenoid valves (Takasago Electronic Inc., Japan). Reproduced from the PhD thesis by Fernando Maya Alejandro [83].	48
Figure 4.3 a) Mixed valve module (Crison Instruments). Reproduced from, the PhD by Fernando Maya Alejandro [83], and b) VICI selection valve Sciware Systems. Reproduced from the website of Sciware Systems S.L.[111]	49
Figure 4.4 LOV made of methacrylate placed on a VICI selection valve (Sciware Systems) with 8 ports, showing the microcolumn channel.	50
Figure 4.5 Configuration menu of AutoAnalysis program to establish the connections.	51
Figure 4.6 Analytical method developed in AutoAnalysis program.	52
Figure 4.7 a) Flow cell; b) Hamamatsu R7600U-200 photomultiplier tube (Hamamatsu Photonics K.K., Shizuoka, Japan). Reproduced from the technical sheet [112] and, c) high-voltage power supply series C4900 (Hamamatsu). Reproduced from the technical sheet [113].....	53
Figure 4.8 Power circuit board with potentiometer. Reproduced from the memory of the external internship carried out by Óscar Pozo at iC-Málaga [114]......	53
Figure 4.9 Example of 3D piece design in Rhinoceros software.....	55
Figure 4.10 Graphical representation of a factorial design 2^3 (2^k).....	59

- Figure 5.1** Automatic system for the dynamic leaching, preconcentration and co-precipitation of ^{226}Ra from phosphogypsum samples. C: three-way connector, HC: holding coil, LOV: Lab-On-Valve, PLC: phosphogypsum lixiviation column, V: external solenoid valve. 69
- Figure 5.2** a) Automatic system for the optimization of the variables that affect the dynamic leaching, preconcentration and co-precipitation of ^{226}Ra from phosphogypsum samples, PLC: phosphogypsum lixiviation column; b) components of the leaching column: 1. top cover, 2. o-ring, 3. filter holder, 4. filter, 5. silicone gasket, 6. cylindrical column, 7. bottom cover; and c) photograph of the lixiviation column..... 71
- Figure 5.3** Pareto chart for the variables affecting the ^{226}Ra lixiviation process. 73
- Figure 5.4** Accumulated percentage of ^{226}Ra release for leached fractions with artificial rainwater at $\text{pH } 2.0 \pm 0.2$. The results are expressed as accumulated percentage average \pm standard deviation ($n=3$). PG 1, PG 2: phosphogypsum samples 1 and 2, PG ref: PG reference sample. 76
- Figure 6.1** Automatic MSFIA-LOV system for the dynamic leaching, extraction and preconcentration of uranium and thorium from solid environmental samples. C: connector; HC: holding coil; PLC: phosphogypsum lixiviation column; LOV: Lab-On-Valve; S: syringes; V: external solenoid valve. 85
- Figure 6.2** Pareto chart of the variables that affect the lixiviation process from soil and sediment. 88
- Figure 6.3** Graph of marginal means of the effect of the interaction between the variables sample weight (mg d.w.), and flow rate (mL min^{-1}). D: desirability. 89
- Figure 6.4** Dynamic lixiviation for U, in solid environmental samples, using artificial rainwater as leaching agent. The results are expressed as average \pm standard deviation ($n=3$). a) Soil sample and soil certified reference material (CRM_soil); b) Sediment certified reference material (CRM_sediment); c) Phosphogypsum sample (PG sample) and phosphogypsum reference material (RM_PG). 92
- Figure 6.5** Dynamic lixiviation for Th, in solid environmental samples, using artificial rainwater as leaching agent. The results are expressed as average \pm standard deviation ($n=3$). a) Soil sample and soil certified reference material (CRM_soil); b) Phosphogypsum sample (PG sample) and phosphogypsum reference material (RM_PG). 93
- Figure 7.1** a) Representation of the 3D printed device (dimensions in mm); b) unmodified device: representation of TEVA resin immobilization and uranium retention in the 3D printed device. 103

Figure 7.2 a) and b) Scanning electron microscopy images of the unmodified 3D printed cubes; c) and d) the same cube after immobilization of 60:40% Aliquat® 336: ACN/MeOH/H₂O (35/35/30, vol%); and e) and f) after the immobilization of TEVA resin. 103

Figure 7.3 Scanning electron microscopy images of the 3D printed device after stirring 15 min at 300 rpm. a) Inner faces with resin beads, and external faces without them; b) and c) enlarged images of the inner faces. 104

Figure 7.4 EDAX spectra of Cl/U from the 3D printed device a) with immobilized 60:40% Aliquat®336: ACN/MeOH/H₂O (35/35/30, vol %); b) with immobilized TEVA resin.... 105

Figure 7.5 Efficiencies of U(VI) extraction obtained by 3D printed device coated with TEVA resin, 60% of Aliquat®336, and the unmodified cube. Extraction conditions: 15 min at 300 rpm. Analyte concentration: 32 mg L⁻¹. 105

Figure 7.6 Optimization of the times of retention and elution steps: a) Conditions of the extraction time: extraction at 300 rpm, elution with 3-times of 5 mL of 1 mol L⁻¹ HNO₃ at 1100 rpm. Analyte mass: 0.33 ng U in both studies; b) Conditions of elution time study: 15 min of extraction at 300 rpm, elution with 10 mL of 1 mol L⁻¹ HNO₃ at 1100 rpm. . 106

Figure 7.7 Analytical response (²³⁸U cps/ ²⁰⁹Bi cps), of solid cube coated with TEVA resin (SC); 3D printed device coated with TEVA resin (C); and 3D printed device coated with TEVA resin, doing the extraction without stir (CWS). Conditions: 15 min of extraction at 300 rpm. Elution, three of 5 mL (1 mol L⁻¹ HNO₃) at 1100 rpm each one. Analyte mass, 0.33 ng. 107

Figure 7.8 Analytical response (²³⁸U cps/ ²⁰⁹Bi cps) of the preconcentration volume. Conditions: 15 min of extraction at 300 rpm. Elution, three of 5 mL (1 mol L⁻¹ HNO₃) at 1100 rpm each one. Analyte mass: 0.2 ng. 108

Figure 7.9 Representation of 3D printed device. a) 3D printed device separated in five parts; b) details of the top and lower taps (parts 1 and 5); c) details of the rings (parts 2 and 4); and d) details of the extraction cavity (part 3). Dimensions are expressed in mm. 110

Figure 7.10 a) Automatic system for the extraction of U using a 3D printed SPE/container device. b) Representation of the automatic magnetic stirring of the 3D printed device, using a ring that contains neodymium magnetic in both sides. HC: holding coil; SV: selection valve. 112

Figure 7.11 Pareto Chart for the variables affecting U retention. 114

Figure 7.12 Pareto Chart for the variables affecting U elution. 116

Figure 7.13 a) Graph of marginal means of the effect of the interaction between the variables eluent volume (mL), and speed stir (rpm). b) eluent molarity (HNO₃ mol L⁻¹), and speed stir (rpm). 116

Figure 7.14 Optimization of eluent molarity (HNO_3 mol L^{-1}). Conditions: 15 min of extraction at 96 rpm, elution 1 min at 96 rpm. U: $10 \mu\text{g L}^{-1}$ 117

Figure 8.1 Representation of 3D printed dark box. a) Perspective view of the 3D printed dark box. b) Details of the lower tap, separated in sections. c) Details of the top cap, separated in sections. d) Details of the slide, separated in sections. 125

Figure 8.2 Representation of 3D printed mixer. a) Four views of the 3D printed mixer, which the Rhinoceros program displays, when the piece is design. b) Perspective view of the 3D printed mixer. 126

Figure 8.3 Automatic system for extraction/ preconcentration and detection of ^{90}Sr using a 3D printed mixer (cocktail to sample ratio 1:1). C: three-way connector, HC: holding coil, PMT: photomultiplier tube, LOV: Lab-on-valve; MSFIA: multisyringe module, S: syringe; V: external solenoid valve. 128

ABSTRACT

In this thesis, different devices have been developed, using 3D printing technology or numerical control tools, which have been integrated into automatic analysis systems that use flow injection analysis techniques.

The first two works describe a device, made by means of numerical control tools, which allows the study of ^{226}Ra , U and Th dynamic lixiviation from residues and environmental samples (phosphogypsum, soil and sediment). The device was integrated into two automatic flow systems, which combine the Lab-On-Valve techniques and multi-syringe flow injection analysis (LOV-MSFIA). The systems allow to perform the on-line lixiviation, extraction and preconcentration of the studied radionuclides. In both works, a subsequent off-line detection is performed, which for ^{226}Ra is carried out in a low background proportional counter, and for U and Th in an ICP-MS. The proposed systems allowed to study the lixiviation process from a new approach, since they are based on a dynamic lixiviation with constant renewal of the extractant, which imitates the natural lixiviation process.

The third work consists of two parts. The first part describes the use of 3D stereolithography technique, which allows the printing in three dimensions of complex structures with high precision. The 3D device manufactured was coated with TEVA resin, for the selective extraction /preconcentration of U(VI) in environmental samples. In the second part, the integration of this 3D device into an automatic flow system is presented, with ICP-MS off-line detection. The proposed method uses the technique of sequential injection analysis (SIA). The results obtained, both in the analytical parameters and in the analysis of samples, have been satisfactory. This work proposes a simple method for the selective extraction of U in environmental samples without the requirement of a pretreatment.

The fourth work presents a completely automated system, which allows the on-line extraction and detection of ^{90}Sr . The detection system was developed in collaboration with the company iC-Málaga and uses a liquid scintillation counter based on photomultiplier tubes. The automatic system combines the flow analysis techniques of LOV and MSFIA, and integrates two 3D printed devices, a dark box to isolate the flow cell from ambient light and a mixer to achieve a homogeneous mixture between the eluate and the scintillation liquid. The constructed sensor prototype allows to carry out all the steps of the analytical protocol, including the extraction and preconcentration of ^{90}Sr , the mixture of the eluate with the scintillation liquid and the on-line count of the beta emissions.

RESUMEN

En esta tesis se han desarrollado diferentes dispositivos, usando la tecnología de impresión 3D o herramientas de control numérico, que se han integrado en sistemas automáticos de análisis que utilizan técnicas de análisis por inyección en flujo.

Los dos primeros trabajos describen un dispositivo, realizado por medio de herramientas de control numérico, que permite el estudio de la lixiviación dinámica de ^{226}Ra , U y Th en residuos y muestras ambientales (fosfoyeso, suelo y sedimento). El dispositivo se integró en dos sistemas automáticos en flujo, que combinan las técnicas Lab-On-Valve y el análisis por inyección en flujo multijeringa (LOV-MSFIA). Los sistemas permiten realizar la lixiviación, extracción y preconcentración en línea de los radionúclidos estudiados. En ambos trabajos se realiza una detección posterior fuera de línea, que para el ^{226}Ra se lleva a cabo en un contador proporcional de bajo fondo, y para el U y el Th en un ICP-MS. Los sistemas propuestos permitieron estudiar el proceso de lixiviación desde un nuevo enfoque, ya que se basan en una lixiviación dinámica con renovación constante del extractante, que imita el proceso de lixiviación natural.

El tercer trabajo consta de dos partes. En la primera parte se describe el uso de la técnica de impresión en 3D por estereolitografía, que permite la impresión en tres dimensiones de estructuras complejas con alta precisión. El dispositivo 3D fabricado fue recubierto con la resina TEVA, para la extracción/ preconcentración selectiva de U(VI) en muestras ambientales. En la segunda parte, se presenta la integración de este dispositivo 3D en un sistema en flujo automático, con posterior detección mediante un ICP-MS. El método propuesto utiliza la técnica de análisis por inyección secuencial (SIA). Los resultados obtenidos, tanto en los parámetros analíticos como en el análisis de muestras, han sido satisfactorios. Este trabajo propone un método simple para la extracción selectiva de U en muestras ambientales sin el requerimiento de un pretratamiento.

El cuarto trabajo presenta un sistema completamente automatizado, que permite la extracción y detección en línea de ^{90}Sr . El sistema de detección fue desarrollado en colaboración con la empresa iC-Málaga y utiliza un contador de centelleo líquido basado en tubos fotomultiplicadores. El sistema automático combina las técnicas de análisis en flujo LOV y MSFIA, e integra dos dispositivos impresos en 3D, una caja oscura para aislar la celda de flujo de la luz ambiental y un mezclador para lograr una mezcla homogénea del eluato y el líquido de centelleo. El prototipo de sensor construido permite llevar a cabo todos los pasos del protocolo analítico, incluyendo la extracción y preconcentración de ^{90}Sr , la mezcla del eluato con el líquido de centelleo y el contaje en línea de las emisiones beta.

RESUM

En aquesta tesi s'han desenvolupat diferents dispositius emprant tecnologies d'impressió 3D, o eines de control numèric, les quals s'han integrat en sistemes automàtics d'anàlisi que utilitzen tècniques d'anàlisi per injecció en flux.

Els dos primers treballs descriuen un dispositiu realitzat per mitjà d'eines de control numèric, que permet l'estudi de la lixiviació dinàmica de ^{226}Ra , U i Th en residus i mostres ambientals (fosfoyeso, terra i sediment). El dispositiu es va integrar en dos sistemes automàtics en flux, que combinen les tècniques Lab-On-Valve i l'anàlisi per injecció en flux multixeringa (LOV-MSFIA). Els sistemes permeten realitzar la lixiviació, extracció i preconcentració en línia dels radionúclids estudiats. En ambdós treballs es realitza una detecció posterior fora de línia, que per al ^{226}Ra es porta a terme en un comptador proporcional de baix fons, i per l'U i el Th en un ICP-MS. Els sistemes proposats van permetre estudiar el procés de lixiviació des d'un nou enfocament, ja que es basen en una lixiviació dinàmica amb renovació constant de l'extractant, que imita el procés de lixiviació natural.

El tercer treball consta de dues parts. A la primera part es descriu l'ús de la tècnica d'impressió en 3D per estereolitografia, que permet la impressió en tres dimensions d'estructures complexes amb alta precisió. El dispositiu 3D fabricat va ser recobert amb la resina TEVA, per a l'extracció / preconcentració selectiva d'U(VI) en mostres ambientals. A la segona part, es presenta la integració d'aquest dispositiu 3D en un sistema en flux automàtic, amb posterior detecció mitjançant un ICP-MS. El mètode proposat utilitza la tècnica d'anàlisi per injecció seqüencial (SIA). Els resultats obtinguts, tant en els paràmetres analítics com en l'anàlisi de mostres, han estat satisfactoris. En aquest treball es proposa un mètode simple per a l'extracció selectiva d'U en mostres ambientals sense el requeriment d'un pretractament.

El quart treball presenta un sistema completament automatitzat, que permet l'extracció i detecció en línia de ^{90}Sr . El sistema de detecció va ser desenvolupat en col·laboració amb l'empresa iC-Màlaga i utilitza un comptador de centelleig líquid basat en tubs fotomultiplicadors. El sistema automàtic combina les tècniques d'anàlisi en flux LOV i MSFIA, i integra dos dispositius impresos en 3D, una caixa fosca per aïllar la cel·la de detecció de la llum ambiental i un mesclador per aconseguir una barreja homogènia de l'eluat i el líquid de centelleig. El prototip de sensor construït permet dur a terme tots els passos del protocol analític, incloent-hi l'extracció i preconcentració de ^{90}Sr , la barreja de l'eluat amb el líquid de centelleig i el comptatge en línia de les emissions beta.

CHAPTER 1

GENERAL INTRODUCTION

1.1. Natural radioactivity

Natural radioactivity can be categorized into three different classes based on the production origin of radionuclides: cosmogenic radionuclides, primordial radionuclides and series of radioactive decay [1].

Cosmic radiation is produced continuously by bombardment of stable nuclides by cosmic rays, mainly in the atmosphere [2,3]. The most important cosmogenic radionuclides are: ^{14}C , ^7Be , ^{10}Be , ^{22}Na and ^3H . These elements are present in air, soil and water, thus incorporating the trophic chain, which explains that the human body itself contains radioactive activity, which is generated mainly by the disintegration of ^{40}K and ^{14}C [4].

Primordial radionuclides, defined as the radionuclides present since the formation of the earth, have half-lives comparable to the age of the earth, it means greater than 100 million years [5]. At least, seventeen individual primary radionuclides with half-lives between 1×10^9 and 1×10^{16} years have been identified. In addition, ^{232}Th , ^{235}U and ^{238}U , which initiate the series of radioactive decay, are also considered primary radionuclides [1].

The successive decay of ^{232}Th , ^{235}U and ^{238}U are essentially responsible for the presence of radioisotopes of lead, polonium, bismuth, radon, astatine, francium and protactinium in the earth [1]. The fact that the decay chains of uranium, thorium and actinides are found in nature is directly related to the long life-average of the parents of these chains [3].

Human beings are exposed to natural radiation from external sources, which include radionuclides in the earth and cosmic radiation, and internal radiation by radionuclides incorporated to the body. The main routes are the ingestion of food and water, and by inhalation [3].

On the other hand, the composition of the ground where the measurements are made, the latitude and the altitude, vary for each area and is known as background radiation [6].

1.1.1. NORM

Materials that may contain the primordial radionuclides or radioactive elements as they occur in nature, such as thorium, radium, uranium, potassium and their radioactive decay products that are not altered as a result of human activities, are called naturally occurring radioactive materials (NORM) [7]. Generally, NORM contain natural radionuclides at low or moderate concentrations, such as some granites and phosphate sedimentary rocks [8]. Some NORM, such as rocks, minerals and soil that are used for the construction of

buildings contain high concentrations of radionuclides, allowing the dispersion of these in the environment as a result of human activity itself [4,9]. Certain industries handle significant amount of NORM, which usually end up in waste streams, or in the case of uranium mining that ends up in tailing dams [10].

1.1.2. TENORM

Technologically enhanced naturally occurring radioactive materials (TENORM) are not a source of production of natural radionuclides, but are responsible for the regional, national and international distribution of many radionuclides in the environment [1].

Conference of Radiation Control Program Directors has defined TENORM as natural materials that are not regulated by the Atomic Energy Law of 1954, whose radionuclides concentrations have increased by or as a result of human practices. The TENORM do not include the natural radioactivity of the rocks or soils, nor the background radiation, but refers to the materials whose radioactivity is technologically enhanced by controllable practices or by human practices carried out in the past [11]. The risk of the TENORM is that they contain enhanced concentration of natural radionuclides [1].

The largest industrial sectors that generate TENORM are: mining, energy productions, water treatment and consumer products [7]. Among the consumer products are [1,9,12,13]:

- a) Antiques: there are items, such as furniture, clothes, jewellery, books, dolls, dishes, which contain radioactive products.
- b) Building materials: Rocks, minerals, and soils containing natural radioactive materials, incorporated into building materials such as brick, cement block, granite countertops and tiles.
- c) Tobacco products: Cigarette smoke contains small amount of radioactive materials that smokers bring that their lungs while inhaling. The radioactive particles lodge in the lung tissue and can be a key factor in lung cancer.
- d) Phosphate fertilizer: These fertilizers contain part of the natural radium (^{226}Ra), uranium and thorium present in the phosphate rock. During the treatment of the phosphate rock with sulfuric acid to form phosphoric acid, the radionuclides present are divided between the products and the waste stream. One of the by-products formed during this treatment is phosphogypsum, which contains percentages of radionuclides of ~80% ^{226}Ra , ~30% ^{232}Th and ~14% ^{238}U .

1.2. Artificial radioactivity

Artificial radionuclides are produced through nuclear reactions that are carried out in nuclear reactors or in a particle accelerator; there are around 1300 artificially produced radionuclides [14].

The existence of artificial radionuclides in the environment is due to several sources such as: nuclear medicine, research laboratories, tests with nuclear weapons, nuclear power generation and the nuclear industry. Being, testing with nuclear weapons and the nuclear industry the most important source of release of artificial radionuclides. This type of source releases almost the same radionuclides in the environment, mainly finding the ^3H , ^{14}C , ^{54}Mn , ^{55}Fe , ^{89}Sr , ^{90}Sr , ^{91}Y , ^{95}Zr , ^{103}Ru , ^{106}Ru , ^{125}Sb , ^{131}I , ^{137}Cs , ^{140}Ba , ^{141}Ce , ^{144}Ce , ^{239}Pu , ^{240}Pu and ^{241}Pu .

The fission between uranium and plutonium forms two radionuclides with long half-lives: ^{137}Cs ($T_{1/2} = 30.02$ years) and ^{90}Sr ($T_{1/2} = 28.63$ years). These radionuclides, are the most active in the environment, and considered the most important from the point of view of nuclear protection at current exposure levels [15].

The US Department of Energy reports that almost 4000 million liters of low-level radioactivity waste and 450 million liters of high-level radioactivity waste were generated associated to nuclear weapons production in the second half of the previous century [16]. In addition, radiostrontium isotopes are present in the environment from atmospheric nuclear weapons testing on a global scale and from approved or unapproved releases from nuclear facilities and nuclear accidents [17]. Besides, transuranium elements are continuously dumped in the waters due to authorized discharges of low activity and they are the most dangerous artificial radionuclides. Most of these radionuclides are alpha emitters and have very long half-lives, keeping them in the environment for several generations so that knowledge of their behaviour is of great importance [5,14].

Therefore, artificial radioactivity is of great public concern in many countries, and it has been recognized as a threat to civilization. For example, the total radioactivity released into the atmosphere of all the years that nuclear tests have been carried out, is comparable to approximately 3 months of radon emission from the surface of the earth, and the Chernobyl accident (Ukraine, 1986) with about 4 days of radon emission [15]. Besides, the Chernobyl nuclear accident caused the greatest release of radiostrontium [18,19]. ^{90}Sr is the most important radiostrontium, and is one of the most harmful because it replaces calcium in bones [20].

1.3. Radionuclides studied

1.3.1. Radium

Radium was one of the first elements discovered thanks to its radioactive properties, and therefore was closely related to the discovery of radioactivity [8]. It is a radioactive element with chemical properties similar to calcium and barium. It is found in nature primarily in rocks, soil, uranium minerals and in mineral and underground waters. It has 13 radioisotopes, of which ^{223}Ra , ^{224}Ra , ^{226}Ra and ^{228}Ra are found in nature and are the products of decay within the radioactive series of ^{238}U , ^{235}U and ^{232}Th . The rest of the isotopes are produced artificially [5,21,22].

^{226}Ra is an alpha and gamma emitter, with a half-life of 1600 years and is the radioisotope of Ra with greater environmental concern, due to its high radiotoxicity, and because it is one of the largest contributors to the internal dose of the population [22,23].

During the 20th century, ^{226}Ra was used in numerous medical and industrial applications. Among the latter, there are consumer products such as toothpaste, hair creams and even foods, due to their supposed beneficial properties for health. Later, these products were banned in many countries due to the possible effects on health. It was also used until the late 1960s and early 1970s in auto-luminous painting for watches, airplane switches and instrument dials [24].

High Ra concentrations, are found in the environment as a result of natural processes, nuclear fuel cycle activities and non-nuclear industry activities [21]. The highest concentrations of ^{226}Ra are found in bitumen slate, shale, volcanic and phosphate rocks, followed by granites, sandstone and clay rocks, finally lime, carbonate and sedimentary rocks. The high levels of ^{226}Ra in bitumen slate and shale are probably due to associations of material rich in clay of organic origin, while the phosphate rocks of sedimentary origin correspond to minerals rich in uranium [8].

The activities of the human being have led to an increase of ^{226}Ra concentrations in the environment, making necessary the development of efficient analytical methods that can mimic their behaviour in nature (leaching) or determine their concentration in the environment, i.e. soil, sediment, biota and water [22].

1.3.2. Uranium

Uranium is a natural radioactive element, alpha and gamma emitter, composed by a mixture of 3 radioisotopes: ^{234}U (0.0055%), ^{235}U (0.75%) and ^{238}U (99.27%) with half-lives of 4.47×10^9 , 7.04×10^8 y 2.46×10^5 years, respectively. Given that they have long-lives, uranium is considered more chemotoxic than radiotoxic.

Uranium can be found in its reduced state (U(IV)), which is generally not very mobile, or in its oxidized state which is more soluble and mobile (U(VI)). Generally, is present in low amounts in rocks, soil, water, plants and animals. The mobility and bioavailability of U in the environment is mainly governed by its oxidation state, complexation by organic and inorganic ligands, pH, and sorption by minerals, including clays and hydroxides, and interactions with organic matter [25].

On the other hand, depleted U is used as counterweight in helicopter motors and aircraft control surfaces, as a shield to protect against ionizing radiation, as a component of ammunition to help them penetrate armored vehicles and as armor in some parts of military vehicles. It is also used to make enriched U, which is used to produce fuel for nuclear power plants.

Besides, U is released naturally by the erosion of wind and water, and by volcanic eruptions. It can also be released by the inactive and active mining and milling industries

The main sources of U exposures for people are food and drinking water. Root crops (potatoes, turnips, parsnips, sweet potatoes) provide the greatest amount of U to the diet. It must be taken into account that the amount of U in these foods is directly related to the amount of U that contains the soil in which are cultivated. Likewise, workers who extract, grind or process U or manufacture articles that contain U, as well as people who work with phosphate fertilizers may also be exposed to higher levels of U, mainly via inhalation [26].

Finally, people with greater exposure to U may have effects on their health, because U has both chemical and radiological toxicity. The radiological effects are usually local, because the alpha radiation has a very short range, causing cancer of the liver, bones and diseases of the blood. But its chemical toxicity allows U to lodge in specific places in the body affecting the normal functioning of the kidney, brain, liver and heart [5].

1.3.3. Thorium

Thorium is a natural radioactive element member of the actinide series of ^{232}Th and U (^{235}U and ^{238}U), and artificially produced by elements such as Pu. It is present in very low levels in practically all rocks, soils and water, and therefore it is also found in plants and animals. However, it is more abundant and in higher concentrations in rocks of the crust, and minerals (monazite and thorium silicate).

The primary anthropogenic source of Th release into air, soil, and water are U and Th mining, processing and milling, phosphate fertilizer production; phosphate rock processing; coal combustion; tin processing; and industrial boilers. Th mobility in water

and soil are governed by its chemical and biological behaviours; commonly Th mobility is very slow, because it will remain strongly sorbed. Wet conditions, acidity and the presence of ions or ligands (CO_3^{-2} , humic matter), which can form soluble complexes with Th can enhance its mobility through the soil. While, the formation of soluble complexes with humic materials, carbonate, or other ligands in water may increase the concentration of dissolved Th in water [27].

Th is composed of 25 different radioisotopes; the most common are ^{224}Th , ^{226}Th , ^{227}Th , ^{229}Th , ^{230}Th , ^{231}Th , ^{232}Th , ^{233}Th and ^{234}Th . These can be naturally and/or artificially produced. The isotopes of Th have different nuclear properties and half-lives ranging from seconds to 10^{10} years. Commonly, there are 6 different isotopes of Th in the environment, such as ^{234}Th , ^{231}Th with β emission, and ^{230}Th , ^{232}Th , ^{228}Th and ^{227}Th with α emission. Among these radioisotopes, ^{230}Th , ^{232}Th and ^{228}Th are particularly important because of their relatively long half-lives, high natural abundance and alpha particle radiation [27]. Furthermore, ^{232}Th in soil health risk is caused by the fast accumulation of ^{228}Ra and its associated gamma radiation. ^{232}Th is generally present with its decay product ^{224}Ra , which will produce ^{220}Rn gas and its decomposition products, which result in lung exposure. Besides, ^{230}Th is usually present along with its decay product ^{226}Ra . It constitutes a health risk because of the gamma radiation from ^{226}Ra decay products, lung exposure from ^{222}Rn gas and its decay products, and ingestion and inhalation exposure [28].

On the other hand, Th is used to make ceramics, flashlight blankets, welding rods, lenses for camera and telescopes, and metals used in the aerospace industry. Studies of workers have shown that inhaling Th powder will cause an increased risk of developing a lung disease, including lung cancer or pancreatic cancer [28].

The determination of Th radioisotopes in nuclear waste is important, due to their long half-lives and high radiological toxicities. In addition, it is necessary for the classification of waste. Th analyses usually require preconcentration and separation of the excess inactive matrix components and highly radioactive fission products. Additionally, a precise characterization of the Th interactions in the environment is necessary, therefore the development of better analytical separation methods for Th is required [27].

1.3.4. Strontium

Strontium is a natural and abundant element, which can exist in two oxidation states: 0 and +2. Under normal environmental conditions, only the oxidation state +2 is stable

enough to be important for the industry. Natural Sr is not radioactive and exists in four stable isotopes (^{84}Sr , ^{86}Sr , ^{87}Sr and ^{88}Sr) [29].

Also, Sr presents radioactive isotopes such as ^{82}Sr , ^{83}Sr , ^{85}Sr , ^{89}Sr and ^{90}Sr . The most important Sr radioisotopes in the environment are ^{89}Sr and ^{90}Sr , because they are the two fission products with long half-lives compared to other radioisotopes. ^{90}Sr has a half-life of 28.6 years and is a pure β^- emitter, decay at ^{90}Y , which has a very short half-life ($T_{1/2} = 2.67$ days), so that normally ^{90}Y and ^{90}Sr are in secular equilibrium in environmental samples [30]. ^{90}Sr is used in medical and agricultural studies. It is also used in thermoelectric devices, electron tubes, radioluminescent markers, as a source of radiation in industrial thickness gauges, and for the treatment of eye disease [31].

In the environment, stable and radioactive Sr compounds are present in the dust of the air. Emissions from burning coal and oil increase stable level of Sr in the air. Likewise, Sr is found naturally in the soil, but this can increase due to the removal of coal ash, ash from incinerators and industrial waste. In general, the amount of ^{90}Sr in the soil is very small [29].

It should be noted that the greatest source of radioactivity in the environment comes from atmospheric test of nuclear weapons. Another secondary source of radiostrontium is released from the nuclear fuel cycle and accidents in nuclear reactors. Nuclear accidents, such as Chernobyl and Fukushima, have released Sr into the atmosphere, which is deposited on the surface of the earth as radioactive fallout. Chernobyl was the nuclear accident that contributed most to the amount of ^{90}Sr released worldwide, a substantial part of the ^{90}Sr released was deposited in the former Soviet Republics, and the rest spread as radioactive fallout worldwide [30,31].

Finally, the population is exposed to ^{90}Sr , either by ingesting food or drink or by small contaminated dust particles that can be inhaled. After ingesting radioactive Sr, 20% to 30% is absorbed in the digestive tract, while the rest is excreted through the stool. Of the portion absorbed, practically all the Sr is deposited in the bones or the skeleton. Affecting people's health in this way, because ^{90}Sr behaves like calcium in the human body and tends to deposit in the bones and in the tissues that make up the blood (bone marrow). Therefore, ^{90}Sr is known as "bone seeker" and exposure will increase the risk of several diseases, including bone cancer, soft tissue cancer near the bone and leukemia [31].

Considering the above mentioned, and that, the use of radionuclides has dramatically increased in the last years, mainly its use to obtain energy in nuclear power plants, the use in medicine for diagnosis and treatments, and industrial uses, e.g. food

and materials sterilization, sheet thickness, welding and leaks monitoring, in fossil and artwork dating, and in research, and therefore, the environmental monitoring of radionuclides has also increased.

The classical approach of radiochemical separations, which are mandatory before detection with radiometric or spectrometric techniques, is time-consuming and encompasses laborious multi-steps analytical protocols. To solve this matter, the automation of the analytical methods is employed providing some advantages, such as:

- Improvement of the analyst safety, by minimizing the manipulation of samples and standards.
- Low cost per analysis, since the volume of reagents is drastically reduced.
- Protection of the environment, by reducing also the waste generated per analysis.
- High versatility, the aimed systems possess a high versatility since instruments, tubes and detectors can be shared.
- Miniaturization of the analysers, reaching a maximum with the development of sensors with integrated detection, providing portability and being very useful for in situ monitoring, e.g. in accidents where onsite determinations are required and the transportation of the samples could be difficult due to its large number and potential activity.

1.4. Flow analysis techniques

The need of the development of flow analysis techniques was due to the clinical tests, since they began to be used in extent for diagnostic purposes in medicine. The large number of samples that could be faced by analysis imposed the use of automatic analytical methods [32].

Flow analysis techniques allow the development of partially or fully automated methods, obtaining a series of advantages such as better sensitivity, selectivity, high frequency of analysis, low cost per parameter, simplicity, low consumption of sample and reagents, use of economic equipment and increases the safety of the analyst by reducing the manipulation of samples and reagents, thus contributing to the reduction of waste generation. Besides, the use of software allows the storage of experimental data, which can be treated later, freeing the specialized personnel from the routine tasks. Actually, automatic analytical methodologies based on flow analysis techniques to monitor elements and parameters of a large number of environmental samples in a short period of time, have been developed in extent [33].

On the other hand, radiochemical analysis is another field where the use of flow analysis techniques has been widely developed, due to the increase of the use of

radionuclides and the consequent increase in their environmental vigilance. The use of radionuclides has drastically increased in energy production, diagnosis and medical therapy and industrial applications. In this way, the advantages of flow analysis techniques are obtained, which is very important when dealing with radioactive samples.

Drawback of the flow techniques are the main impediment to achieve a fully automatic system in this field, because the low activities of the radionuclides in the environmental, requiring counting times about 1 day by radiometric detection. However, even partially automated methods allow the automation of the more laborious, time-consuming and manipulative steps [34,35].

The fully automated determination of radionuclides, that is, with on-line detection, can be carried out by coupling the analytical system with a radiometric detector, commonly liquid scintillation counting that require counting times of minutes to a few hours, due to its highest counting efficiencies. Another alternative is to manufacture a sensor based in liquid scintillation counter (LSC) by means the use of photomultipliers tubes (PMT) [35,36].

1.5. Extraction techniques

The radionuclide determination requires a prior treatment separation and preconcentration of the analyte of interest, to subsequently measured its activity using radiometric or spectrometric techniques. Thus, the low activities of the radionuclides, found in environmental samples, can be measure without interferences.

1.5.1. Extraction by selective resin

Solid phase extraction (SPE) is a technique that uses the extractant supported on beads or disk for the preparation of samples. The development of this separation technique has grown, due to the optimization of the adsorbent formats, the automation and the increase of the extraction selectivity, thanks to the introduction of new solid phases in the market.

The main objectives of SPE are the trace enrichment (preconcentration), the simplification of the matrix (sample clean-up) and the exchange of the medium (transfer of the sample matrix to an eluent) [37]. In addition, SPE provides advantages with respect to liquid-liquid extraction (LLE), which present an incomplete separation of phases by the emulsions that can be formed, the use of expensive and breakable specialized glass material, and the large quantities of organic solvent, wastes. Besides, SPE is more efficient, because it is fast and produces quantitative extractions easy to perform [38].

Chromatographic resins are widely used for the separation of radionuclides from different sample types, because it combines the selectivity of LLE with the ease operation of a chromatographic column. A chromatographic extraction resin consists mainly of an inert support, a stationary phase and a mobile phase. Liquid extractants are used in the stationary phase. The diluents can also be used to help solubilize the extractant and increase the hydrophobicity of the stationary phase. The mobile phase is usually an acidic solution, for example, nitric acid or hydrochloric acid, although complexing agents, such as oxalic or hydrofluoric acids, are frequently used to improve the selectivity or separation of metal ions strongly retained by the resin.

1.5.2. Extraction by co-precipitation

Co-precipitation is a phenomenon that occurs when impurities are incorporated into the precipitate during its formation. There are four types of co-precipitation [39–41]:

- a) Inclusion: Refers to a single substitution of an ion of similar size in the crystal lattice. For this substitution to occur it is necessary that the two ions have the same charge and their size does not differ by more than 5%. In addition, the two salts must belong to the same class of crystals.
- b) Occlusion: Occurs when the precipitation procedure is performed quickly, and spectator ions and pocket of solvent can be trapped within the crystal.
- c) Surface adsorption: It occurs when a normally soluble compound is entrained as contaminants on the surface of a coagulated colloid, as a result of which it contains large areas of internal surface area that leave many ions exposed to the solution, which attracts ions of opposite charge.
- d) Mechanical entrapment: It happens when the crystals stay close together during growth. In this case, several crystals grow together and as a consequence a portion of the solution is trapped in small holes.

Radium is often extracted by co-precipitation with barium or other alkaline earth metals. The distribution equation for Ra in the precipitate is derived from the equilibrium of the lattice replacement reaction between the Ra^{2+} ion and the carrier ions (e.g., Ba^{2+} and Sr^{2+}) in aqueous and solid phases [42]. The mechanisms involved in the co-precipitation process depend to a great extent on the present ions, the ionic strength of the medium, reaction time and the existing crystals.

1.6. Detection techniques

For the detection of radioactive elements at environmental levels, it is necessary to use techniques for the pretreatment of the sample, because the radionuclide of interest is generally at trace level, and usually an environmental matrix contains a large number of inactive compounds that make direct analysis very difficult. On the other hand, a preconcentration of the radionuclide will not be required if the sample comes from a nuclear test or accident.

The most used detection techniques for the determination of ^{226}Ra at trace levels are by means of a low background proportional counter (LBPC), a liquid scintillation counter (LCS), gamma spectrometry and alpha spectrometry [43–46]. In the case of elemental uranium and thorium the detection techniques commonly used are: inductively coupled plasma optical emission spectrometry (ICP-OES) [47,48], photon/electron-rejecting alpha liquid scintillation system (PERALS) [49–51], and inductively coupled plasma mass spectrometry (ICP-MS). The latter being the most used, due to its high sensitivity and rapidity of analysis [52–55].

For the detection of total strontium at trace levels the following techniques are commonly used: atomic absorption spectroscopy (AAS) [56], ICP-MS [57,58], and ICP-OES [59,60]. The determination of ^{90}Sr can be carried out through LBPC, [61,62], LSC [63,64], and the Cherenkov radiation count produced by ^{90}Y [65,66]. In addition, ^{90}Sr is a radionuclide of interest for its rapid measurement, when a nuclear accident has occurred or it is required to measure some residue of a nuclear power plant. LSC detection technique is commonly used for this purpose [20,67–69].

1.7. 3D printing technology

The concept of 3D printing, also known as additive manufacturing (AM), rapid prototyping (RP) or solid-free-form (SFF) technology, was developed to manufacture plastic devices from photopolymers in the early 1980s [70].

3D printing has become a key technology for the advancement of multiple scientific fields, such as medicine [71], biology [72], chemistry [73,74], biochemistry [75] and nanotechnology [76]. Therefore, it has been found in different types of industrial applications.

Nowadays, different 3D printing techniques have been developed based on [70,77,78]:

- a) **Stereolithography (SLA)**: Additive technology that converts liquid materials into solid parts, layer by layer. Then, they are cured using a light source in a process called light curing.

- b) Fused deposition modelling (FDM): 3D models are fabricated by extruding thermoplastic materials and depositing the semi-molten materials layer by layer.
- c) Inkjet printing: A powder based method where the layer of solid particles is joined by a printed liquid material to generate a 3D model.
- d) Selective laser sintering (SLS): It uses a high-power laser to synthesize polymeric powders to generate a 3D model.
- e) PolyJet technology: It injects into a tray layers of photopolymers that are instantly hardened by ultraviolet light.

The FDM technology was the first to be used to manufacture templates for microfluidic devices with poly(dimethylsiloxane) [79]. Due to the SLA resolution and accessibility evolved, as well as the complexity of the devices that have been manufactured, 3D micromixers and devices with integrated valves could be printed [80].

In the field of analytical chemistry, the deposition of layer material has been explored allowing 3D printing for the design of unprecedented and low-cost devices for the automation of different methodologies. 3D technology also allows to manufacture mesofluidics devices with complex geometries, decreasing time and costs [81].

CHAPTER 2

TECHNIQUES USED

2.1. Flow analysis techniques

For the development of this thesis, different flow analysis injection techniques were used, such as sequential injection analysis (SIA), multisyringe flow injection analysis (MSFIA) and Lab-On-Valve (LOV).

2.1.1. Sequential injection analysis

The technique of sequential injection analysis (SIA) was developed by J. Ruzicka and G. Marshall in 1990, as an alternative to the flow injection analysis (FIA). This technique is based on the use of a bidirectional syringe pump [82]. The operation mode of the piston pump with a syringe is the following: in the syringe head it houses a three-way solenoid valve, allowing four operations in the handling of fluids (loading or dispensing the liquid into a reservoir or a manifold).

SIA is based on the use of a selection valve, in which the central port of the valve is connected to the syringe pump previously described, by means of a holding coil (HC). The central port is connected with the different lateral ports of the selection valve, allowing the loading of different reagents/ samples in the flow system. Also, a detector can be connected to a lateral port.

On the other hand, this type of technique allows the development of multiparameter analysers without the excessive increase in the complexity of the manifold, as well as a considerable saving in the consumption of samples and reagents, and a greater flexibility in the change of parameters without having to perform a reconfiguration in the manifold. It also allows the elimination of the Tygon® pipe, which deteriorates with aggressive chemicals (strong acids and organic solvents), not being affected by the glass syringe and resistant polymeric tubing used in this technique.

Besides, SIA has instrumental robustness since it is capable of withstanding high pressures [83]. SIA technique has been widely used for the determination of radionuclides of interest in nuclear waste, nuclear reactor coolants and environmental samples [16,34,84].

2.1.2. Multisyringe flow injection analysis

The multisyringe flow injection analysis (MSFIA) was developed in 1999 by the group of Analytical Chemistry, Automation and Environment of the University of the Balearic Islands together with Crison (Alella, Barcelona, Spain). The objective was to combine the advantages of previously designed flow techniques and avoid their disadvantages. In this way, a new multichannel technique was designed that combines the high

performance and multichannel operation of FIA, together with the robustness and versatility of SIA [32].

The module consists of a conventional automatic burette that can be equipped with up to 4 syringes which are used as liquid controllers. Each syringe has a three-way solenoid valve in the head, which facilitates the application of multiple switching schemes. These valves have the capacity to withstand an overpressure of up to approximately 2 bars, allowing analytical methods with extraction columns, taking into account that the flow velocity must be moderate. The piston is mounted on a common steel bar driven by a one-step motor. Therefore, all pistons move simultaneously and unidirectionally for liquid delivery (dispense) or aspiration (pick up) [4,32].

Furthermore, this technique gives a high chemical resistance, which is provided by the use of poly(ethylene-co-tetrafluoroethylene) resistant polymer (head valves) and polytetrafluoroethylene (PTFE) or glass tubes. Besides, the use of organic solvents and aggressive reagents are allowed. Likewise, it allows the precise and constant control of the hydrodynamic variables for each sample and reagent through the use of software that controls the multisyringe module.

Nowadays, MSFIA has been successfully coupled with other techniques such as LOV [43,52,85], low pressure chromatography [86–88] and multipumping flow systems [89,90] for the determination of environmental parameters and radionuclides of environmental interest [34,91]. MSFIA systems with 3D printed devices integrated for the heavy metal determinations have been recently reported [81,92].

2.1.3. Lab-On-Valve

Lab-On-Valve (LOV) was developed by J. Ruzicka with the aim of compacting SIA. The channel system and the flow cell are manufactured as a monolithic structure mounted on a conventional multiposition selection valve. LOV allows the manipulation of samples in the sequential injection mode, in which a wide variety of assays can be programmed within the same microfluidic device. The measurement, mixing, dilution and monitoring of the solution can be executed in any desired sequence in a channel system, integrated with a multipurpose flow cell [93].

In addition to the compactness and robustness of LOV, other advantages that it presents, are the permanent rigid position of the sample processing channels that guarantees the repetitiveness of the microfluidic manipulations.

It is worth mentioning that LOV has flexibility in the handling of fluids, being able to handle homogeneous and heterogeneous solutions. Likewise, it allows the manipulation of particles. One of the channels of LOV can be used as a microcolumn to

carry out the bead injection (BI) process, thus allowing the automatic regeneration of the solid phase. This type of concept has been widely exploited for the separation, preconcentration of analytes in the presence of complex matrix components [32].

2.2. Extraction techniques

In this thesis, selective chromatographic extraction resins were used (Triskem International, France) [94]. As previously mentioned, this type of resins allows the chromatographic separation of two or more radionuclides, but in the works developed, they have been used for the separation and preconcentration of one or two radionuclides (eluted at the same time). Three types of resin were used: UTEVA resin for the extraction and preconcentration of ^{238}U and ^{232}Th , TEVA resin for the extraction of ^{238}U , and Sr resin for the extraction of ^{90}Sr .

2.2.1. UTEVA resin

UTEVA resin (Uranium and TEtraValents Actinides) is used for the separation of uranium and tetravalent actinides such as Np, Th and Pu. Figure 2.1 shows the functional group that gives it the extractant capacity, being the DP[PP] (Dipentyl pentylphosphate).

The retention of uranium(VI), thorium(IV), neptunium(IV) and plutonium(IV), depends on the concentration of nitrate in the solution, the higher nitrate concentration there is a better absorption of actinides.

On the other hand, different types of biological or environmental samples may contain phosphates, which affect negatively the absorption. Because the phosphate anions compete easily with the tetravalent actinides, preventing the absorption of neptunium or thorium to the resin. Fortunately, the addition of aluminium to the sample can significantly reduce this problem, avoiding the interference of phosphate in the absorption of radionuclides [95].

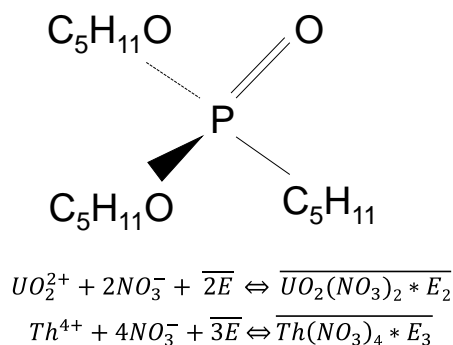


Figure 2.1 UTEVA resin component and equilibrium extraction, E= extractant. Dipentyl pentylphosphate DP[PP], also called Diamyl amyolphosphate (DAAP).

2.2.2. TEVA resin

TEVA resin (TetraValent Actinides and technetium) is commonly used for the separation of technetium(VII) and actinides(IV). The extractant that gives specificity to TEVA resin is a quaternary ammonium salt, also called Aliquat®336, which can be seen in Figure 2.2. Acts as a strongly basic anion exchange material [96].

The retention of tetravalent actinides has a direct relationship with the concentration of nitric acid; this means that as the acid concentration decrease, the retention of the tetravalent actinides decreases as well. In high concentrations of hydrochloric acid, Pu(IV), Np(IV) and U(VI) are strongly retained, but Th(IV) and Am(III) are not. By adjusting acid concentration and valences, several separations can be established. For example, after loading actinides and washing the column, the unretained Am will be removed, and the uranium can be eluted with 2 mol L⁻¹ nitric acid, followed by thorium with 3 mol L⁻¹ hydrochloric acid. The tetravalent actinides such as Pu(IV) and Np(IV) can be eluted with 0.5 mol L⁻¹ hydrochloric acid [97].

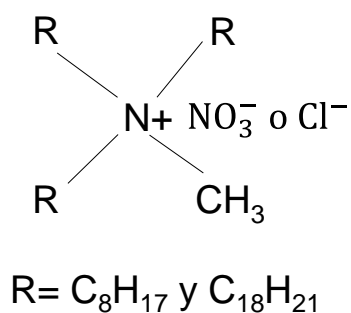


Figure 2.2 TEVA resin component, a quaternary ammonium salt (Aliquat®336).

2.2.3. Sr-resin

Sr-resin is used mainly for strontium separation. The stationary phase consists of a dicyclohexano 18-crown-6 derivative dissolved in octanol (Figure 2.3). The concentration of the crown in the resin is 1 mol L⁻¹ and the experimental capacity of the resin is 8 mg Sr mL⁻¹ resin.

The affinity of strontium in the Sr-resin increases with direct relation to the concentration of nitric acid, obtaining good results in a range between 3 and 8 mol L⁻¹. Except for the barium, all the alkaline and alkaline earth elements show no affinity for the resin, especially in 8 mol L⁻¹.

Calcium that is chemically analogous to strontium shows very little affinity for Sr-resin, however it has been reported that when the concentration of calcium, passing it in a 2 mL column exceeds 300 mg, it behaves as interfering, reducing the chemical recovery of strontium [98].

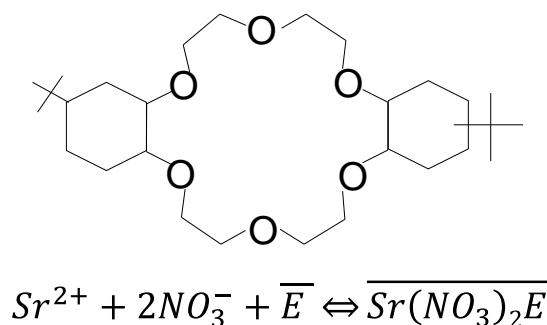


Figure 2.3 Sr-resin and equilibrium extraction, E= 4,4'(5')-di-t-butylcyclohexano-18-crown-6 (2).

2.2.4. Cellulose beads

For the extraction of ^{226}Ra , macroporous bead cellulose (MBD) was used, manufactured by the company Iontosorb (Czech Republic). This type of pearls has a hydrophilic matrix and spherical particles. They occur in various types of porosity and various particle sizes.

MBD is highly porous regenerated cellulose with heterogeneous matrix (partially microcrystalline) and polymer structure stabilized only by hydrogen bonds. Due to its high-pressure stability, it belongs to the category of swollen semi-rigid gels for low pressure chromatography.

In addition, the gels are characterized by their excellent mechanical properties, are easy to handle, resistant to destruction, high chemical resistance and compatibility with the most commonly used solvents and buffers, and applicability over a wide range of pH and salt with minimal changes (swelling or contraction) in the gel bed [99].

In this thesis, MBD of type MT-50, with a particle size of 50-100 μm , was used.

2.3. Detection techniques

The determination of many specific radionuclides can be done by radiometric and mass spectrometric techniques. Their applications are directly related to the analytical accuracy, detection limits, and accessibility of the equipment. In addition, parameters as sample preparation procedure in terms of complexity, duration, counting time and interference, should be considered in the choice of the analytical method [100].

In this thesis, detection techniques such as ICP-MS and LBPC were used to measure radionuclides at trace levels, and a prototype sensor based on LSC was manufactured.

2.3.1. Inductively coupled plasma mass spectrometry

The inductively coupled plasma mass spectrometry (ICP-MS) is a powerful tool for analysing traces and ultra-trace metals in environmental samples. Therefore, this

technique is applied to a wide variety of fields, mainly in chemistry, food, petrochemicals, drugs, geology, environmental, biomedical, semiconductor and nuclear. Undoubtedly its great advantage is due to its ability to carry out rapid determinations of multiple elements at ultra-trace level; this means that concentrations can be quantified in a minimum range of 5 orders of magnitude. In addition, it has the advantages of having an isotopic capacity, possessing high precision [101,102].

An ICP-MS system works in the following way: first the sample is introduced into argon plasma as aerosol droplets. Subsequently, the plasma dries the aerosol, dissociates the molecules and then removes an electron from the components, thus forming single charge ions, which are directed to a mass filtration device known as the mass spectrometer.

Upon exiting the mass spectrometer, the ions hit the first dynode of an electron multiplier, which serves as a detector. The impact of the ions releases a cascade of electrons that are amplified until it becomes a measurable pulse. Finally, the software compares the intensities of the pulses measured with those of the standards, which make up the calibration curve, to determine the concentration of the element [103].

Commonly an ICP-MS consists of the following components [5,103,104]:

- Sample introduction system: it is composed of a nebulizer and a spray chamber; it provides the means to insert samples in the instrument.
- The plasma source (torch system and radiofrequency coil): The argon gas is continuously flowing through the quartz torch, and a radio frequency (RF) generator supplies the energy to the RF coil. Generating in this way the plasma in the ICP-MS torch. The RF coil reaches high temperatures, in which by supplying an abundant amount of argon, it allows the plasma to reach equilibrium and to maintain a constant temperature of around 6,000°C during the analysis.
- Interface of ICP-MS: It can be described as the point at which the sample of the ICP part of the instrument is entered in the mass spectrometry part (MS) of the instrument. The interface part of the instrument is used to allow the ICP and MS portions to be coupled.
- Vacuum system: Provides a high vacuum for the quadrupole, detector and ion optics.
- Mass spectrometer: Acts as a mass filter to sort the ions by their mass to charge ratio. This quadrupole filter consists of four cylindrical molybdenum bars. When the ions enter the quadrupole they avoid that they deviate and are subjected to an oscillatory path by means of a radiofrequency voltage. With an adequate radiofrequency voltage, only the ions with a specific mass/ charge ratio are able to pass through the entire quadrupole filter.

- Detector: Operates in high vacuum conditions and has the function of counting the individual ions excited in the quadrupole.

Commonly, ICP-MS is sensitive for long-lived radionuclides, while radiometric methods are generally sensitive for short-lived radionuclides ($T_{1/2} < 10$ years), especially those with γ -rays emission. In addition, an ICP-MS has better detection limits, rapid analytical capacity, and reduces the sample amount needed for the analysis in comparison to the radiometric techniques. However, the disadvantage of an ICP-MS with respect to radiometric techniques is their isobaric interference, less accessibility, low stability, high cost and noise of equipment [100].

In this thesis, an ICP-MS Elan DRC-e (Perkin Elmer, United States), equipped with a cross flow nebulizer and Scott spray chamber (Perkin Elmer) was used.

2.3.2. Low background proportional counter

The low background proportional counter (LBPC) is a gaseous ionization detector, commonly with cylindrical or hemispheric geometry, that take advantage of the multiplying effect of the electric field when working polarized in the proportional zone.

Counters with cylindrical geometry are usually used in the detection of low energy X photons, since the body of the detector is equipped with a window of little mass thickness (aluminium or beryllium) that allows easy access to radiation.

Additionally, counters with hemispheric geometry are generally employed in the detection of alpha and beta particles. The flat part of the cathode in some models of detectors is composed of a thin window through which the radiation penetrates. In other models, this flat part is a removable cover, in which the radioactive source can be introduced inside the detector, thus allowing the absorption of the less energetic fraction of the beta radiation spectrum to be eliminated [105].

Generally, a proportional counter operates in the following way: when the incident particle enters the proportional counter, the ionization occurs, which is through the interactions of the particles with the detection gas. The secondary electrons produced through these interactions are accelerated towards the anode as a result of the bias applied to the system. Free electrons gain enough kinetic energy during acceleration to produce secondary ionization as they migrate towards the anode. This effect is known as "gas multiplication", which is used to amplify the load collected from the anode. This charge is collected by means of a resistor-capacitor circuit resulting in a charge in the potential through a capacitor [106].

The proportional counters that allow the simultaneous measurement of alpha and beta particles are based on the reach of the particles is larger to the radius of the detection chamber, causing that the impulses produced are proportional to the specific ionization that produces the particle and not to their energy; allowing differential measurement of alpha and beta radiation [105].

In this thesis, a LBPC Canberra LB4200 was used. This instrument has the lowest background specifications of any alpha/beta system that has been published, because it uses a proportional gas flow detector of 5.7 cm in diameter. It also has a shield of 10 cm, especially qualified, low background. Likewise, each detector has an additional shield to reduce the interference of adjacent detectors. It uses P-10 detection gas, which is a mixture of argon (90%) and methane (10%).

LBPC is equipped with 4 independent detectors, and allows the simultaneous measurement of 4 samples. Each detector has a cylindrical geometry, with a diameter of 5.7 cm, with a window that formed by a thin mylar sheet of $500 \mu\text{g cm}^{-2}$, which allows the passage of most of the alpha and beta particles emitted by the sample. The body of the detector is composed of the anode and cathode. The cathode is formed by a layer of copper of 0.2 cm of thickness and in its interior is the anode, which is a metallic wire of tungsten of $50 \mu\text{m}$ in diameter [107].

2.3.3. Prototype sensor based on liquid scintillation counting

The liquid scintillation counter (LSC) is a popular detector used for quantitative measurement of radioactivity since the early 1950s. Liquid scintillation analysis has been widely employed in the fields of environmental radioactivity, and in the measurement of higher levels of radioactivity used in research, radioisotope applications and nuclear energy [108]. LSC is applicable to all forms of emission of nuclear disintegration (alpha and beta particles, radionuclides emitting gamma rays and electron capture).

The scintillation technique is based on the excitation of the molecules in the solution; being the scintillation solution (cocktail), a mixture of solvent and solute (scintillator). Excited solvent molecules can transfer energy to each other and also to the solute. A molecule of excited solvent, that transfers its energy to a molecule of solute, disturbs the electron cloud of the orbital of the solute, elevating it to its state of arousal. As the electron in the excited orbital of the solute molecule returns to their ground state, a radiation (photon of light) is produced. Therefore, a single particle will manifest its presence colliding with solvent molecules and the excitation of many scintillator molecules. Having released the energy in the form of a flash of light, it can be measured

at a wavelength between the ranges of 375-430 nm for each process of radioactive decay. The emission wavelength depends on the scintillator dissolved in the solvent.

In order to measure this wavelength, a photomultiplier tube (PMT) is required, which has the internal part uniformly coated with a photosensitive material that releases photoelectrons with negative charge, by converting the light emitted into electrical energy. These electrons are attracted by an electrode inside the tube by the positive potential of the electrode, resulting in the production of more electrons.

In addition, the tube consists of a series of electrodes (usually 11-13). When the electron produced pass through the electrodes, a cascade of electrons is produced in the final electrode, thus creating an electrical pulse. Since the PMT is a linear device, the amplitude of the pulse is directly proportional to the number of photons detected by the photocathode.

In this thesis, a device based on the LSC technique was designed for the measurement of ^{90}Sr . The sensor uses two diametrically opposite PMT, thus allowing the detection of pulse by coincidence. This being an electron logic circuit that compares the signal output of both PMTs. The signal of each PMT is fed to a circuit that produces an output only if the two signals are produced together, called coincidence circuit (Figure 2.4), obtaining a coincidence pulse as output. The electrical noise of the PMT originates randomly over time, but occurs at a rate low enough to be excluded by the matching circuit [108,109].

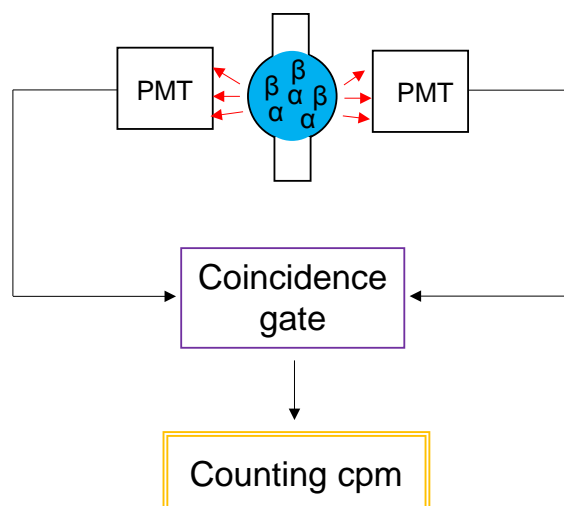


Figure 2.4 Coincidence circuit. PMT: photomultiplier tube, cpm: counts per minute.

2.4. 3D printing technology: stereolithography

The stereolithography (SLA) process was created at the beginning of 1970 and later it was patented in 1986 by Charles W. Hull. SLA allows the creation of 3D objects by successively printing thin layer of curable material by ultraviolet light, starting from the bottom layer to the top layer.

Since patents began to expire in the late 2000s, the introduction of desktop 3D printing expanded access to this technology.

Later in 2011, Formlabs expanded desktop 3D printing by adapting it to SLA technology allowing 3D printing to be accessible for a variety of custom applications including engineering, chemistry, design and manufacturing of products for the dental and jewellery industries [77].

There are two types of 3D printers base on SLA technology. The first type is shown in Figure 2.5, being right-side SLA with a direct curing process, which are built around a large tank containing liquid photopolymer (resin) and the construction platform. Basically, a single laser moves along the surface of the resin, row by row, until the desired layer is completely cured. To start the next layer, the construction platform sinks further down into the resin tank until a new layer of liquid resin covers the surface and the curing process is repeated. The process builds consecutive layers on top of each other until the piece is finished.

Among the advantages of this type of printers, it should be noted the high precision, being their main focuses in large-scale industrial systems. By the contrary, these machines are highly sensitive to any inconsistency that causes printing failures.

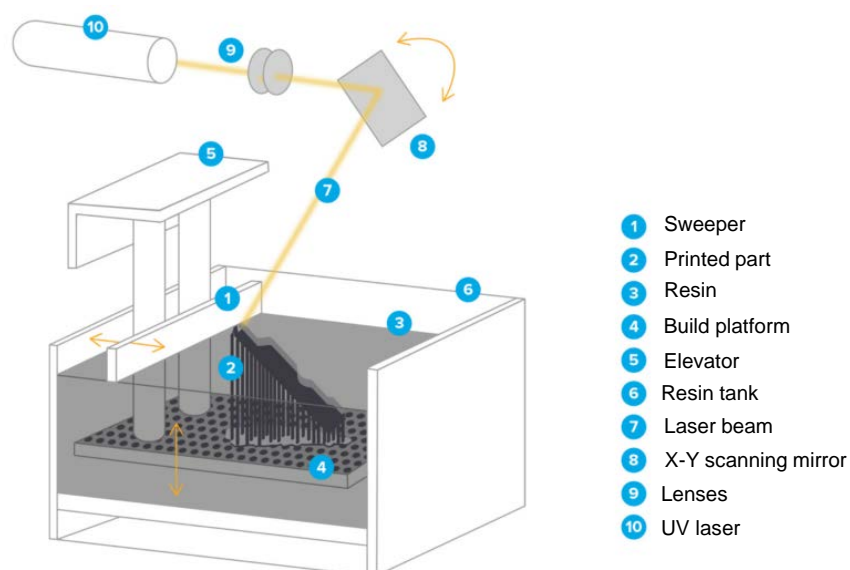


Figure 2.5 Right-side up SLA. Reproduced from the ultimate guide to stereolithography (SLA) 3D printing [77].

The second type of 3D printer is an upside-down (inverted) SLA (Figure 2.6). This method uses a tank with a transparent bottom and non-stick surface, which serves as a substrate for the liquid resin to cure, allowing the soft detachment of the newly formed layer. The printing process of a device starts when the construction platform is submerged at a defined distance in a resin tank. Next, the UV laser points to two mirror galvanometers, which direct the light to the correct coordinates in a series of mirrors, focusing light up through the bottom of the tub and curing a layer of photopolymeric resin against the background of the tank. A combination of the vertical construction platform and the horizontal movement of the tank separate the cured layer from the bottom of the tank, and the construction platform moves upward to allow the resin to flow underneath. The process is repeated until printing is completed.

One of the advantages of this type of printer is that the volume of construction can substantially exceed the volume of the tank, since the printer only requires enough material to keep the lower part of the construction platform continuously covered with liquid; allowing in this way that it is easier to maintain, clean, exchange materials, and also allows a much smaller and less expensive machine size, making it possible to bring SLA technology to the desktop. Among its disadvantages is that when the building the 3D piece inverted, the volume of construction is limited and larger support structures are required to keep the piece attached to the constructed platform [70,77].

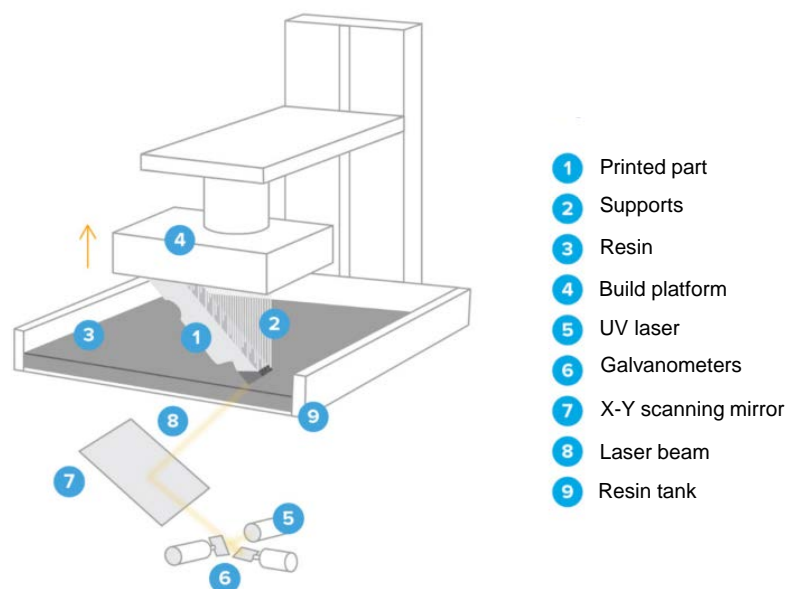


Figure 2.6 Upside-down (inverted) SLA. Reproduced from the ultimate guide to stereolithography (SLA) 3D printing [77].

In this thesis, desktop printers Form 1 and Form 2 from Formlabs based on the mechanism of upside-down (inverted) SLA were used.

CHAPTER 3

OBJECTIVES AND WORK METHODOLOGY

3.1. General objective

The main objective of this thesis is the development of devices to integrate in automatic methodologies for determining radionuclides in residues and environmental samples, which are object of environmental monitoring programmes, through miniaturized automatic systems.

3.1.1. Specific objectives

The specific objectives to achieve the general one, are the following:

- a. Design, construction and testing of a flow cell that allows to perform studies of dynamic lixiviation of radionuclides from solid matrices.
- b. Development of automatic systems, integrating the developed flow cell, for the study of radionuclide dynamic lixiviation from solid samples exploiting radiometric and spectrometric detection.
- c. Design, construction and testing of a 3D printed device to perform the selective extraction of radionuclides.
- d. Development of an automatic system, integrating the developed 3D printed device, for the selective radionuclide extraction.
- e. Design, construction and testing of 3D printed devices to perform the on-line preparation and detection of radionuclides.
- f. Development of a prototype sensor based on flow techniques encompassing the on-line extraction, preconcentration, preparation and detection of radionuclides, using 3D printed devices.

3.1.2. Work methodology

The basic work methodology to achieve the specific objectives proposed was the following:

1. Design and construction of devices based on 3D printing technology and numerical control tools. Test of the degradation of the materials used to construct the devices with different organic solvents and scintillation liquids.

2. Construction of flow systems based on flow injection analysis techniques, in which the devices will be assembled.
3. Optimization of the variables that influence the flow systems, by means of multivariate and univariate techniques.
4. Determination of the analytical parameters, including extraction efficiency, limits of detection and quantification, intra- and interday precision, durability, sample volume to be preconcentrated, and analysis frequency. Validation of the proposed methodologies, analysing certified reference materials and reference materials.
5. Application of the developed systems to the analysis of real samples, carrying out addition/recovery assays.

CHAPTER 4

MATERIALS AND METHODS

4.1. Flow systems configuration

In this section detailed information on the instrumentation and materials used for the development of the flow systems are given.

4.1.1. Multisyringe burette

The multisyringe burette (Crison Instruments, Alella, Spain) is a module that can be equipped with a range of 1 to 4 syringes of different volumes: 0.5, 1, 2.5, 5 and 10 mL (Hamilton, Switzerland) (Figure 4.1 (I)). The syringes are fixed on a joint bar, allowing them to move simultaneously at a same flow. In this way, it dispenses liquids with high precision, since the piston stroke is divided into 40,000 steps.

The syringes exert the function of a piston pump that allows the propulsion of liquids in the system. Each one has a three-way solenoid valve (N-Research, Caldwell, NJ, USA) in the upper part, which has a common port (COM). When, the valve is deactivated, the port is called “normally open port” (NO), while if the valve is activated, it is called “normally closed port” (NC). This means that when the valve is disconnected, it is said in the Off position, while if it is connected, it is said in the On position, as shown in Figure 4.1 (II).

The burette contains four ports on the back, which have an output voltage up to a maximum of 13 volts. These allow the control of four additional solenoid valves, or agitators, micro-pumps, fans and relays. At each additional connection, an electronic circuit must be incorporated to prevent overheating.

Additionally, in the back of the burette there is another output that allows the chain connections with another device, which should share the same communication channel. In this way the development of more complex automatic system is performed.

All instrumentation is controlled through the AutoAnalysis program (Sciware Systems, SL, Bunyola, Spain) through the RS232C interface.

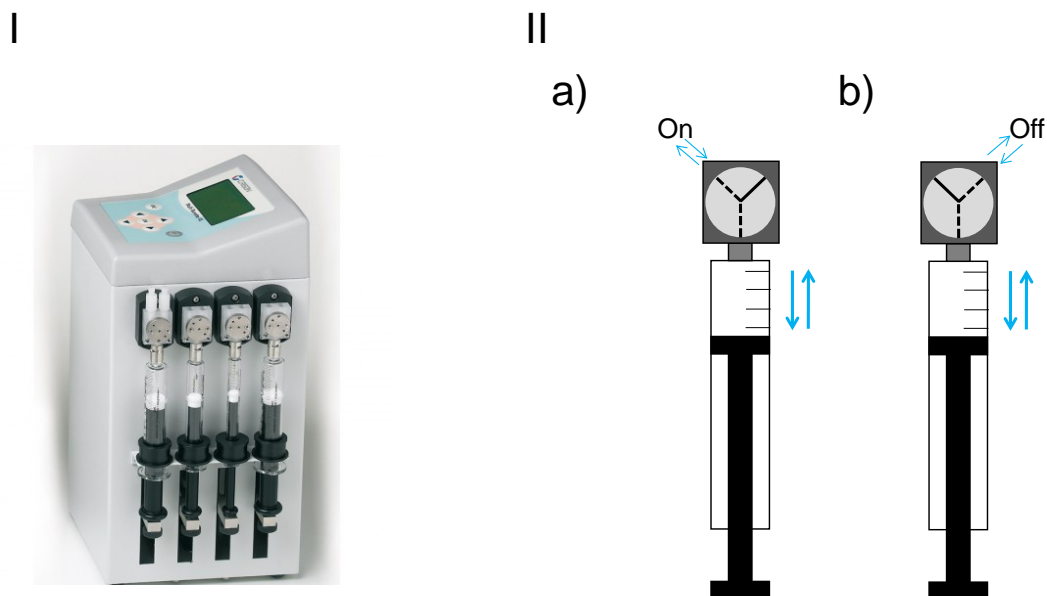


Figure 4.1 (I) Multisyringe burette, Multi-Burette 4S-D. Reproduced from the website of Crison [110]. (II) Diagram of the operation of a solenoid valve located on the top of each syringe. a) Solenoid valve activated in the On position and, b) solenoid valve deactivated in the Off position.

4.1.2. Solenoid valve

The external solenoid valves Takasago Electronic Inc. (Japan), powered by the ports located in the back of the burette withstand pressures between 2 and 6 bar (Figure 4.2).



Figure 4.2 External solenoid valves (Takasago Electronic Inc., Japan). Reproduced from the PhD thesis by Fernando Maya Alejandro [83].

4.1.3. Selection valve and Lab-on-Valve

Selection valve module contains between 6, 8 and 10 ports, and can be used in systems of low and high pressure.

In this thesis, two different low-pressure selection valve modules were used. The first one is VA1+1 (Crison Instruments), which contains an 8-port rotatory selection valve in its upper part, and a 6-port injection valve in its lower part (Figure 4.3a). This type of module can be connected in series with the burette or an autosampler, through the ports located on the back of the burette and the selection valve.

The second one is a VICI module (08V-0449L) (Sciware Systems) with 8 ports (Figure 4.3b), which can be operated using the AutoAnalysis software with a DLL (Dynamic Link Library) specific to this module (DLL Switching Valve modules Sciware Systems).

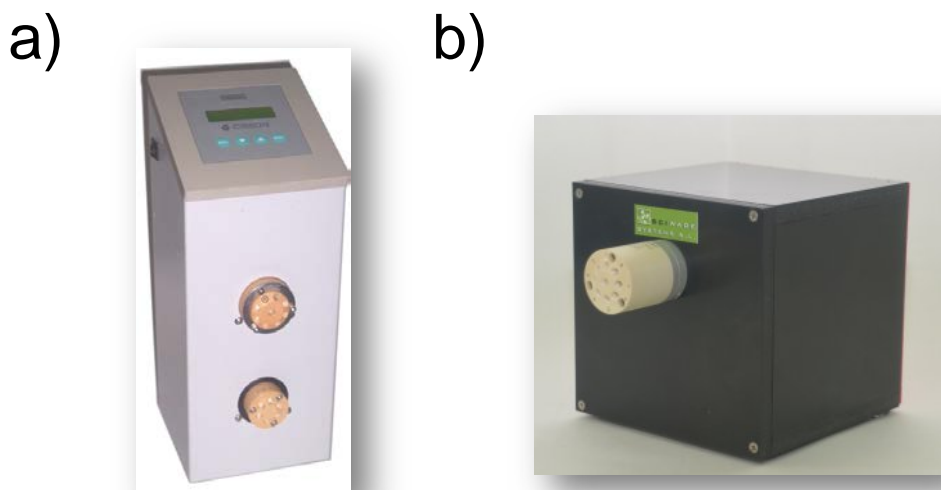


Figure 4.3 a) Mixed valve module (Crison Instruments). Reproduced from, the PhD by Fernando Maya Alejandro [83], and b) VICI selection valve Sciware Systems. Reproduced from the website of Sciware Systems S.L.[111]

Lab-On-Valve is a monolithic piece made of methacrylate with 8 integrated channels, of which 7 are 1.5 mm i.d. and 16.0 mm long, and one of 3.2 mm i.d which is used as microcolumn. The piece is placed on the rotor of the selection valve, to which the outer cover was removed.

The channel of LOV that works like a microcolumn (Figure 4.4), is filled with cellulose beads or resin in order to perform a solid phase extraction. The column is filled with a quantity of beads or suitable resin, avoiding the overpressure and compaction of the column packing. One of the advantages of LOV is that allows the automatic

regeneration of the resin, which is contained by means of glass wool or fiberglass pre-filter placed at the exit of the column.

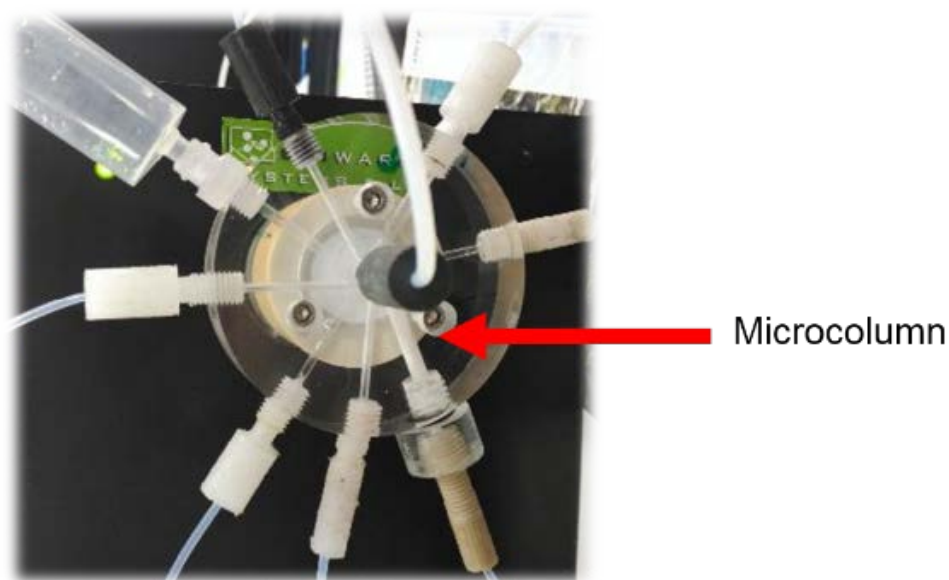


Figure 4.4 LOV made of methacrylate placed on a VICI selection valve (Sciware Systems) with 8 ports, showing the microcolumn channel.

4.1.4. Pipes, connectors and lixiviation column

The manifold was constructed with polytetrafluoroethylene (PTFE) of 0.8 and 1.5 mm i.d. The connections were made with connectors of methacrylate, polyvinylidene fluoride (PVDF), delrin® acetal resin and, polyether ether ketone (PEEK).

In addition, a lixiviation column made of methacrylate was used to carry out dynamic leaching studies of radionuclides of environmental interest (^{226}Ra , ^{238}U and ^{232}Th). The cell consists of three main parts: the first part is the one that contains the solid sample, which has a cylindrical shape (25.5 mm long, 16 mm i.d.). The other two parts are conic sections with connectors (1 and 7). More details in chapter 5.

4.1.5. AutoAnalysis software

AutoAnalysis is a software developed by the Analytical Chemistry, Automation and Environment Group of the Balearic Island University, which allows to integrate the control of the instruments for the development of flow systems, such as: multisyringe burette, selection valve, external solenoid valves, and magnetic stirrers used in this thesis.

This software uses dynamic link libraries (DLL) of 32 bits, when being developed in Delphi 5.0 and Visual C++ 6.0. It is a program that allows the instrumentation control and data acquisition and processes.

It also accepts variables and conditional commands, which has its own language, facilities the development of intelligent routines. Therefore, AutoAnalysis is able to make decision for itself based on the analytical results collected at a certain point without the intervention of the analyst.

The program contains a configuration menu, in which required instrumentation can be connected to develop a flow system. In this menu, the communication channel or DLL is connected; considering that more than one instrument can be installed at the same time in the same channel, e.g. the multisyringe burette and the selection valve module from Crison are connected through a Crison series channel (Figure 4.5).

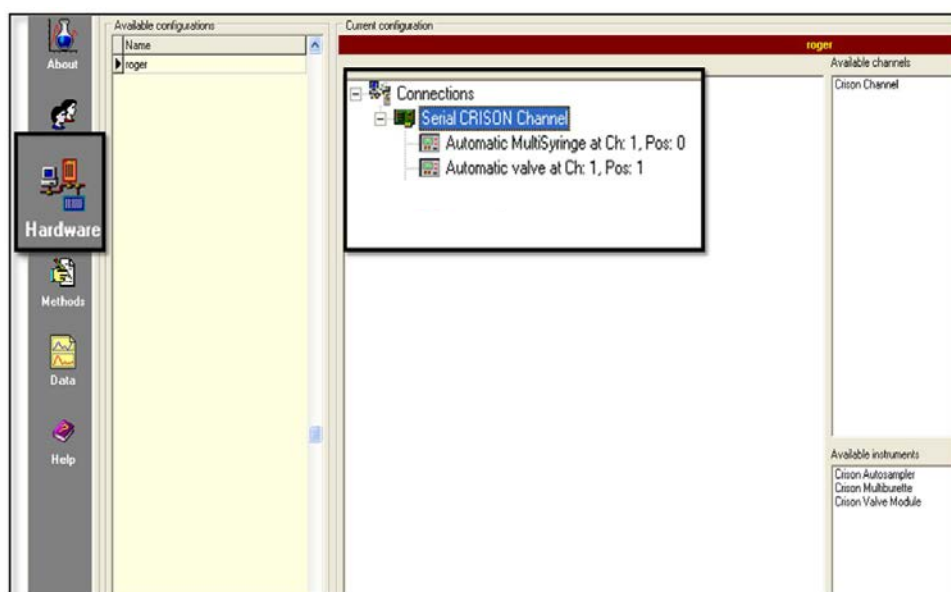


Figure 4.5 Configuration menu of AutoAnalysis program to establish the connections.

Once the necessary instruments are connected, they are controlled automatically through the development of an analytical method (creation of instruction sequences). Each instruction is executed by the instruments connected in the program or it can also be a series of additional commands defined by the system, which do not affect the instruments but are essential for the development of an analytical methodology. Some examples of these commands are: time control, command to highlight marks, conditional commands and, commands for repeating procedures.

Figure 4.6 shows an example of an analytical method used in this thesis, in which the written orders execute the cleaning of LOV pipe.

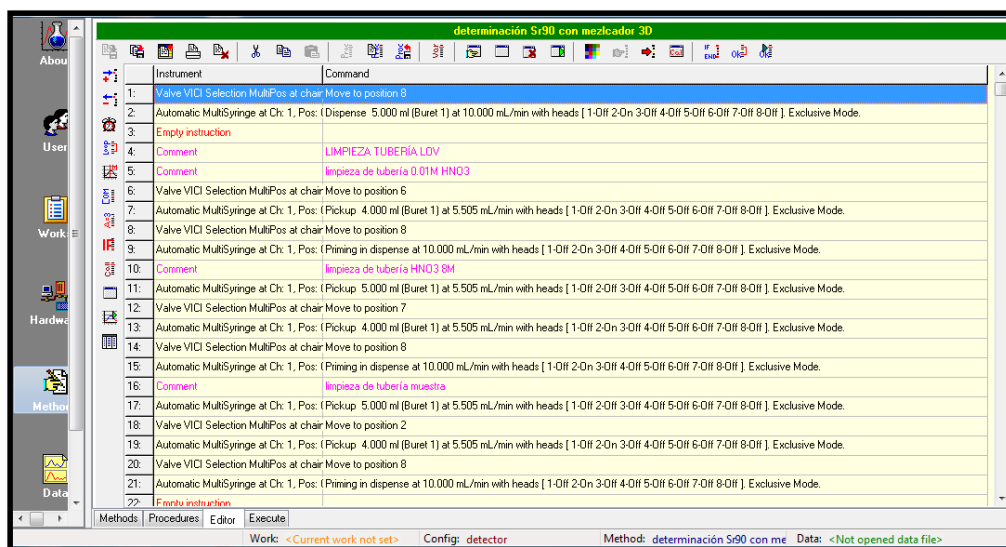


Figure 4.6 Analytical method developed in AutoAnalysis program.

4.2. Components of the liquid scintillation prototype detector

The prototype sensor consists of a flow cell (Figure 4.7a) of 20 mm e.d. and 37.6 mm long, made from glass with a capacity of 10 mL.

Two R7600U-200 photomultiplier tubes (PMT, Hamamatsu Photonics K.K., Shizuoka, Japan), contained in a 3D printed black box are responsible for the detection. The PMTs are compact, they weight approximately 33 g, have a wide dynamic range and respond with high speed; their section size is 30 x 30 mm (Figure 4.7b). The effective photocathode area is squared with a size of 18 x 18 mm, which has an approximate efficiency of 35% at a wavelength of 420 nm and has a spectral response between 300-650 nm wavelength [112].

In addition, a high-voltage power supply series C4900 (Hamamatsu) was used to power both PMTs (Figure 4.7c). The power supply has an input voltage of 12V, with dimensions of 46 x 24 x 12 mm (L x H x W). Among its features it is worth noting its compactness and lightweight, the high stability, the low power consumption, and its fast response [113].

This high-voltage power supply is fed by means of an auxiliary 15 V (90 mA) power source, and provides an output voltage between 0 and -1250 V and by a maximum current of 0.6 mA.

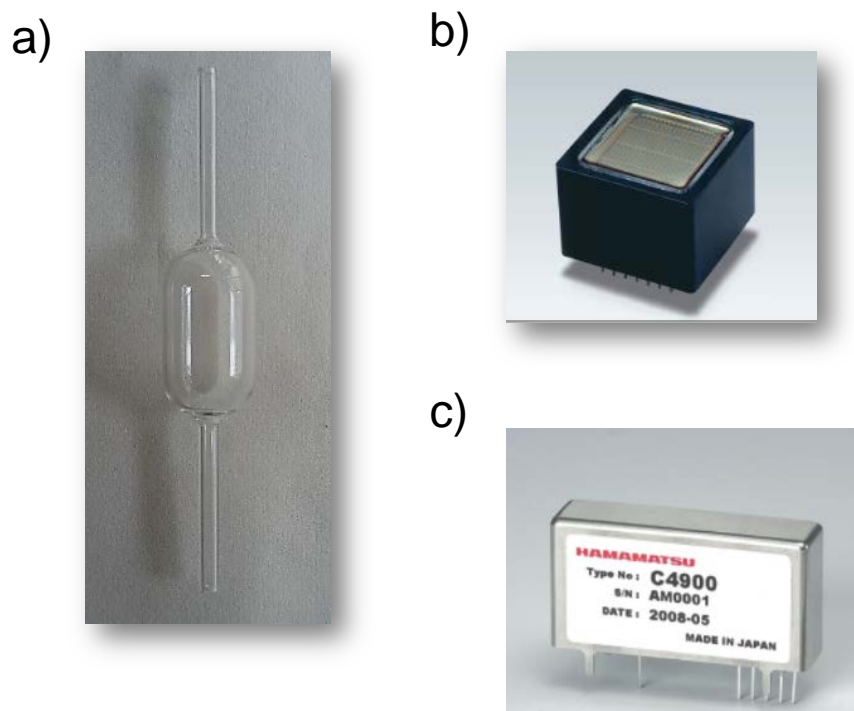


Figure 4.7 a) Flow cell; b) Hamamatsu R7600U-200 photomultiplier tube (Hamamatsu Photonics K.K., Shizuoka, Japan). Reproduced from the technical sheet [112] and, c) high-voltage power supply series C4900 (Hamamatsu). Reproduced from the technical sheet [113].

The output voltage can be regulated by means of a 50 k Ω potentiometer or by an auxiliary power source that provides a signal between 0 and 5 V.

Two PMTs were used for the development of the prototype sensor, so two different power electronic circuit boards were designed and constructed to independently set the proper high voltage and to perform the PMTs signal readout (Figure 4.8).

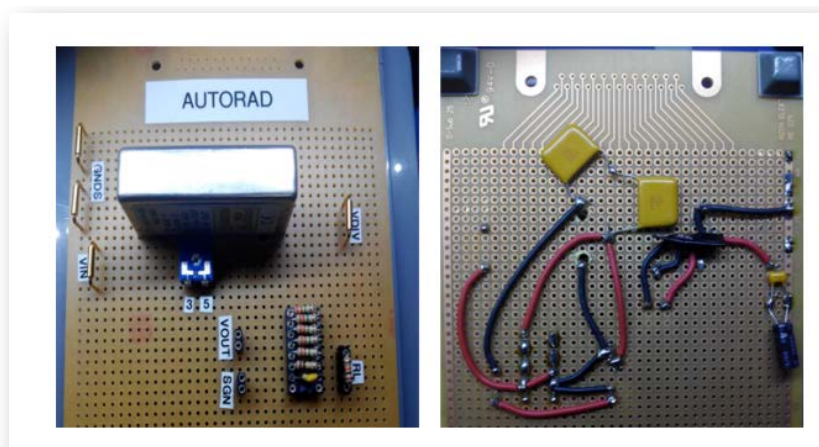


Figure 4.8 Power circuit board with potentiometer. Reproduced from the memory of the external internship carried out by Óscar Pozo at iC-Málaga [114].

4.3. 3D printing technology

In this thesis, several devices were designed and printing exploiting 3D printing technology, which formed an active part of the developed flow systems, and allowed the design of more complex automatic methods.

4.3.1. Rhinoceros software

Rhinoceros 5 SR11 32 software (McNeel & Associates, USA) allows to design devices for subsequent 3D printing. Among its features it is worth highlighting [115]:

- It allows to model 3D devices in an unlimited way, being software with an accessible price without any maintenance fee.
- It is accessible software, since it is very easy to use and learn to design pieces.
- It is compatible with most design, drawing, engineering, prototype, analysis, illustration and animation programs.
- It has a great precision for the design of prototypes, of any type of products.

In Rhinoceros program, it is possible to create pieces in 3D (Figure 4.9) by means of the geometric objects that the program provides, which are [116–119]:

- Curves: Are similar to wireframe, can be straight or wavy, open or closed. Rhino offers several tools for the creation arcs, lines, circles, curves of free form and combinations of all. It is also possible to draw polylines formed by segments of connected lines, helices, spirals, ellipses and polygons.
- Surfaces: Rhino has several commands that allow to build surfaces directly or from existing curves or from points. It also has tools to build closed and open surfaces.
- Polysurfaces and extrusion objects: It is formed by the union of two or more surfaces. It is able to build closed or open polysurfaces. The commands allowing create pyramid, cone and truncated cone. The commands such as box, cylinder, tube; extrudeCrv and extrudeSup, can also create polysurface and extrusion objects.
- Solids: A solid is constituted by a polysurface or surface that encloses a volume of space. Rhino, allows creating solids of a surfaces (sphere, toroid, ellipsoid), polysurface (pyramid, cone, box, cylinder, paraboloid, truncated cone, truncated pyramid and tube) or created from curves or surfaces (relief, pipe, slab, etc.)
- Extrusion of curves and surfaces: The extrusion function allows making an open shape from a curve or surface. It also has commands to draw extrusions such as: box, cylinder, pipe and slab. In addition, the extrusion objects can be closed with

an open or lid flat. There are special extrusions such as relief, normal extrusion, pipe, tape and slab.

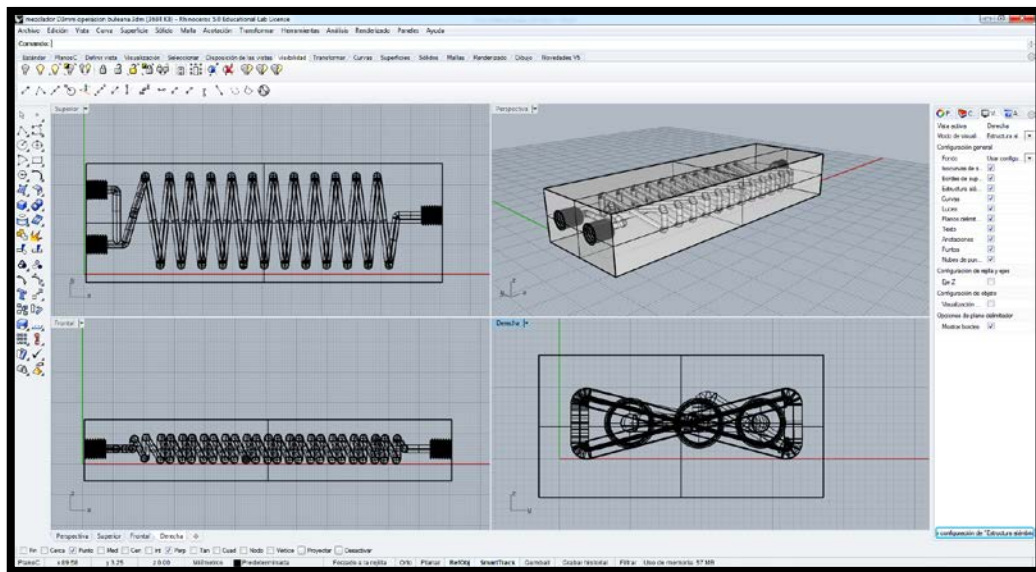


Figure 4.9 Example of 3D piece design in Rhinoceros software.

4.3.2. 3D printers

In this thesis, two printers from Formlabs Inc. (Massachusetts, USA) were used for printing the 3D devices, Form 1+ and Form 2.

Form 1+ has dimensions 30 x 28 x 45 cm, weight 8 kg, and the operating temperature is 18-28°C. Inside the printing properties are: the technology that uses is SLA, the build volume is 125 x 125 x 165 mm, feature size is of 300 microns and the layer thickness (axis resolution) is 25, 50 or 100 microns. The supports for printing the device are auto-generated and can be easily removable [120].

The features of Form +1 are [121]:

- A system laser of second generation with higher power for faster print speeds. The laser specifications are class one laser product (405 nm violet laser).
- A galvanometer control system redesigned, for more accurate and precise control.
- For a better durability and wear, it was used re-engineered mechanical components.
- For a better print, it was used a light-blocking injection molded resin tank consistency (allowing to store the tank outside the Form 1+). Additionally, the tank comes with a stackable lid, to help manage of multiple resins more easily.

The Form 2 has a more advanced system in which the tank is heated to provide a controlled environment, and a cleaner passes through the tank between the layers to circulate the resin and remove clusters of semicured resin. Also, has a resin wiper to remove any particulate from the build tank by properly agitating the resin, improving in that way the print consistency.

The heart of this printer is found in the potent optical engine guided by custom-built galvanometers, which offer big prints with impressive details. A laser of high precision draws pieces at 25-100 microns resolution, bringing precision on par with industrial 3D printers.

The dimensions of Form 2 are 35 x 33 x 52 cm, with a weight of 13 kg. As is already said the temperature control is self-heating resin tank with an operating temperature of 35 °C. Inside the printing properties are: uses a SLA technology, the build volume is 145 x 145 x 175 mm, the layer thickness (axis resolution) is 25, 50, 100 microns, the laser spot size (FWHM) is 140 microns and, the supports are auto-generated and easy removable. In addition, this printer has an automated resin refill that means, a level sensing to ensure that tank is automatically filled during the printing [122].

4.3.3. Photopolymeric resins

For the 3D printed devices, it was used black and clear photopolymeric resins from Formlabs Inc. (MA, USA).

The photopolymeric resins are thermosetting plastics. This means that after the resin is cured remain in a permanent solid state by forming an irreversible chemical bond [77].

Black photoreactive resin used for 3D printed box that contain the flow cell and both PMTs (components of the prototype sensor), is a liquid of black colour and acrylic odour. Also, is very slightly soluble in cold and hot water, and is soluble in organic solvents, has a boiling point >100°C, and dynamic density (room temperature) of 850 to 900 mPa·s. The resin is a mixture of methacrylic acid esters, photoinitiators, proprietary pigment and additive package. This resin is for use in both Formlabs printers, Form 1+ and Form 2, but in this case 3D box was printed with the Form 1+ [123].

Clear photoreactive resin used to print 3D mixer and 3D device for SPE, is a liquid of yellow colour, and a characteristic acrylic odour. Besides, is very slightly soluble in cold and hot water, and is soluble in organic solvents. Has a boiling point >100°C, and dynamic density (room temperature) of 850 to 900 mPa·s; like the black resin previously described. This resin is a mixture of methacrylic acid esters, and photoinitiator. Also clear

resin is for use in Formlabs 3D printers, in this case for printing the mixer and SPE devices Form 2 printer was used [124].

4.3.4. PreForm software

PreForm software 2.15.1 is a free software that can be downloading in Fomlabs web page, allowing a simple, fast and effective process to print 3D devices by automatic tools for supporting and orientation [120].

The features of the software are [120,125]:

- Allows the detail adjustment like individual support placement (adding and deleting manual supports), geometry, and density.
- Generates internal support if the piece requires it.
- Volume and print time estimation to calculate costs.
- Optimal print position by auto-orient.
- Allows the duplication, rotation, and scaling of the piece for print.
- Path inspection by layer slicer (allows to make and inspection of the piece layer by layer).
- Generates a FORM file, which is charged in the 3D printer for print the 3D device.
- STL and OBJ file input.

4.3.5. Ultraviolet crosslinker

Once the 3D device was printed and cleaned with isopropyl alcohol (IPA), the polymerization reaction is not yet completed. For that reason, it was used a post-cure chamber CL-100 Ultraviolet Crosslinker (UVP, Upland, Canada) to finalizes the polymerization process and stabilizes the resin mechanical properties [77].

The CL-100 UV Crosslinker is an instrument that utilizes a 254 nm shortwave ultraviolet (UV) radiation. Its external dimensions are of 22.2 x 34.9 x 40.0 cm (H x D x W), a weight of 7.5 kg, tubes of 5 x 8 watt UV dual bipin discharge type. It is designed to control and measure the UV radiation inside the exposure chamber. Contains a unique UV sensor that allows the continuous measures of UV energy and adjust automatically to variations in the UV intensity that occurs as the UV tubes age. Has a large interior UV exposure chamber, internal safety interlock, UV blocking viewing window, and multiple set functions (the pre-set exposure UV time and UV energy; the user set, exposure to UV energy and UV time) [126]. This UV Crosslinker allows a maximum UV time exposure adjustment of 16.7 h, and for cure the photopolymer resin of the 3D printed device is used between 8 and 10 h.

4.4. Multivariate optimization

The term optimization in analytical chemistry refers to finding the best conditions in which an analytical method is developed, generally in terms of reproducibility and sensitivity. Typically, these optimizations are performed in a univariate way, this means studying the influence of a single factor each time on the analytical response. The disadvantage of univariate optimization is that does not consider the possible significant interactions between the factors. This involves the risk of misinterpretation and, in the worst case, moving away from the true optimal values [127].

Multivariate statistic techniques try to solve these problems, by designing experiments in which different factors are varied simultaneously. These methods allow to extract a large volume of information from the system with the realization of a minimum number of experiments, since take into account the interactions between the factors. The response surface methodology (RSM) is one of the most relevant multivariate techniques used, being that, can be well applied when a set of responses or a response of interest are influenced by several variables. The objective is the simultaneous optimization of these variables levels to achieve the best system performance [128–131].

Before applying RSM, is necessary to choose an experimental design, and the independent experimental variables that will defines which experiments should be carried out in the experimental domain (minimum and maximum limits of the experimental variables studied) being studied [130].

For this purpose, there are some experimental matrices like experimental design for first-order models (factorial design) used when the data set do not present curvature. If curvature is presented, to achieve the optimal working conditions is necessary applying experimental design for quadratic response surfaces, such as three level factorial, Box-Behnken, central composite and Doehlert designs.

4.4.1. Screening of variables

Screening assay allows the establishment of the independent variables and their interactions that present significant effect in the experimental domain studied, measured in one or several responses. Full (2^k) or fractional two-level (2^{k-n}) factorial design can be used to study the influence of all experimental factors, variables, and interactions effects on the response investigated [129,130].

As can see in Figure 4.10 from a geometrical point of view, the factorial design explores the corner of a cube. It will be a hypercube, when the variables are more than three. Full factorial designs are commonly used when the number of factors is relatively limited. The factors (n) are varied in only two levels (-1, +1), involving the performance

of k^n experiments, where k is the number of variables under study. The variables can be qualitative (e.g., type of apparatus, type of catalyst, sequence of separation) or quantitative (e.g., pressure, temperature, time of stir, amount of an ingredient) [128].

The set of data obtained after carried out this type of design can be adjusted to a linear model with interactions according to the number of variables. Its recommended to add 3 replicates of the same experiment performed in the central point of each variable, which allows to study both the curvature of the system and the design error (pure error) that defines the confidence intervals.

The significance of the curvature indicates that within the studied experimental domain, there may be variables with values capable of offering a critical response (maximum, minimum or saddle). As a result, information is obtained on the significance of the influence of all the experimental factors studied and their interactions, if exist.

Screening provides useful information as p-value of variables, lack of fit, curvature, correlation coefficient and residuals; to make the relevant decision under probabilistic risk defined by the user (confidence level). These decisions allow defining the representative variables and its ranges. In the case of presenting a significant curvature, is necessary to determine the polynomial function that contains the quadratic terms (response surface) that best describes our chemical process to be able to establish the critical values of the variables.

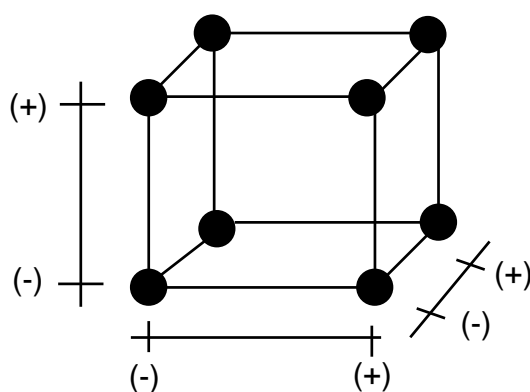


Figure 4.10 Graphical representation of a factorial design 2^3 (2^k).

4.5. Calculations

The calculation used for the quantification of the activities, uncertainty and minimum detectable activity (MDA), of the radionuclides measured in radiometric detectors, are presented.

4.5.1. Total alpha measurements

The total alpha activity (A_α) expressed in Bq, is calculated as:

$$A_\alpha = \frac{\text{cpm } \alpha - \text{cpm } b\alpha}{60 * E * F} \quad \text{Equation 1}$$

cpm α : counts per minute of alpha in the sample

cpm $b\alpha$: counts per minute of the background

E: efficiency of the count, expressed in decimals

F: self-absorption factor corresponding to the mass thickness of the sample

The uncertainty of the activity (2σ) in Bq is calculated by the expression:

$$u_{Act} = \frac{2}{60 * E * F} * \sqrt{\frac{\text{cpm } \alpha}{t(m)} + \frac{\text{cpm } b\alpha}{t(b)}} \quad \text{Equation 2}$$

cpm α : counts per minute of alpha in the sample

cpm $b\alpha$: counts per minute of the background

E: efficiency of the count, expressed in decimals

F: self-absorption factor corresponding to the mass thickness of the sample

t(m): time of measurement of the sample, in minutes.

t(b): time of measurement of the blank, in minutes.

The MDA in Bq, for a confidence level of 95% ($k=2$), is calculated by the following expression, according to ISO 11929 [132].

$$MDA = \frac{3.29 * \sqrt{\frac{\text{cpm } b\alpha}{t(m)} + \frac{\text{cpm } b\alpha}{t(b)}} + 2.7 * \left(\frac{1}{t(m)} + \frac{1}{t(b)} \right)}{60 * E * F} \quad \text{Equation 3}$$

cpm $b\alpha$: counts per minute of the background

E: efficiency of the count, expressed in decimals

F: self-absorption factor corresponding to the mass thickness of the sample

t(m): time of measurement of the sample, in minutes.

t(b): time of measurement of the blank, in minutes.

4.5.2. Total beta measurements

The total beta activity (A_β) expressed in Bq, is calculated as:

$$A_\beta = \frac{(\text{cpm } \beta - \text{cpm } b\beta) - \gamma * (\text{cpm } \alpha - \text{cpm } b\alpha)}{60 * E * F} \quad \text{Equation 4}$$

cpm β : counts per minute of beta in the sample

cpm $b\beta$: counts per minute of beta background

cpm α : counts per minute of alpha in the sample

cpm $b\alpha$: counts per minute of alpha background

E: efficiency of the count, expressed in decimals

F: self-absorption factor corresponding to the mass thickness of the sample

γ : spill-over of beta measure, expressed as:

$$\gamma = \frac{\text{counts } \alpha(\beta) \text{ standard}}{\text{counts } \alpha(\alpha) \text{ standard}} \quad \text{Equation 5}$$

Counts $\alpha(\beta)$ standard: are the counts of an alpha emitter standard registered in beta channel.

Counts $\alpha(\alpha)$ standard: are the counts of an alpha emitter standard registered in alpha channel.

The uncertainty of the activity (2σ) in Bq is calculated by the expression:

$$u_{Act} = \frac{2}{60 * E * F} * \sqrt{\frac{\text{cpm } \beta + \gamma^2 * \text{cpm } \alpha}{t(m)} + \frac{\text{cpm } b\beta + \gamma^2 * \text{cpm } b\alpha}{t(b)}} \quad \text{Equation 6}$$

cpm β : counts per minute of beta in the sample

cpm $b\beta$: counts per minute of beta background

cpm α : counts per minute of alpha in the sample

cpm $b\alpha$: counts per minute of alpha background

E: efficiency of the count, expressed in decimals

F: self-absorption factor corresponding to the mass thickness of the sample

γ : spill-over of beta measure

4.5.3. Z-score value

The z value is calculated as:

$$z = \frac{(x - X)}{\sigma_p} \quad \text{Equation 7}$$

x: activity concentration obtained from the sample

X: activity concentration of the reference value

σ_p : standard deviation of the data set.

For the evaluation of the z values obtained the following criteria were established:

$|z| \leq 2$ satisfactory

$2 < |z| < 3$ acceptable

$|z| \geq 3$ unsatisfactory

The activity concentration of the reference value (X) is calculated as:

$$X = \frac{\sum_i \left(\frac{A_i}{I(A_i)^2} \right)}{\sum_i \left(\frac{1}{I(A_i)^2} \right)} \quad \text{Equation 8}$$

A_i : activity concentration of each determination

$I(A_i)$: uncertainty in A_i

The uncertainty $I(X)$ in X value is calculated as:

$$I(X) = \sqrt{\frac{\sum_i \left(\frac{(A_i - X)^2}{I(A_i)^2} \right)}{(n - 1) \sum_i \left(\frac{1}{I(A_i)^2} \right)}} \quad \text{Equation 9}$$

CHAPTER 5
 ^{226}Ra DYNAMIC LIXIVIATION FROM
PHOSPHOGYPSUM SAMPLES BY AN
AUTOMATIC FLOW-THROUGH SYSTEM WITH
INTEGRATED RENEWABLE SOLID-PHASE
EXTRACTION

5.1. Introduction

^{226}Ra is part of the decay chain of uranium, is an alpha emitter and has a half-life of 1600 years, which increases the interest in controlling it, in the environment. Elevated radium concentration in some environmental compartments, can be cause from natural process, fuel cycle and nonnuclear industry activities [21].

Phosphogypsum (PG) is a by-product in the phosphate fertilizer industry, and is produced in large quantities through the production of phosphoric acid by wet process [12,13,133]. PG contains natural radionuclides, mainly ^{226}Ra and its decay products [134–136]. After wet process between 80-90% of ^{226}Ra originally present in the phosphate rock remains in the PG, by it is classified as a Technologically Enhanced Naturally Occurring Radioactive Material (TENORM) [12,137–139]. Much of the PG produced is stored in stockpiles, being exposed to meteorological processes [140,141] causing damage to the environment, especially in coastal areas [142], such as the region of Huelva, located in southeaster Spain.

^{226}Ra activity in PG varies if the sample is collected in different stacks within the same geographic area and if it is collected at different points within the same raft [139]. These variations may be due by the fact, that the origin of the phosphate rock can vary over time in the same plant for market reasons, causing variations in the production process, and consequently in the generation of PG.

The actual PG lixiviation processes that take place in stockpiles are very complex to model, and experimentally reproduce. The process of contact between PG and water does not occur only with rainwater, in which the dynamic process of water percolation can vary through the piles: most stacks are formed by transporting PG in suspension with water (static process), to the stacks where PG is decanted, and the waters are either discharged to the environment or recirculated. Therefore, in order to achieve an efficient PG management, is crucial to study some possible scenarios, i.e. its releases in static, semi-static and dynamic conditions.

The study of radionuclides lixiviation from PG is of great environmental, and industry importance due to its possibilities of reuse. Also, can cause the transfer of radionuclides present in PG matrix to the rainwater or to water of adjacent zones, causing environmental damages [142–144].

^{226}Ra leachability from PG stockpiles has been studied mainly in a static approach, i.e. using a large amount of sample and lixiviation agent; maintaining the contact time between the sample and the lixiviation agent for a long time [12,13,44,145,146]. The conventional static lixiviation methods have some limitations, including the re-adsorption of ^{226}Ra that can reach up to 89% of the leached content

[146]. In addition, long periods in leaching tests are more susceptible to experimental errors, and the methods are laborious and time-consuming.

In order to study the main differences between the more frequently studied static scenery, and dynamic lixiviation conditions, in this paper is proposed a dynamic lixiviation of ^{226}Ra exploiting flow injection analysis techniques. This approach allows the development of an automatic system avoiding re-adsorption processes, needing lower reagent and sample consumption. Besides, it increases the analyst security, by the reduction of sample and reagent handling [32,34].

The continuous flow of the lixiviation agent through the sample allows its constant renewal, avoiding the re-adsorption process by continuous solid-liquid equilibrium variation [147]. The combination of multisyringe flow injection analysis (MSFIA) [32] and Lab-On-Valve (LOV) [148] combines the advantages of both system in one. MSFIA supplies multi-channel operation with an accurate control of reagents volume and flow rate; whilst LOV allows the integration of several analytical units in the valve, and the automatically regenerating the extraction column.

The main objective of this work, is the evaluation of dynamic lixiviation of ^{226}Ra from PG samples, and to compare it, to more frequently considered static lixiviation process. Artificial rainwater was used as lixiviation agent at two different pHs. MSFIA-LOV system facilitates the simulation of lixiviation process in which rainwater can pass through PG without staying enough time in contact with it, avoiding the re-adsorption process typical in static lixiviation approach. Thus, after each lixiviation cycle, eight leachates and a residual fraction were analysed allowing the evaluation of dynamic lixiviation of ^{226}Ra .

5.2. Experimental

5.2.1. Reagents and solutions

All solutions were prepared from analytical grade reagents with ultra-pure water obtained from a Milli-Q water purification system from Millipore (Bedford, MA, USA).

Stock solution of artificial rainwater was prepared by exact weight of magnesium sulfate (3.55 mg L^{-1} , Probus, Barcelona, Spain), sodium nitrate (12.2 mg L^{-1} , Probus), potassium sulfate (0.98 mg L^{-1} , Panreac, Barcelona, Spain), calcium chloride (4.43 mg L^{-1} , Probus), sodium chloride (1.69 mg L^{-1} , Scharlau, Barcelona, Spain) and ammonium sulfate (7.67 mg L^{-1} , Probus) and dissolved in Milli-Q water. Working solutions of artificial rainwater (diluting 100 times the stock solution) were prepared with Milli-Q water [149] and the pH was adjusted with diluted nitric acid. Besides, NaOH 0.22 mol L^{-1} (Scharlau) was used to adjust PG leachate to $\text{pH}=7.0\pm 0.5$, before the extraction and

preconcentration protocol. A cleaning solution of $0.05 \text{ mol L}^{-1} \text{ HNO}_3$ (Scharlau) was used to clean the leachate collector before each lixiviation.

^{226}Ra standard solutions were prepared with an appropriate quantity of the ^{226}Ra certified standard material with an initial activity of $34.68 \pm 0.69 \text{ Bq g}^{-1}$ in HNO_3 1 mol L^{-1} (CIEMAT, Madrid, Spain, ref FRC-2015-453).

The reagents and materials for ^{226}Ra extraction and preconcentration were: macroporous bead cellulose (MBC, Iontosorb® MT50) of 50–100 μm particle size, 0.025 mol L^{-1} potassium permanganate (Scharlau), 0.5 mol L^{-1} sodium sulfate (Scharlau), 2 mol L^{-1} acetic acid-acetate buffer at pH 3 with $50 \text{ mg L}^{-1} \text{ Ba}^{2+}$ (Scharlau), 0.1 mol L^{-1} hydroxylamine (Scharlau) in $0.2 \text{ mol L}^{-1} \text{ HCl}$ (Scharlau).

In addition, $0.22 \mu\text{m}$ pore size nitrocellulose filters (Millipore), $0.45 \mu\text{m}$ pore size nylon filters (Millex®), syringe filter units of $0.45 \mu\text{m}$ pore size and 25 mm diameter (Millipore) and fiberglass wool were used.

5.2.2. Phosphogypsum samples

The three PG samples were obtained from a non-active PG stack owned by Fertiberia and located in Huelva, Spain. Two were randomly collected from the stockpiles of Huelva, and one used as reference material in an intercomparison exercise of Nuclear Safety Council of Spain (CSN). The reference PG material (MatControl CSN-CIEMAT 2008) was prepared by the Laboratory for the Preparation of Quality Control Materials (Mat Control) in collaboration with the Environmental Radiology Laboratory (LRA), both from the Analytic Chemistry Department of the University of Barcelona (Spain).

PG samples were placed in ceramic melting pots and dried until constant weight in an oven at $55 \pm 5^\circ\text{C}$. To measure the total ^{226}Ra activity concentration present in the PG samples, in the reference PG material (400 mg), and in the residual fraction a microwave (Multiwave Go, Anton Paar) assisted digestion was carried out with 10 mL of concentrated HNO_3 (69%, Scharlau), the microwave digestion program consisted in elevating the temperature within 10 min up to 180°C and maintaining this temperature during 9.5 min. After the digestion, the HNO_3 was evaporated to dryness and residues were diluted in 25 mL of Milli-Q water. The sample solutions were filtrated through a $0.45 \mu\text{m}$ syringe filter and finally, the pH was adjusted to 7.0 ± 0.5 .

5.2.3. Analytical procedure

The lixiviation, extraction and preconcentration of ^{226}Ra were carried out with a MSFIA-LOV system presented in Figure 5.1.

One of LOV ports was used as reservoir of MBC suspended in 20:80 methanol:water (v/v) contained in a 5 mL plastic syringe. Fiberglass wool was placed at the outlet of the column in order to retain MBC.

The analytical procedure is detailed in Table 5.1, and can be summarized as follows: first PG leaching is obtained, by placing an adequate amount of PG sample in PG lixiviation column (PLC), approx. 0.4000 g d.w., and passing 30 mL fractions of artificial rainwater through PLC. The leached fraction was collected in the leachate collector, an appropriate amount of NaOH (port 2) was loaded, and then dispensed to the leachate collector (port 5), to adjusted the pH at 7.0 ± 0.5 , this dissolution was stirred to homogenize the leachate.

When analysing the entire sample or the residual fraction, the analytical procedure starts here, with the digested sample at pH 7.0 ± 0.5 . Secondly, MBC column (port 8) was conditioned with 5 mL of hot deionized water (70°C), and then 4 mL of KMnO_4 (port 7) were passed through the column in order to form a coating of MnO_2 .

Thirdly, the leachate was loaded into HC1 and dispensed at 1.5 mL min^{-1} through the MBC with V in "Off" position (to the waste). Afterward, ^{226}Ra retained in the column was eluted with 2.5 mL of $\text{NH}_2\text{OH}\cdot\text{HCl}$ (port 1), with V in "On" position. This eluent reduced the MnO_2 adsorbed in the MBC, and it was eluted jointly with the ^{226}Ra deposited.

Finally, ^{226}Ra was co-precipitated dispensing 8 mL of Na_2SO_4 (syringe 3) and 4 mL of acetate buffer/ Ba^{+2} (syringe 4) into the fraction collector. The leachate collector was cleaned first with cleaning solution and finally with deionized water. Waiting time of 30 min was needed, for achieve the $\text{Ba}(\text{Ra})\text{SO}_4$ formation. The resulting co-precipitated was filtered through a $0.22\ \mu\text{m}$ nylon filter and brought to dryness over a stainless-steel planchette under an infrared lamp.

After five reuses, the MBC column packing was automatically regenerated replacing the old one, dispensed to waste, by new MBC from the reservoir (port 4).

The measurements were carried out immediately after separation in a low-background proportional counter (LBPC) Canberra LB4200 with the voltage adjusted to 1320 V for simultaneous alpha/beta mode and a counting time of 1000 min. The Apex software was used for data acquisition. In addition, the LBPC calibration was carried out using a certified standard of ^{226}Ra for efficiency and autoabsorption calibration curve.

Reagent blanks were also made in order to calculate the minimum detectable activity (MDA) of each detector.

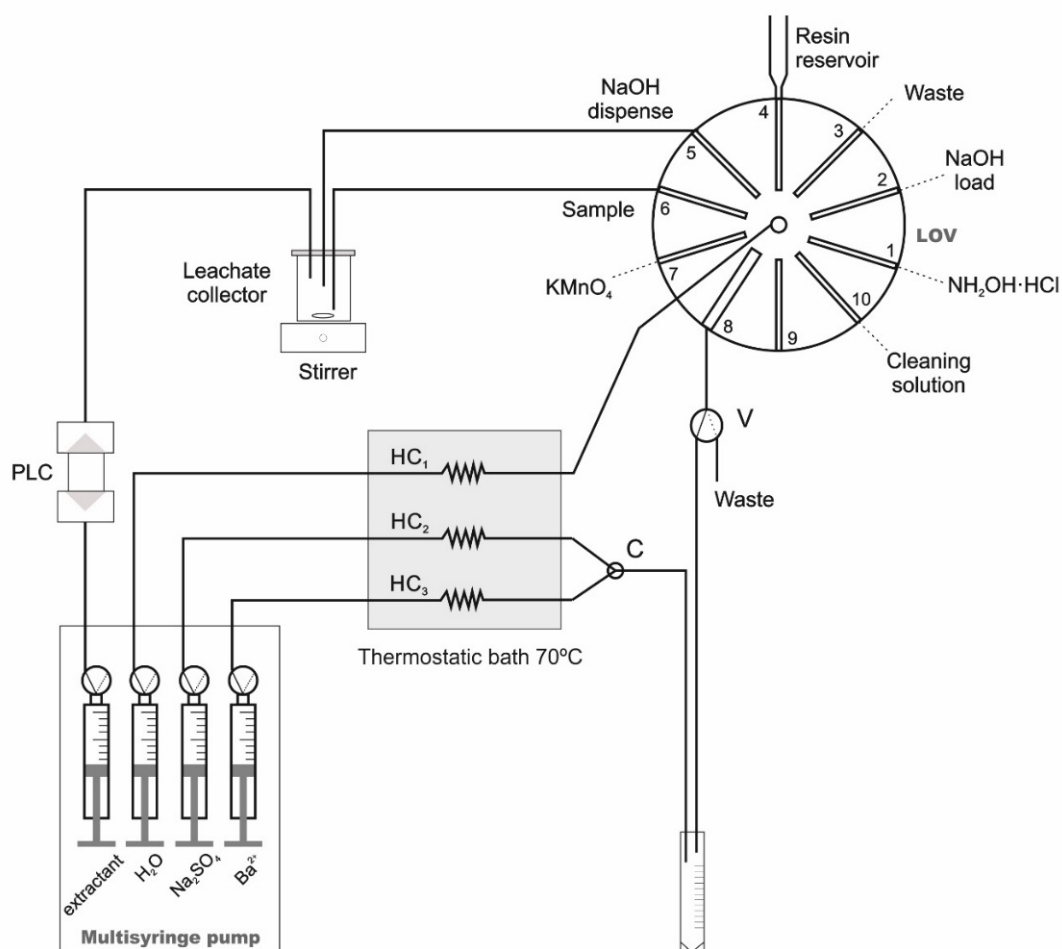


Figure 5.1 Automatic system for the dynamic leaching, preconcentration and co-precipitation of ^{226}Ra from phosphogypsum samples. C: three-way connector, HC: holding coil, LOV: Lab-On-Valve, PLC: phosphogypsum lixiviation column, V: external solenoid valve.

Table 5.1 General procedure for lixiviation, extraction and preconcentration of ^{226}Ra from PG samples by a MSFIA-LOV system.

Step	Flow rate (mL min ⁻¹)	LOV position	S1	S2	S3	S4	V
1. PG leaching and pH adjust							
a. Load 10 mL of extractant	10		Off	Off	Off	Off	Off
b. Dispense 10 mL of extractant	3.5		On	Off	Off	Off	Off
c. Stage a and b repeat 3 times							
d. Load 0.17 mL of NaOH	1.8	2	Off	On	Off	Off	Off
e. Dispense 0.17 mL NaOH	1.8	5	Off	On	Off	Off	Off
f. Waiting time for homogenize the leachate (2 min)							
2. MBC column conditioning							
a. Dispense 5 mL of hot deionized water MnO ₂ formation	1.5	8	Off	On	Off	Off	Off
b. Load 4 mL of KMnO ₄ into HC1	5	7	Off	On	Off	Off	Off
c. Dispense 4 mL of KMnO ₄	1.5	8	Off	On	Off	Off	Off
d. Dispense 5 mL of deionized water	1.5	8	Off	On	Off	Off	Off
e. Waiting time for MnO ₂ formation (2 min)							
3. Sample loading							
a. Load X mL of sample into HC1	5	6	Off	On	Off	Off	Off
b. Dispense X mL of sample	1.5	8	Off	On	Off	Off	Off
4. Elution of ^{226}Ra							
a. Load 2.5 mL of NH ₂ OH·HCl	5	1	Off	On	Off	Off	Off
b. Dispense 2.5 mL of NH ₂ OH·HCl	1.5	8	Off	On	Off	Off	On
5. Co-precipitation formation							
a. Load 8 mL of Na ₂ SO ₄ into HC2 and 4 mL of acetate buffer/Ba ⁺² into HC3	5		Off	Off	Off	Off	Off
b. Dispense 8 mL of Na ₂ SO ₄ and 4 mL of acetate buffer/Ba ⁺²	5		Off	Off	On	On	Off
c. Waiting time for co-precipitation formation (30 min)							

S1: extractant, S2: H₂O, S3: Na₂SO₄, S4: acetate buffer/Ba⁺². S1, S2, S3, S4 and V: Off indicates liquid to the container, while the position On to the system.

5.3. Results and discussion

5.3.1. Optimization of experimental conditions

For this work, a methacrylate cell was constructed and dedicated to contain the PG samples. The variables that affect the PG lixiviation process were optimized using a separate manifold (see Fig. 5.2). Then both manifolds were coupled to a unique automatic system in order to achieve the ^{226}Ra release, extraction and preconcentration with a high degree of automation and miniaturization.

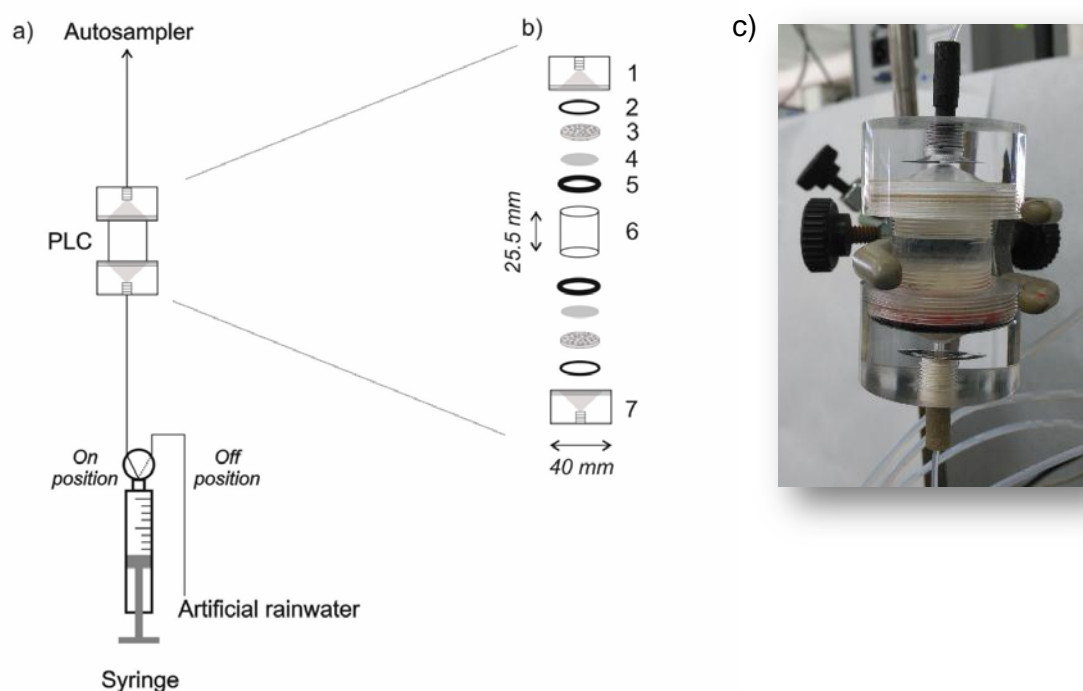


Figure 5.2 a) Automatic system for the optimization of the variables that affect the dynamic leaching, preconcentration and co-precipitation of ^{226}Ra from phosphogypsum samples, PLC: phosphogypsum lixiviation column; b) components of the leaching column: 1. top cover, 2. o-ring, 3. filter holder, 4. filter, 5. silicone gasket, 6. cylindrical column, 7. bottom cover; and c) photograph of the lixiviation column.

The factors studied as independent variables were the PG sample weight in the PLC (200-600 mg d.w.) and the lixiviation flow rate ($2.0\text{-}5.0\text{ mL min}^{-1}$). In Table 5.2 the full performed factorial design (2^2) is presented. The maximum values of both experimental domains were set in order to avoid overpressure in the system, while the minimum values were the lowest amount of PG that guarantees reproducibility, and the minor flow rate allowed by the system. The analytical response (CPM, counts per minute) was evaluated by the analysis of variance (ANOVA) represented graphically through the Pareto chart (Figure 5.3). The analysed variables did not produce significant changes in

the response at 95% of confidence ($p=0.05$). The Statistica software was used for the experimental design and data processing.

Table 5.2 Variables, levels and experimental matrix of the full factorial design for the PG lixiviation process.

Variables		Levels		
		Low (-)	Central Point (0)	High (+)
PG sample weight (mg d.w.)		200	400	600
Flow rate (mL min ⁻¹)		2.0	3.5	5.0
Assay	PG sample weight	Flow rate	Analytical response CPM (counts per minute)	
1	-	-	0.21	
2	+	-	0.14	
3	-	+	0.17	
4	+	+	0.18	
5	0	0	0.15	
6	0	0	0.16	
7	0	0	0.18	

Since the central points of the ranges for PG sample weight and lixiviation flow rate, 400 mg and 3.5 mL min⁻¹, respectively, present the best precision in terms of RSD (%), they were used for future assays. The fact that the signal does not increase significantly with increasing amounts of sample is linked to the hygroscopic nature of PG, which causes the formation of preferential channels (observed after each test), preventing further contact between sample and extractant. In addition, it was not possible to maintain a fluidized bed, even at the maximum tested flow rate.

The optimal pH value of the sample, e.g. leached fraction, residual fraction and entire sample, to introduce in the extraction/preconcentration manifold was determined in a univariate way. The pH was studied among 6.0 and 8.0 with a ²²⁶Ra standard solution with an activity of 0.05 Bq, not obtaining significant differences between the results in a pH 6.5 to 7.5.

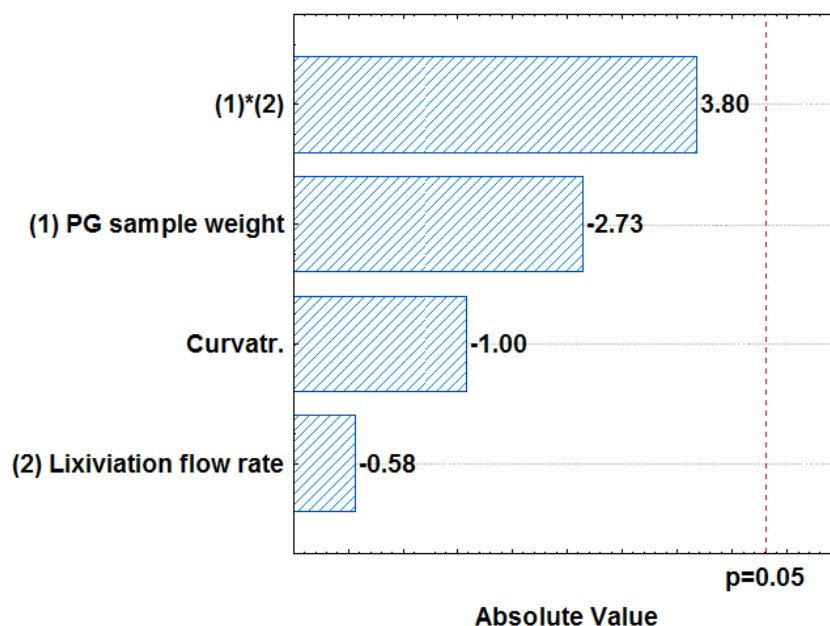


Figure 5.3 Pareto chart for the variables affecting the ^{226}Ra lixiviation process.

The automatic system for extraction and preconcentration of ^{226}Ra had been previously optimized [43].

5.3.2. Validation

The validation of the method was performed with a reference PG material (MatControl CSN-CIEMAT 2008). The reference sample was analysed according to the protocol described above, leached with artificial rainwater at $\text{pH } 2.0 \pm 0.2$. After the lixiviation cycle, eight leachates and a residual fraction were obtained for each PG replicate sample ($n=3$). Besides, the total content of ^{226}Ra was determined in the entire PG reference material. Lixiviation fractions were directly analysed, while each residual fraction (PG sample and nylon filters), and the entire sample were dried at $55 \pm 5^\circ\text{C}$ until constant weight, digested and posteriorly analysed.

The validation results are presented in Table 5.3. Since 3 replicates were analysed of each fraction and for entire sample, ^{226}Ra activity concentration is presented as weighted average \pm uncertainty (external variance) following the IUPAC recommendations [150]. The weighted average was calculated taking into account the relationship of each activity concentration with its uncertainty calculated following ISO11929 [132]. The external variance considers the dispersion of the informed activity values. Significant differences were not found, by means of z-score [151], when comparing the sum of the leached fractions and the residual fraction to the reference material ^{226}Ra total content.

The complete dataset of ^{226}Ra values obtained in the intercomparison exercise (n=38) for the same reference material was available [152]. Hence, a new standard deviation was estimated taking into account the values obtained in this study (n=40), allowing the use of z-score as a statistical measurement that realizes the comparison between each value in a group of scores to the mean of the dataset. Z-score less than or equal to 2 were obtained, indicating a satisfactory validation [151].

Table 5.3 Validation results of reference PG material (MatControl CSN-CIEMAT 2008).

	Activity concentration* (Bq kg ⁻¹ d.w.)	^{226}Ra (%)	Z-score
$\sum_{F=1}^8 F$ (sum of leached fractions)	295±14	52	
Residual fraction	276±13	48	
Sum of fractions (leached+ residual)	571±19	100	-0.03
Total digestion	585±8		0.13
Reference value	573±115		--

* The activity concentration is expressed as weighted average of three replicates ± uncertainty (external variance); n=3, three replicates of one sample. The percentage of leached ^{226}Ra is expressed respect the sum of fractions (leached + residual fractions).

5.3.3. ^{226}Ra dynamic lixiviation

The total content of ^{226}Ra in the entire sample was determined and the lixiviation assays were performed in the three samples by triplicate. Thus, ^{226}Ra total content between 280 – 585 Bq Kg⁻¹ d.w. were obtained, resulting similar to the lower values found in previous works, which were in a range of 330 – 1390 Bq Kg⁻¹d.w [137,138]

The dynamic lixiviation of ^{226}Ra from PG was studied with artificial rainwater at pH commonly found in normal conditions, i.e. pH of 5.4±0.2, and also with a lower pH (2.0±0.2) in order to study the behaviour of the radium release in an acid medium. In all cases, ^{226}Ra was determined in eight 30 mL leached fractions, the ninth fraction overlapped with MDA (7 Bq kg⁻¹). The activity concentration of ^{226}Ra in the leached and residual fractions in PG samples, using artificial rainwater as extracting agent at pH 5.4 and 2.0 are shown in Table 5.4. Using artificial rainwater at pH 5.4, the released ^{226}Ra reached 37%, which is higher than those obtained in static leaching studies. For assays

with artificial rainwater at pH 2.0 the released ²²⁶Ra reached between 49–52% of the total content of ²²⁶Ra in PG sample.

Table 5.4 Activity concentration of ²²⁶Ra in the leached fractions and the residual fraction in samples of phosphogypsum, using artificial rainwater as extracting agent at pH 5.4 and 2.0.

	pH=5.4±0.2		pH=2.0±0.2	
	Activity concentration* (Bq kg ⁻¹ d.w.)	²²⁶ Ra (%)	Activity concentration* (Bq kg ⁻¹ d.w.)	²²⁶ Ra (%)
Fraction 1	17±3	6	28±4	8
Fraction 2	17±3	6	25±3	8
Fraction 3	15±3	5	22±3	7
Fraction 4	10±3	4	18±3	5
Fraction 5	10±3	4	23±3	7
Fraction 6	12±3	4	18±3	5
Fraction 7	12±3	4	19±3	6
Fraction 8	11±3	4	12±3	4
Σ _{F=1} ⁸ F (sum of leached fractions)	105±8	37	166±9	50
Residual fraction	177±36	63	163±18	50
Sum of fractions (leached+ residual)	282±37	100	329±20	100

* The activity concentration is expressed as weighted average of three replicates ± uncertainty (external variance); n=6, three replicates of two samples. The percentage of ²²⁶Ra leached is respect the sum of fractions (leached + residual fractions).

²²⁶Ra release decreases for successive fractions. In terms of mass and volume can be expressed as 240 mL of leaching agent were necessary to extract ²²⁶Ra of 400 mg of PG, which represents that each fraction of 30 mL at pH 5.4 extracts between 4–6% of the total content of ²²⁶Ra (see Table 5.4). In the case of lixiviation at pH 2.0, each fraction extracts between 4–8 % of the ²²⁶Ra total content. Depending on the ²²⁶Ra total content of PG sample, these percentages will have different implications. For the

analysed PG samples, 37% represents about 100 Bq kg⁻¹ d.w. of ²²⁶Ra, which can be considerably increased due to the high variability of the total ²²⁶Ra content, which can be up to 4 times higher [137,138]. The cumulative percentage of ²²⁶Ra released in the dynamic lixiviation is similar across different samples, as can be seen in Figure 5.4.

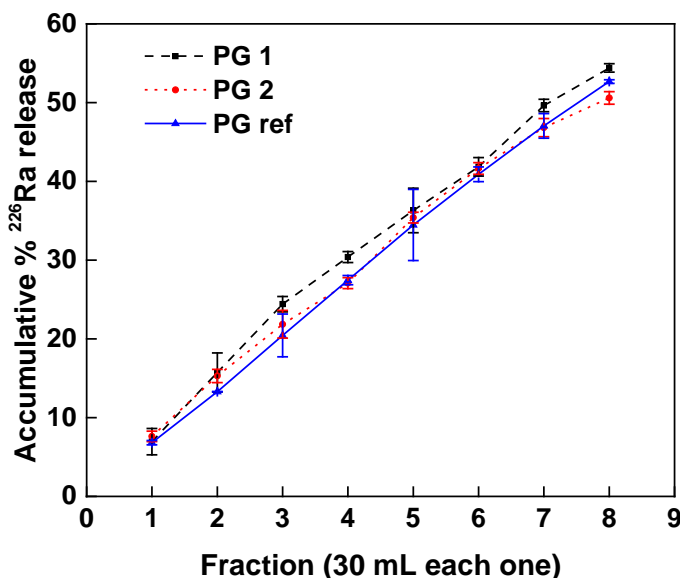


Figure 5.4 Accumulated percentage of ²²⁶Ra release for leached fractions with artificial rainwater at pH 2.0±0.2. The results are expressed as accumulated percentage average ± standard deviation (n=3). PG 1, PG 2: phosphogypsum samples 1 and 2, PG ref: PG reference sample.

Besides, a static lixiviation was carried out in order to compare it to the results obtained by the dynamic lixiviation process. Artificial rainwater at pH 5.4±0.2 and pH 2.0±0.2 was again used as leaching agent. The contact time between the leaching agent and PG sample was set to 24 h. To compare both lixiviation approaches, results from the dynamic lixiviation fraction F1 are compared to those with static lixiviation, maintaining the same proportion of PG sample: rainwater, i.e., 400 mg: 30mL. The dynamic lixiviation using rainwater at pH 5.4±0.2 and pH 2.0±0.2 releases respectively 50% and 38% more ²²⁶Ra than the static process, as can be seen in Table 5.5.

On a previous study on static lixiviation, different proportions of PG sample: rainwater (pH 5.5), between 10 g: 100 mL and 10 g: 10000 mL, were considered for a fixed contact time of 24 h. Each PG sample: rainwater proportion was repeated up to 5 times by adding new rainwater into the same PG sample. The cumulative percentage of released ²²⁶Ra increased 1-25% with the proportion of used rainwater [13].

Table 5.5 Comparison between static (24 h) and dynamic lixiviation of ²²⁶Ra from PG samples with rainwater at pH 5.4 and 2.0.

	Dynamic lixiviation		Static lixiviation (24 h)	
	pH=5.4±0.2	pH=2.0±0.2	pH=5.4±0.2	pH=2.0±0.2
²²⁶ Ra leached (%)	6±1	8±1	3±1	5±1
PG dissolved (%)	19±1	20±2	26±5	36±1
I-PG sample mass (mg)	400	400	400	400
F-PG sample mass (mg)	324±4	320±8	296±20	256±4

The percentage of ²²⁶Ra leached is referred to the first leached fraction, using the proportion PG: rainwater 400 mg: 30 mL. Results are expressed as percentage average± standard deviation (n=9, three replicates of three samples). I-PG: Initial PG sample mass, F-PG: final PG sample mass.

Higher ²²⁶Ra contents in the leached fractions, both in the dynamic vs. static processes and using a more acidic extractant, are due to direct dependence on the leaching conditions such as pH of the extractant and the contact time between sample and extractant [13]. In this sense, in the dynamic approach, the contact time between the sample and the extractant is given by the lixiviation flow rate used. In this work, taking into account the PLC capacity and the flow rate of 3.5 mL min⁻¹, the contact time is of 9 min since the agent enters the cell until it leaves.

Thus, it can be considered that the leaching agent is renewed constantly and the equilibrium is displaced to benefit the extraction. Contrary, the contact time in static studies can reach up to days without lixiviation agent renewal, in which equilibrium between extractant-radium is reached.

Besides, in a study of static lixiviation, the dependence of ²²⁶Ra leachability in PG samples with the contact time was studied. Different contact times between 10 min to 250 days were considered, indicating that the percentage of leached ²²⁶Ra activity decreased with increasing contact times [13], probably caused by re-adsorption processes of ²²⁶Ra by PG, achieving up to 89% of the total content [146]. Therefore, the increase of ²²⁶Ra release in the dynamic lixiviation is probably caused by the absence of the re-adsorption process, which does not occur with the extractant agent constant renovation.

In addition to the leaching process itself, ²²⁶Ra determined in each fraction partially comes from the dissolution of PG. In order to quantify such contribution, the remanent sample together with the filters that help to contain it into the PLC, were dried

in oven at 55°C up to constant weight after each lixiviation cycle, and weighted (324±4 mg). Results indicate that PG solubility reaches between 19±1%. Besides, in the static assays the dissolved amount of PG was also evaluated (Table 5.4) and the results are in accordance with previously reported values (6 –40%) [12,13,133].

5.4. Conclusions

The hyphenation of flow injection analysis techniques allows the on-line lixiviation, extraction and preconcentration of ²²⁶Ra, showing that the activity concentration decreases for successive fractions.

At pH 5.4, about 240 mL of leaching agent, divided in eight 30 mL fractions, were needed to release up to 37% of the total ²²⁶Ra content present in 400 mg of PG samples. Increasing the acidity to pH 2.0 raised the release up to 50%.

In the case of the analysed PG samples, the 37% represents about 100 Bq kg⁻¹ d.w. of ²²⁶Ra, which can increase considerably due to the high variability of the total content of ²²⁶Ra.

The main difference between static and dynamic lixiviation is the contact time between the sample and the extractant. In the result obtained comparing the static and dynamic lixiviation of ²²⁶Ra from phosphogypsum samples using the same proportion in both cases of PG sample: rainwater, i.e., 400 mg: 30 mL, indicate that the ²²⁶Ra release is 50% and 38% higher in dynamic lixiviation than in static one, at pH 5.4 and pH 2.0 respectively, of the leaching agent.

It is therefore crucial to develop detailed models of the lixiviation processes that take place in the stockpiles and to determine in which cases the static, semi-static or dynamic scenarios better resemble the actual lixiviation process.

CHAPTER 6
AN INTEGRATED AUTOMATIC SYSTEM TO
EVALUATE U AND Th DYNAMIC LIXIVIATION
FROM SOLID MATRICES, AND TO EXTRACT/
PRECONCENTRATE LEACHED ANALYTES
PREVIOUS TO ICP-MS DETECTION

6.1. Introduction

Uranium and thorium are naturally occurring radioactive elements, widely distributed in the Earth's crust, and both are quite useful in industries. Uranium and thorium mining, milling, and processing; phosphate fertilizer production; tin processing; phosphate rock processing; coal combustion; and industrial boilers are some of the primary anthropogenic sources of uranium and thorium released into the air, soil, and water [25,27,145]. Whilst the mobility of Th in soil is very low, because it will remain strongly sorbed, the mobility and bioavailability of U is ruled by oxidation state, having more solubility as U(VI) and less in the reduced state (U(IV)), by the complexation in inorganic and organic ligands, pH, interaction with organic matter and sorption by minerals including hydroxides and clays [25,27].

The leaching process of solid samples (e.g. soil, sediment, sludge, phosphogypsum) has consolidated importance for the potential impact of trace elements or radionuclides in the environment, causing their transference to water of adjacent zones or rainwater [144,147,153]. The lixiviation to the water or rainwater is dependent of several factors as the pH, concentration of complexing anion, porosity of the medium, temperature, presence of organic and inorganic compounds, redox potential, amount of water available for the leaching, and microbial activity. It is important to know the activity concentration of U and Th in soil, sediment, waste or rock and the mobile fraction of each one, to assess the impact of the different matrices in the environment [154].

Many leaching tests have been developed in static or semi-static way, which are used to understand an environmental process that occur frequently [12,143,154–157]. Nevertheless, dynamic processes also occur, being the natural leaching conditions more difficult to be duplicated in a laboratory.

An approach to the study of leaching under dynamic conditions is possible using flow analysis techniques in which the leaching flow rate is constant and reproducible. In this sense, the combination of the multisyringe flow injection analysis (MSFIA) [158] and lab-on-valve (LOV) [148] enabling the advantages of both techniques: MSFIA contributes with ruggedness, versatility and provides multi-channel operation with a precise control of reagents volume and flow rate, whilst the LOV permits the automatic regeneration of the column packing and the integration of several channels in a unique device [32].

Besides, the reduction of reagent and samples amounts together with the minimization of sample handling, increasing of the analyst security working with radioactive samples [34,158].

Because of the low concentration of U and Th in environmental samples, it is expected that the leached fractions have ultra-trace levels, for which the sensitivity of an

ICP-MS as detector is mandatory. ICP-MS allows the determination of long-lived radionuclides, specifically actinides elements at low concentration, in a sensitive and fast way [52,159].

Thus, once the leached fraction has been obtained, it is passed through the microcolumn packing with a selective resin in order to make the matrix fraction clean-up and preconcentrate both analytes of interest. UTEVA resin was chosen as selective extraction material for U and Th, allowing the simultaneous retention and elution [95].

The main objective of this work is the study of the dynamic lixiviation of U and Th in different environmental solid matrices using rainwater (pH 5.4) as leaching agent exploiting an automatic MSFIA-LOV system for lixiviation, extraction and preconcentration previous to ICP-MS detection. The proposed system was optimized by experimental design in order to assess the optimal conditions that affect the leaching process.

6.2. Experimental

6.2.1. Reagents and solutions

All the solutions were prepared with Milli-Q water (Bedford, MA, USA) and analytical grade reagents: nitric acid (HNO_3) (65%, Scharlau, Barcelona, Spain), hydrofluoric acid (HF) (48%, Panreac Barcelona, Spain), aluminium nitrate ($\text{Al}(\text{NO}_3)_3 \cdot 9\text{H}_2\text{O}$, Scharlau) and oxalic acid ($\text{H}_2\text{C}_2\text{O}_4$, Panreac). From atomic absorption standards solution of uranium (1001 mg L^{-1} in 2% HNO_3), thorium (1012 mg L^{-1} in 5.1 % HNO_3) and bismuth (1000 mg L^{-1} in 0.5 mol L^{-1} HNO_3), were prepared the stock solutions (U and Th in 3 mol L^{-1} HNO_3). Bismuth was used as internal standard solution as a factor correction for ICP-MS measures.

The stock solution of artificial rainwater was prepared by precise weight of ammonium sulfate (7.67 mg L^{-1} , Probus, Barcelona, Spain), calcium chloride (4.43 mg L^{-1} , Probus), magnesium sulfate (3.55 mg L^{-1} , Probus), sodium nitrate (12.2 mg L^{-1} , Probus), sodium chloride (1.69 mg L^{-1} , Scharlau) and potassium sulfate (0.98 mg L^{-1} , Panreac) and dissolved in Milli-Q water [149].

Besides, UTEVA (Uranium and TEtraVAleNT actinides) resin of 50-100 μm particle size (Triskem International, France), syringe filter units of 0.45 μm pore size (Millipore), nitrocellulose filters of 0.8 μm pore size (Millipore) and fiberglass wool for chromatography were employed.

6.2.2. Environmental solid samples

The proposed methodology was applied to different kind of environmental solid matrices, i.e. soil, sediment and phosphogypsum (PG).

Two soil samples were analysed: a certified reference material from International Atomic Energy Agency (IAEA-375), collected on the field of the collective farm “Staryi Vishkov” Novozybkov district, Bryansk region, Russia, in July 1990 (zone affected by Chernobyl accident) [160]; and a soil reference material (MatControl CSN-CIEMAT 2016), prepared by the Laboratory for the Preparation of Quality Control Materials (MatControl) in collaboration with the Environmental Radiology Laboratory (LRA), from Analytic Chemistry Department of the University of Barcelona (Spain).

A sediment channel certified reference material (BCR-320R) from the Institute for Reference Material and Measurements (IRMM) of Joint Research Centre from the European Commission was also analysed for the U and Th determination.

Two PG samples from a non-active PG stack owned by Fertiberia, Huelva, Spain: a sample randomly collected from the stockpiles and a PG reference material (MatControl CSN-CIEMAT 2008), also prepared by MatControl and LRA from the University of Barcelona (Spain). The PG is a by-product of phosphate fertilizer industry, and it is produced by wet chemical treatment with H_2SO_4 .

As a result of this process the ^{238}U with its decays products are fractionated between the PG and the phosphoric acid, estimating that <40 % is remaining in the PG [12], and is categorized as Technologically Enhanced Naturally Occurring Radioactive Material (TENORM) [137–139], although in this work the PG is categorized as an environmental sample by its growing use and dissemination in agricultural soils as soil amendment [161].

Besides, the U in the PG is quite variable depending of its treatment and age. The fresh PG (just after its generation in the factory) has a bigger fraction of U due to presence of impurities of soluble phosphoric acid that was not fully separated in the production process. When the PG is disposed in the piles, the U associated to the phosphoric acid quickly is leached remaining in the PG a fraction of U that is clearly more insoluble (generally this insoluble U is associated to some undissolved phosphate rock material) [12].

6.2.3. Sample treatment

All samples were settled in ceramic melting pots and placed in an oven at $55\pm 5^\circ C$ for drying until constant weight.

The total content of U and Th present in soil and PG samples and in their residual fractions was determined following a microwave digestion program with 10 mL of HNO₃ concentrated (increasing the temperature to 180 °C in 10 min and maintaining this temperature during 9.5 min with a microwave Multiwave Go, Anton Paar). After that, the HNO₃ was evaporated to dryness and residues were diluted up to 250 mL with 3 mol L⁻¹ HNO₃. For determining the total content of U and Th in sediment sample and in its residual fraction, the digestion was performed with 9 mL of HNO₃ concentrated and 2 mL of HF concentrated following the microwave digestion program described previously. In addition, after digestion, the acid mixture was evaporated to dryness and residues were diluted up to 250 mL with 3 mol L⁻¹ HNO₃.

Since the higher U and Th contents in the whole sample and in their residual fractions, an additional dilution was necessary, in all samples.

In the case of PG samples, 4 mL of the digested solution were diluted up to 25 mL with 3 mol L⁻¹ HNO₃/ 0.5 mol L⁻¹ Al(NO₃)₃. While, for the soil and sediment samples 2 mL of the digested solution were diluted up to 50 mL with 3 mol L⁻¹ HNO₃.

Finally, all solutions were filtered through a 0.45 µm syringe filter, and analysed by the proposed automatic methodology.

The leaching fractions were directly analysed by the proposed automatic methodology.

6.2.4. Analytical procedure

The automatic system used for the leaching and extraction/preconcentration of U and Th is presented in Figure 6.1; and the analytical procedure is detailed in Table 6.1

Firstly, approx. 0.4500±0.0500 g d.w. of samples is placed into (phosphogypsum lixiviation column) PLC, and 10 or 15 mL of artificial rainwater (syringe 1), for soil/sediment and PG samples, respectively, is passed through the LC. Then, the leached fraction is mixed through the HC1 with 5 mL of 6 mol L⁻¹ HNO₃ for soil/sediment samples, and 7.5 mL of 6 mol L⁻¹ HNO₃/ 1 mol L⁻¹ Al(NO₃)₃ (syringe 2) for PG samples, in order to achieve the optimal medium for U and Th retention. The leached fraction was collected in a fraction collector. When the residual fraction or the entire sample is analysed, the analytical procedure starts from this step.

The second step is the conditioning of UTEVA resin with 1 mL of 3 mol L⁻¹ HNO₃ (port 4). Then, the leached fraction or entire sample/residual fraction was dispensed through the microcolumn (port 7) at 0.8 mL min⁻¹ with V in “off” position (to the waste). 0.2 mL of 3 mol L⁻¹ HNO₃ was eluted through the microcolumn to avoid interferences.

After that, U and Th retained in the column were eluted with 1.4 mL of 0.05 mol L⁻¹ H₂C₂O₄ (port 6) with V in “On” position to autosampler.

Finally, the internal standard of Bi (14.6 µg L⁻¹) (syringe 4), HNO₃ 2% (port 1), and the eluate were mixed in HC3, and collected in the autosampler. The UTEVA resin was replaced when required in automatic way, discarding the old one to the waste and loading new one from the resin reservoir.

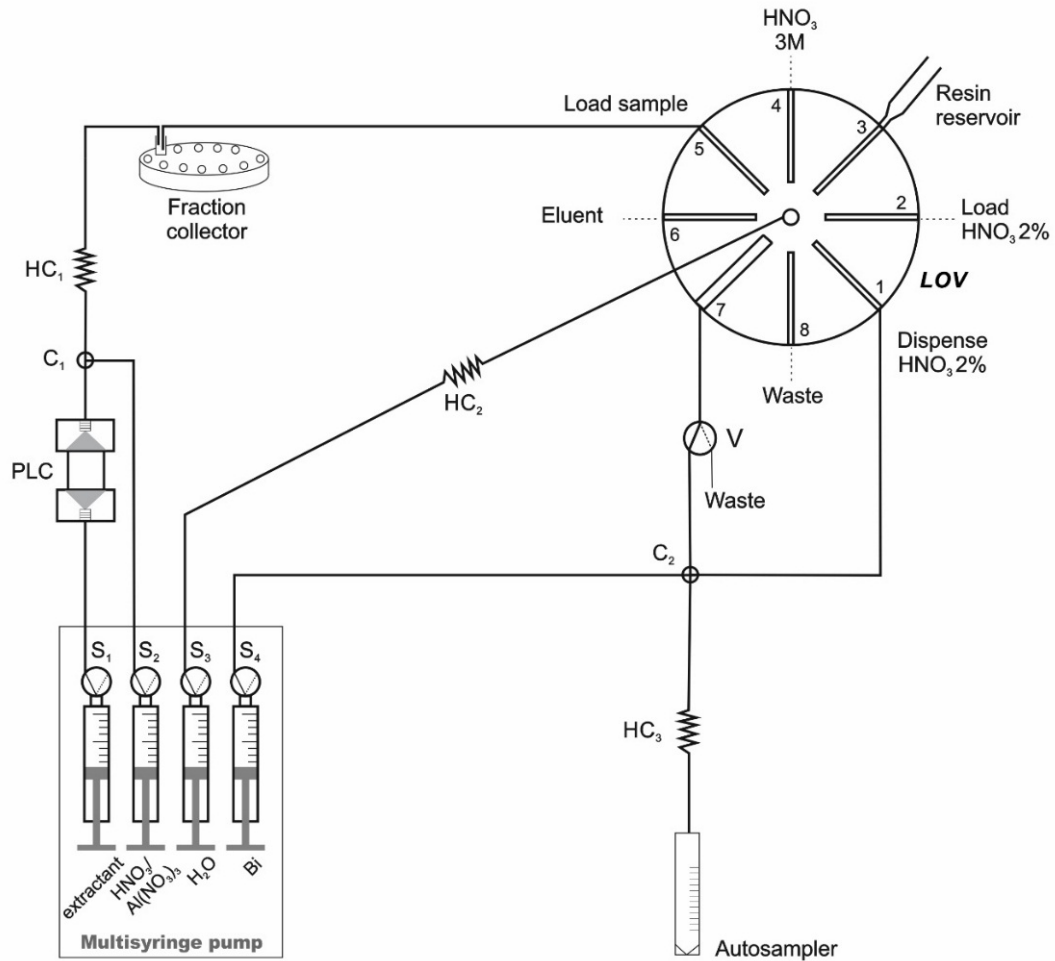


Figure 6.1 Automatic MSFIA-LOV system for the dynamic leaching, extraction and preconcentration of uranium and thorium from solid environmental samples. C: connector; HC: holding coil; PLC: phosphogypsum lixiviation column; LOV: Lab-On-Valve; S: syringes; V: external solenoid valve.

Table 6.1 General procedure for lixiviation, extraction and preconcentration of U and Th from solid matrices by a MSFIA-LOV system.

Step	Flow rate (mL min ⁻¹)	LOV position	S1	S2	S3	S4	V
1. Solid matrices leaching							
a. Load 10 mL of extractant for soil/sediment samples, and 15 mL for PG samples	10	8	Off	Off	Off	Off	Off
b. Dispense 10 mL of extractant for soil/sediment samples, and 15 mL for PG samples	3.5	8	On	Off	Off	Off	Off
c. Load 5 mL of 6 mol L ⁻¹ HNO ₃ for soil/sediment samples, and 7.5 mL of 6 mol L ⁻¹ HNO ₃ / 1 mol L ⁻¹ Al(NO ₃) ₃	5	8	Off	Off	Off	Off	Off
d. Dispense 5 mL of 6 mol L ⁻¹ HNO ₃ for soil/sediment samples, and 7.5 mL of 6 mol L ⁻¹ HNO ₃ / 1 mol L ⁻¹ Al(NO ₃) ₃ into HC1	1.8	8	Off	On	Off	Off	Off
2. Column conditioning							
a. Load 1 mL of HNO ₃	5	4	Off	Off	On	Off	Off
b. Dispense 1 mL of HNO ₃	2	7	Off	Off	On	Off	Off
3. Sample loading							
a. Load X mL of sample into HC1	5	5	Off	Off	On	Off	Off
b. Dispense X mL of sample	0.8	7	Off	Off	On	Off	Off
4. Interference elimination							
a. Load 0.1 mL of HNO ₃	5	4	Off	Off	On	Off	Off
b. Rinsing 0.2 mL on the column	2	7	Off	Off	On	Off	Off
5. Elution of U and Th							
a. Load 1 mL of eluent	5	6	Off	Off	On	Off	Off
b. Rinsing 1.1 mL on the column	0.8	7	Off	Off	On	Off	On
6. Addition of Bi and HNO ₃ 2%							
a. Dispense 1.8 mL of HNO ₃ 2%	5	1	Off	Off	On	Off	Off
b. Dispense 0.18 mL of Bi	0.5	8	Off	Off	Off	On	Off

S1: extractant, S2: HNO₃/ Al(NO₃)₃, S3: H₂O, S4: Bi. S1, S2, S3, S4 and V: Off indicates liquid to the container, while position On to the system.

6.3. Results and discussion

6.3.1. Optimization of experimental conditions

The independent variables studied in order to find the best conditions for the lixiviation process from soil and sediment, were the solid sample weight into the PLC and the lixiviation flow rate. A full factorial design 2^2 was performed. The experimental domain, the analytical response (U or Th cps / Bi cps), the matrix design and the global desirability (D) of the system are shown in Table 6.2. With the aim to evaluate multiple responses, D is used transforming two analytical responses into one [162]. The range of variables were set considering the lowest amount of solid sample that guarantee reproducibility and the lowest flow rate that can set in the multisyringe module, whereas the maximum of both values, were those that avoid overpressure, preventing the membrane filter rupture.

The results obtained within the experimental domain studied can be observed in the Pareto Chart (Figure 6.2), indicating that the flow rate and sample weight are significant with negative effects, entailing that a lower flow rate and a lower sample weight increase the analytical response. This result can be attributed to a slow leaching of U and Th and particularly to the low solubility of Th in water that tends to remain bound to the particulate matter [25,27,163].

Also, a $D = 1$ is observed in the assay with the lowest flow rate and lowest sample weight (Table 6.2), indicating that more contact time between the extractant and the sample is required for an efficient extraction of U and Th. A small amount of sample (30 mg) for a better effective contact surface area between the extractant and the solid sample was essential in a previous work, in which a column for soil lixiviation was employed [164].

In addition, a significant positive interaction between the two variables is observed for both radionuclides. Evaluating the marginal means (Figure 6.3), it is established that the positive interaction is due to the combination of the two lowest values of the variables (i.e. increase of the analytical signal (+) = low flow rate (-) x low sample weight (-). Through the function D, the optimized values within the range studied were 500 mg of sample weight and 0.6 mL min^{-1} leaching flow rate, and these values were set for the performance of future assays.

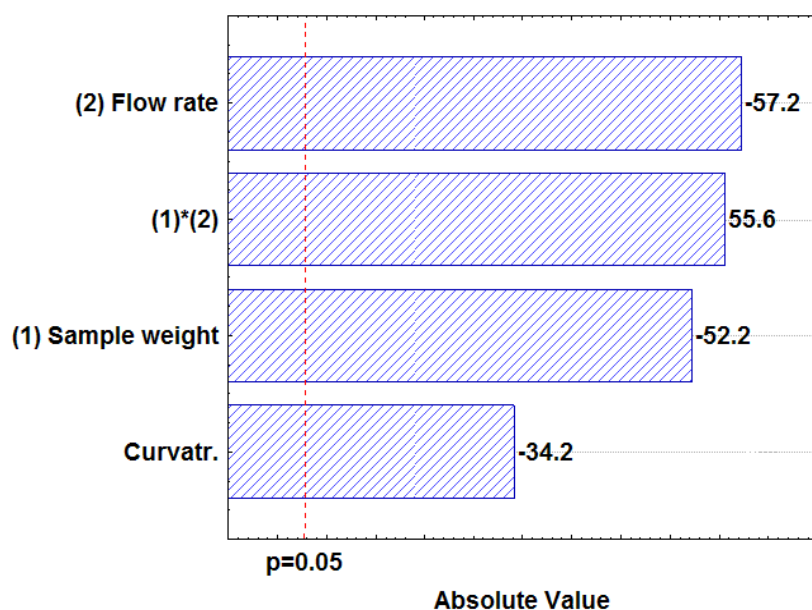


Figure 6.2 Pareto chart of the variables that affect the lixiviation process from soil and sediment.

Table 6.2 Variables, levels and experimental matrix of the full factorial design for lixiviation process from soil and sediment samples.

Variables	Levels		
	Low (-)	Central Point (0)	High (+)
Sample weight (mg d.w.)	500	1000	1500
Flow rate (mL min ⁻¹)	0.6	2.8	5.0

Assay	Sample weight	Flow rate	Analytical response*		
			U	Th	D
1	-	-	1.2047	0.1164	1.00
2	+	-	0.0920	0.0112	0.04
3	-	+	0.0561	0.0092	0
4	+	+	0.0767	0.0096	0.03
5	0	0	0.0637	0.0041	0
6	0	0	0.0728	0.0053	0.01
7	0	0	0.0688	0.0048	0

*The analytical response is presented as U or Th cps/ Bi cps; D: global desirability.

In the case of variables that affect the lixiviation process from the PG samples an univariate optimization was carried out, since preliminary results are available for this kind of sample. The experimental domain for PG sample weight was between 400 and 800 mg d.w., and leaching flow rate between 0.6 and 5 mL min⁻¹. Results indicate that optimal values were 400 mg d.w. of PG sample and 3.5 mL min⁻¹ for the leaching flow rate. The differences, of these variables with respect those for soil and sediment probably is due to hygroscopic nature of the PG sample.

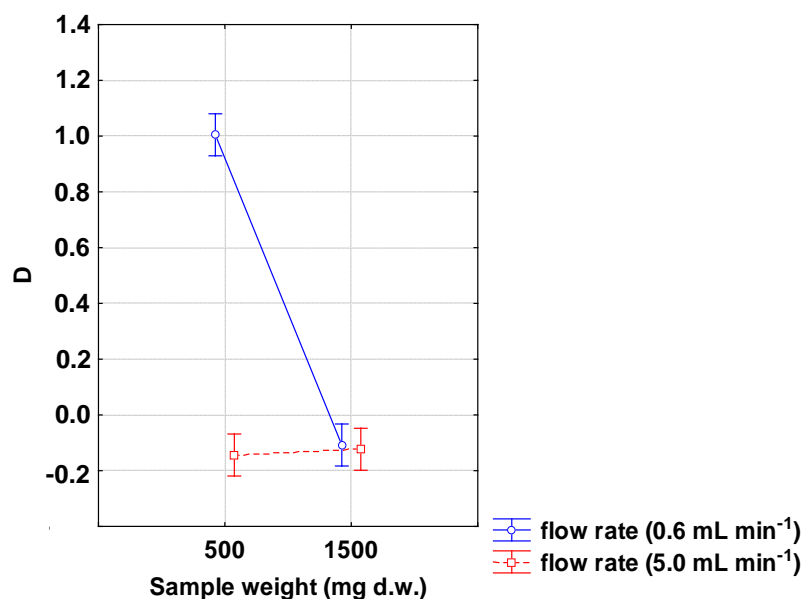


Figure 6.3 Graph of marginal means of the effect of the interaction between the variables sample weight (mg d.w.), and flow rate (mL min⁻¹). D: desirability.

The automatic system for extraction and preconcentration of U and Th had been previously optimized [52]. In the case of PG, since the sample matrix has an elevated content of phosphates, the medium of retention was HNO₃/Al(NO₃)₃ because of the aluminium can avoid the interference of phosphates on the Th uptake by the UTEVA resin, following the manufacturer recommendation [95].

6.3.2. Validation of the automatic system

The validation of the proposed methodology was carried out for each kind of sample. Thus, three solid matrices samples, i.e. a certified soil reference material (IAEA-375), a certified sediment reference material (BCR-320R) and a PG reference material (MatControl CSN-CIEMAT 2008) were analysed. The analyses were performed by triplicate for each solid matrix (n=3), in which 10 leached fractions and a residual fraction were obtained for each one, and all of them were analysed by the proposed automatic methodology.

The sum of the leached fractions plus the residual fraction did not show significant differences with the certified and reference values of U and Th, comparing with t-test at a confidence level of 95%. Although the leached percentage was extremely low (less than 0.06%) respect to the total content this together with the residual fraction, was analysed with the developed system, considering the results satisfactory.

The results of solid matrices validation are presented in Table 6.3 as average of three replicates (n=3) for each solid sample \pm uncertainty (k=2), that was calculated in accordance with the Guide for the expression of uncertainty in measurements [165].

Table 6.3 U and Th in leached fractions and residual fraction analysed by the MSFIA-LOV system for lixiviation, extraction and preconcentration steps previous to ICP-MS detection, from reference materials.

	Uranium (mg kg ⁻¹ d.w.)		Thorium (mg kg ⁻¹ d.w.)	
	Sum of fractions ($\sum_{F=1}^{10} F+$ residual)	Reference or certified value	Sum of fractions ($\sum_{F=1}^{10} F+$ residual)	Reference or certified value
Soil (IAEA-375)	1.80 \pm 0.18 ^a	1.99 \pm 0.08 ^b	4.93 \pm 0.53 ^a	5.15 \pm 0.66 ^b
Sediment (BCR- 320R)	1.84 \pm 0.08 ^a	1.56 \pm 0.20 ^a	4.88 \pm 0.30 ^a	5.3 \pm 0.40 ^a
PG (MatControl 2008)	5.11 \pm 0.23 ^a	4.50 \pm 0.82 ^c	1.23 \pm 0.29 ^a	1.50 \pm 0.29 ^c

Results are expressed as (a) average \pm uncertainty (k=2) (n=3); (b) average \pm uncertainty (k=2) (n=6); (c) average \pm uncertainty (k=2) (n=21 and n= 18 for U and Th, respectively). Significant differences were not found at a confidence level of 95%. PG: phosphogypsum.

The limits of detection (LOD) and quantification (LOQ) were calculated following the IUPAC recommendations [166]. The system reached LODs of 0.1 and 0.7 ng kg⁻¹ of U and Th, respectively.

Mass calibrations curves (cps of analyte/cps of internal standard ratio versus mass in ng of U, and Th) were performed for each radionuclide, obtaining $y=6.2674x+0.004$ ($r^2=0.9999$, n=7) for U and $y=5.8029x+0.0058$ ($r^2=0.9986$, n=7) for Th.

6.3.3. Dynamic lixiviation of U and Th from solid environmental samples

The developed automatic MSFIA-LOV system was applied to study the dynamic lixiviation of U and Th in three different solid environmental matrices, i.e. soil, sediment and PG. In general, the dynamic lixiviation behaviour of U and Th in the analysed samples was similar, i.e. the content of radionuclides decreases with the successive

extractions (except the U content in PG samples in which the fraction 2 is higher than fraction 1), and it is maintained constant in the last five fractions. In addition, the U release was always two or three orders of magnitude higher than Th, which is in concordance with the low mobility of Th, which generally tends to remain bound to the particulate matter [25,27,163].

The lixiviation process for soil and sediment samples consisted, of 10 fractions of 10 mL each one. In the case of U, all fractions were quantified, while only the first five fractions contained Th above the LOD. Figure 6.4a and 6.5a shows the dynamic lixiviation behaviour for U, and Th in two soil samples, respectively.

It can be seen that, although the behaviour is similar, the percentage vary, thus varying the amount of U released, e.g. between 0.004% (68 ng kg⁻¹) and 0.016% (221 ng kg⁻¹) from soil samples with a total U content of 1.77 and 1.42 mg kg⁻¹, respectively. In case of Th, a release of 0.0004% (18 ng kg⁻¹) was obtained from soil samples with 4.93 and 4.87 mg kg⁻¹ Th, respectively.

Figure 6.4b shows U dynamic lixiviation behaviour for sediment sample, since Th was below the LOD in all the leached fractions analysed. The percentage of U released respect to the total content was 0.002% (44 ng kg⁻¹) from sample with 1.84 and 4.88 mg kg⁻¹ of U and Th, respectively.

The lixiviation process for PG samples was performed with 10 fractions of 15 mL each one. Figure 6.4c, and 6.5b, shows U and Th release behaviour in PG samples, respectively.

Th presents similar behaviour that mentioned above, i.e. decreasing with the successive extractions, varying the leached percentage between 0.005% (67 ng kg⁻¹ d.w.) and 0.0004% (11 ng kg⁻¹ d.w.) from PG samples with a total content 1.23 and 3.10 mg kg⁻¹ Th. The exception is the U release from PG, since the maximum appears in the second fraction. The percentage of U released respect to the total content was between 0.015% (782 ng kg⁻¹ d.w.) and 0.05% (13,967 ng kg⁻¹ d.w.). The total content of U in PG sample was between 5.10 and 26.71 mg kg⁻¹ d.w. Also, in PG sample, it is observed that U has more mobility than Th, since in all the leached fractions U can be quantified, while Th only in the first three fractions. U total content of PG sample agree with those reported in previous works, which were in a range of 5.89– 36.53 mg kg⁻¹ [12,137,157].

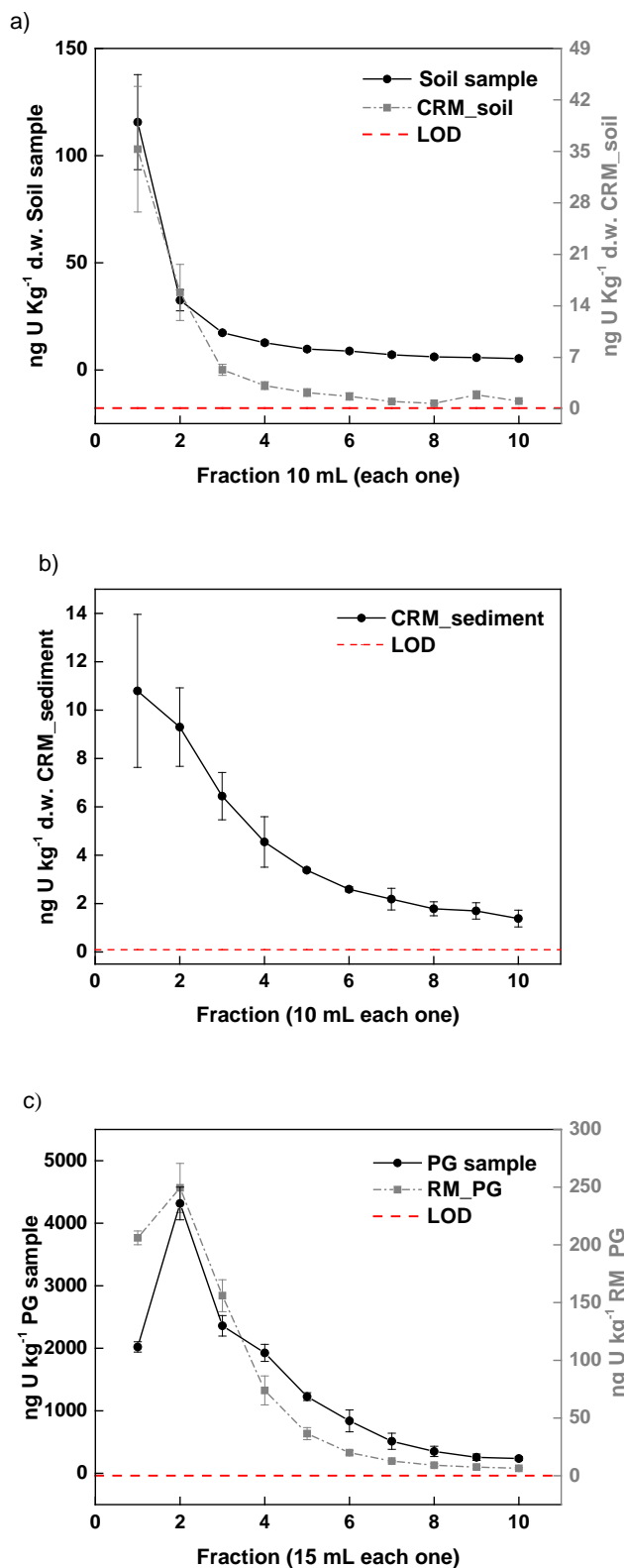


Figure 6.4 Dynamic lixiviation for U, in solid environmental samples, using artificial rainwater as leaching agent. The results are expressed as average ± standard deviation (n=3). a) Soil sample and soil certified reference material (CRM_soil); b) Sediment certified reference material (CRM_sediment); c) Phosphogypsum sample (PG sample) and phosphogypsum reference material (RM_PG).

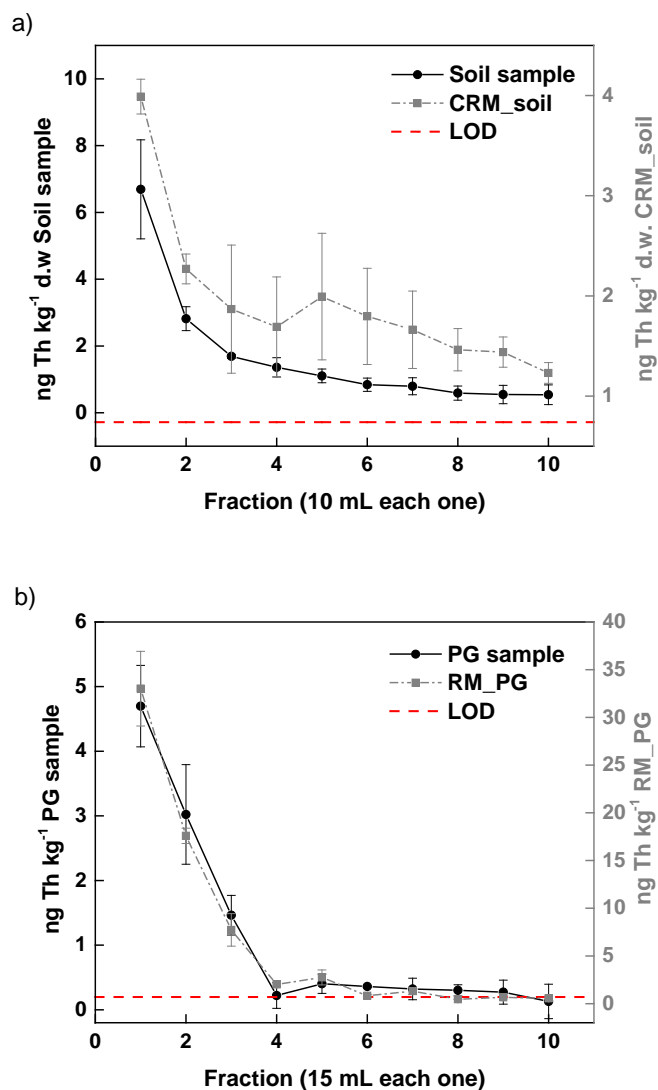


Figure 6.5 Dynamic lixiviation for Th, in solid environmental samples, using artificial rainwater as leaching agent. The results are expressed as average \pm standard deviation ($n=3$). a) Soil sample and soil certified reference material (CRM_soil); b) Phosphogypsum sample (PG sample) and phosphogypsum reference material (RM_PG).

The results obtained in a static leaching study were very different from those presented here. In static tests, using fresh and marine water as extractants, the percentage of ^{238}U release from PG samples was between 40 – 60% for periods of stirring time between 600 – 2880 min, concluding that elevated U mobilization depends on the acidity of the leachates, i.e. by the presence of phosphoric acid in the PG [12].

Besides, the high percentage of U leached (40-60%) was in agreement with the fresh PG sample used. The low U leached observed in this study corresponds to the “U washed sample” analysed.

Other static lixiviation study carried out with PG agitated for 20 h and varying the pH among 2 – 9, indicates that the variation of the rates of leaching and the dissolved mass of PG is a function of extractant pH. Thus, the leached radionuclides appear to be associated with the elements exclusively absorbed on the solid surface, regardless of the chemical form, while those that were not leached should be absorbed in sites less soluble with structures of type CaSO_4 [145].

The mass ratios of Th/U found in the leached fractions (0.002 – 0.04 PG sample and 0.0015 – 0.0088 CRM_PG) and in bulk PG (0.12 – 0.24), indicating that the PG sample collected in the stockpiles from Huelva are enriched in U in relation to Th, as well as U release is higher than Th.

Therefore, the lixiviation process of U and Th under dynamic conditions from the environmental solid matrices analysed, shows U and Th releases extremely low, up to 0.05 and 0.005% of U and Th, respectively, using rainwater at pH 5.4 as extractant. This behaviour can probably be explained, by the direct dependence on the leaching conditions such as the composition of the leaching agent and its pH, the contact time between the sample and the extractant, the porosity of the medium and the amount of water available for the leaching [12,133,154]. A semi-static lixiviation study, in which the solid sample was placed in contact with two different extractants (distilled water and $0.1 \text{ mol L}^{-1} \text{ NaNO}_3$) by a period of 142 days, replacing the extractant each 15 days (9 times), obtained a low uranium release, up to a 0.59 %. Authors propose that the processes that govern the release of mobile U are the diffusion and the surface wash-off [154].

Otherwise, at the end of the leaching process a decrease of the amount of solid samples was observed, being a 7 ± 3 % for soil, 11 ± 1 % for sediment and 19 ± 1 % for PG. U and Th content of this dissolved fraction are added to the leached fraction percentage. PG solubility reported in previous works of static lixiviation were between 6 – 40% [12,13,133].

The great variability found in different environmental sample matrices, especially of U releases, e.g. between 44 ng U kg^{-1} (0.5 mBq kg^{-1}), and $13,967 \text{ ng U kg}^{-1}$ (173 mBq kg^{-1}), demonstrate the relevance of the lixiviation assays in dynamic conditions for holistic environmental impact studies.

6.4. Conclusions

A rapid evaluation of dynamic lixiviation of uranium, and thorium from solid environmental samples was possible thanks to the hyphenation of flow analysis techniques, a dedicated sample cell and a selective resin. A multisyringe flow injection analysis (MSFIA) - Lab-On-Valve (LOV) system allows the on-line lixiviation, extraction and preconcentration of

U and Th in different environmental solid matrices. The automatic MSFIA-LOV system was combined with an ICP-MS enabling the detection of both radionuclides at ultra-trace levels in the leached fractions, and in the residual fractions. The use of multivariate techniques allows a quick and efficient optimization of the independent variables that affect the lixiviation process.

A similar behaviour of U and Th releases under dynamic lixiviation conditions, from environmental solid matrices, i.e. soil, sediment and phosphogypsum, was observed using rainwater at pH 5.4 as extractant. U and Th content decrease for successive fractions, being the mobility of both radionuclides was extremely low, obtaining up to 0.05% and 0.005% of U and Th release, respectively, remaining almost all them in the residual fraction (>99.95%). Nevertheless, the great variability found in different environmental sample matrices analysed, especially of U releases; highlight the importance of the dynamic lixiviation assays for holistic environmental impact studies.

CHAPTER 7
3D PRINTED DEVICE FOR URANIUM(VI)
EXTRACTION AND ITS INTEGRATION IN AN
AUTOMATIC FLOW-THROUGH SYSTEM

7.1. Introduction

3D printing or additive manufacturing has gained significant interest [167]. In several fields, including analytical chemistry, the integration of 3D printed devices in different automated methodologies has been successfully achieved [70,80].

Recently, 3D printing technology has allowed the fabrication of devices conveniently modified to fit experimental requirements [73], e.g. it has been applied in flow-cells for chemiluminescence detection [168], for fabrication of flow-based devices [92,169–173], SPE devices [73,81,174,175], fluidic valves and pumps [176], among others [177,178]. Also, the combination of flow techniques with 3D printing technology opens new possibilities in the miniaturization and integration of automated analytical methods [73,81,176].

Solid phase extraction (SPE) method is the most useful for sample pretreatment, typically based on the use of columns or cartridges packed with ion exchange resins, is currently the most useful for the extraction/preconcentration of radionuclides with the use of different commercial selective chromatographic extraction resins [179–182]. Additionally, this technique facilitates the automation of the extraction process using flow analysis techniques, obtaining high reproducibility and low consumption of reagents, and the increasing of the analyst working security by minimization the handling of radioactive samples [34,158].

Uranium is a naturally occurring radioactive element, unfortunately it is of great concern due to the human activities such as mining and milling activities, nuclear weapons, and nuclear fuel fabrication have caused widespread environmental contamination. Also, burning of fossil fuel (oil and coal), manufacture and use of phosphate fertilizers, phosphate rock processing are some of the primary anthropogenic source of U released into the air, soil and water, causing contamination in groundwater in proximity to populated areas [25,145,183]. The simplest way that can be incorporated the U in a human body is through the water, for that reason, Work Health Organization (WHO) recommends that U should not exceed $30 \mu\text{g L}^{-1}$ in drinking water. Thus, the determination of uranium levels present in environmental samples is required, needing previous separation and preconcentration steps before its detection [184]. The determination of uranium is carried out by radiometric detectors [16,34] and by spectrometric techniques, such as inductively coupled plasma optical emission spectrometry (ICP-OES) [47,48], and inductively coupled plasma mass spectrometry (ICP-MS), being the last one the most used [52,53,159]. Even the ICP-MS is a selective technique, the analytical performance may be enhanced by sample clean-up and preconcentration [91].

A number of studies have been reported for the extraction of uranium using the commercial chromatographic resins together with the advantages of the flow analysis techniques [52,179,184,185]. However, these studies rely on packed columns, which can be clogged with complex matrices requiring tedious digestion, filtration or centrifugation previous procedures.

The main objective of this study is to design a 3D printed device to provide a high surface area in a small volume with a coat of a selective extractant of uranium(VI), i.e. Aliquat®336 for liquid extraction and TEVA resin for SPE (Section A).

Next, it is intended to integrate the optimized 3D printed device in a SIA system for U extraction in water matrices, without doing any previous pretreatment. In order to improve the on-line U extraction efficiency, a magnetic-stirring assisted (MSA) system was developed. The proposed SIA system was optimized by experimental design, and ICP-MS was used, allowing the determination of uranium at low concentrations, in a fast and sensitive way [52,53,159](Section B).

Section A) 3D printed device for selective uranium extraction

7.2. Experimental

7.2.1. Reagents and solutions

The chemicals used were from analytical grade, and all the solutions were prepared with Milli-Q water (Bedford, MA, USA). Nitric acid (HNO₃ 65%, Scharlau, Barcelona, Spain); hydrochloric acid (HCl 37%, Panreac, Barcelona, Spain), trioctylmethylammonium chloride (Aliquat®336, Sigma Aldrich, St. Louis, MO, USA), methanol ACS Basic (MeOH, Scharlau), acetonitrile analytical standard (ACN, Scharlau), standard solution of uranium (998 ± 2 mg L⁻¹ in 5% HNO₃, VHG Labs, Manchester, USA), and bismuth (1000 mg L⁻¹ in 0.5 mol L⁻¹ HNO₃), were used.

Syringe filter units of 0.45 µm pore size (Millipore), and TEVA (TEtraVAlent actinides) resin of 50-100 µm particle size (Triskem International, France), were employed.

Clear photoactive resin composed by methacrylated monomers, oligomers, and an initiator (Formlabs), was used.

7.2.2. Instrumentation and software

The 3D printed device was designed using Rhinoceros 5SR11 32 software (MacNeel& Associates, USA), and printed with Perform Software (Formlabs).

The 3D printer Form +2 (Formlabs Inc., Somerville, USA) was employed. The printing time for one device with 408 layers was 64 min, while 72 min were required to print 8 devices simultaneously, and 157 min for 16 devices, oriented 40° in x-axis for printing with stand, and 0.05 mm of resolution. The weight of the device is 573 mg, and consumes a volume of 1.32 mL of polymeric resin.

7.2.3. Immobilization of TEVA resin on the 3D printed device

The 3D printed device was cleaned with 2-propanol for removing the unreacted monomers, and placed in a plastic centrifuge tube of 50 mL, containing an appropriate amount of TEVA resin, and shaken during 1 min. After that, the 3D printed device was removed from the centrifuged tube using tweezers, and it was cured by placed in a CL-100 Ultraviolet Crosslinker (VP, Upland, Canada) between 8 and 10 h, which has a lamp of 365 nm of wavelength. The non-immobilized TEVA resin was removed by washing it with Milli-Q water three times. About a 0.055 ± 0.012 g (n=8) of TEVA resin is coated in the sticky surface of the 3D printed device.

7.2.4. Immobilization of the Aliquat®336 on the 3D printed device

3D printed device cured using a CL-100 Ultraviolet Crosslinker were placed in a plastic centrifuge tube of 50 mL, containing 5 mL of Aliquat®336 at different percentages (40, 60, 80 %) diluted with ACN/MeOH/H₂O (35/35/30, vol %), and stirred during 18 min at 800 rpm. After that, the 3D device was removed from the centrifuge tube using tweezers, and washed three times with Milli-Q water, for removing the non-immobilized Aliquat®336.

7.2.5. Characterization and detection

The device characterization was carried out by scanning electron microscopy (SEM) Hitachi S-3400N, equipped with a Bruker AXS Xflash 4010 energy-dispersive X-ray spectroscopy (EDS) system. A low-background proportional counter (LBPC) Canberra LB4200, equipped with four detectors, with an average alpha efficiency of 20%, was used for the uranium detection from Aliquat®336's and TEVA's eluates. The measurements were performed at 1320 V, for simultaneous alpha/beta mode, and a counting time of 1000 min. Apex software was used for data acquisition and processes. Also, an ICP-MS Elan DRC-e (Perkin Elmer), fitted with a cross flow nebulizer and Scott spray chamber (Perkin Elmer) was used for uranium detection from TEVA's eluates. ²³⁸U was selected for measurement since it is the most abundant occurring isotope of

uranium[25], and ^{209}Bi was simultaneously measured in order to correct the instrumental drift.

7.2.6. Sample preparation

The phosphogypsum reference material (MatControl CSN-CIEMAT 2008) was analysed by weighing an appropriate amount (approx. 56 mg), which was dried until constant weight (placed in an oven at $55\pm 5^\circ\text{C}$). Phosphogypsum was dissolved with 9 mol L^{-1} HCl (up to 50 mL). The reference water material (CSN/CIEMAT 2011) was prepared in 9 mol L^{-1} HCl.

7.2.7. Analytical procedure

First, the 3D printed device coated with TEVA resin was conditioned with 5 mL of 9 mol L^{-1} HCl by stirring for 1 min at 300 rpm; then the device was submerged in the sample for 15 min stirring at 300 rpm allowing the uranium(VI) extraction. Then sample matrix was removed by washing with 5 mL of 9 mol L^{-1} HCl for 1 min. After that, the uranium elution was carried out with 3 x 5 mL of 1 mol L^{-1} HNO_3 by stirring for 1 min at 1100 rpm. Finally, the 3D printed device with immobilized TEVA resin was cleaned with 5 mL of 1 mol L^{-1} HNO_3 , stirring 1 min at 1100 rpm. The eluate was evaporated to dryness, and the residue was dissolved in 2.87 mL of HNO_3 2%, this was filtered through a $0.45\mu\text{m}$ syringe filter, and added 0.03 mL of the internal standard of Bi ($10\text{ }\mu\text{g L}^{-1}$). The eluate fractions were analysed in an ICP-MS.

7.3. Results and discussion

The 3D printed device is a cube with a diameter and height of 10.62 mm (Figure 7.1a). The small cubes that composed the cube structure have a volume of 0.8 mm^3 , between each small cube there is a separation of 0.6 mm, and are superposed by an area of 0.1 mm. This structure provides a high superficial area coated by the extractant and, at the same time, it provides channels through which the raw matrix of the sample flows without presenting problems of obstruction as in a resin column or extraction disk.

The selected extractant is a quaternary ammonium salt, which was tested for liquid extraction using different percentages of Aliquat®336, and for SPE employing TEVA resin with an extracting loading of 40% (w/w)[182], both forming a coat supported by the 3D printed device. In Figure 7.1b is shown the schematic representation of the immobilization of TEVA resin on the 3D printed device, and the uranium retention.

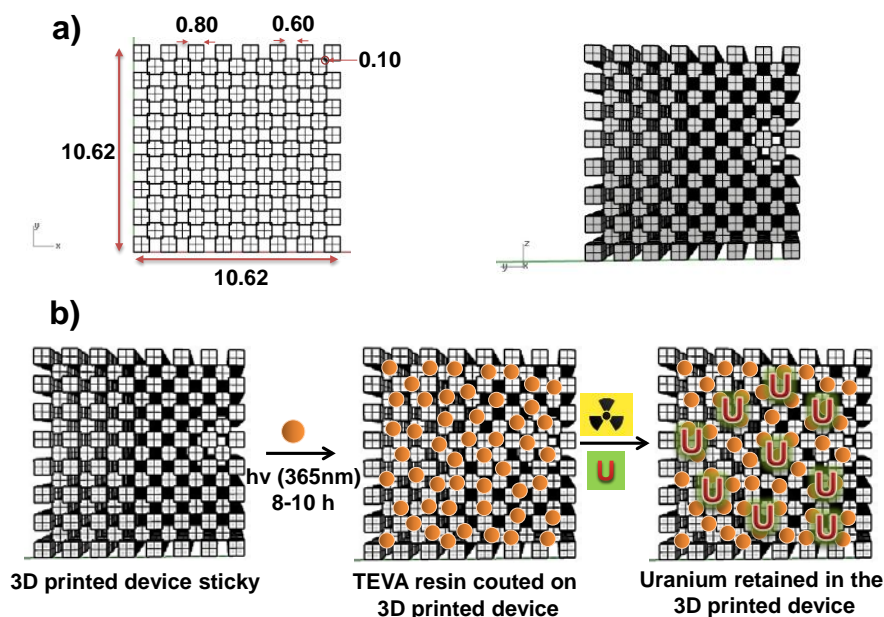


Figure 7.1 a) Representation of the 3D printed device (dimensions in mm); b) unmodified device: representation of TEVA resin immobilization and uranium retention in the 3D printed device.

The 3D printed device was characterized by scanning electron microscopy (SEM). In Figure 7.2a and b are presented the SEM images of the unmodified 3D printed device, while the 3D printed device after immobilization of 60:40% Aliquat®336: ACN/MeOH/H₂O (35/35/30 vol %) is shown in Figure 7.2c and d. In addition, in Figure 7.2e and f are presented the SEM images of the 3D printed device with immobilized TEVA resin.

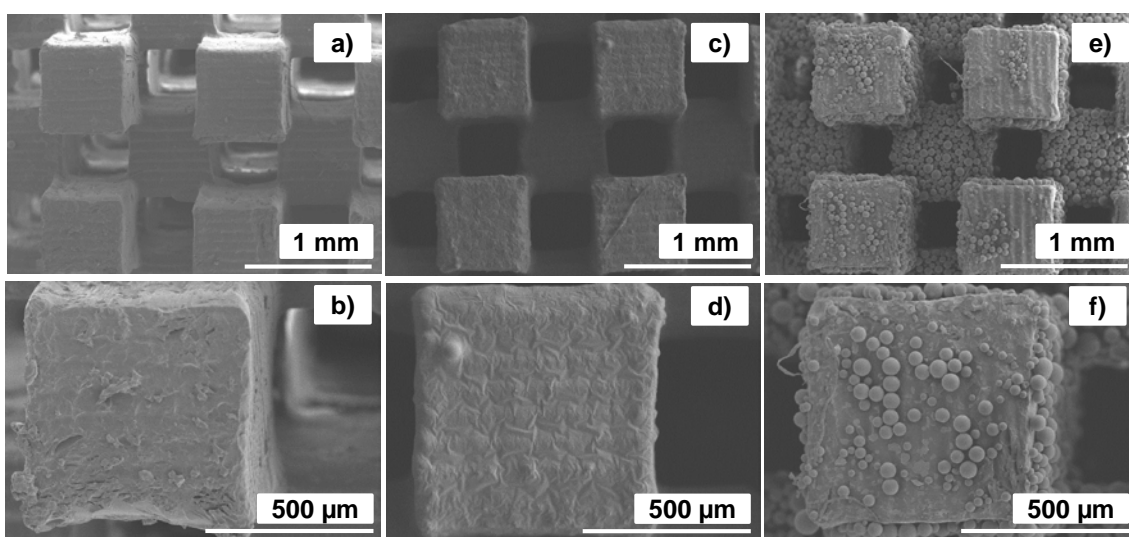


Figure 7.2 a) and b) Scanning electron microscopy images of the unmodified 3D printed cubes; c) and d) the same cube after immobilization of 60:40% Aliquat® 336: ACN/MeOH/H₂O (35/35/30, vol%); and e) and f) after the immobilization of TEVA resin.

In Figure 7.3 is shown the SEM images of the 3D printed device coated with TEVA resin, which were taken after the 3D printed device was stirred with water during 15 min at 300 rpm. It can be observed that TEVA resin remains immobilized in the inner faces of the cubes, which conform the 3D printed device, while the resin took off from the external faces (see Figure 7.3.a).

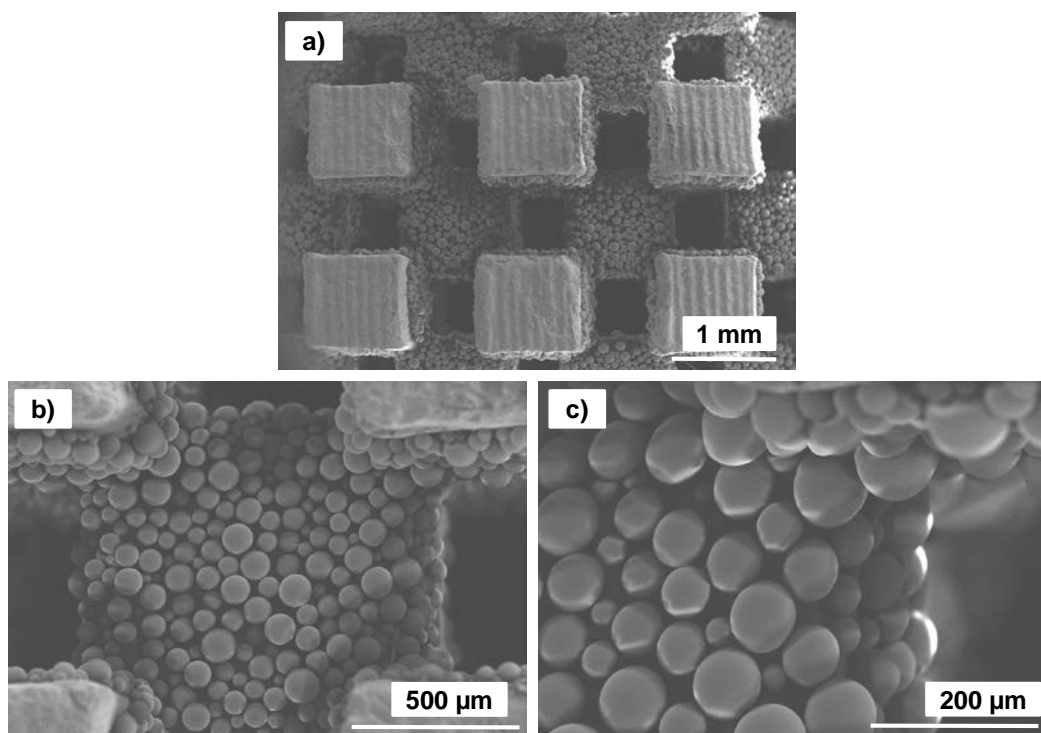


Figure 7.3 Scanning electron microscopy images of the 3D printed device after stirring 15 min at 300 rpm. a) Inner faces with resin beads, and external faces without them; b) and c) enlarged images of the inner faces.

EDS spectra for uranium retained in 60:40% Aliquat®336: ACN/MeOH/H₂O (35/35/30, vol%) (Figure 7.4a), and TEVA resin (Figure 7.4b), immobilized in 3D printed device, present two peaks, one of Cl (Aliquat®336 or TEVA resin), and the other one of the uranium retained in the 3D printed device. Demonstrating that, 3D printed device as support of liquid and solid extractant is useful for uranium extraction.

Thus, assays were carried out with 32 mg L⁻¹ (activity of 2 Bq) of U(VI) in 9 mol L⁻¹ HCl [96,159], using an extraction time of 15 min at 300 rpm.

The eluates coming from the liquid extraction presented traces of Aliquat®336, thus the U(VI) detection was made measuring the U alpha activity in a LBPC. The eluate was dried and the residue was dissolved in Milli-Q water to remove the HCl medium. Then, the solution was transferred to a stainless-steel planchette with Milli-Q water; and evaporated to dryness with an infrared lamp.

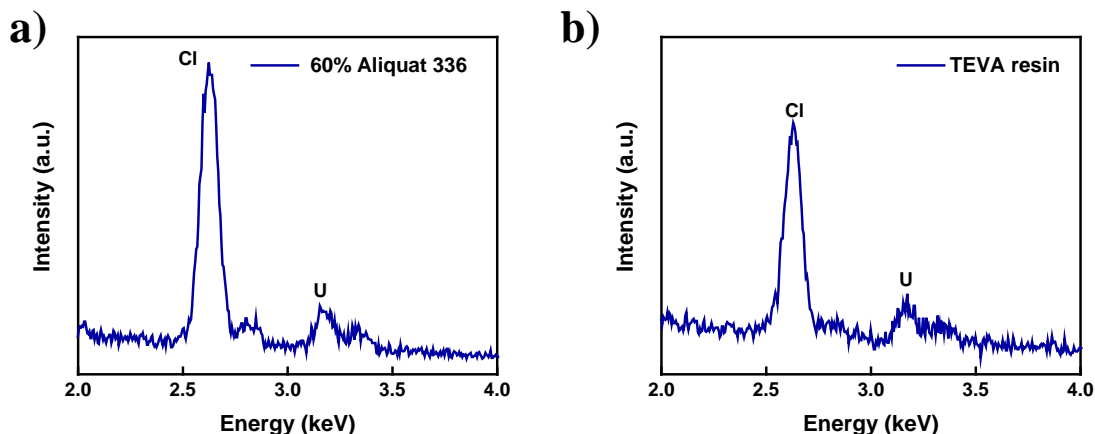


Figure 7.4 EDAX spectra of Cl/U from the 3D printed device a) with immobilized 60:40% Aliquat®336: ACN/MeOH/H₂O (35/35/30, vol %); b) with immobilized TEVA resin.

The results obtained with the 3D printed device as support of Aliquat®336 (40, 60, and 80%) show a uranium extraction of 88 ± 3 %, 93 ± 3 %, and 92 ± 4 % ($n=3$), respectively. Therefore, a coat conformed by 60% Aliquat®336 is enough for a satisfactory extraction efficiency.

A comparison of extraction efficiencies was carried out between the unmodified 3D printed device, coated with TEVA resin, and coated with Aliquat®336, making 7 continuous U(VI) extractions with each one (Figure 7.5). The cubes modified with TEVA and Aliquat®336 present a similar extraction efficiency (~ 90 %). Nevertheless, a better reproducibility in terms of RSD was obtained with the 3D printed device coated with TEVA resin (2.9%) compared with the RSD obtained with 60% Aliquat®336 as extractant (4.6%).

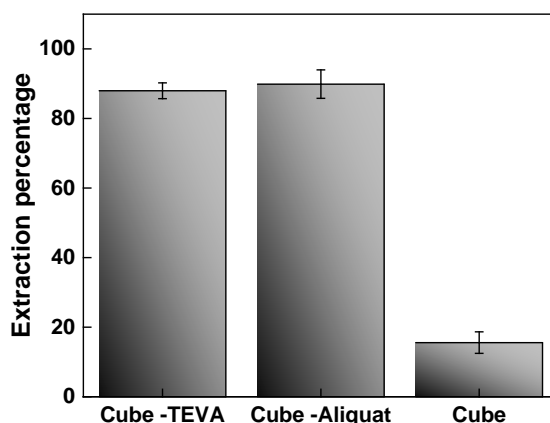


Figure 7.5 Efficiencies of U(VI) extraction obtained by 3D printed device coated with TEVA resin, 60% of Aliquat®336, and the unmodified cube. Extraction conditions: 15 min at 300 rpm. Analyte concentration: 32 mg L^{-1} .

Since the best results for uranium extraction, in terms of extraction efficiency together with reproducibility, were accomplished using the 3D printed device coated with TEVA resin, so an ICP-MS was used allowing to detect ultra-trace levels of uranium in a fast approach.

The variables that affect the process of uranium extraction, i.e. the retention and elution time, and the eluent volume, were studied in a univariant way. Uranium retention time was studied in a range of 5 to 30 min (Figure 7.6a), showing an increment of the analytical signal with the time, up to an extraction time of 15 min, which was set for future assays. The effect of the elution time was evaluated varying in a range between 1 – 7 min. The results indicate that the elution time does not affect the analytical signal in the studied range, so 1 min was set for future assays (Figure 7.6b) in order to not affect negatively the analysis time. Then, the effect of the eluent volume was studied in a range between 10 – 15 mL. Moreover, the way to do the elution was evaluated by using 1 – 3 consecutive elutions, obtaining an improvement of 16 % in the analytical response using 3 elutions of 5 mL each one, setting the total eluent volume to 15 mL.

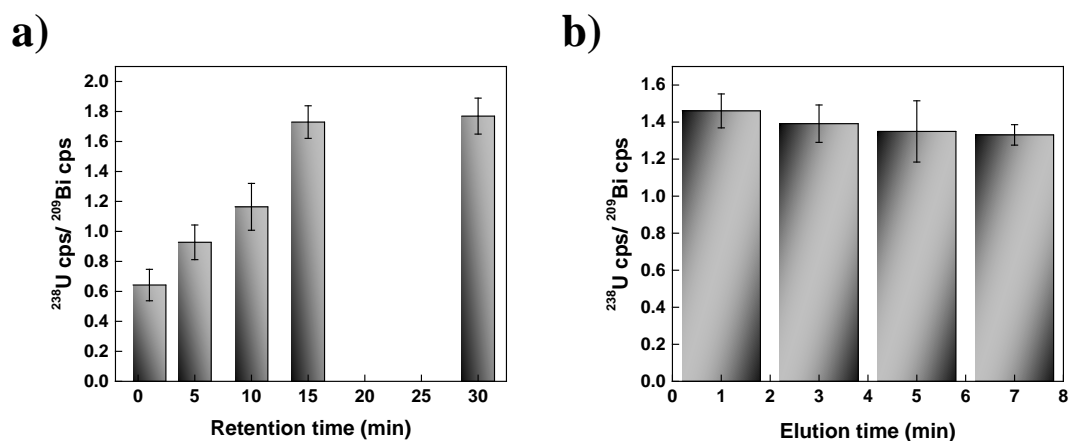


Figure 7.6 Optimization of the times of retention and elution steps: a) Conditions of the extraction time: extraction at 300 rpm, elution with 3-times of 5 mL of 1 mol L⁻¹ HNO₃ at 1100 rpm. Analyte mass: 0.33 ng U in both studies; b) Conditions of elution time study: 15 min of extraction at 300 rpm, elution with 10 mL of 1 mol L⁻¹ HNO₃ at 1100 rpm.

In addition, the design of the 3D printed device and the stir step in the uranium extraction were evaluated. Thus, the 3D printed device was compared with and without stir, and also with 3D printed solid cube, all of them with identical size and coated with TEVA resin (Figure 7.7). The best results were obtained with the design of the 3D printed device conformed by a network of small cubes and stir, evidencing the importance of both, the design of the 3D printed device, and the stir in the extraction process. The 3D printed device with small cubes compared with the solid one, has more surface area,

allowing five-times more amount of resin can be coated in the sticky surface on the 3D printed device. Besides, the stir permits more contact between the TEVA resin and the U, doubling the analytical signal.

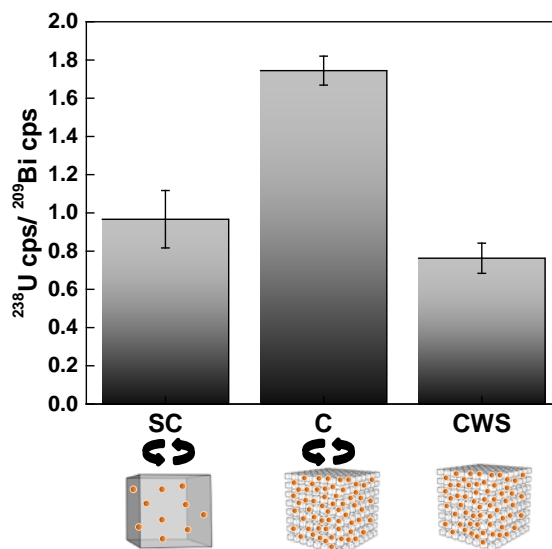


Figure 7.7 Analytical response (^{238}U cps / ^{209}Bi cps), of solid cube coated with TEVA resin (SC); 3D printed device coated with TEVA resin (C); and 3D printed device coated with TEVA resin, doing the extraction without stir (CWS). Conditions: 15 min of extraction at 300 rpm. Elution, three of 5 mL ($1 \text{ mol L}^{-1} \text{ HNO}_3$) at 1100 rpm each one. Analyte mass, 0.33 ng.

In order to study the durability of the 3D printed device coated with TEVA resin, 30 consecutive uranium extractions using 0.2 ng of U(VI) were performed using the same device. The results indicate that an extraction efficiency of 90% (RSD 5%), 84% (RSD 8%), and 81% (RSD 10%) were obtained for 10, 20 and 30 consecutive extractions, respectively. Thus, in order not to worsen extraction efficiency nor precision, it is recommended to use the device 10 times and then change it. The preconcentration volume was studied in a range between 5 to 30 mL (Figure 7.8). The 3D printed device coated with TEVA resin is able to extract and preconcentrate uranium(VI) up to a sample volume of 30 mL.

The limit of detection (LOD) and limit of quantification (LOQ) were calculated following the IUPAC recommendation [166], obtaining a LOD of 0.032 ng, and LOQ of 0.107 ng of U.

Mass calibration curves (ng U(VI) vs $^{238}\text{U} / ^{209}\text{Bi}$) were performed obtaining a good correlation ($y=4.3271x+0.0082$, $r^2=0.9985$, $n=7$) in a linear working range between 0 to 0.7 ng U(VI).

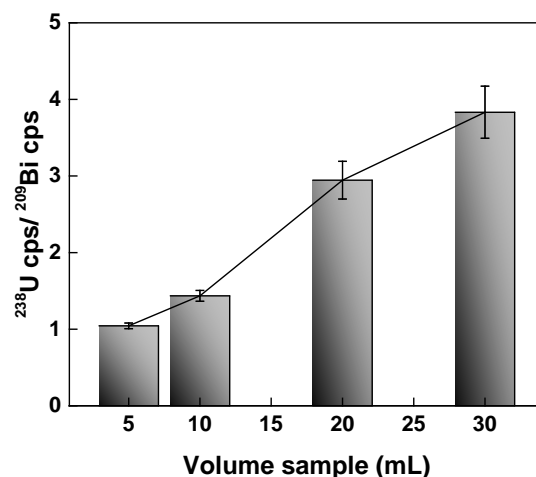


Figure 7.8 Analytical response ($^{238}\text{U cps} / ^{209}\text{Bi cps}$) of the preconcentration volume. Conditions: 15 min of extraction at 300 rpm. Elution, three of 5 mL ($1 \text{ mol L}^{-1} \text{ HNO}_3$) at 1100 rpm each one. Analyte mass: 0.2 ng.

Finally, the validation of the 3D printed device with TEVA resin was performed analysing reference material, e.g. phosphogypsum and water matrices from intercomparison exercises. The results were satisfactory at a confidence level of 95% (Table 7.1). It should be noted that these results were obtained without any pretreatment of the samples.

Table 7.1 Analysis of the reference materials using the 3D printed device coated with TEVA resin, for uranium(VI) extraction and ICP-MS detection.

	U(VI) extracted by 3D printed device coated with TEVA resin	U(VI) reference value
Water reference material (CSN/CIEMAT 2011) ($\mu\text{g L}^{-1}$)	$17.7 \pm 3.0^{\text{a}}$	$20.0 \pm 3.6^{\text{b}}$
Phosphogypsum reference material (CSN/CIEMAT 2008) ($\text{mg Kg}^{-1} \text{ d.w}$)	$3.77 \pm 0.31^{\text{a}}$	$4.50 \pm 0.82^{\text{c}}$

Results are expressed as (a) average \pm standard deviation ($k=2$) ($n=3$); (b) average \pm uncertainty ($k=2$) ($n=5$); (c) average \pm uncertainty ($k=2$) ($n=21$). Significant differences were not found at a confidence level of 95%.

Section B) 3D printed SPE device integrated in an automatic system

7.4. Experimental

7.4.1. Reagents and solutions

The chemicals used were from analytical grade, and all the solutions were prepared with Milli-Q water (Bedford, MA, USA). Nitric acid (HNO_3 65%, Scharlau, Barcelona, Spain); hydrochloric acid (HCl 37%, Panreac, Barcelona, Spain), standard solution of uranium ($998 \pm 2 \text{ mg L}^{-1}$ in 5% HNO_3 , VHG Labs, Manchester, USA), and bismuth (1000 mg L^{-1} in 0.5 mol L^{-1} HNO_3 , employed as internal standard solution, were used.

Stock, and working solutions of uranium were prepared with an appropriate amount of uranium standard solution in HCl 6 mol L^{-1} .

Besides, TEVA (TEtraVAalent actinides) resin of 50-100 μm particle size (Triskem International, France) were employed and nylon syringe filter units of $0.45 \mu\text{m}$ pore size (Millipore).

7.4.2. Sample preparation

The reference water material (CSN/CIEMAT 2011) was diluted up to 50 mL with 6 mol L^{-1} HCl.

Water samples were also prepared in a final solution of 6 mol L^{-1} HCl, without any previous filtration.

7.4.3. 3D printed device

In order to integrate the above described 3D printed SPE device in a flow system for the on-line extraction of U, it was necessary to design a device container. Therefore, as can be seen in Figure 7.9a, the 3D printed device/container consists in 5 parts. Figure 7.9b shows the dimension of parts 1 and 5, both are the external pieces that contain the connectors. The liquid input is located in part 5, which is connected to port 5 of the selection valve. The liquid output is located in part 1, which is connected directly to the waste. The internal diameter of the flow channels of each part is 2 mm.

Part 2 and 4 are rings, holding neodymium magnetic in both sides, allowing the automatic magnetic stirring of the stir bar, which is inside the 3D printed device. Figure 7.9c shows their respective dimensions.

Figure 7.9d shows the part 3, which is the central part that contains SPE device. At the end of part 3, where the cube is fixed, there is a reduction of 7.52 mm to facilitate the on-line emptying of the piece.

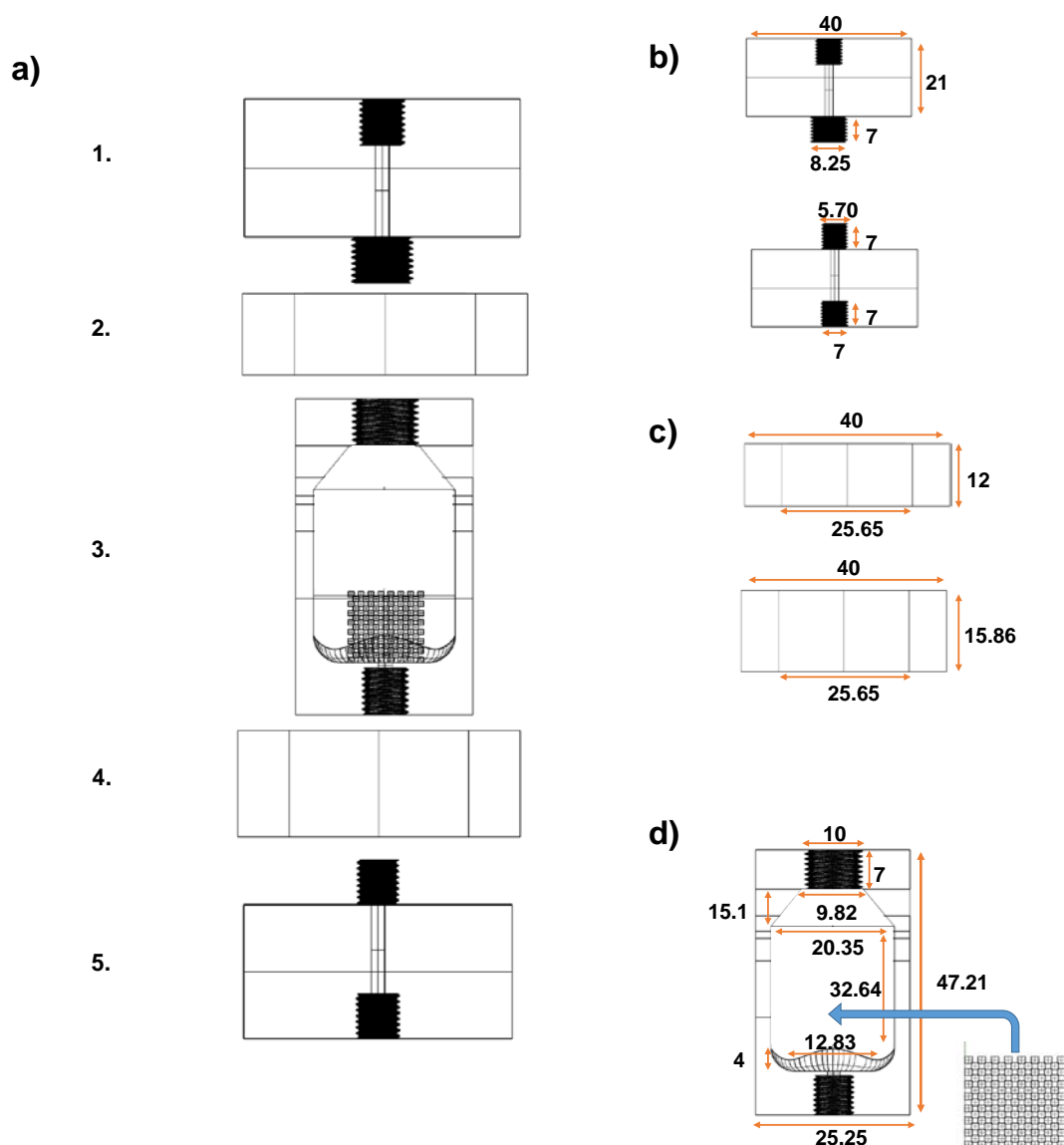


Figure 7.9 Representation of 3D printed device. a) 3D printed device separated in five parts; b) details of the top and lower taps (parts 1 and 5); c) details of the rings (parts 2 and 4); and d) details of the extraction cavity (part 3). Dimensions are expressed in mm.

3D printed devices were printed with a 3D printer Form +2 (Formlabs Inc., Somerville, USA). Clear photoactive resin (Formlabs) was used. After printed the 3D SPE/container device, the unreacted monomers were cleaned by pumping isopropyl alcohol using a HPLC pump (Waters, Milford, USA). Then, the 3D printed parts were dried at room temperature for 15 min, and cured by placed in a CL-100 Ultraviolet Crosslinker (VP, Upland, Canada) between 8 and 10 h.

The parts 1 and 5 were printed together, the printing time was of 198 min, with 350 layers and vertical printing with stand. In addition, the parts 2 and 4 were printed together, with a printing time of 96 min, 190 layers, and vertical printing with stand. All these pieces were printed with a resolution of 0.1 mm.

The part 3 was printed separately, with a printing time of 177 min for 1003 layers, while 348 min were necessary to print four devices simultaneously, and 562 min for 8 devices, with 0.05 mm resolution, vertical printing with stand.

The part 3 has a weight of 16.2 g, and 15.34 mL of volume of polymeric resin consumed. The total weight of all the parts that make up the 3D printed device is 101 g, and 100 mL of volume of polymeric resin consumed.

7.4.4. Automatic system set-up

The on-line extraction of U exploiting the 3D printed SPE/container device was carried out with the manifold shown in Figure 7.10.

The automatic SIA system is composed by a multisyringe burette module (BU4S, Crison Instruments), and a selection valve of 6 ports (Sciware Systems). The burette module is equipped with 1 syringe of 10 mL (Hamilton, Switzerland), at the head is located a three-way solenoid valve that redirects the liquid depending of its position (“off” position connects to the reagent reservoirs, and “on” position to the manifold).

The syringe is connected to the central port of the selection valve via a holding coil (HC). The configuration of the lateral ports are: sample/ standard (port 1), 1 mol L⁻¹ HNO₃ (port 2), eluate collector (port 3), 6 mol L⁻¹ HCl (port 4), 3D printed SPE/container device (port 5), waste (port 6). Approximately 0.065±0.014 g (n=8) of TEVA resin was immobilized on the 3D printed device.

Manifold was constructed with poly(tetrafluoroethylene) (PTFE) tubing of 1.5 mm i.d., HC had 720 cm long. All connections were made with polyvinylidene fluoride (PVDF) connectors.

Software AutoAnalysis 5.0 (Sciware Systems) was used for the instrumental control.

The detector used is an ICP-MS Elan DRC-e (Perkin Elmer), fitted with a cross flow nebulizer and Scott spray chamber (Perkin Elmer). For measurement, ²³⁸U channel was selected since it is the most abundant occurring isotope of uranium [25]. In order to correct the instrumental drift, ²⁰⁹Bi was simultaneously measured.

Experimental design and data processing were carried out with Statistica software for a confidence level of 95%.

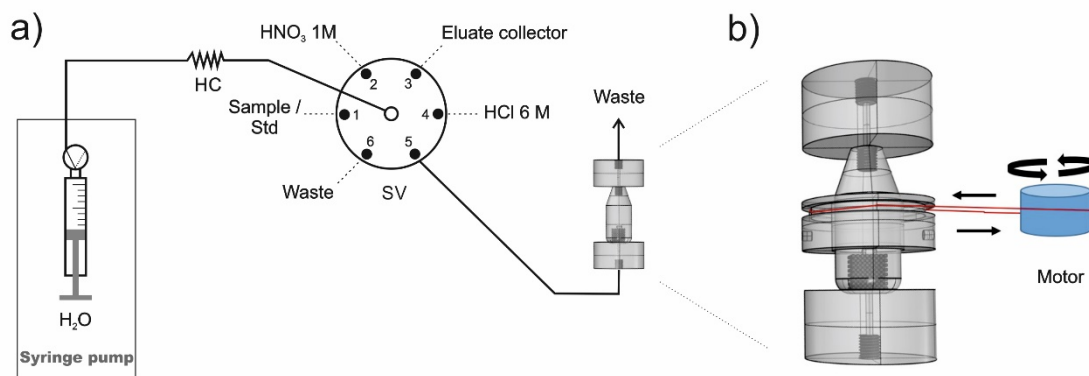


Figure 7.10 a) Automatic system for the extraction of U using a 3D printed SPE/container device. b) Representation of the automatic magnetic stirring of the 3D printed device, using a ring that contains neodymium magnetic in both sides. HC: holding coil; SV: selection valve.

7.4.5. Analytical procedure

Firstly, the 3D printed device coated with TEVA resin was conditioned with 9 mL of 6 mol L⁻¹ HCl, maintaining a constant stirring at 96 rpm. Then, 9 mL of the sample/standard were dispensed through the 3D printed SPE/container device at 3.5 mL min⁻¹, maintaining the stirring during 15 min at 96 rpm, in order to ensure an optimum extraction. To avoid interferences, the 3D SPE/container device was rinsed with 9 mL of 6 mol L⁻¹ HCl, stirring at 96 rpm. After that, the rinse liquid was dispensed to the waste.

The second step was the elution of U retained in TEVA resin with 9 mL of 1 mol L⁻¹ HNO₃, maintaining the stirring during 1 min at 96 rpm. The eluate was dispensed via HC in the eluate collector.

Finally, the 3D printed SPE/container device was cleaned by passing three times 9 mL of 1 mol L⁻¹ HNO₃ at 3.5 mL min⁻¹, and stirring at 72 rpm. The 3D printed SPE/container device was used for 12 consecutive extractions, after that, it was replaced by a new 3D printed SPE/container device.

The eluate collected was evaporated to dryness, and the residue was dissolved in 2.87 mL of HNO₃ 2%, filtered through a 0.45µm syringe filter, and added 0.03 mL of the internal standard of Bi (10 µg L⁻¹). The eluate fractions were analysed in an ICP-MS detector.

7.5. Results and discussion

7.5.1. Optimization of experimental conditions

The variables that affect the extraction and elution of U were studied by performing a full factorial design. First, it was studied the molarity of HCl as retention medium, column conditioner, and for removal other anions, comparing a solution of 9 mol L⁻¹, as the manufacturer recommends [96,186], with other of 6 mol L⁻¹ HCl studied by others authors [180,181]. Better results were obtained with 6 mol L⁻¹ HCl, which was set for future assays.

A full factorial design was performed for the study of the independent variables that affect U retention, i.e. time and velocity of stir. The range of the time stir was set according to the previous assays performed in Section A, while the velocity of stir was established according the speed reached by the on-line motor.

In Table 7.2, variable levels and the experimental matrix of the full factorial design (2²) are presented.

Table 7.2 Variables, levels and experimental matrix of the full factorial design for U retention. U: 10 µg L⁻¹.

Variables	Levels		
	Low (-)	Central Point (0)	High (+)
Time stir (min)	6	18	30
Speed stir (rpm)	48	72	96
Assay	Time stir	Speed stir	Analytical response U cps/ Bi cps
1	-	-	0.36
2	+	-	0.42
3	-	+	0.40
4	+	+	0.56
5	0	0	0.46
6	0	0	0.46
7	0	0	0.47

The results obtained within the experimental domain studied can be observed in the Pareto Chart (Figure 7.11), which indicates that the time and speed stir are significant, both with a positive effect, entailing that more time and speed stir increase the analytical response. This result can be attributed that U retention needs more contact time with the resin, and a higher speed stir to permit the interaction of the sample/standard with the TEVA resin impregnated in the 3D cube. Other authors have reported that the on-line retention of uranium using the same resin should be carried out at a low flow rate allowing more contact time between the resin and the sample /standard [53,179,185].

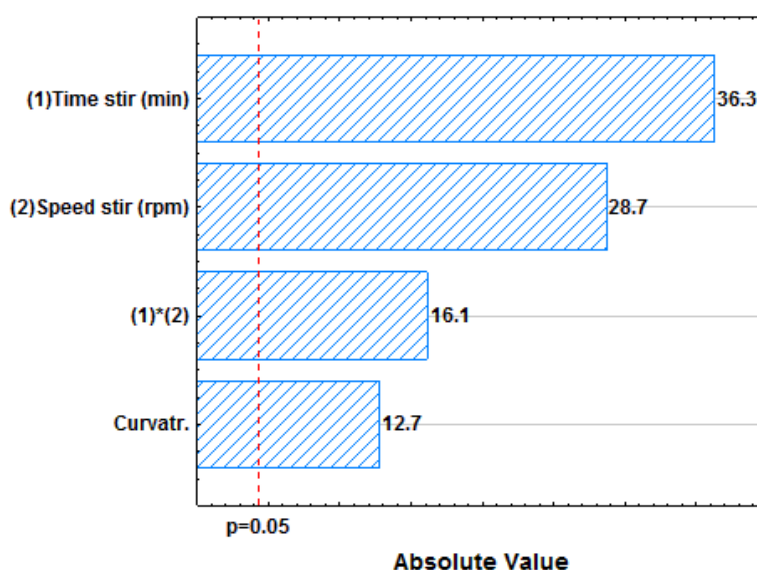


Figure 7.11 Pareto Chart for the variables affecting U retention.

Additionally, a significant curvature is observed indicating that within the experimental domain studied could be determined a critical condition of maximum signal. Since the maximum speed allowed by the on-line motor is 96 rpm, it was set for future assays. In the case of the time of stir, 15 min were set due to it allows an enough sensibility without worse the analysis frequency.

After optimizing the variables that affect the retention process, the elution process was optimized by performing a full factorial design encompassing the following independent variables that affect this process: stir elution time (min), stir elution speed (rpm), eluent volume (mL), and eluent molarity (HNO_3).

The experimental domain of stir elution time (min) and eluent molarity (HNO_3) were set according to previous assays. Besides, an eluent molarity of 2 mol L^{-1} of HNO_3 was recommended by the manufacturer [182,186]. The eluent volume was set according to the capacity of the 3D printed SPE/container device, requiring at least 6 mL to cover

the 3D printed cube, and 9 mL to fill the device. Stir elution speed was set in the same way that U retention.

In Table 7.3 is presented the full factorial design (2^4) performed, and the experimental domains.

Table 7.3 Variables, levels and experimental matrix of the full factorial design for U elution. U: $10 \mu\text{g L}^{-1}$.

Variables	Levels		
	Low (-)	Central Point (0)	High (+)
Time stir (min)	6	18	30
Speed stir (rpm)	48	72	96
Eluent volume (mL)	6.0	7.5	9.0
Eluent molarity (HNO_3 , mol L^{-1})	1.0	2.0	3.0

Assay	Stirring Time	Stirring Speed	Eluent volume	Eluent molarity	Analytical response
					U cps/ Bi cps
1	-	-	-	-	0.33
2	+	-	-	-	0.66
3	-	+	-	-	0.55
4	+	+	-	-	0.68
5	-	-	+	-	0.67
6	+	-	+	-	0.84
7	-	+	+	-	0.96
8	+	+	+	-	0.71
9	-	-	-	+	0.53
10	+	-	-	+	0.20
11	-	+	-	+	0.08
12	+	+	-	+	0.25
13	-	-	+	+	0.60
14	+	-	+	+	0.57
15	-	+	+	+	0.67
16	+	+	+	+	0.48
17	0	0	0	0	0.73
18	0	0	0	0	0.74
19	0	0	0	0	0.84

The results obtained within the experimental range studied (Figure 7.12) indicate that stir elution speed and stir elution time are not significant. Thus, the stir elution time was set to the lower level studied (1 min), and the stir elution speed was set in 96 rpm for future assays. The stirring elution speed was set in the maximum level studied, because its interaction with the eluent volume and eluent molarity observed in the graph of marginal means (Figure 7.13), indicates that a maximum analytical response was obtained at stir elution speed of 96 rpm.

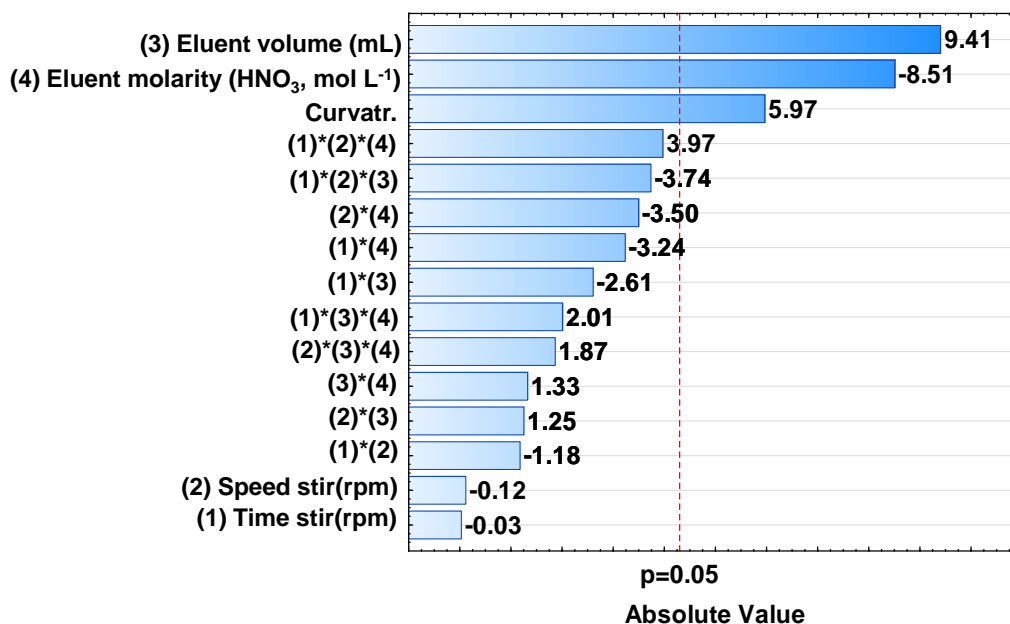


Figure 7.12 Pareto Chart for the variables affecting U elution.

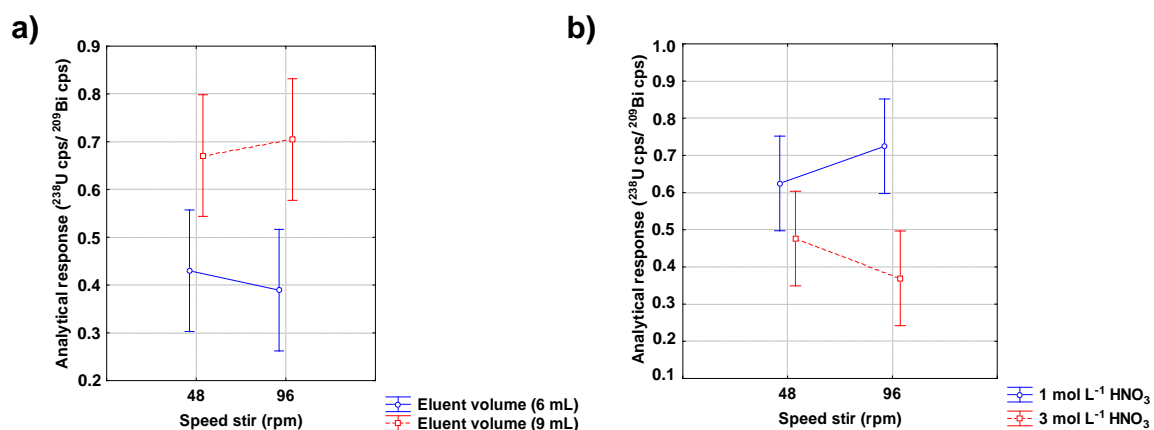


Figure 7.13 a) Graph of marginal means of the effect of the interaction between the variables eluent volume (mL), and speed stir (rpm). b) eluent molarity (HNO₃ mol L⁻¹), and speed stir (rpm).

The eluent volume and molarity were significant with a confidence level of 95%. The eluent volume shows a positive effect, indicating that a best analytical response is obtained when the volume is used at the maximum level, i.e. 9 mL of eluent.

The eluent molarity ($\text{mol L}^{-1} \text{HNO}_3$) shows a negative effect. So, this parameter was studied in a univariate approach. The eluent molarity assays were 0.5, 1, 1.5, and 2 $\text{mol L}^{-1} \text{HNO}_3$, obtaining (represented in Figure 7.14) the best results using an eluent molarity of 1 and 1.5 $\text{mol L}^{-1} \text{HNO}_3$. Thus, 1 $\text{mol L}^{-1} \text{HNO}_3$ was used for future assays.

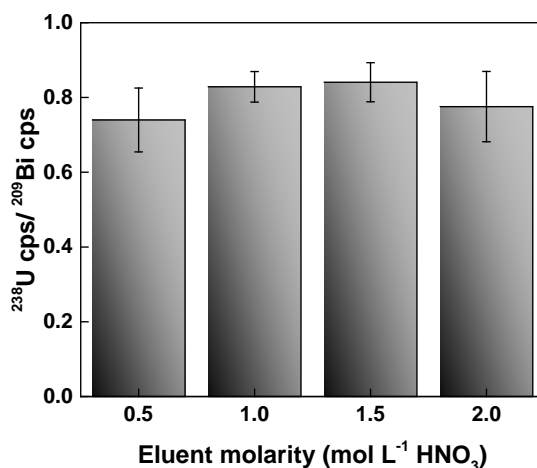


Figure 7.14 Optimization of eluent molarity ($\text{HNO}_3 \text{ mol L}^{-1}$). Conditions: 15 min of extraction at 96 rpm, elution 1 min at 96 rpm. U: $10 \mu\text{g L}^{-1}$.

7.5.2. Analytical features

The analytical parameters are summarized in Table 7.4.

Table 7.4 Figures of merit.

Figures of merit	Value
Limit of detection (ng)	0.03
Limit of quantification (ng)	0.09
Regression coefficient (n=7)	0.9984
Intra-day precision (RSD%) (n=10)	9
Inter-day precision (RSD%) (n=5)	13
3D printed device reusability (extractions)	11
Linear working range (ng)	0-1
Extraction frequency (h^{-1})	1

The limit of detection (LOD) and limit of quantification (LOQ) were calculated according the IUPAC recommendation [166], based on the standard deviation of the blank signal and the slope of calibration curve. The mass calibration curve (ng U(VI) vs $^{238}\text{U}/^{209}\text{Bi}$) was statistically satisfactory fitted ($y=4.0667x+0.0531$, $r^2=0.9984$, $n=7$) in a linear range of 0 to 1 ng U(VI).

Intra-day precision and reusability of 3D printed SPE/container device are intimately linked, since both indicate the number of consecutive analyses feasible without changing the 3D printed device coated with TEVA resin. So, both parameters were studied at the same time. The first ten extractions give an intra-day precision of 9% expressed as RSD. The reusability of the 3D printed device reaches 12 consecutive extractions with an extraction efficiency of 91% (RSD 11%).

Inter-day precision was calculated considering five extractions doing in five different days by changing the 3D printed SPE/ container device.

7.5.3. Application to water matrices

A reference water material (CSN/CIEMAT 2011) was analysed to validate the automatic SIA system. Besides, three different water matrices, e.g. mineral water, ground water and tap water were analysed. The analyses were performed by triplicate ($n=3$), and the results are presented in Table 7.5.

Significance differences were not found between the reference value of the water sample and the value obtained using the proposed SIA system, at a confidence level of 95%.

The procedure was applied to the three water matrices by adding a known U(VI) mass, obtaining satisfactorily results, with recoveries higher than 95%, in all the samples.

Table 7.5 Analysis of the different type of water samples.

Sample (n=3)	Added U ($\mu\text{g L}^{-1}$)	Found U ($\mu\text{g L}^{-1}$)	Recovery (%)
Groundwater	0.0	< LOD	
	2.5	2.4 \pm 0.1 ^a	95
	5.0	5.3 \pm 0.8 ^a	106
Tap water	0.0	< LOD	
	2.5	2.5 \pm 0.4 ^a	100
	5.0	4.8 \pm 0.3 ^a	96
Mineral water	0.0	< LOD	
	2.5	2.5 \pm 0.5 ^a	100
	5.0	5.0 \pm 0.7 ^a	99
Sample (n=3)	Reference value ($\mu\text{g L}^{-1}$)	Found U ($\mu\text{g L}^{-1}$)	Significant differences $\alpha=0.05$
reference water sample (CSN/CIEMAT 2011)	20.0 \pm 3.6 ^b	16.7 \pm 3.4 ^a	Not found

Results are expressed as (a) average \pm standard deviation (k=2) (n=3); (b) average \pm uncertainty (k=2) (n=5).

7.6. Conclusions

A 3D printed device coated with TEVA resin for the selective extraction of U has been designed, fabricated using SLA technology, and characterized. All steps included in the analytical protocol, i.e. pretreatment, extraction and preconcentration, are attained using a single device.

Then, the 3D printed SPE device coated with TEVA resin was included into a container and integrated in a SIA system configuration, as a reliable analytical strategy for the determination of U in complex water matrices without doing any pretreatment. The method developed is simple, effective and miniaturized, being a useful tool for U determination in water matrices.

Both 3D printed devices, the cube tested in a manual approach and the cube included in a container integrated to a SIA system, have given satisfactory analytical results, and are suitable for the application to real samples without any pretreatment, as

has been demonstrated by U determination in references materials, and by addition/recovery assays.

The integration of 3D printed device in an automatic methodology is a step forward for the extraction of radionuclides in complex matrices, allowing the pretreatment, treatment, extraction and preconcentration in a two-step protocol, increasing the analyst safety. Besides, it allows the customization of the 3D device with the aim to fit to different samples matrices, i.e. soil, vegetable ash, sediment channel, and also, the immobilization of different commercial resins for the selective extraction of radionuclides.

CHAPTER 8
FULLY AUTOMATED SYSTEM WITH
INTEGRATED LIQUID SCINTILLATION
DETECTOR FOR THE FAST DETECTION OF
RADIOSTRONTIUM

8.1. Introduction

Atmospheric nuclear weapon testing is considered the main source of radiostrontium in the environment, and gave rise to the posterior deposition of radionuclides known as global fallout [187]. Additionally, other secondary sources of radiostrontium have been nuclear accidents as Chernobyl (Ukraine, 1986) and Fukushima (Japan, 2011) [18,19,187,188]. Chernobyl nuclear accident resulted in a major release of volatile radionuclides meaning a contamination also outside the evacuation zone, and in a lot of European countries [18,189]. Besides, Fukushima accident released a great number of radionuclides into the atmosphere and sea [18].

The most important strontium radioisotope is ^{90}Sr , which is the most widespread anthropogenic radionuclide worldwide, because of its origin in global fallout [187]. ^{90}Sr is one of the most hazardous fission product because is chemical analogous to calcium and has long biological and radioactive half-live ($T_{1/2}=28.6$ years) [20,187,190]. ^{90}Sr decays in ^{90}Y by β^- emission ($E_{\text{max}}= 546$ keV), and due to the short half-life of ^{90}Y ($T_{1/2}=2.57$ d, $E_{\text{max}}= 2282$ keV), it is usually in secular equilibrium with ^{90}Sr in environmental samples [187].

^{90}Sr can be quantified by β counting using a LBPC previous isolation, by following the ingrowth of ^{90}Y , or after the secular equilibrium is reached by counting the total β activity (^{90}Sr and ^{90}Y) [191]. Since ^{90}Sr is a pure β^- emitting, is also common to detect its activity using a liquid scintillation counter (LSC). In any case, a previous radiochemical separation is mandatory. The procedure involved for chemical separation and detection is laborious and time-consuming, preventing a fast response in case of an emergency or an accident.

To solve this, some methodologies have been reported accomplishing simple and short procedures [67,192,193]. Besides, previous homemade detectors based on liquid scintillation have been developed for the determination of pure electron capture (EC), and pure β^- massic activity [36,68,69]. Grate et. al [20] have reported a SIA system with on-line detector based on liquid scintillation, able to detect ^{90}Sr as transient signal, and also the system can be operated in a stopped flow mode for longer counting times. Nevertheless, to the best of our knowledge, the combination of the advantages of three techniques as 3D printing, flow analysis techniques and liquid scintillation counter has not been reported yet.

Therefore, the main objective of this work is to combine the advantages of 3D printing, flow analysis injection techniques and the liquid scintillation counting for developing a fast, low-cost and miniaturized system, that allows the precise detection of ^{90}Sr in case of nuclear emergency. Sr-resin was used as solid phase extraction, since it

is a chromatographic material of high selectivity for Sr. In order to reach a fully automated system the on-line detection was performed with a homemade LSC detector based on two PMTs.

8.2. Experimental

8.2.1. Reagents and solutions

All the chemicals used were of analytical grade and prepared with Milli-Q water (Bedford, MA, USA). Nitric acid (HNO₃) (65%, Scharlau, Barcelona, Spain), hydrochloric acid (HCl) (37.5%, Panreac, Barcelona, Spain), ⁹⁰Sr certified standard with an initial activity of 0.965±0.014 Bq mg⁻¹ (CIEMAT, Madrid, Spain, ref. FRC-2015-00404), and 0.978±0.015 Bq mg⁻¹ (CIEMAT ref. FRC-2015-00451), both prepared in 0.1 mol L⁻¹ HCl, were used. Standard working solutions of ⁹⁰Sr were prepared with an appropriate quantity of ⁹⁰Sr certified standard in HNO₃ 8 mol L⁻¹.

Sr-resin 50-100 µm particle size (Triskem International) was used for the ⁹⁰Sr extraction and fiberglass wool for chromatography was employed to retain the resin beads into the microcolumn.

Low viscosity liquid Ultima Flo M (PerkinElmer, Waltham, MA, USA), was used as liquid scintillation cocktail for the on-line measurement of ⁹⁰Sr.

8.2.2. 3D printed devices

A dark box dedicated to contain the flow cell, was designed like a puzzle in 4 parts (Figure 8.1a). The lower tap is cross-shaped, and in turn it has several sections (Figure 8.1b). Section 1 has 156 x 37 x 37 mm (L x H x W), and section 2 has 126 x 46 x 37 mm (L x H x W). Section 3 has 31 mm leaving 3 mm to fit with the leads. The windows (4) are separated by a distance of 50 mm, and they have 25 mm width and 3 mm of thickness. The two pieces that hold the flow cell (5) are separated by 45.6 mm and have 15.3 x 13.3 x 5 mm (L x H x W). To fit the top cap, section 6 has 40 mm.

The top cap (Figure 8.1c) is also cross-shaped, and has the same size as the bottom part with the width difference being 4 mm. To fit the lids and the top part a reduction of 0.3 mm was made. The section 1 has 30.4 mm and section 2 has 39.4 mm to fit with the bottom part. The two pieces that secure the flow cell (3) have 15.3 x 12 x 5 mm (L x H x W).

The lids (Figure 8.1d) are squares of four equal sides, 37 (1) x 37 x 4 mm (L x H x W). Also, in the lids was made a reduction of 0.3 mm to fit the bottom and the top cap, remaining the section 2 in 30.4 mm.

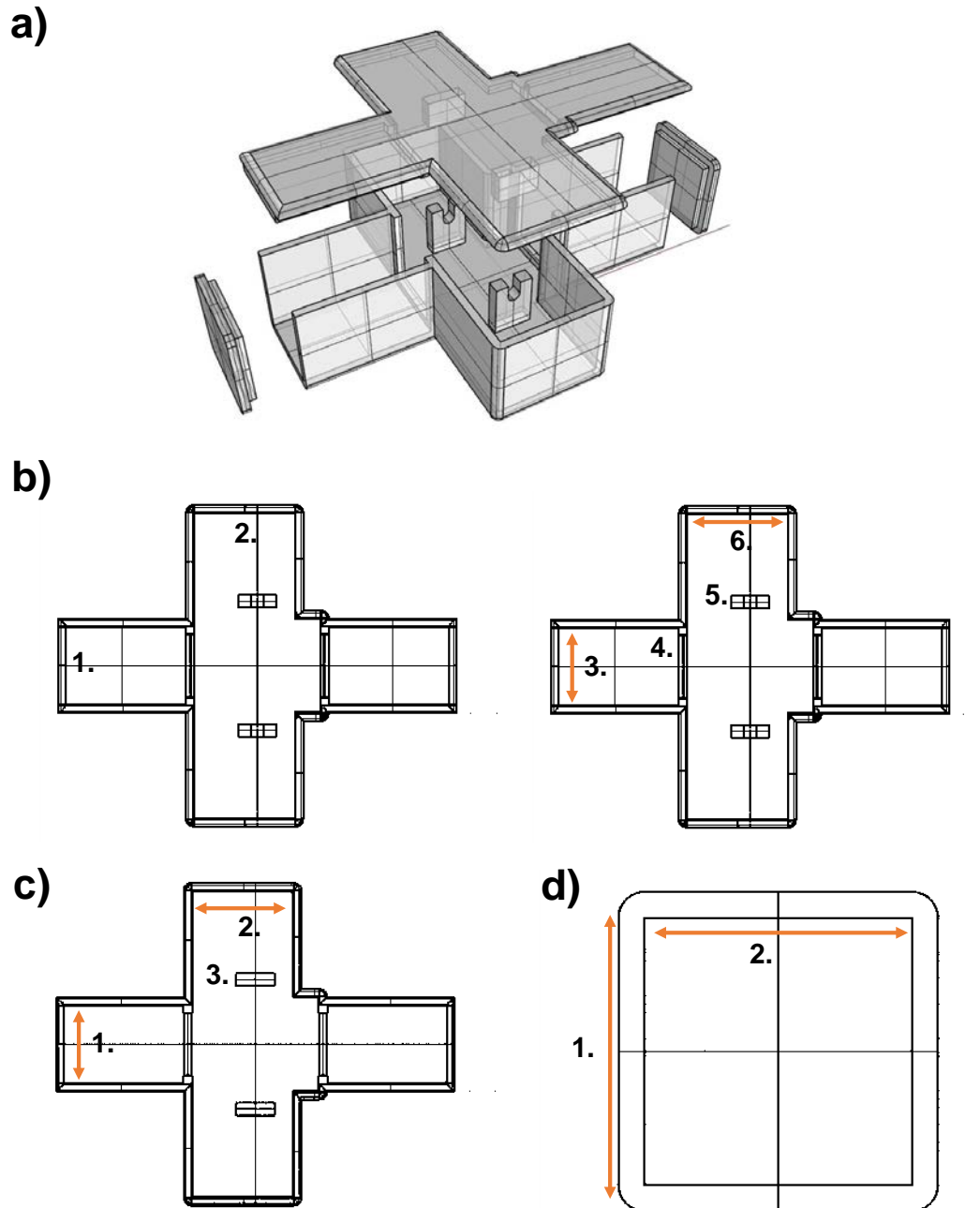


Figure 8.1 Representation of 3D printed dark box. a) Perspective view of the 3D printed dark box. b) Details of the lower tap, separated in sections. c) Details of the top cap, separated in sections. d) Details of the slide, separated in sections.

In Figure 8.2a is shown the 3D printed mixer in four views (superior, frontal, perspective and right), that the Rhinoceros program displays for the design of the piece. It has a zigzag form, with 3 mm i.d., and 120 x 20 x 40 mm (L x H x W). Figure 8.2b presents a perspective view, showing that the 3D mixer has 2 inputs: one for the air (S4) and the second one to a four-way connector (to connect with C1, Ultima Flo M, the eluate and the cleaning solution); and one output that leads to the flow cell.

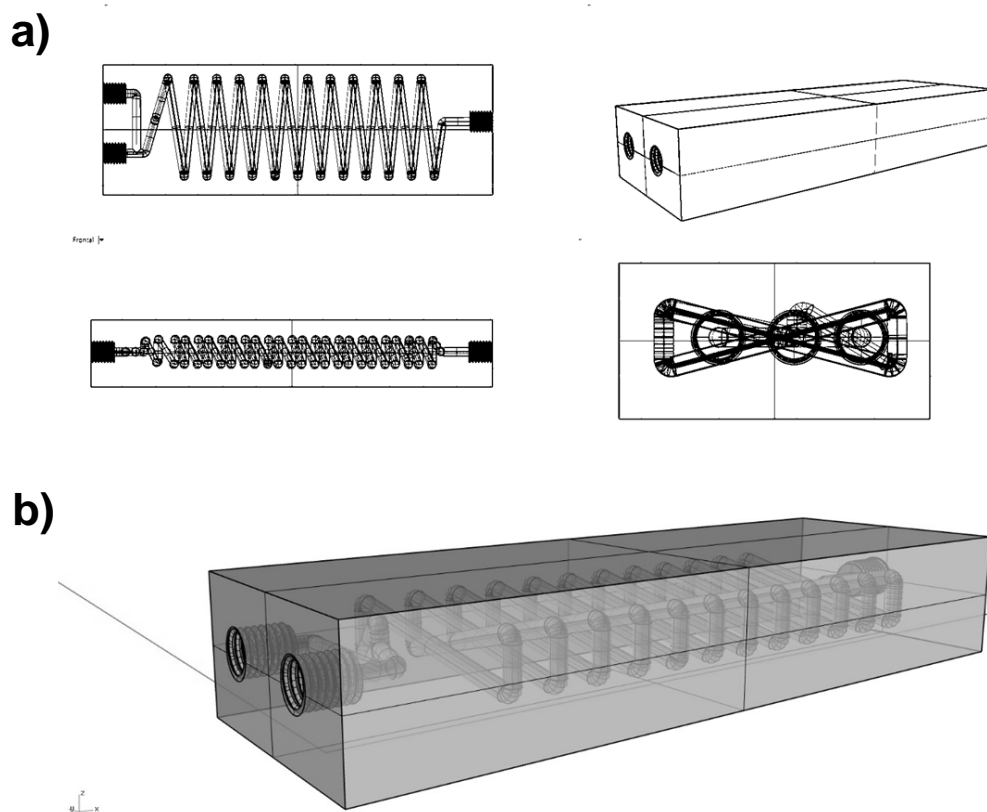


Figure 8.2 Representation of 3D printed mixer. a) Four views of the 3D printed mixer, which the Rhinoceros program displays, when the piece is design. b) Perspective view of the 3D printed mixer.

Both 3D printed devices were performed using a 3D printer Form+1 and Form+2 (Formlabs Inc., Somerville, USA). The resins used were black and clear photoactive (Formlabs), for dark box and mixer, respectively.

In the case of 3D printed mixer, isopropyl alcohol was pumped using a HPLC pump (Waters, Milford, USA) for rinsing the channels filled with unreacted monomers. The 3D printed parts were dried for 15 min at room temperature, and settled between 8-10 hours in a CL-1000 Ultraviolet Crosslinker (UVP, Upland, Canada) using a lamp of 365 nm wavelength.

Each part of the 3D dark box was printed separately, being the printing time for the lower cap 10 h 46 min, with 1503 layers and oriented 50° on the y-axis with stand. The top cap has a printing time of 8 h 37 min, with 1107 layers and oriented 40° on the y-axis with stand. The two side lids were printed in 2 h 30 min, with 333 layers, oriented 40° on the y-axis with stand. Printing time for the 3D mixer was 5h 54 min, with 395 layers, oriented 20° on the x-axis with stand. All the 3D pieces were printed with a resolution of 0.1 mm.

8.2.3. On-line radioactivity detection

The prototype liquid scintillation counter sensor was equipped with a 10 mL flow cell (20 mm e.d. and 37.4 mm of length) made of glass (Anorsa) and two photomultipliers R7600U-200 series (PMT, Hamamatsu Photonics K.K., Shizuoka, Japan) contained in the 3D printed dark and opaque box.

Each PMT has a section size 30 x 30 mm, the photocathode area shape is squared with an effective size of 18 x 18 mm, and it has an efficiency of 35% at 420 nm, its spectral response is between 300-650 nm [112]. Two high voltage power supplies C4900 series (Hamamatsu) were used to power each PMT; it has an input voltage of 12 V and dimension 46 x 24 x 12 mm (L x H x W) [113]. Being supplied by another auxiliary source of 15 V (90 mA), it is possible to obtain an output voltage between 0 and -1250 V.

Two electronic circuits (see Chapter 4, Figure 4.9) were designed to control and independently set the voltage provided to the PMTs. The readout of their output signal was also controlled by these two electronic circuits. A voltage signal was then sent to an analog-to-digital converter (CAEN DT5725, 8 channels 250MS/s, digitizer 640 kS/ch) to detect the peaks corresponding to each disintegration.

The data obtained from both PMTs were treated offline, and a FORTRAN code was developed to perform the coincidence peak detection.

8.2.4. Automatic system set-up

The automatic system for the extraction and detection of ^{90}Sr is shown in Figure 8.3.

The automatic MSFIA-LOV system consists in a multisyringe burette module (BU4S, Crison Instruments, Alella, Barcelona, Spain) of 40000 steps and a monolithic device LOV (Sciware Systems) mounted over an 8 ports selection valve (Crison). LOV was fabricated from methacrylate with 8 integrated microchannels of 1.5 mm i.d. and 16 mm length, except the microcolumn channel that it has 3.2 mm i.d.

The MSFIA module was equipped with two syringes of 5 mL (S1 and S2) and two syringes of 10 mL (S3 and S4) (Hamilton, Switzerland). A three-way solenoid valve is located at the head of each syringe, redirecting the liquid depending of its position ("On" position connects to the manifold and the "Off" position connects to the reservoir).

S1 is connected to the central port of LOV via a holding coil (HC1), and the lateral ports are configured as follows: reservoir of Sr-resin suspended in $8 \text{ mol L}^{-1} \text{ HNO}_3$ and contained in a plastic syringe of 5 mL (port 1), sample or standard solution (port 2), microcolumn of Sr-resin (port 5), $8 \text{ mol L}^{-1} \text{ HNO}_3$ (port 6), $0.01 \text{ mol L}^{-1} \text{ HNO}_3$ (port 7). The microcolumn is packed with 0.055 g of Sr-resin, at the end fiberglass wool to retain the

beads, is placed. The output of microcolumn is connected to an external solenoid valve (V1, MTV-3-n ¼ UKG, Takasago, Japan) to conduct the liquid to the waste or to the 3D printed mixer, via a four-way connector (C1).

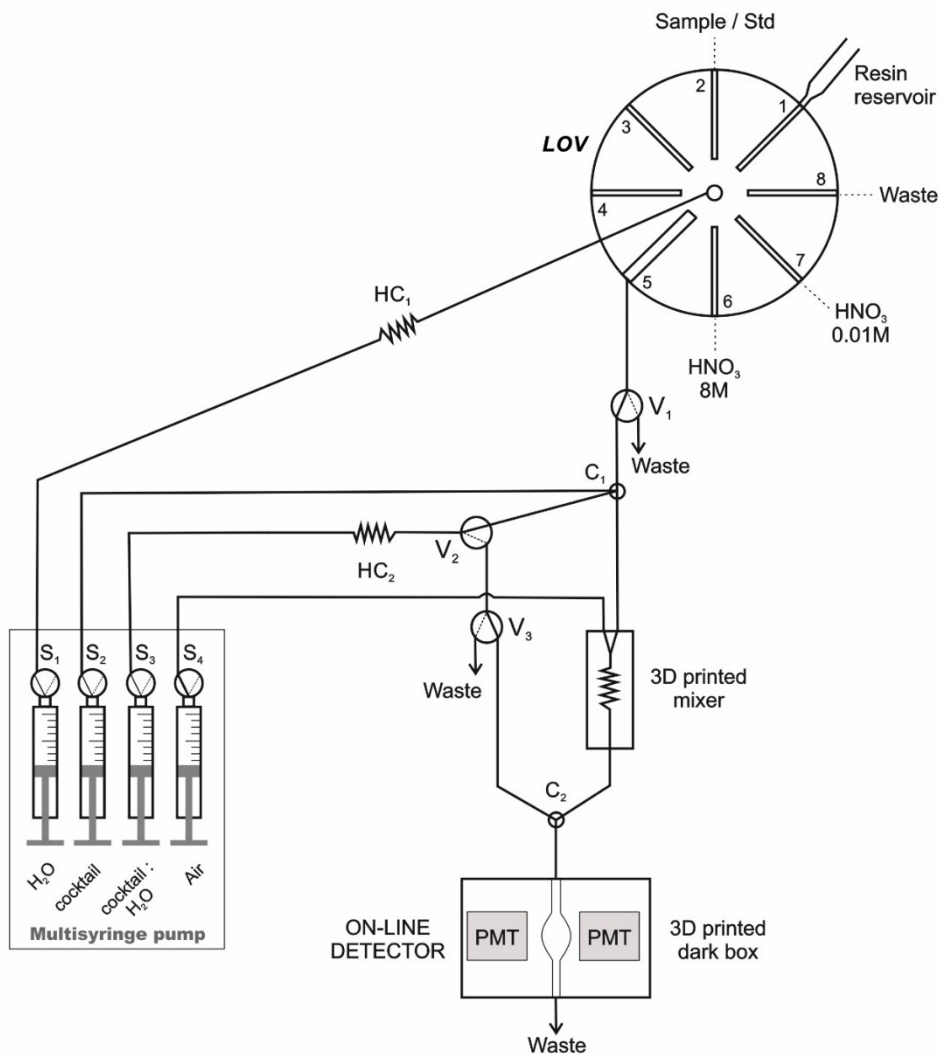


Figure 8.3 Automatic system for extraction/ preconcentration and detection of ⁹⁰Sr using a 3D printed mixer (cocktail to sample ratio 1:1). C: three-way connector, HC: holding coil, PMT: photomultiplier tube, LOV: Lab-on-valve; MSFIA: multisyringe module, S: syringe; V: external solenoid valve.

S2 containing liquid scintillation cocktail and port 5 of the LOV (microcolumn of Sr-resin) were connected to a four-way connector (C1) located previous to the 3D printed mixer.

S3 containing Milli-Q water: Ultima Flo M (proportion 1:1) is connected to V2 via a HC2, and the “On” position connects to C1 to the 3D printed mixer, the “Off” position

connects to V3 (“On” position connects to a three-way connector, C2 to the flow cell for the on-line detection, and the “Off” position connects to the waste).

S4 contains air, and it is directly connected to the 3D printed mixer, to empty the mixer and to ensure the mix between the liquid scintillation and the eluate contained in the flow cell for the on-line detection.

Manifold was made with poly(tetrafluoroethylene) (PTFE) tubing of 1.5 mm i.d., the HC1 and HC2 are 0.72 m and 0.66 m long respectively. C1, C2 were fabricated with polyacetal (Delrin®) and all the connections with polyvinylidene fluoride (PVDF).

The instrumental control was performed with AutoAnalysis 5.0 software (Sciware Systems).

8.2.5. Analytical procedure

The analytical procedure is detailed in Table 8.1, and can be summarized as follows: firstly, the number of dark counts for the prototype sensor was determined: 3 replicates with an update time (i.e. time to accumulate counts) of 100 s each one. Then, Sr-resin was conditioned with 4 mL of 8 mol L⁻¹ HNO₃, and after that ⁹⁰Sr standard was passed through the microcolumn at 0.6 mL min⁻¹ with V1 in “Off” position directed to the waste.

The second step was the elution of ⁹⁰Sr, carried out with 5 mL of 0.01 mol L⁻¹ HNO₃, setting V1 in “On” position directed to the 3D printed mixer at 0.8 ml min⁻¹. Simultaneously, 5 mL of liquid scintillation cocktail (Ultima Flo M) were dispensed, and both, i.e. elution and cocktail (ratio 1:1), are mixed in the 3D printed mixer. After that, S4 is activated picking up 5 mL of air and passed through the 3D printed mixer to empty it. Then, the on-line detection is performed doing 3 replicates, of 100 s detection cycle each one.

The final step consisted in cleaning the system, passing through the microcolumn 4 mL of 8 mol L⁻¹ HNO₃ and 10 mL of Milli-Q water with V1 in the “On” position directed to the 3D mixer. This procedure was repeated 2 times to ensure the total cleaning. After that, the flow cell was emptied; picking up the liquid with S3 and V3 in “On” position, V2 in “Off” position kept in HC2; then the liquid is dispensed to the waste with V2 and V3 in “Off” position, S3 in “On” position.

To remove traces of the reagents used in the microcolumn, 3D printed mixer and the flow cell, a cleaning cycle using 7 mL of 1:1 Milli-Q water: Ultima Flo M with V2 in “On” position was carried out. Again, the flow cell was emptied, carrying out the previously described procedure. After 16 analyses the microcolumn was regenerated, i.e. the used resin was discarded and a new resin was packed into the column.

Table 8.1 General procedure for the extraction and detection of ^{90}Sr .

Step	Flow rate (mL min ⁻¹)	LOV position	S1	S2	S3	S4	V1	V2	V3
1. Column conditioning									
a. Load 4 mL of 8 mol L ⁻¹ HNO ₃	5	6	On	Off	Off	Off	Off	Off	Off
b. Dispense 4 mL of 8 mol L ⁻¹ HNO ₃	1.6	5	On	Off	Off	Off	Off	Off	Off
2. Standard / sample loading									
a. Load X mL of standard / sample into HC1	5	2	On	Off	Off	Off	Off	Off	Off
b. Dispense X mL of standard /sample	1.6	5	On	Off	Off	Off	Off	Off	Off
3. Elution of ^{90}Sr and mixing with the cocktail (Ultima Flo M)									
a. Dispense 5 mL of 0.01 mol L ⁻¹ HNO ₃	0.8	5	On	Off	Off	Off	On	Off	Off
b. Dispense 5 mL of Ultima Flo M	0.8	8	Off	On	Off	Off	Off	Off	Off
4. Emptying the 3D mixer and on-line detection									
a. Dispense 10 mL of air	3	8	Off	Off	Off	On	Off	Off	Off
b. Wait for the on-line detection by doing 3 replicates, of 100 s detection cycle each one									
5. Cleaning procedure									
a. Dispense 4 mL of 8 mol L ⁻¹ HNO ₃	1.6	5	On	Off	Off	Off	On	Off	Off
b. Dispense 10 mL of Milli-Q water	1.6	5	On	Off	Off	Off	On	Off	Off
c. Repeat stage a and b two times									
d. Dispense 7 mL of 1:1 Milli-Q water: Ultima Flo M	3	8	Off	Off	On	Off	Off	On	Off
6. Emptying the flow cell									
a. Load 9 mL of the liquid contained in the flow cell into HC2	1.9	8	Off	Off	On	Off	Off	Off	On
b. Dispense 10 mL of the liquid kept in HC2	5.5	8	Off	Off	On	Off	Off	Off	Off

S1: H₂O, S2: Ultima Flo M, S3: Milli-Q water: Ultima Flo M, S4: air. S1, S2, S3, S4 and V: Off indicates liquid to the container and position On to the system.

8.3. Results and discussion

8.3.1. Optimization of the mix between the cocktail and eluate

Different devices dedicated to mix the eluate and the scintillation cocktail (Ultima Flo M) were tested, in order to achieve a clear mixture avoiding a milky mix. Moreover, as the automatic systems are highly precise, the mixture will be always the same, i.e. exactly the same proportion between the eluate and the scintillation liquid, and the same flow systems conditions, and therefore the detection is performed at a constant quench. Thus, quenching calibration curves are not necessary.

The optimization of the mix between the cocktail (Ultima Flo M) and the eluate was carried out with two different 3D printed mixers. One is presented in Figure 7.2, and its design is based on a gradient generation published by Shallan et. al [169]. The other one has a helicoidal microflow channel; and its design is based on the work published by Frizzarin et. al [92]. Both 3D printed mixer designs, have an i.d. of 3 mm, 120 mm of length, 20 mm of height, with the only difference that 3D printed mixer with a helicoidal microflow channel has 13.5 mm more width than the other one.

The i.d. of the 3D printed mixer was of 3 mm, because the cocktail has a high viscosity. Thus, in order to avoid overpressure, it was used a higher i.d. for making easier the pass of the cocktail through the channel of the 3D printed mixers.

Besides, tubing reaction coils were tested, assaying two different lengths of 57 and 463 cm, fabricated with PTFE tubing of 1.5 mm i.d.

The best result was obtained with the 3D printed mixer, which design is based on a gradient generation, obtaining a clear and homogeneous mixture.

8.3.2. Optimization of experimental conditions

The optimal working conditions for the extraction of ^{90}Sr using Sr-resin were already studied in previous works [20,59,61,194], using $8 \text{ mol L}^{-1} \text{ HNO}_3$ as retention medium. Sr retention increases continuously with the increasing concentration of HNO_3 up to 8 mol L^{-1} approximately [20]. The strontium elution can be performed with water or dilute nitric acid [20], in this work it was used $0.01 \text{ mol L}^{-1} \text{ HNO}_3$ [61].

The optimization of the flow and chemical variables was carried out with the manifold, but doing off-line detection exploiting a LBPC Canberra LB4200, equipped with four detectors, employing an average beta efficiency of 32%. The measurements were carried out with the voltage adjusted to 1320 V for simultaneous alpha/beta mode and a counting time of 1000 s. For the data acquisition it was used Apex software. Once this part of optimization was completed, the flow system was coupled to the on-line detector.

The eluent volume was studied for two volumes 5 and 7.5 mL, making elution of 120, 240, 360 and 480 Bq.

The quantification of ^{90}Sr beta activity in a LBPC was performed, as described below: the eluted fraction was recollected and transferred to a stainless-steel planchette with Milli-Q water and evaporated to dryness with an infrared lamp [59].

For both volumes (5 and 7.5 mL), satisfactory recoveries were obtained between 82-110%. Therefore, an eluent volume of 5 mL was chosen as working volume in order to decrease the eluent time, and the reagent consumption.

Two flow cells were tested with capacities of 10 and 15 mL, in order to study the proportion between eluate and scintillation cocktail, 1:1 and 1:2 respectively. Results indicate that the flow cell of 10 mL using a proportion 1:1 of eluate: liquid scintillation cocktail is enough to make the detection.

In addition, the durability of the resin packing of the microcolumn was studied, by doing 16 consecutive injections of 120 Bq with the same packing column obtaining recoveries of $108\pm 10\%$ with an RSD 9%. The results obtained from 9 consecutive injections show a low RSD (5%) with recoveries of $113\pm 4\%$.

8.3.3. Cleaning procedure

In order to study the cross-contamination, reagent blanks were run after 16 consecutive ^{90}Sr standard analysis (durability assay). Performing one cleaning cycle (4 mL of $8\text{ mol L}^{-1}\text{ HNO}_3$ and 10 mL of Milli-Q water) between standard and blank analysis, it was obtained a blank signal corresponding to carry-over of 1% of the sample activity in the first blank, in concordance with a previous work [20]. With the objective to decrease the cross-contamination, two cleaning cycles were made with 4 mL of $8\text{ mol L}^{-1}\text{ HNO}_3$ and 10 mL of Milli-Q water. Thus, a carry-over of 0.4% in the blank signal was obtained after analyzing a standard of 120 Bq ^{90}Sr .

With the aim to eliminate traces of nitric acid used in the previous cleaning step, one additional cleaning cycle was made with 7 mL Milli-Q water: scintillation liquid (proportion 1:1).

8.3.4. Background

The background of the sensor was 10 Bq, obtained from the background counts corrected with the efficiency of the analysis. The background counts are the sum of all the counts during the 100 s corresponds to the detection cycle.

8.4. Conclusions

A prototype of the sensor including all the steps of the analytical protocol and the on-line detection was satisfactorily developed. The hyphenation of flow analysis techniques with an on-line detector makes possible to achieve the highest degree of automation for ^{90}Sr determination. MSFIA provides the versatility, ruggedness and a precise control of the flow rate and reagent volumes, whereas LOV allows the integration of some channels in a unique device and the automatic regeneration of the column packing. Additionally, the analyst safety is incremented with the minimization of radioactive samples handling, and also decrease the sample and reagent consumption. The fully automated method allows the analysis of ^{90}Sr in less than 2 h, which is very fast response-time compared with 2 days required by the manual analytical protocol and a conventional radiometric detection. Regarding the future, this work opens a new approach to the determination of ^{90}Sr and ^{89}Sr , both present in a nuclear accident by making a slight modification in the flow system.

The use of 3D printing technology allowed the miniaturization of the system to a portable setup, with the objective to transport the system to a contaminated area, so the transport radioactive samples from nuclear accident areas would no longer be mandatory. Besides, this technology enables the precise deposition layer-by-layer, which has been explored in analytical chemistry field, for the design of unprecedented flow-based and low-cost devices for the automation of different methodologies.

CHAPTER 9

FINAL CONCLUSIONS

This thesis involves the development of different devices based on 3D printing technology and numerical control tools, for its integration in automatic flow systems for determining radionuclides in residues and environmental samples.

The first device, a flow cell designed to contain solid matrices, was fabricated with numerical control tools, and successfully integrated in a system based on two flow injection analysis techniques, i.e. MSFIA and LOV, which allowed the on-line lixiviation, extraction and preconcentration of ^{226}Ra , U and Th. The proposed system made possible the development of two dynamic lixiviation studies, one for ^{226}Ra from phosphogypsum (PG) samples, and the other one for U and Th from environmental solid matrices, i.e. soil, sediment and PG. A similar behaviour of the three radionuclides was observed under dynamic lixiviation conditions, showing that the activity concentration of each radionuclide decrease for successive fractions. The main difference was observed by using rainwater at pH 5.4 as extractant, showing a great release of ^{226}Ra (up to 25%) compared with the low release of U and Th (up to 0.05% and 0.005%, respectively) from PG samples. The proposed systems allowed a new approach to the leaching process, based on dynamic leaching with constant renewal of the extractant that simulates the characteristics of the actual leaching process given in the environment.

The second device, a cube to support a selective extractant, was fabricated using SLA 3D technology, and coated with TEVA resin for the extraction of U. This device allowed the pretreatment, extraction and preconcentration of U in environmental samples, and it was successfully included in a container and integrated in a SIA system configuration with ICP-MS off-line detection. Both 3D printed devices have shown satisfactory analytical results, and were applied to the U extraction in real samples without any pretreatment, e.g. PG and different kind of water samples (tap, mineral and groundwater). The main features of the proposed extraction technique are simplicity, selectivity, low operational costs and robustness, attaining self-manufacturing techniques to design novel analytical tools.

A prototype sensor is a fully automated system, which allowed the extraction and on-line detection of ^{90}Sr . The detection system, developed in collaboration with the company iC-Málaga, is based on a liquid scintillation counter using photomultiplier tubes. The automatic system combines the LOV and MSFIA techniques, integrating two 3D printed devices into the automatic system, a dark box to isolate the flow cell to the light and a mixer to achieve a homogeneous mixture between the eluate and the scintillation liquid. The prototype allowed to involve all steps of the analytical protocol, including the extraction and preconcentration of ^{90}Sr , the mixture of the eluate with the scintillation liquid and the on-line count of the beta emissions. This hyphenation allowed the highest degree of automatization, and the increase the safety of the analyst by decreasing the

manipulation of radioactive samples. The use of 3D printing technology allowed the miniaturization of the system, by being transported in a contaminated area.

Summarizing, it is considered that the integration of the devices designed and fabricated in this thesis, offer a new alternative to different studies and applications, by allowing both, the automation and the miniaturization of the systems.

REFERENCES

- [1] D. Larivière, N. Guérin, Natural Radioactivity, in: D.A. Atwood (Ed.), Radionucl. Environ., First edit, John Wiley & Sons, Ltd., Chichester, West Sussex, United Kingdom., 2010: pp. 1–17.
- [2] M. Eisenbud, T. Gesell, Natural Radioactivity, in: Environ. Radioact., Elsevier, 1997: pp. 134–200.
- [3] National Academy of Science, Environmental Protection Agency, Evaluation of Guidelines for Exposures to Technologically Enhanced Naturally Occurring Radioactive Materials, National Academies Press, Washington, D.C. 20418, 1999.
- [4] Y. Fajardo González, Desarrollo de nuevos métodos de análisis en flujo para la determinación de isótopos estables y radioactivos, Universidad de las Islas Baleares, 2007.
- [5] R. Rodríguez Maese, Automatización de métodos radioquímicos para la separación y preconcentración de radionúclidos en muestras ambientales, Universidad de las Islas Baleares y Centro de Investigación en Materiales Avanzados, S.C., 2016.
- [6] U. United Nations Scientific Committee on the Effects of Atomic Radiation, Sources and Effects of Ionization Radiation. Report to the General Assembly Volume I: Sources, United Nations, New York, 2000.
- [7] Environmental Protection Agency (EPA), Technologically Enhanced Naturally Occurring Radioactive Materials (TENORM), (2017). <https://www.epa.gov/radiation/technologically-enhanced-naturally-occurring-radioactive-materials-tenorm> (accessed January 30, 2018).
- [8] International Atomic Energy Agency (IAEA), The environmental behaviour of radium: revised edition, Vienna (Austria), 2014.
- [9] Environmental Protection Agency (EPA), TENORM: Consumer Products, (2017). <https://www.epa.gov/radiation/tenorm-consumer-products#self> (accessed January 31, 2018).
- [10] R. Rodríguez, J. Avivar, L. Ferrer, L.O. Leal, V. Cerdà, Uranium monitoring tool for rapid analysis of environmental samples based on automated liquid-liquid microextraction, Talanta. 134 (2015) 674–680.
- [11] Association of State and Territorial, Solid Waste Management Officials, Incidental TENORM : A Guidance for State Solid Waste Managers, Washington, D.C. 20001, 2011.
- [12] J.L. Aguado, J.P. Bolívar, E.G. San Miguel, R. García-Tenorio, Ra and U isotopes

- determination in phosphogypsum leachates by alpha-particle spectrometry, *Radioact. Environ.* 7 (2005) 160–165.
- [13] P.P. Haridasan, C.G. Maniyan, P.M.B. Pillai, A.H. Khan, Dissolution characteristics of ^{226}Ra from phosphogypsum, *J. Environ. Radioact.* 62 (2002) 287–294.
- [14] M.F. L'Annunziata, Radiation Physics and Radionuclide Decay, in: M.F. L'Annunziata (Ed.), *Handb. Radioact. Anal.*, Third edit, Elsevier Inc., Waltham, MA 02451 USA, 2012: pp. 33–42.
- [15] J.W. Mietelski, Anthropogenic Radioactivity, in: D.A. Atwood (Ed.), *Radionucl. Environ.*, First edit, John Wiley & Sons, Ltd., Chichester, West Sussex, United Kingdom., 2010: pp. 19–34.
- [16] M. Trojanowicz, K. Kołacińska, J.W. Grate, A review of flow analysis methods for determination of radionuclides in nuclear wastes and nuclear reactor coolants, *Talanta.* 183 (2018) 70–82.
- [17] N. Vajda, C.K. Kim, Determination of radiostrontium isotopes: A review of analytical methodology, *Appl. Radiat. Isot.* 68 (2010) 2306–2326.
- [18] G. Steinhauser, A. Brandl, T.E. Johnson, Comparison of the Chernobyl and Fukushima nuclear accidents: A review of the environmental impacts, *Sci. Total Environ.* 470–471 (2014) 800–817.
- [19] S.P. Gaschak, Y.A. Makliuk, A.M. Maksimenko, M.D. Bondarkov, I. Chizhervsky, E.F. Caldwell, G.T. Jannik, E.B. Farfán, Frequency distributions of ^{90}Sr and ^{137}Cs concentrations in an ecosystem of the “red forest” area in the Chernobyl exclusion zone, *Health Phys.* 101 (2011) 409–415.
- [20] J.W. Grate, R. Strebin, J. Janata, O. Egorov, J. Ruzicka, Automated analysis of radionuclides in nuclear waste: rapid determination of ^{90}Sr by sequential injection analysis., *Sect. Title Nucl. Technol.* 68 (1996) 333–340.
- [21] H. Vandenhove, F. Verzezen, E.R. Landa, Radium, in: D.A. Atwood (Ed.), *Radionucl. Environ.*, First edit, John Wiley & Sons, Ltd., Chichester, West Sussex, United Kingdom., 2010: pp. 97–106.
- [22] Y. Fajardo, E. Gómez, F. Garcias, V. Cerdà, M. Casas, Development of an MSFIA-MPFS pre-treatment method for radium determination in water samples, *Talanta.* 71 (2007) 1172–1179.
- [23] M. Villa, H.P. Moreno, G. Manjón, Determination of ^{226}Ra and ^{224}Ra in sediments samples by liquid scintillation counting, *Radiat. Meas.* 39 (2005) 543–550.
- [24] Agency for Toxic Substance and Disease Registry, U.S. Public Health Service, U.S. Environmental Protection Agency, Toxicological Profile for Radium, 1990.
- [25] H. Vandenhove, C. Hurtgen, Uranium, in: D.A. Atwood (Ed.), *Radionucl. Environ.*,

- First edit, John Wiley & Sons, Ltd., Chichester, West Sussex, United Kingdom., 2010: pp. 261–271.
- [26] Agency for Toxic Substances and Disease Registry (ATSDR), Environmental Protection Agency (EPA), Toxicological Profile for Uranium, Atlanta, Georgia, 2013.
- [27] Z.U.W. Mahmood, C.A.R. Mohamed, Thorium, in: D.A. Atwood (Ed.), Radionucl. Environ., First edit, John Wiley & Sons, Ltd., Chichester, West Sussex, United Kingdom., 2010: pp. 247–252.
- [28] Environmental Protection Agency (EPA), EPA Facts about Thorium, 1–2.
- [29] Agency for Toxic Substances and Disease Registry (ATSDR), Environmental Protection Agency (EPA), Toxicological Profile for Strontium, 2004.
- [30] F.J. Guillén, A. Baeza, A. Salas, Strontium, in: D.A. Atwood (Ed.), Radionucl. Environ., First edit, John Wiley & Sons, Ltd., Chichester, West Sussex, United Kingdom., 2010: pp. 79–93.
- [31] Environmental Protection Agency (EPA), EPA Facts about Strontium-90, United States.
- [32] V. Cerdà, L. Ferrer, J. Avivar, A. Cerdà, Evolution and Description of the Principal Flow Techniques, in: Flow Anal. A Pract. Guid., first edit, Elsevier Science Ltd, Amsterdam, The Netherlands, 2014: pp. 1–42.
- [33] M. Trojanowicz, Advances in flow analysis, Wiley-VHC, Weinheim, Germany, 2008.
- [34] Y. Fajardo, J. Avivar, L. Ferrer, E. Gómez, V. Cerdà, M. Casas, Automation of radiochemical analysis by applying flow techniques to environmental samples, TrAC Trends Anal. Chem. 29 (2010) 1399–1408.
- [35] V. Cerdà, L. Ferrer, J. Avivar, A. Cerdà, Automating Radiochemical Analysis, in: Flow Anal. A Pract. Guid., First edit, Elsevier Science Ltd, Amsterdam, The Netherlands, 2014: pp. 247–264.
- [36] R. Broda, A review of the triple-to-double coincidence ratio (TDCR) method for standardizing radionuclides, Appl. Radiat. Isot. 58 (2003) 585–594.
- [37] C.F. Poole, New trends in solid-phase extraction, TrAC - Trends Anal. Chem. 22 (2003) 362–373.
- [38] Supelco, Sigma-Aldrich Co., Guide to Solid Phase Extraction, Bellefonte, USA, 1998.
- [39] D.T. Harvey, Chapter 8. Gravimetric Methods, in: Anal. Chem. 2.0: pp. 355–410. [https://chem.libretexts.org/Textbook_Maps/Analytical_Chemistry/Book%3A_Analytical_Chemistry_2.0_\(Harvey\)](https://chem.libretexts.org/Textbook_Maps/Analytical_Chemistry/Book%3A_Analytical_Chemistry_2.0_(Harvey)).
- [40] Chapter 3, Gravimetry. <http://www5.csudh.edu/oliver/che230/textbook/ch03.htm>

- (accessed August 18, 2018).
- [41] I.M. Kolthoff, Theory of Coprecipitation. The Formation and Properties of Crystalline Precipitates, *Anal. Chem.* 36 (1932) 860–881.
- [42] T. Zhang, K. Gregory, R.W. Hammack, R.D. Vidic, Co-precipitation of radium with barium and strontium sulfate and its impact on the fate of radium during treatment of produced water from unconventional gas extraction, *Environ. Sci. Technol.* 48 (2014) 4596–4603.
- [43] R. Rodríguez, A. Borràs, L. Leal, V. Cerdà, L. Ferrer, MSFIA-LOV system for ^{226}Ra isolation and pre-concentration from water samples previous radiometric detection, *Anal. Chim. Acta.* 911 (2016) 75–81.
- [44] J.L. Aguado, J.P. Bolívar, ^{226}Ra determination in phosphogypsum by alpha-particle spectrometry, *Czechoslov. J. Phys.* 49 (1999) 439–444.
- [45] M. Rodas Ceballos, A. Borràs, R. García-Tenorio, R. Rodríguez, J.M. Estela, V. Cerdà, L. Ferrer, ^{226}Ra dynamic lixiviation from phosphogypsum samples by an automatic flow-through system with integrated renewable solid-phase extraction, *Talanta.* 167 (2017) 398–403.
- [46] G. Jia, J. Jia, Determination of radium isotopes in environmental samples by gamma spectrometry, liquid scintillation counting and alpha spectrometry: a review of analytical methodology, *J. Environ. Radioact.* 106 (2012) 98–119.
- [47] S. Shariati, Y. Yamini, M. Zanjani Khalili, Simultaneous preconcentration and determination of U(VI), Th(IV), Zr(IV) and Hf(IV) ions in aqueous samples using micelle-mediated extraction coupled to inductively coupled plasma-optical emission spectrometry, *J. Hazard. Mater.* 156 (2008) 583–590.
- [48] S.R. Yousefi, S.J. Ahmadi, F. Shemirani, M.R. Jamali, M. Salavati-Niasari, Simultaneous extraction and preconcentration of uranium and thorium in aqueous samples by new modified mesoporous silica prior to inductively coupled plasma optical emission spectrometry determination, *Talanta.* 80 (2009) 212–217.
- [49] N. Clavier, E. du F. de Kerdaniel, N. Dacheux, P. Le Coustumer, R. Drot, J. Ravaux, E. Simoni, Behavior of thorium–uranium (IV) phosphate–diphosphate sintered samples during leaching tests. Part II. Saturation processes, *J. Nucl. Mater.* 349 (2006) 304–316.
- [50] N. Dacheux, N. Clavier, J. Ritt, Behavior of thorium–uranium (IV) phosphate–diphosphate sintered samples during leaching tests. Part I – Kinetic study, *J. Nucl. Mater.* 349 (2006) 291–303.
- [51] N. Dacheux, J. Aupiais, Determination of Uranium, Thorium, Plutonium, Americium, and Curium Ultratracés by Photon Electron Rejecting α Liquid Scintillation, *Anal. Chem.* 69 (1997) 2275–2282.

- [52] J. Avivar, L. Ferrer, M. Casas, V. Cerdà, Fully automated lab-on-valve-multisyringe flow injection analysis-ICP-MS system: an effective tool for fast, sensitive and selective determination of thorium and uranium at environmental levels exploiting solid phase extraction, *J. Anal. At. Spectrom.* 27 (2012) 327–334.
- [53] M. Rodas Ceballos, R. García-Tenorio, J.M. Estela, V. Cerdà, L. Ferrer, An integrated automatic system to evaluate U and Th dynamic lixiviation from solid matrices, and to extract/pre-concentrate leached analytes previous ICP-MS detection, *Talanta.* 175 (2017) 507–513.
- [54] F.A. Aydin, M. Soylak, Solid phase extraction and preconcentration of uranium(VI) and thorium(IV) on Duolite XAD761 prior to their inductively coupled plasma mass spectrometric determination, *Talanta.* 72 (2007) 187–192.
- [55] E.R. Unsworth, J.M. Cook, S.J. Hill, Determination of uranium and thorium in natural waters with a high matrix concentration using solid-phase extraction inductively coupled plasma mass spectrometry, *Anal. Chim. Acta.* 442 (2001) 141–146.
- [56] J.E. Azparren, A. Fernandez-Rodriguez, G. Vallejo, Diagnosing death by drowning in fresh water using blood strontium as an indicator, *Forensic Sci. Int.* 137 (2003) 55–59.
- [57] C.M. Almeida, M.T.S.D. Vasconcelos, ICP-MS determination of strontium isotope ratio in wine in order to be used as a fingerprint of its regional origin, *J. Anal. At. Spectrom.* 16 (2001) 607–611.
- [58] P. Roos, Analysis of radionuclides using ICP-MS, *Radioact. Environ.* 11 (2008) 295–330.
- [59] Y. Fajardo, E. Gómez, F. Mas, F. Garcias, V. Cerdà, M. Casas, Multisyringe flow injection analysis of stable and radioactive strontium in samples of environmental interest, *Appl. Radiat. Isot.* 61 (2004) 273–277.
- [60] H. Altundag, M. Tuzen, Comparison of dry, wet and microwave digestion methods for the multi element determination in some dried fruit samples by ICP-OES, *Food Chem. Toxicol.* 49 (2011) 2800–2807.
- [61] R. Rodríguez, J. Avivar, L. Ferrer, L.O. Leal, V. Cerdà, Automated total and radioactive strontium separation and preconcentration in samples of environmental interest exploiting a lab-on-valve system, *Talanta.* 96 (2012) 96–101.
- [62] J.J. Mateos, E. Gómez, F. Garcias, M. Casas, V. Cerdà, Rapid $^{90}\text{Sr}/^{90}\text{Y}$ determination in water samples using a sequential injection method, *Appl. Radiat. Isot.* 53 (2000) 139–144.
- [63] H. Amano, N. Yanase, Measurement of ^{90}Sr in environmental samples by cation-

- exchange and liquid scintillation counting, *Talanta*. 37 (1990) 585–590.
- [64] K.H. Hong, Y.H. Cho, M.H. Lee, G.S. Choi, C.W. Lee, Simultaneous measurement of ^{89}Sr and ^{90}Sr in aqueous samples by liquid scintillation counting using the spectrum unfolding method, *Appl. Radiat. Isot.* 54 (2001) 299–305.
- [65] Z. Grahek, N. Zecevic, S. Lulic, Possibility of rapid determination of low-level Sr-90 activity by combination of extraction chromatography separation and Cherenkov counting, *Anal. Chim. Acta.* 399 (1999) 237–247.
- [66] D.D. Rao, S.T. Mehendarge, S. Chandramouli, A.G. Hegde, U.C. Mishra, Application of Cherenkov radiation counting for determination of ^{90}Sr in environmental samples, *J. Environ. Radioact.* 48 (2000) 49–57.
- [67] M. Uesugi, R. Watanabe, H. Sakai, A. Yokoyama, Rapid method for determination of ^{90}Sr in seawater by liquid scintillation counting with an extractive scintillator, *Talanta*. 178 (2018) 339–347.
- [68] K. Kossert, O.J. Nähle, Disproof of solar influence on the decay rates of $^{90}\text{Sr}/^{90}\text{Y}$, *Astropart. Phys.* 69 (2015) 18–23.
- [69] J.W. Grate, O.B. Egorov, M.J. O'Hara, T.A. DeVol, Radionuclide sensors for environmental monitoring: From flow injection solid-phase absorptiometry to equilibrium-based preconcentrating minicolumn sensors with radiometric detection, *Chem. Rev.* 108 (2008) 543–562.
- [70] B.C. Gross, J.L. Erkal, S.Y. Lockwood, C. Chen, D.M. Spence, Evaluation of 3D printing and its potential impact on biotechnology and the chemical sciences, *Anal. Chem.* 86 (2014) 3240–3253.
- [71] M. Biggs, A. Pandit, D.I. Zeugolis, 2D imprinted substrates and 3D electrospun scaffolds revolutionize biomedicine, *Nanomedicine*. 11 (2016) 989–992.
- [72] S. Tsuda, J. Hussain, D. Doran, M. Hezwani, P.J. Robinsons, M. Yoshida, L. Cronin, Customizable 3D Printed 'Plug and Play' Millifluidic Devices for Programmable Fluidics, *PLoS One*. 10 (2015) 1–13.
- [73] C.K. Su, P.J. Peng, Y.C. Sun, Fully 3D-Printed Preconcentrator for Selective Extraction of Trace Elements in Seawater, *Anal. Chem.* 87 (2015) 6945–6950.
- [74] J. Prikryl, F. Foret, Fluorescence Detector for Capillary Separations Fabricated by 3D Printing, *Anal. Chem.* 86 (2014) 11951–11956.
- [75] M. Vaezi, H. Setiz, S. Yang, A review on 3D micro-additive manufacturing technologies, *Int. J. Adv. Manuf. Technol.* 67 (2013) 1721–1754.
- [76] V. Ferreras Paz, M. Emons, K. Obata, A. Ovsiankov, K. Frenner, S. Peterhänsel, B. Chichkov, C. Reinhardt, U. Morgner, W. Osten, Development of functional sub-100 nm structures with 3D two-photon polymerization technique and optical methods for characterization, *J. Laser Appl.* 24 (2012) 420024.

- [77] Formlabs Inc., The Ultimate Guide to Stereolithography (SLA) 3D Printing, (2017) 1–23. <https://formlabs.com/blog/ultimate-guide-to-stereolithography-sla-3d-printing/>.
- [78] Stratasys, Tecnología PolyJet. <http://www.stratasys.com/es/impresoras-3d/technologies/polyjet-technology> (accessed February 5, 2018).
- [79] J.C. McDonald, G.M. Whitesides, Poly(dimethylsiloxane) as a material for fabricating microfluidic devices, *Acc. Chem. Res.* 35 (2002) 491–499.
- [80] N.P. Macdonald, S.A. Currivan, L. Tedone, B. Paull, Direct Production of Microstructured Surfaces for Planar Chromatography Using 3D Printing, *Anal. Chem.* 89 (2017) 2457–2463.
- [81] C. Calderilla, F. Maya, V. Cerdà, L.O. Leal, 3D printed device including disk-based solid-phase extraction for the automated speciation of iron using the multisyringe flow injection analysis technique, *Talanta.* 175 (2017) 463–469.
- [82] J. Ruzicka, G.D. Marshall, Sequential injection: a new concept for chemical sensors, process analysis and laboratory assays, *Anal. Chim. Acta.* 237 (1990) 329–343.
- [83] F. Maya, Desarrollo de nuevas metodologías analíticas de interés medioambiental y clínico mediante la técnica de análisis por inyección en flujo multijeringa, Universidad e las Islas Baleares, 2010.
- [84] A. Economou, Sequential-injection analysis (SIA): A useful tool for on-line sample-handling and pre-treatment, *TrAC Trends Anal. Chem.* 24 (2005) 416–425.
- [85] B. Beltrán, J. Avivar, M. Mola, L. Ferrer, V. Cerdà, L.O. Leal, Automated method for simultaneous lead and strontium isotopic analysis applied to rainwater samples and airborne particulate filters (PM10), *Environ. Sci. Technol.* 47 (2013) 9850–9857.
- [86] H.M. Oliveira, M.A. Segundo, J.L.F.C. Lima, V. Cerdà, Multisyringe flow injection system for solid-phase extraction coupled to liquid chromatography using monolithic column for screening of phenolic pollutants, *Talanta.* 77 (2009) 1466–1472.
- [87] F. Maya, J.M. Estela, V. Cerdà, Multisyringe ion chromatography with chemiluminescence detection for the determination of oxalate in beer and urine samples, *Microchim. Acta.* 173 (2010) 33–41.
- [88] F. Maya, J.M. Estela, V. Cerdà, Interfacing on-line solid phase extraction with monolithic column multisyringe chromatography and chemiluminescence detection: An effective tool for fast, sensitive and selective determination of thiazide diuretics, *Talanta.* 80 (2010) 1333–1340.
- [89] Y. Fajardo, L. Ferrer, E. Gómez, F. Garcias, M. Casas, V. Cerdà, Development of

- an automatic method for americium and plutonium separation and preconcentration using an multisyringe flow injection analysis-multipumping flow system, *Anal. Chem.* 80 (2008) 195–202.
- [90] P. Phansi, C. Henríquez, E. Palacio, D. Nacapricha, V. Cerdà, An automated in-chip-catalytic–spectrophotometric method for determination of copper(II) using a multisyringe flow injection analysis-multipumping flow system, *Anal. Methods*. 6 (2014) 8494–8504.
- [91] R. Rodríguez, J. Avivar, L.O. Leal, V. Cerdà, L. Ferrer, Strategies for automating solid-phase extraction and liquid-liquid extraction in radiochemical analysis, *TrAC - Trends Anal. Chem.* 76 (2016) 145–152.
- [92] R. M. Frizzarin, E. Aguado, L.A. Portugal, D. Moreno, J.M. Estela, F.R.P. Rocha, V. Cerdà, A portable multi-syringe flow system for spectrofluorimetric determination of iodide in seawater, *Talanta*. 144 (2015) 1155–1162.
- [93] J. Ruzicka, Lab-on-valve: universal microflow analyzer based on sequential and bead injection, *Analyst*. 125 (2000) 1053–1060.
- [94] Triskem International, Extraction Chromatography: Technical Documentation, 1–39. http://www.triskem-international.com/iso_album/technical_doc_general_v6_en_ht_web.pdf (accessed February 7, 2018).
- [95] Triskem International, UTEVA resin specifications, France, n.d. http://www.triskem-international.com/iso_album/ft_resine_uteva_en_160927.pdf.
- [96] Triskem International, TEVA Resin, (2016) 2–5.
- [97] J.W. Grate, M.J. O’Hara, O.B. Egorov, Automation of extraction chromatographic and ion exchange separations for radiochemical analysis and monitoring, in: B.A. Moyer (Ed.), *Ion Exch. Solvent Extr. A Ser. Adv.*, volume 19, CRC Press, Taylor & Francis Group, United States of America, 2010: pp. 515–562.
- [98] Triskem International, Triskem Sr Resin Product Sheet, 33 (2016) 3–6.
- [99] Iontosorb bed cellulose derivatives. <http://www.iontosorb.cz/> (accessed February 25, 2016).
- [100] X. Hou, P. Roos, Critical comparison of radiometric and mass spectrometric methods for the determination of radionuclides in environmental, biological and nuclear waste samples, *Anal. Chim. Acta.* 608 (2008) 105–139.
- [101] R. Díaz Zamora, Ventajas y Desventajas del Análisis por ICP-MS de metales pesados en muestras biológicas, (2017) 54–59.
- [102] R. Thomas, *Practical Guide to ICP-MS*, Marcel Dekker, Inc., United States of America, 2004.
- [103] PerkinElmer Ink., *The 30-minute Guide to ICP-MS*, Waltham, MA 02451 USA.

- [104] A. Bazilio, J. Weinrich, *The Easy Guide to: Inductively Coupled Plasma- Mass Spectrometry (ICP-MS)*, 2012.
- [105] M. Sevilla, I. Vallés, J.R. Rosell, X. Dies, *Detección y Medidas de la radiación*, in: X. Aramburu Ortega, J. Bisbal Jorba (Eds.), *Radiac. Ioniz. Util. y Riesgos I*, Primera ed, Edicions UPC, Universitat Politècnica de Catalunya, Barcelona, España, 1994: pp. 247–352.
- [106] *Standard Practice for the Measurement of Radioactivity, Nuclear Counting Instrumentation*, American Society for Testing and Materials, West Conshohocken, PA 19428, 2001.
- [107] Mirion Technologies (Canberra) Inc., LB4200: Multi-Detector Low Background Alpha/Beta Counting System, 2017.
- [108] M.J. Kessler, M.F. L'Annunziata, *Liquid Scintillation Analysis: Principles and Practice*, in: M.F. L'Annunziata (Ed.), *Handb. Radioact. Anal.*, Third edit, Elsevier Inc., Waltham, MA 02451 USA, 2012: pp. 424–542.
- [109] I. PerkinElmer, *Liquid Scintillation Analysis. Science and Technology*, Waltham, MA 02451 USA, 2015. www.perkinelmer.com.
- [110] Crison. Líderes en electroquímica, Bureta dispensadora Multi-Burette 4S-D, (n.d.) 1–4. www.crisoninstruments.com (accessed February 28, 2018).
- [111] Sciware Systems S.L., Selection Valve module, 8 ports, (2018). <https://www.sciware-sl.com/products/injection-selection-valves/item/136-sel-low8hplc> (accessed March 2, 2018).
- [112] Hamamatsu Photonics K.K., Photomultipliers tubes R7600U series, (2016). <https://www.hamamatsu.com/us/en/R7600U-200.html> (accessed September 20, 2017).
- [113] Hamamatsu Photonics K.K., Compact high voltage power supply C4900 series, (2012). https://www.hamamatsu.com/resources/pdf/etd/C4900_TACC1013E.pdf (accessed September 26, 2017).
- [114] Ó. Pozo Ocaña, *Memoria Prácticas Externas: Colaboración en el proyecto AUTORAD*, Mallorca, España, 2016.
- [115] Robert McNeel & Associates, *Características de Rhino 6*, (2018) 1–7. <https://www.rhino3d.com/la/features#large> (accessed March 3, 2018).
- [116] Robert McNeel & Associates., *Objetos de Rhino*, (2017) 1–7. http://docs.mcneel.com/rhino/6/help/es-es/index.htm#information/rhinoobjects.htm%3FTocPath%3DCrear%2520objetos%7C_____1 (accessed March 5, 2018).
- [117] Robert McNeel & Associates., *Dibujar líneas y curvas*, (2017) 1–4. http://docs.mcneel.com/rhino/6/help/es-es/index.htm#seealso/sak_curve.htm

- (accessed March 5, 2018).
- [118] Robert McNeel & Associates., *Objetos Sólidos*, (2010) 1–3. http://docs.mcneel.com/rhino/6/help/es-es/index.htm#seealso/sak_solid.htm (accessed March 5, 2018).
- [119] Robert McNeel & Associates., *Extrusión de curvas y superficies*, (2017) 1–4. http://docs.mcneel.com/rhino/6/help/es-es/index.htm#seealso/sak_extrude.htm (accessed March 5, 2018).
- [120] Formlabs Inc., *Form 1+: An introducing to desktop SLA*, (2014) 1–8.
- [121] Formlabs Inc., *Introducing the Form 1+*, (2014). <https://formlabs.com/blog/introducing-form-1-plus/> (accessed April 10, 2018).
- [122] Formlabs Inc., *Form 2: The most advanced desktop 3D printer ever created*. <https://formlabs.com/3d-printers/form-2/> (accessed April 10, 2018).
- [123] Formlabs Inc., *Safety Data Sheet. Black: Photoreactive resin for Form1+, Form 2*, (2017) 1–8.
- [124] Formlabs Inc., *Safety Data Sheet. Clear: Photoreactive resin for Form1, Form 1+, Form 2*, (2016) 1–8. https://formlabs.com/media/upload/Clear-SDS_u324bsC.pdf.
- [125] Formlabs Inc., *PreForm Software 2.15.1: Print preparation software for Formlabs 3D printers*. <https://formlabs.com/tools/preform/> (accessed April 11, 2018).
- [126] Ultra-Violet Products Limited, *Ultraviolet Crosslinkers Operating Instructions and Service Manual*, 1–16. www.uvp.com.
- [127] V. Cerdà, J.L. Cerdà, A.M. Idris, Optimization using the gradient and simplex methods, *Talanta*. 148 (2016) 641–648.
- [128] R. Leardi, Experimental design in chemistry: A tutorial, *Anal. Chim. Acta*. 652 (2009) 161–172.
- [129] T. Lundstedt, E. Seifert, L. Abramo, B. Thelin, Å. Nyström, J. Pettersen, R. Bergman, Experimental design and optimization, *Chemom. Intell. Lab. Syst.* 42 (1998) 3–40.
- [130] M.A. Bezerra, R.E. Santelli, E.P. Oliveira, L.S. Villar, L.A. Escaleira, Response surface methodology (RSM) as a tool for optimization in analytical chemistry, *Talanta*. 76 (2008) 965–977.
- [131] J.L. Brasil, L.C. Martins, R.R. Ev, J. Dupont, S.L.P. Dias, J.A.A. Sales, C. Airoldi, É.C. Lima, Factorial design for optimization of flow-injection preconcentration procedure for copper(II) determination in natural waters, using 2-aminomethylpyridine grafted silica gel as adsorbent and spectrophotometric detection, *Int. J. Environ. Anal. Chem.* 85 (2005) 475–491.
- [132] International Organization for Standardization (ISO), *ISO 11929: 2000. Determination of the detection limit and decision threshold for ionizing radiation*

- measurements. Part 1, 2, 3 and 4, Geneva, Switzerland, 2000.
- [133] J.M. Rutherford, P. M., Dudas, M. J., Arocena, Radium in phosphogypsum leachates, *J. Environ. Qual.* 24 (1995) 307–314.
- [134] M.J. Gázquez, J.P. Bolívar, R. García-Tenorio, F. Galán, Natural occurring radionuclide waste in Spain: the Huelva phosphogypsum stacks case, in: 1st Spanish Natl. Conf. Adv. Mater. Recycl. Eco – Energy, 2009: pp. 75–78.
- [135] M.S. Al-Hwaiti, J.F. Ranville, P.E. Ross, Bioavailability and mobility of trace metals in phosphogypsum from Aqaba and Eshidiya, Jordan, *Chemie Der Erde - Geochemistry.* 70 (2010) 283–291.
- [136] U.S. Government Publishing Office. Subpart R- National Emission Standard for Radon Emissions from phosphogypsum stacks. http://www.ecfr.gov/cgi-bin/text-idx?SID=3fb89e719353c5dbee592eac8d84c73a&mc=true&node=sp40.9.61.r&rgn=div6#se40.9.61_1201 (accessed April 18, 2016).
- [137] J.-M. Abril, R. García-Tenorio, G. Manjón, Extensive radioactive characterization of a phosphogypsum stack in SW Spain: ^{226}Ra , ^{238}U , ^{210}Po concentrations and ^{222}Rn exhalation rate., *J. Hazard. Mater.* 164 (2009) 790–797.
- [138] J.P. Bolívar, R. García-Tenorio, J. Mas, Radioactivity of Phosphogypsum in the South-West of Spain, *Radiat. Prot. Dosimetry.* 76 (1998) 185–189.
- [139] EPA, Potential uses of phosphogypsum and associated risks. Background information document for 40 CFR 61 Subpart R National Standard for Radon emissions from phosphogypsum stacks, U.S. Environmental Protection Agency Office of Radiation Programs, Washington, D.C. 20460, 1992.
- [140] M. Villa, F. Mosqueda, S. Hurtado, J. Mantero, G. Manjón, R. Periañez, F. Vaca, R. García-Tenorio, Contamination and restoration of an estuary affected by phosphogypsum releases, *Sci. Total Environ.* 408 (2009) 69–77.
- [141] E. Rodríguez López, Movilidad de radionucleidos naturales en fosfoyeso, Universidad Internacional de Andalucía, 2016.
- [142] P.M. Rutherford, M.J. Dudas, R.A. Samek, Environmental impacts of phosphogypsum, *Sci. Total Environ.* 149 (1994) 1–38.
- [143] M.B. Nisti, C.R. Saueia, L.H. Malheiro, G.H. Groppo, B.P. Mazzilli, Lixiviation of natural radionuclides and heavy metals in tropical soils amended with phosphogypsum, *J. Environ. Radioact.* 144 (2015) 120–126.
- [144] G. Olszewski, A. Boryło, B. Skwarzec, The radiological impact of phosphogypsum stockpile in Wiślinka (northern Poland) on the Martwa Wisła river water, *J. Radioanal. Nucl. Chem.* 307 (2016) 653–660.
- [145] M. Azouazi, Y. Ouahidi, S. Fakhi, Y. Andres, J. Abbe, M. Benmansour, Natural radioactivity in phosphates, phosphogypsum and natural waters in Morocco., *J.*

- Environ. Radioact. 54 (2001) 231–242.
- [146] A. May, J.W. Sweeney, Evaluation of radium and toxic element leaching characteristics of Florida phosphogypsum stockpiles, (1984) 140–149.
- [147] J.R. Bacon, C.M. Davidson, Is there a future for sequential chemical extraction?, *Analyst*. 133 (2008) 25–46.
- [148] J. Wang, E.H. Hansen, Sequential injection lab-on-valve: the third generation of flow injection analysis, *TrAC Trends Anal. Chem.* 22 (2003) 225–231.
- [149] J. Zhang, S.M. Liu, X. Lü, W.W. Huang, Characterizing Asian wind-dust transport to the Northwest Pacific Ocean. Direct measurements of the dust flux for two years, *Tellus*. 45B (1993) 335–345.
- [150] M. Thompson, R. Wood, Harmonized guidelines for internal quality control in analytical chemistry laboratories (Technical Report), *Pure Appl. Chem.* 67 (1995) 649–666.
- [151] International Organization for Standardization (ISO), Proficiency testing by interlaboratory comparisons-guidelines. ISO/IEC Guide 43-1: 1997, 1997.
- [152] M. Lourdes Romero González, M. Barrera Izquierdo, F. Valiño García, Evaluación de las intercomparación analítica de radionucleidos en muestras ambientales campaña 2008-2009 (fosfoyeso), 2009.
- [153] C.R.M. Rao, A. Sahuquillo, J.F. Lopez Sanchez, A review of the different methods applied in environmental geochemistry for single and sequential extraction of trace elements in soils and related materials, *Water. Air. Soil Pollut.* 189 (2008) 291–333.
- [154] A.C. Patra, C.G. Sumesh, S. Mohapatra, S.K. Sahoo, R.M. Tripathi, V.D. Puranik, Long-term leaching of uranium from different waste matrices, *J. Environ. Manage.* 92 (2011) 919–925.
- [155] D.H. Moon, D. Dermatas, An evaluation of lead leachability from stabilized/solidified soils under modified semi-dynamic leaching conditions, *Eng. Geol.* 85 (2006) 67–74.
- [156] R.O. Abdel Rahman, A.A. Zaki, A.M. El-Kamash, Modeling the long-term leaching behavior of ^{137}Cs , ^{60}Co , and $^{152,154}\text{Eu}$ radionuclides from cement–clay matrices, *J. Hazard. Mater.* 145 (2007) 372–380.
- [157] M.J. Gázquez, J. Mantero, F. Mosqueda, J.P. Bolívar, R. García-Tenorio, Radioactive characterization of leachates and efflorescences in the neighbouring areas of a phosphogypsum disposal site as a preliminary step before its restoration., *J. Environ. Radioact.* 137 (2014) 79–87.
- [158] V. Cerdà, J.M. Estela, R. Forteza, A. Cladera, E. Becerra, P. Altimira, P. Sitjar, Flow techniques in water analysis, *Talanta*. 50 (1999) 695–705.

- [159] D. Lariviere, V.F. Taylor, R.D. Evans, R.J. Cornett, Radionuclide determination in environmental samples by inductively coupled plasma mass spectrometry, *Spectrochim. Acta Part B At. Spectrosc.* 61 (2006) 877–904.
- [160] J. Merešová, W. Uwe, T. Altizizoglou, Evaluation of EC Interlaboratory Comparison on Radionuclides in Soil, Belgium, 2012.
- [161] J.-M. Abril, R. García-Tenorio, S.M. Enamorado, M.D. Hurtado, L. Andreu, A. Delgado, The cumulative effect of three decades of phosphogypsum amendments in reclaimed marsh soils from SW Spain: ^{226}Ra , ^{238}U and Cd contents in soils and tomato fruit., *Sci. Total Environ.* 403 (2008) 80–8.
- [162] G. Derringer, R. Suich, Simultaneous Optimization of Several Response Variables, *J. Qual. Technol.* 12 (1980) 214–219.
- [163] A.J.G. Santos, B.P. Mazzilli, D.I.T. Fávaro, P.S.C. Silva, Partitioning of radionuclides and trace elements in phosphogypsum and its source materials based on sequential extraction methods, *J. Environ. Radioact.* 87 (2006) 52–61.
- [164] M.P. Beeston, H.J. Glass, J.T. van Elteren, Z. Šlejkovec, Assessment of elemental mobility in soil using a fluidised bed approach with on-line ICP-MS analysis, *Anal. Chim. Acta.* 599 (2007) 264–270.
- [165] International Organization for Standardization (ISO), Evaluation of measurement data - Guide to the expression of Uncertainty in Measurement, in: Geneva, Switzerland, 2008.
- [166] L.A. Currie, Detection and quantification limits: origins and historical overview, *Anal. Chim. Acta.* 391 (1999) 127–134.
- [167] S. Waheed, J.M. Cabot, N.P. Macdonald, T. Lewis, R.M. Guijt, B. Paull, M.C. Breadmore, 3D printed microfluidic devices: enablers and barriers, *Lab Chip.* 16 (2016) 1993–2013.
- [168] K.B. Spilstead, J.J. Learey, E.H. Doeven, G.J. Barbante, S. Mohr, N.W. Barnett, J.M. Terry, R.M. Hall, P.S. Francis, 3D-printed and CNC milled flow-cells for chemiluminescence detection, *Talanta.* 126 (2014) 110–115.
- [169] A.I. Shallan, P. Smejkal, M. Corban, R.M. Guijt, M.C. Breadmore, Cost-effective three-dimensional printing of visibly transparent microchips within minutes, *Anal. Chem.* 86 (2014) 3124–3130.
- [170] C.-K. Su, S.-C. Yen, T.-W. Li, Y.-C. Sun, Enzyme-Immobilized 3D-Printed Reactors for Online Monitoring of Rat Brain Extracellular Glucose and Lactate, *Anal. Chem.* 88 (2016) 6265–6273.
- [171] N.P. Macdonald, J.M. Cabot, P. Smejkal, R.M. Guijt, B. Paull, M.C. Breadmore, Comparing Microfluidic Performance of Three-Dimensional (3D) Printing Platforms, *Anal. Chem.* 89 (2017) 3858–3866.

- [172] É.M. Kataoka, R.C. Murer, J.M. Santos, R.M. Carvalho, M.N. Eberlin, F. Augusto, R.J. Poppi, A.L. Gobbi, L.W. Hantao, Simple, Expendable, 3D-Printed Microfluidic Systems for Sample Preparation of Petroleum, *Anal. Chem.* 89 (2017) 3460–3467.
- [173] C. Chen, Y. Wang, S.Y. Lockwood, D.M. Spence, 3D-printed fluidic devices enable quantitative evaluation of blood components in modified storage solutions for use in transfusion medicine, *Analyst.* 139 (2014) 3219–3226.
- [174] C. Calderilla, F. Maya, V. Cerdà, L.O. Leal, 3D printed device for the automated preconcentration and determination of chromium (VI), *Talanta.* 184 (2018) 15–22.
- [175] R.M. Frizzarin, C. Palomino Cabello, M. del M. Bauzà, L.A. Portugal, F. Maya, V. Cerdà, J.M. Estela, G. Turnes Palomino, Submicrometric Magnetic Nanoporous Carbons Derived from Metal–Organic Frameworks Enabling Automated Electromagnet-Assisted Online Solid-Phase Extraction, *Anal. Chem.* 88 (2016) 6990–6995.
- [176] A.K. Au, N. Bhattacharjee, L.F. Horowitz, T.C. Chang, A. Folch, 3D-printed microfluidic automation., *Lab Chip.* 15 (2015) 1934–1941.
- [177] C.-K. Su, S.-C. Hsia, Y.-C. Sun, Three-dimensional printed sample load/inject valves enabling online monitoring of extracellular calcium and zinc ions in living rat brains, *Anal. Chim. Acta.* 838 (2014) 58–63.
- [178] S.K. Anciaux, M. Geiger, M.T. Bowser, 3D Printed Micro Free-Flow Electrophoresis Device, *Anal. Chem.* 88 (2016) 7675–7682.
- [179] J. Avivar, L. Ferrer, M. Casas, V. Cerdà, Lab on valve-multisyringe flow injection system (LOV-MSFIA) for fully automated uranium determination in environmental samples, *Talanta.* 84 (2011) 1221–1227.
- [180] S. Uchida, R. Garcia-Tenorio, K. Tagami, M. Garcia-León, Determination of U isotopic ratios in environmental samples by ICP-MS, *J. Anal. At. Spectrom.* 15 (2000) 889–892.
- [181] K. Tagami, S. Uchida, Use of TEVA resin for the determination of U isotopes in water samples by Q-ICP-MS, *Appl. Radiat. Isot.* 61 (2004) 255–259.
- [182] E.P. Horwitz, M.L. Dietz, R. Chiarizia, H. Diamond, S.L. Maxwell, M.R. Nelson, Separation and Preconcentration of Actinides by Extraction Chromatography Using a Supported Liquid Anion-Exchanger - Application to the Characterization of High-Level Nuclear Waste Solutions, *Anal. Chim. Acta.* 310 (1995) 63–78.
- [183] J.S. Santos, L.S.G. Teixeira, W.N.L. dos Santos, V.A. Lemos, J.M. Godoy, S.L.C. Ferreira, Uranium determination using atomic spectrometric techniques: An overview, *Anal. Chim. Acta.* 674 (2010) 143–156.
- [184] J. Avivar, L. Ferrer, M. Casas, V. Cerdà, Automated determination of uranium(VI)

- at ultra trace levels exploiting flow techniques and spectrophotometric detection using a liquid waveguide capillary cell., *Anal. Bioanal. Chem.* 397 (2010) 871–878.
- [185] M. Mola, A. Nieto, A. Peñalver, F. Borrull, C. Aguilar, Uranium and thorium sequential separation from norm samples by using a SIA system., *J. Environ. Radioact.* 127 (2014) 82–87.
- [186] B.A. Moyer, ed., *Ion Exchange and Solvent Extraction: A series of advances*, volume 19, CRC Press, Taylor & Francis Group, Boca Raton, FL, 2009.
- [187] J.W. & S. Ltd, ed., *Radionuclides in the environment*, First edit, Chichester, West Sussex, United Kingdom., 2010.
- [188] O. Masson, A. Baeza, J. Bieringer, K. Brudecki, S. Bucci, M. Cappai, F.P. Carvalho, O. Connan, C. Cosma, A. Dalheimer, D. Didier, G. Depuydt, L.E. De Geer, A. De Vismes, L. Gini, F. Groppi, K. Gudnason, R. Gurriaran, D. Hainz, Ó. Halldórsson, D. Hammond, O. Hanley, K. Holeý, Z. Homoki, A. Ioannidou, K. Isajenko, M. Jankovic, C. Katzlberger, M. Kettunen, R. Kierepko, R. Kontro, P.J.M. Kwakman, M. Lecomte, L. Leon Vintro, A.P. Leppänen, B. Lind, G. Lujaniene, P. Mc Ginnity, C.M. Mahon, H. Malá, S. Manenti, M. Manolopoulou, A. Mattila, A. Muring, J.W. Mietelski, B. Møller, S.P. Nielsen, J. Nikolic, R.M.W. Overwater, S.E. Pálsson, C. Papastefanou, I. Penev, M.K. Pham, P.P. Povinec, H. Ramebäck, M.C. Reis, W. Ringer, A. Rodriguez, P. Rulík, P.R.J. Saey, V. Samsonov, C. Schlosser, G. Sgorbati, B. V. Silobritiene, C. Söderström, R. Sogni, L. Solier, M. Sonck, G. Steinhauser, T. Steinkopff, P. Steinmann, S. Stoulos, I. Sýkora, D. Todorovic, N. Tooloutalaie, L. Tositti, J. Tschiersch, A. Ugron, E. Vagena, A. Vargas, H. Wershofen, O. Zhukova, Tracking of airborne radionuclides from the damaged Fukushima Dai-Ichi nuclear reactors by European Networks, *Environ. Sci. Technol.* 45 (2011) 7670–7677.
- [189] B.L. Rosenberg, J.E. Ball, K. Shozugawa, G. Korschinek, M. Hori, K. Nanba, T.E. Johnson, A. Brandl, G. Steinhauser, Radionuclide pollution inside the Fukushima Daiichi exclusion zone, part 1: Depth profiles of radiocesium and strontium-90 in soil, *Appl. Geochemistry.* 85 (2017) 201–208.
- [190] A.F. Seliman, V.N. Bliznyuk, T.A. DeVol, Development of stable extractive scintillating materials for real-time quantification of radiostrontium in aqueous solutions, *J. Radioanal. Nucl. Chem.* 314 (2017) 743–751.
- [191] M.J. O'Hara, S.R. Burge, J.W. Grate, Automated Radioanalytical System for the Determination of Sr-90 in Environmental Water Samples by Y-90 Cherenkov Radiation Counting, *Anal. Chem.* 81 (2009) 1228–1237.
- [192] S.L. Maxwell, B.K. Culligan, Rapid method for determination of radiostrontium in

- emergency milk samples, *J. Radioanal. Nucl. Chem.* 279 (2009) 757–760.
- [193] E. Kabai, L. Hornung, B.T. Savkin, A. Poppitz-Spuhler, L. Hiersche, Fast method and ultra fast screening for determination of ^{90}Sr in milk and dairy products, *Sci. Total Environ.* 410–411 (2011) 235–240.
- [194] E.P. Horwitz, R. Chiarizia, M.L. Dietz, A novel strontium-selective extraction chromatographic resin, *Solvent Extr. Ion Exch.* 10 (1992) 313–336.

ANNEX

Publications resulting from this thesis

1. **^{226}Ra dynamic lixiviation from phosphogypsum samples by an automatic flow-through system with integrated renewable solid-phase extraction.** Melisa Rodas Ceballos, Antoni Borràs, Rafael García-Tenorio, Rogelio Rodríguez, José Manuel Estela, Víctor Cerdà, Laura Ferrer. *Talanta* 167 (2017) 398-403.
2. **An integrated automatic system to evaluate U and Th dynamic lixiviation from solid matrices, and to extract/ pre-concentrate leached analytes previous ICP-MS detection.** Melisa Rodas Ceballos, Rafael García-Tenorio, José Manuel Estela, Víctor Cerdà, Laura Ferrer. *Talanta* 175 (2017) 507-513.

These publications are enclosed at the end of this section.

Manuscripts in evaluation

3. **3D printed device for selective uranium(VI) extraction.** Melisa Rodas Ceballos, Francisco González Serra, José Manuel Estela, Víctor Cerdà, Laura Ferrer.
4. **Automated extraction of uranium(VI) exploiting a 3D printed device.** Melisa Rodas Ceballos, José Manuel Estela, Víctor Cerdà, Laura Ferrer.
5. **Fully automated system with integrated liquid scintillation detector for the fast detection of ^{90}Sr .** Melisa Rodas Ceballos, Óscar Pozo, Antoni Borràs, Bartomeu Servera, Álvaro Pineda, José Manuel Estela, Víctor Cerdà, Laura Ferrer.

Additional publications not included in this thesis

6. **Monitoring of ^7Be and gross beta in particulate matter of surface air from Mallorca Island, Spain.** Melisa Rodas Ceballos, Antoni Borràs, Esteve Gomila, José Manuel Estela, Víctor Cerdà, Laura Ferrer. *Chemosphere* 152 (2016) 481-489.
7. **Parabens determination in cosmetic and personal care products Exploiting a Multi-Syringe Chromatographic (MSC) system and**

chemiluminescent detection. Melisa Rodas, L.A. Portugal, J. Avivar, José Manuel Estela, Víctor Cerdà. *Talanta* 143 (2015) 254-262.

Conference contributions

Oral Communications

1. **Hyphenation of MSFIA-LOV system with a homemade liquid scintillation detector for radionuclide determination at environmental levels.** Melisa Rodas Ceballos, Antoni Borràs, José Manuel Estela, Víctor Cerdà, Laura Ferrer. 21st International Conference on Flow Injection Analysis and Related Techniques (ICFIA). Saint Petersburg, Russia. 2017.
2. **Dynamic lixiviation of uranium and thorium from phosphogypsum by an MSFIA-LOV system previous ICP-MS detection.** Melisa Rodas Ceballos, Rafael García-Tenorio, José Manuel Estela, Víctor Cerdà, Laura Ferrer. 20th International Conference on Flow Injection Analysis and Related Techniques (ICFIA). Palma de Mallorca, Spain. 2016.
3. **Estudio de la cinética de la lixiviación dinámica de ²²⁶Ra de muestras de fosfoyeso implementando un sistema automático.** Melisa Rodas Ceballos, Antoni Borràs, Rafael García-Tenorio, José Manuel Estela, Víctor Cerdà, Laura Ferrer. IX Conference on the quality control of environmental radioactivity. Sitges, Spain. 2016.

Poster Presentations

4. **Study of the dynamic lixiviation of ²²⁶Ra form phosphogypsum by an automatic system previous radiometric detection.** Melisa Rodas Ceballos, Antoni Borràs, Rafael García-Tenorio, José Manuel Estela, Víctor Cerdà, Laura Ferrer. Second International Conference on Radioecological Concentration Process (50 years later). Sevilla, Spain. 2016.
 5. **3D printed device for uranium extraction by a SIA system.** Melisa Rodas Ceballos, José Manuel Estela, Víctor Cerdà, Laura Ferrer. 14th International Conference on Flow Analysis. Bangkok, Thailand. 2018.
-



^{226}Ra dynamic lixiviation from phosphogypsum samples by an automatic flow-through system with integrated renewable solid-phase extraction



Melisa Rodas Ceballos^{a,b}, Antoni Borràs^a, Rafael García-Tenorio^c, Rogelio Rodríguez^a, José Manuel Estela^d, Víctor Cerda^d, Laura Ferrer^{a,*}

^a Environmental Radioactivity Laboratory (LaboRA), University of the Balearic Islands, 07122 Palma de Mallorca, Spain

^b Sciware Systems, S.L., R & D department, 07193 Bunyola, Spain

^c Dpto. Física Aplicada II, Universidad de Sevilla, ETSA, Avda. Reina Mercedes s/n, 41012 Seville, Spain

^d Environmental Analytical Chemistry Laboratory (LQA²), University of the Balearic Islands, 07122 Palma de Mallorca, Spain

ARTICLE INFO

Keywords:

^{226}Ra
Phosphogypsum
Dynamic lixiviation
Automatic flow system

ABSTRACT

The release of ^{226}Ra from phosphogypsum (PG) was evaluated by developing a novel tool for fully automated ^{226}Ra lixiviation from PG integrating extraction/pre-concentration using a renewable sorbent format. Eight leached fractions (30 mL each one) and a residual fraction were analyzed allowing the evaluation of dynamic lixiviation of ^{226}Ra . An automatic system allows this approach coupling a homemade cell with a ^{226}Ra extraction/pre-concentration method, which is carried out combining two procedures: Ra adsorption on MnO_2 and its posterior co-precipitation with BaSO_4 . Detection was carried out with a low-background proportional counter, obtaining a minimum detectable activity of 7 Bq kg^{-1} . Method was validated by analysis of a PG reference material (MatControl CSN-CIEMAT 2008), comparing the content found in fractions (sum of leached fractions + residual fraction) to the reference value. PG samples from Huelva (Spain) were studied. ^{226}Ra average activity concentration of the sum of leached fractions with artificial rainwater at $\text{pH } 5.4 \pm 0.2$ was $105 \pm 3 \text{ Bq kg}^{-1} \text{ d.w.}$ representing a ^{226}Ra lixiviation of 37%; while at $\text{pH } 2.0 \pm 0.2$, it was $168 \pm 3 \text{ Bq kg}^{-1} \text{ d.w.}$, which represents a 50%. Also, static lixiviation, maintaining the same experimental conditions, was carried out indicating that, for both considered pH, the ^{226}Ra release from PG is up to 50% higher in a dynamic leaching than in a static one, may have both environmental and reutilization implications.

1. Introduction

^{226}Ra belongs to the uranium decay series, it is an alpha emitter and has a long half-life (1600 years), implying an environmental concern owing to its high radiotoxicity. In addition to natural processes, fuel cycle activities and nonnuclear industry activities can cause elevated radium concentrations in some environmental compartments [1].

The phosphogypsum (PG) is a by-product of phosphate fertilizer industries, and is produced in large amount by wet phosphoric acid process [2–4]. PG contains high levels of some natural radionuclides, especially ^{226}Ra and its decay products [5–7]. After the wet process, between 80–90% of ^{226}Ra originally present in the phosphate rock stays in PG, so it is classified as a Technologically Enhanced Naturally Occurring Radioactive Material (TENORM) [8–10]. Most produced PG is stored in stockpiles, causing in their surroundings environmental damages like radioactive and chemical contamination, especially in coastal regions [11,12]. ^{226}Ra activity in PG varies for samples recollected at different stacks inside the same geographical area, and

also at different sampling locations in the same stack [10]. These variations may be due to the fact that the origin of the phosphate rock can vary over time in the same plant for market reasons, causing variations in the production process, and therefore in the generation of phosphogypsum.

It is complex to model and experimentally reproduce the actual PG lixiviation processes that take place in stockpiles. The process of contact between PG and water does not occur only with rainwater in which the dynamic process of water percolation can vary through the piles: most rafts are formed by transporting the PG in suspension with water (static process) to the rafts where PG is decanted and the waters are either discharged to the environment or recirculated. Therefore, in order to achieve an efficient PG management, it is crucial to study the leaching of radionuclides from phosphogypsum providing several possible scenarios, i.e. its release in static, semi-static and dynamic conditions. The leaching process can cause the transference of radionuclides present in the PG matrix to the rainwater or to water of the adjacent zones, causing environmental damages [13–15]. ^{226}Ra leach-

* Corresponding author.

E-mail address: laura.ferrer@uib.es (L. Ferrer).

ability from PG stockpiles has been mainly studied in a static approach, i.e. using a large quantity of leaching agent and PG sample and maintaining the contact between them for a long time [2,16–18]. These conventional static leaching methods have some limitations, including the re-adsorption of the leached radionuclides. In some cases, such as for ^{226}Ra , its re-adsorption can reach the 89% of the leached content [18]. Moreover, extended leaching periods tests are laborious and time consuming methods, which are more susceptible to accidental errors.

In order to study the main differences between dynamic leaching conditions and the more frequently studied static scenario, in this paper a dynamic lixiviation of ^{226}Ra is proposed exploiting flow injection analysis techniques. This approach allows the development of an automatic system avoiding re-adsorption processes, needing lower sample and reagent consumption and increasing the analyst security by the reduction of reagent and sample handling [19,20]. The continuous flow of the leaching agent through the sample allows its constant renewal, avoiding the re-adsorption process by continuous solid-liquid equilibrium variation [21]. The combination of multi-syringe flow injection analysis (MSFIA) [22] and lab-on-valve (LOV) [23] combines the advantages of both techniques in one system: MSFIA supplies multi-channel operation with an accurate control of reagents volume and flow rate, while LOV allows to automatically regenerate the extraction column and the integration of several analytical units in the valve.

The main objective of this work is to evaluate the dynamic leaching of ^{226}Ra from PG samples and to compare it to the more frequently considered static leaching process. Artificial rainwater was used as leaching agent, discarding re-adsorption processes typical in the static lixiviation approach. It also facilitates to simulate lixiviation processes in which rainwater can pass through the PG without staying enough time in contact with it for the re-adsorption to occur. Thus, after each lixiviation cycle, eight leachates and a residual fraction were analyzed allowing the evaluation of dynamic lixiviation of ^{226}Ra , testing two different pHs for the leaching agent.

2. Experimental

2.1. Reagent and solutions

All solutions were prepared from analytical grade reagents with ultra-pure water obtained from a Milli-Q water purification system from Millipore (Bedford, MA, USA).

Stock solution of artificial rainwater was prepared by exact weight of magnesium sulfate (3.55 mg L^{-1} , Probus, Barcelona, Spain), sodium nitrate (12.2 mg L^{-1} , Probus), potassium sulfate (0.98 mg L^{-1} , Panreac, Barcelona, Spain), calcium chloride (4.43 mg L^{-1} , Probus), sodium chloride (1.69 mg L^{-1} , Scharlau, Barcelona, Spain) and ammonium sulfate (7.67 mg L^{-1} , Probus) and dissolved in Milli-Q water. Working solutions of artificial rainwater (diluting 100 times the stock solution) were prepared with Milli-Q water [24] and the pH was adjusted with diluted nitric acid. Besides, NaOH 0.22 mol L^{-1} (Scharlau) was used to adjust the PG leachate to $\text{pH } 7.0 \pm 0.5$, before the extraction and pre-concentration protocol. A cleaning solution of $0.05 \text{ mol L}^{-1} \text{ HNO}_3$ (Scharlau) was used to clean the leachate collector before each lixiviation.

^{226}Ra standard solutions were prepared with an appropriate quantity of the ^{226}Ra certified standard material with an initial activity of $34.68 \pm 0.69 \text{ Bq g}^{-1}$ in HNO_3 1 mol L^{-1} (CIEMAT, Madrid, Spain, ref. FRC-2015-453).

The reagents and materials for ^{226}Ra extraction and pre-concentration were: macroporous bead cellulose (MBC, Iontosorb MT50) of 50–100 μm particle size, 0.025 mol L^{-1} potassium permanganate (Scharlau), 0.5 mol L^{-1} sodium sulfate (Scharlau), 2 mol L^{-1} acetic acid-acetate buffer at pH 3 with $50 \text{ mg L}^{-1} \text{ Ba}^{2+}$ (Scharlau), 0.1 mol L^{-1} hydroxylamine (Scharlau) in $0.2 \text{ mol L}^{-1} \text{ HCl}$ (Scharlau).

In addition, $0.22 \mu\text{m}$ pore size nitrocellulose filters (Millipore), $0.45 \mu\text{m}$ pore size nylon filters (Millex®), syringe filter units of $0.45 \mu\text{m}$ pore size and 25 mm diameter (Millipore) and fiberglass wool were used.

2.2. Phosphogypsum samples

Three PG samples were obtained from a non-active PG stack owned by Fertiberia and located in Huelva, Spain. Two were randomly collected from the stockpiles of Huelva, and one used as reference material in an intercomparison exercise of Nuclear Safety Council of Spain (CSN). The reference PG material (MatControl CSN-CIEMAT 2008) was prepared by the Laboratory for the Preparation of Quality Control Materials (Mat Control) in collaboration with the Environmental Radiology Laboratory (LRA), both from the Analytical Chemistry Department of the University of Barcelona (Spain).

PG samples were placed in ceramic melting pots and dried until constant weight in an oven at $55 \pm 5 \text{ }^\circ\text{C}$. To measure the total ^{226}Ra activity concentration present in the PG samples, in the reference PG material, and in the residual fraction, a microwave (Multiwave Go, Anton Paar) assisted digestion was carried out with 10 mL of concentrated HNO_3 (69%, Scharlau), the microwave digestion program consisted in elevating the temperature within 10 min up to $180 \text{ }^\circ\text{C}$ and maintaining this temperature during 9.5 min. After the digestion, the HNO_3 was evaporated to dryness and residues were diluted in 25 mL of Milli-Q water. The sample solutions were filtrated through a $0.45 \mu\text{m}$ syringe filter and finally, the pH was adjusted to 7.0 ± 0.5 .

2.3. Automatic system set-up

A homemade PG lixiviation column (PLC) was fabricated with methacrylate. It consists of three main parts: the section containing the PG sample has a cylindrical form (25.5 mm long, 16 mm i.d.), and two conic sections with connectors, O-rings and filter holders equipped with $0.45 \mu\text{m}$ pore size nylon filters, that were placed at the end of both column sides to retain the PG sample (Fig. 1).

The automatic system involved a 16000 steps multisyringe burette

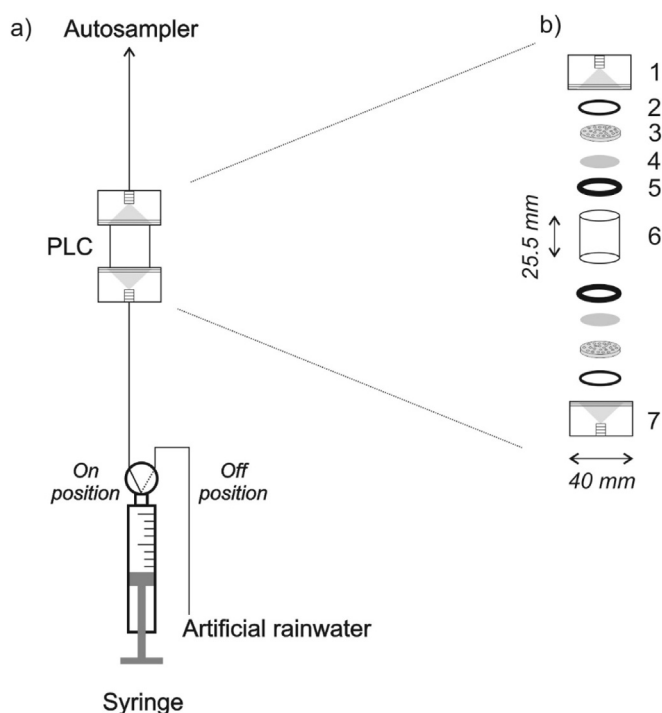


Fig. 1. Homemade phosphogypsum lixiviation column (PLC). a) General location in the system. b) Components of PLC: 1) top cap, 2) O-ring, 3) filter holder, 4) nylon filter, 5) rubber gasket, 6) PG sample container, 7) lower cap.

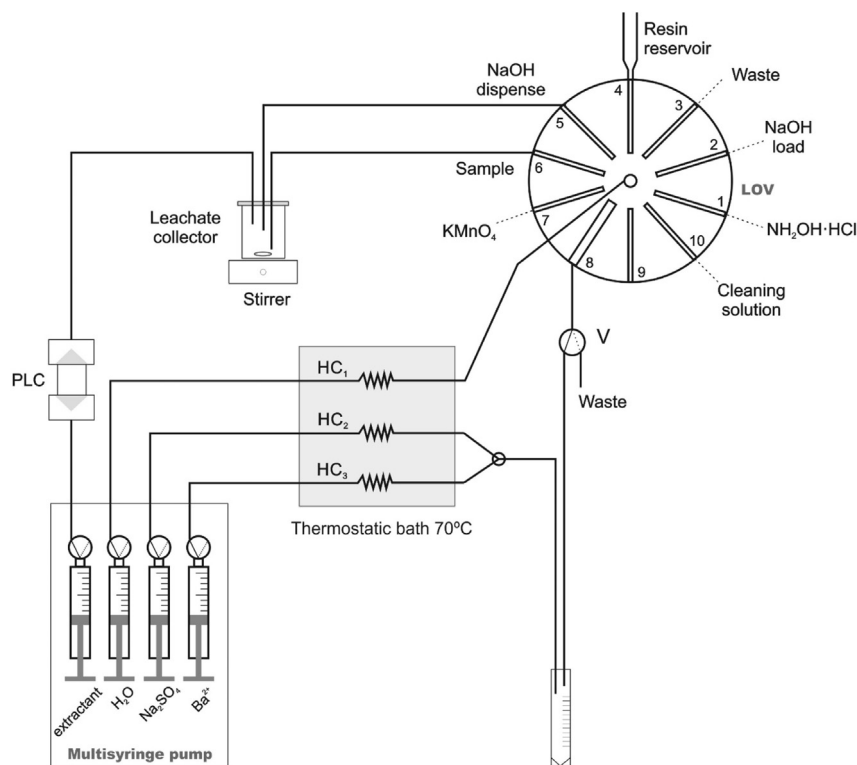


Fig. 2. Automatic system for the dynamic leaching, extraction/pre-concentration and co-precipitation of ^{226}Ra from phosphogypsum samples. C: three-way connector, HC: holding coil, LBPC: low background proportional counter, LOV: Lab-on-valve; MSFIA: multisyringe module, PLC: phosphogypsum lixiviation column, S: syringe; V: external solenoid valve.

module (BU4S, Crison Instruments, Alella, Barcelona, Spain) and a 10 ports multi-selection valve (Crison Instruments). A monolithic device LOV (Sciware Systems, Bunyola, Spain) was fabricated from methacrylate including ten integrated microchannels of 1.5 mm i.d. and 16 mm length, excepting the column channel with 3.2 mm i.d., and it was mounted atop of multi-selection valve (Fig. 2).

The multisyringe burette module was equipped with 3 syringes of 10 mL (S_1 , S_2 , S_3) and 1 syringe of 5 mL (S_4) (Hamilton, Switzerland). Each syringe has a three way-solenoid valve located at the head and the liquid is redirected depending on the position of the valve. In this system, the “On” position connects to the manifold and the “Off” position connects to the reservoir.

S_2 was connected to the central LOV port via a holding coil (HC_1), in which the lateral ports have the following configuration: $\text{NH}_2\text{OH}\cdot\text{HCl}$ (port 1), load NaOH (port 2), waste (port 3), reservoir of MBC suspended in 20:80 methanol: water (v/v) contained in a 5 mL plastic syringe (port 4), dispense NaOH (port 5), sample (e.g. leached fraction, residual fraction, entire sample) (port 6), KMnO_4 (port 7), MBC column (port 8) and cleaning solution (port 10). The column packed with 0.3 g of MBC and fiberglass wool at the end to retain the beads, is connected to an external solenoid valve (V, MTV-3-n 1/4 UKG, Takasago, Japan) to lead the liquids to the waste or to collect the fraction with ^{226}Ra .

S_3 containing the Na_2SO_4 and S_4 containing Ba^{+2} , were connected through a three way connector (C) to dispense the liquids to the fraction with ^{226}Ra .

The manifold is fabricated with 0.8 mm i.d. poly(tetrafluoroethylene) (PTFE) tubing, while HC_1 , HC_2 and HC_3 are constructed with 1.5 mm i.d. PTFE tubing, 10, 5.5 and 3.5 m long, respectively. All holding coils were submerged in the thermostatic bath at 70 °C. All connections were made using polyvinylidene fluoride (PVDF) connectors.

The AutoAnalysis 5.0 software (Sciware Systems) was used for the instrumental control.

A low-background proportional counter (LBPC) Canberra LB4200, equipped with four detectors and an average alpha efficiency of 20% was employed. The measurements were carried out immediately after separation with the voltage adjusted to 1320 V for simultaneous alpha/beta mode and a counting time of 1000 min. The Apex software was used for data acquisition. In addition, the LBPC calibration was carried out using a certified standard of ^{226}Ra for efficiency and autoabsorption calibration curves, reagent blanks were also made in order to calculate the minimum detectable activity (MDA) of each detector, following ISO11929 [25].

2.4. Analytical procedure

The analytical procedure can be summarized as follows: first, the PG leachate is obtained, putting approx. 0.4 g d.w. of the PG sample in the PLC and passing 30 mL fractions of artificial rainwater throughout the PLC. The leached fraction was collected in the leachate collector and the pH was adjusted to 7.0 ± 0.5 adding NaOH, this dissolution was stirred to homogenize the leachate. When analyzing the residual fraction or the entire sample, the analytical procedure starts here, with the digested sample at $\text{pH } 7.0 \pm 0.5$. Secondly, the MBC column was conditioned with 5 mL of hot deionized water (70 °C), and then 4 mL of KMnO_4 were passed through the column in order to form a coating of MnO_2 . In the next step, the leachate was loaded into the HC_1 and dispensed at 1.5 mL min^{-1} through the MBC column with V in “Off” position (to the waste). After that, ^{226}Ra retained in the column was eluted with 2.5 mL of $\text{NH}_2\text{OH}\cdot\text{HCl}$, with V in “On” position. This eluent reduced the MnO_2 adsorbed in the MBC and it was eluted jointly with the ^{226}Ra deposited.

Finally, the ^{226}Ra was co-precipitated dispensing 8 mL of Na_2SO_4 and 4 mL of acetate buffer/ Ba^{+2} into the fraction collector. The leachate collector was cleaned first with cleaning solution and finally with deionized water. In order to achieve the $\text{Ba}(\text{Ra})\text{SO}_4$ formation, a 30 min waiting time was needed. The resulting co-precipitated was

filtered through a 0.22 μm nylon filter and brought to dryness over a stainless-steel planchette under an infrared lamp.

After five reuses, the MBC column packing was automatically regenerated replacing the old one, dispensed to waste, by new MBC from the reservoir.

The efficiency of the radiochemical process was evaluated, obtaining an analyte recovery higher than 90% over 54 consecutive injections, using a certified standard of ^{226}Ra (CIEMAT).

3. Results and discussion

3.1. Optimization of experimental conditions

For this work, a methacrylate cell was constructed and dedicated to contain the PG samples. The variables that affect the PG lixiviation process were optimized using a separate manifold (see Fig. 1). Then both manifolds were coupled to a unique automatic system in order to achieve the ^{226}Ra release, extraction and pre-concentration with a high degree of automation and miniaturization.

The factors studied as independents variables were the PG sample weight in the PLC (200–600 mg d.w.) and the lixiviation flow rate (2.0–5.0 mL min^{-1}). In Table 1, the full performed factorial design (2^2) is presented. The maximum values of both experimental domains were set in order to avoid overpressure in the system, while the minimum values were the lowest amount of PG that guarantees reproducibility and the minor flow rate allowed by the system. The analytical response (CPM, counts per minute) was evaluated by the analysis of variance (ANOVA) represented graphically through the Pareto chart (Fig. 3). The analyzed variables did not produce significant changes in the response at 95% of confidence ($p=0.05$). The Statistica software was used for the experimental design and data processing.

Since the central points of the ranges for PG sample weight and lixiviation flow rate, 400 mg and 3.5 mL min^{-1} , respectively, present the best precision in terms of RSD (%), they were used for future assays. The fact that the signal does not increase significantly with increasing amounts of sample is linked to the hygroscopic nature of PG, which causes the formation of preferential channels (observed after each test), preventing further contact between sample and extractant. In addition, it was not possible to maintain a fluidized bed, even at the maximum tested flow rate.

The optimal pH value of the sample, e.g. leached fraction, residual fraction and entire sample, to introduce in the extraction/pre-concentration manifold was determined in a univariate way. The pH was studied among 6.0 and 8.0 with a ^{226}Ra standard solution with an activity of 0.05 Bq, not obtaining significant differences between the

Table 1.

Variables, levels and experimental matrix of the full factorial design for the PG lixiviation process.

Variables	Levels		
	Low (-)	Central Point (0)	High (+)
PG sample weight (mg d.w.)	200	400	600
Flow rate (mL min^{-1})	2.0	3.5	5.0
Assay	PG sample weight	Flow rate	Analytical response CPM (counts per minute)
1	–	–	0.21
2	+	–	0.14
3	–	+	0.17
4	+	+	0.18
5	0	0	0.15
6	0	0	0.16
7	0	0	0.18

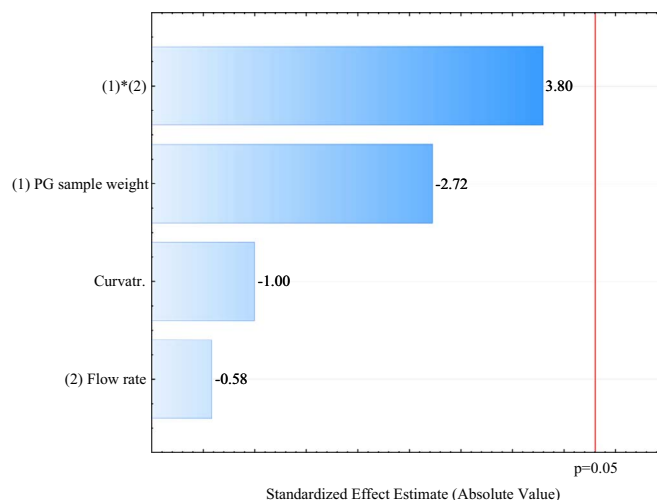


Fig. 3. Pareto chart for the estimated effects for the variables affecting the ^{226}Ra lixiviation process.

results in a pH 6.5–7.5.

The automatic system for extraction and pre-concentration of ^{226}Ra had been previously optimized [26].

3.2. Validation

The validation of the method was performed with a reference PG material (MatControl CSN-CIEMAT 2008). The reference sample was analyzed according to the protocol described above, leached with artificial rainwater at $\text{pH } 2.0 \pm 0.2$. After the lixiviation cycle, eight leachates and a residual fraction were obtained for each PG replicate sample ($n=3$). Besides, the total content of ^{226}Ra was determined in the entire PG reference material. Lixiviation fractions were directly analyzed, while each residual fraction (PG sample and nylon filters), and the entire sample were dried at 55 ± 5 $^{\circ}\text{C}$ until constant weight, digested and posteriorly analyzed.

The validation results are presented in Table 2. Since 3 replicates were analyzed of each fraction and for entire sample, ^{226}Ra activity concentration is presented as weighted average \pm uncertainty (external variance) following the IUPAC recommendations [27]. The weighted average was calculated taking into account the relationship of each activity concentration with its uncertainty calculated following ISO11929 [24]. The external variance considers the dispersion of the informed activity values. Significant differences were not found, by means of z-score [26] when comparing the sum of the leached fractions and the residual fraction to the reference material ^{226}Ra total content. The complete dataset of ^{226}Ra values obtained in the intercomparison exercise ($n=38$) for the same reference material was available [28].

Table 2

Validation results of reference PG material (MatControl CSN-CIEMAT 2008).

	Activity concentration ^a ($\text{Bq Kg}^{-1}\text{d.w.}$)	^{226}Ra (%)	Z-score
$\sum_{F=1}^8 F$ (sum of leached fractions)	295 ± 14	52	
Residual fraction	276 ± 13	48	
Sum of fractions (leached+residual)	571 ± 14	100	-0.03
Total digestion	585 ± 8		0.13
Reference value	573 ± 115		–

^a The activity concentration is expressed as weighted average \pm uncertainty (external variance); $n=3$, three replicates of one sample. The percentage of leached ^{226}Ra is expressed respect the sum of fractions (leached + residual fractions).

Hence, a new standard deviation was estimated taking into account the values obtained in this study ($n=40$), allowing the use of z-score as a statistical measurement that realizes the comparison between each value in a group of scores to the mean of the dataset. Z-score less than or equal to 2 were obtained, indicating a satisfactory validation [29].

3.3. ^{226}Ra dynamic lixiviation

The total content of ^{226}Ra in the entire sample was determined and the lixiviation assays, both dynamic and static, were performed in the three samples by triplicate. Thus, ^{226}Ra total content between 280 and 585 Bq Kg⁻¹ d.w. were obtained, resulting similar to the lower values found in previous works, which were in a range of 330 – 1390 Bq Kg⁻¹ d.w. [8,9].

The dynamic lixiviation of ^{226}Ra from PG was studied with artificial rainwater at pH commonly found in normal conditions, i.e. pH of 5.4 ± 0.2 , and also with a lower pH 2.0 ± 0.2 in order to study the behavior of the radium release in an acid medium. In all cases, ^{226}Ra was determined in eight 30 mL leached fractions, the ninth fraction overlapped with the MDA (7 Bq kg⁻¹). The activity concentration of ^{226}Ra in the leached and residual fractions in PG samples, using artificial rainwater as extracting agent at pH 5.4 and 2.0 are shown in Table 3. Using artificial rainwater at pH 5.4, the released ^{226}Ra reached 37%, which is higher than those obtained in static leaching studies. For assays with artificial rainwater at pH 2.0 the released ^{226}Ra reached between 49–52% of the total content of ^{226}Ra in PG sample.

^{226}Ra release decreases for successive fractions. In terms of mass and volume can be expressed as 240 mL of leaching agent were necessary to extract ^{226}Ra of 400 mg of PG, which represents that each fraction of 30 mL at pH 5.4 extracts between 4–6% of the total content of ^{226}Ra (see Table 3). In the case of lixiviation at pH 2.0, each fraction extracts between 4–8% of the ^{226}Ra total content. Depending on the ^{226}Ra total content of PG sample, these percentages will have different implications. For the analyzed PG samples, 37% represents about 100 Bq kg⁻¹d.w. of ^{226}Ra , which can be considerably increased due to the high variability of the total ^{226}Ra content, which can be up to 4 times higher [8,9]. The cumulative percentage of ^{226}Ra released in the dynamic lixiviation is similar across different samples, as can be seen in

Table 3

Activity concentration of ^{226}Ra in the leached fractions and the residual fraction in samples of phosphogypsum, using artificial rainwater as extracting agent at pH 5.4 and 2.0.

	pH 5.4 ± 0.2		pH 2.0 ± 0.2	
	Activity concentration ^a (Bq Kg ⁻¹ d.w.)	^{226}Ra (%)	Activity concentration ^a (Bq Kg ⁻¹ d.w.)	^{226}Ra (%)
Fraction 1	17 ± 3	6	28 ± 4	8
Fraction 2	17 ± 3	6	25 ± 3	8
Fraction 3	15 ± 3	5	22 ± 3	7
Fraction 4	10 ± 3	4	18 ± 3	5
Fraction 5	10 ± 3	4	23 ± 3	7
Fraction 6	12 ± 3	4	18 ± 3	5
Fraction 7	12 ± 3	4	19 ± 3	6
Fraction 8	11 ± 3	4	12 ± 3	4
$\sum_{F=1}^8$ F (sum of leached fractions)	105 ± 3	37	166 ± 3	50
Residual fraction	177 ± 36	63	163 ± 18	50
Sum of fractions (leached+residual)	282 ± 25	100	329 ± 13	100

^a The activity concentration is expressed as weighted average ± uncertainty (external variance); $n=6$, three replicates of two samples. The percentage of ^{226}Ra leached is respect the sum of fractions (leached + residual fractions).

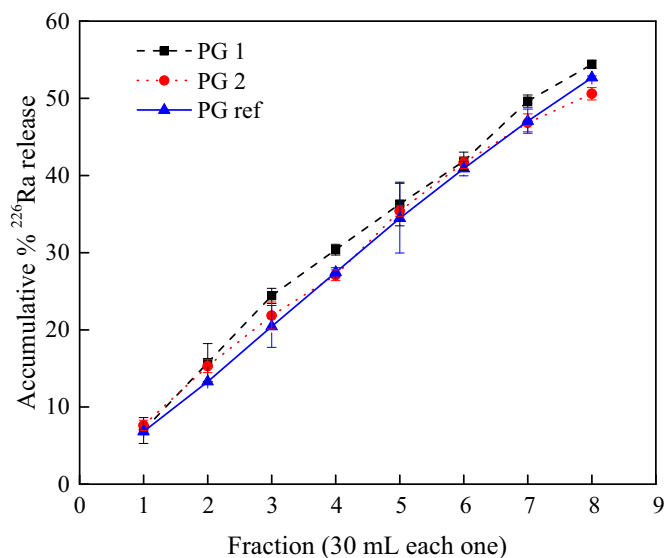


Fig. 4. Accumulated percentage of ^{226}Ra release for leached fractions with artificial rainwater at pH 2.0 ± 0.2 . The results are expressed accumulated percentage average ± standard deviation ($n=3$). PG 1,2: phosphogypsum samples, PG ref: PG reference sample.

Fig. 4.

Moreover, a static lixiviation was carried out in order to compare it to the results obtained by the dynamic lixiviation process. Artificial rainwater at pH 5.4 ± 0.2 and pH 2.0 ± 0.2 was again used as leaching agent. The contact time between the leaching agent and PG sample as set to 24 h. To compare both lixiviation approaches, results from the dynamic lixiviation fraction F1 are compared to those with static lixiviation, maintaining the same proportion of PG sample: rainwater, i.e., 400 mg:30 mL. The dynamic lixiviation using rainwater at pH 5.4 ± 0.2 and pH 2.0 ± 0.2 releases respectively 50% and 38% more ^{226}Ra than the static process, as can be seen in Table 4.

On a previous study on static lixiviation, different proportions of PG sample: rainwater (pH 5.5), between 10 g: 0.1 L and 10 g: 10 L, were considered for a fixed contact time of 24 h. Each PG sample: rainwater proportion was repeated up to 5 times by adding new rainwater into the same PG sample. The cumulative percentage of released ^{226}Ra increased 1–25% [3].

Higher ^{226}Ra contents in the leached fractions, both in the dynamic vs. static processes and using a more acidic extractant, are due to direct dependence on the leaching conditions such as pH of the extractant and the contact time between sample and extractant [3]. In this sense, in the dynamic approach, the contact time between the sample and the extractant is given by the lixiviation flow rate used. In this work, taking into account the PLC capacity and the flow rate of 3.5 mL min^{-1} , the contact time is of 9 min since the agent enters the cell until it leaves.

Table 4

Comparison between static (24 h) and dynamic lixiviation of ^{226}Ra from PG samples with rainwater at pH 5.4 and 2.0.

	Dynamic lixiviation		Static lixiviation (24 h)	
	pH 5.4 ± 0.2	pH 2.0 ± 0.2	pH 5.4 ± 0.2	pH 2.0 ± 0.2
^{226}Ra (%)	6 ± 1	8 ± 1	3 ± 1	5 ± 1
^{226}Ra dissolved (%)	19 ± 1	20 ± 2	26 ± 5	36 ± 1
I-PG sample mass (mg)	400	400	400	400
F-PG sample mass (mg)	324 ± 4	320 ± 8	296 ± 20	256 ± 4

The percentage of ^{226}Ra leached is referred to the first leached fraction, using the proportion PG: rainwater 400 mg: 30 mL. Results are expressed as percentage average ± standard deviation ($n=9$, three replicates of three samples). I-PG: Initial PG sample mass, F-PG: final PG sample mass.

Thus, it can be considered that the leaching agent is renewed constantly and the equilibrium is displaced to benefit the extraction. Contrary, the contact time in static studies can reach up to days without lixiviation agent renewal, in which equilibrium between extractant-radium is reached. Besides, in a study of static lixiviation, the dependence of ^{226}Ra leachability in PG samples with the contact time was studied. Different contact times between 10 min to 250 days were considered, indicating that the percentage of leached ^{226}Ra activity decreased with increasing contact times [3], probably caused by re-adsorption processes of ^{226}Ra by PG, achieving up to 89% of the total content [18]. Therefore, the increase of ^{226}Ra release in the dynamic lixiviation is probably caused by the absence of the re-adsorption process, which does not occur with the extractant agent constant renovation.

In addition to the leaching process itself, ^{226}Ra determined in each fraction partially comes from the dissolution of PG. In order to quantify such contribution, the remanent sample together with the filters that help to contain it into the PLC, were dried in oven at 55 °C up to constant weight after each lixiviation cycle, and weighted (0.324 ± 0.004 g). Results indicate that PG solubility reaches between $19 \pm 1\%$. Besides, in the static assays the dissolved amount of PG was also evaluated (see Table 4) and the results are in accordance with previously reported values (6–40%) [2–4].

4. Conclusion

The hyphenation of flow injection analysis techniques allows the on-line lixiviation, extraction and pre-concentration of ^{226}Ra , showing that the activity concentration decreases for successive fractions.

At pH 5.4, about 240 mL of leaching agent, divided in eight 30 mL fractions, were needed to release up to 37% of the total ^{226}Ra content present in 400 mg of PG samples. Increasing the acidity to pH 2.0 raised the release up to 50%.

In the case of the analyzed PG samples, the 37% represents about 100 Bq kg⁻¹ d.w. of ^{226}Ra , which can increase considerably due to the high variability of the total content of ^{226}Ra .

The main difference between static and dynamic lixiviation is the contact time between the sample and the extractant. In the result obtained comparing the static and dynamic lixiviation of ^{226}Ra from phosphogypsum samples using the same proportion in both cases of PG sample: rainwater, i.e., 400 mg: 30 mL, indicate that the ^{226}Ra release is 50% and 38% higher in dynamic lixiviation than in static one, at pH 5.4 and pH 2.0, respectively.

It is therefore crucial to develop detailed models of the lixiviation processes that take place in the stockpiles and to determine in which cases the static, semi-static or dynamic scenarios better resemble the actual lixiviation process.

Acknowledgements

Financial support from the State Research Agency (AEI) cofinanced by European Regional Development's funds (FEDER) (CTM2013-42401-R, AEI/FEDER, UE), are gratefully acknowledged. M. Rodas acknowledges MINECO for the allowance of an Industrial PhD fellowship (DI-14-06961).

References

- [1] D.A. Atwood, Radionuclides in the environment, First ed., Chichester, West Sussex, United Kingdom, 2010.
- [2] J.L. Aguado, J.P. Bolívar, E.G. San Miguel, R. García-Tenorio, Ra and U isotopes determination in phosphogypsum leachates by alpha-particle spectrometry, *Radioact. Environ.* 7 (2005) 160–165.
- [3] P.P. Haridasan, C.G. Maniyan, P.M.B. Pillai, A.H. Khan, Dissolution characteristics of ^{226}Ra from phosphogypsum, *J. Environ. Radioact.* 62 (2002) 287–294.
- [4] J.M. Rutherford, P.M. Dudas, M.J. Arocena, Radium in phosphogypsum leachates, *J. Environ. Qual.* 24 (1995) 307–314.
- [5] M.J. Gázquez, J.P. Bolívar, R. García-Tenorio, F. Galán, Natural occurring radionuclide waste in Spain: the Huelva phosphogypsum stacks case, in: Proceedings of the 1st Spanish Natl. Conference Adv. Mater. Recycl. Eco – Energy: pp. 75–78, 2009.
- [6] M.S. Al-Hwaiti, J.F. Ranville, P.E. Ross, Bioavailability and mobility of trace metals in phosphogypsum from Aqaba and Eshidiya, Jordan, *Chem. Der Erde - Geochem.* 70 (2010) 283–291.
- [7] U.S. Government Publishing Office. Subpart R- National Emission Standard for Radon Emissions from phosphogypsum stacks. (http://www.ecfr.gov/cgi-bin/text-idx?SID=3fb89e719353c5dbec592ea8d84c73a&mc=true&node=sp40.9.61.r&rgn=div6#se40.9.61_1201) (Accessed 18 April 16).
- [8] J.P. Bolívar, R. García-Tenorio, J. Mas, Radioactivity of Phosphogypsum in the South-West of Spain, *Radiat. Prot. Dosim.* 76 (1998) 185–189.
- [9] J.M. Abril, R. García-Tenorio, G. Manjón, Extensive radioactive characterization of a phosphogypsum stack in SW Spain: ^{226}Ra , ^{238}U , ^{210}Po concentrations and ^{222}Rn exhalation rate, *J. Hazard. Mater.* 164 (2009) 790–797.
- [10] EPA, Potential uses of phosphogypsum and associated risks. Background information document for 40 CFR 61 Subpart R National Standard for Radon emissions from phosphogypsum stacks, U.S. Environmental Protection Agency Office of Radiation Programs, Washington, D.C. 20460, 1992.
- [11] H. Tayibi, M. Choura, F.A. López, F.J. Alguacil, A. López-Delgado, Environmental impact and management of phosphogypsum, *J. Environ. Manag.* 90 (2009) 2377–2386.
- [12] F. Papageorgiou, A. Godelitsas, T.J. Mertzimekis, S. Xanthos, N. Voulgaris, G. Katsantonis, Environmental impact of phosphogypsum stockpile in remediated Schistos waste site (Piraeus, Greece) using a combination of γ -ray spectrometry with geographic information systems, *Environ. Monit. Assess.* 188 (2016) 1–14.
- [13] P.M. Rutherford, M.J. Dudas, R.A. Samek, Environmental impacts of phosphogypsum, *Sci. Total Environ.* 149 (1994) 1–38.
- [14] M.B. Nisti, C.R. Saueia, L.H. Malheiro, G.H. Groppo, B.P. Mazzilli, Lixiviation of natural radionuclides and heavy metals in tropical soils amended with phosphogypsum, *J. Environ. Radioact.* 144 (2015) 120–126.
- [15] G. Olszewski, A. Boryło, B. Skwarzec, The radiological impact of phosphogypsum stockpile in Wiślinka (northern Poland) on the Martwa Wisła river water, *J. Radioanal. Nucl. Chem.* 307 (2016) 653–660.
- [16] M. Azouazi, Y. Ouahidi, S. Fakhri, Y. Andres, J. Abbe, M. Benmansour, Natural radioactivity in phosphates, phosphogypsum and natural waters in Morocco, *J. Environ. Radioact.* 54 (2001) 231–242.
- [17] J.L. Aguado, J.P. Bolívar, ^{226}Ra determination in phosphogypsum by alpha-particle spectrometry, *Czechoslov. J. Phys.* 49 (1999) 439–444.
- [18] A. May, J.W. Sweeney, Evaluation of radium and toxic element leaching characteristics of Florida phosphogypsum stockpiles, *Chem. Technol. Gypsum* (1984) 140–149.
- [19] Y. Fajardo, J. Avivar, L. Ferrer, E. Gómez, V. Cerdà, M. Casas, Automation of radiochemical analysis by applying flow techniques to environmental samples, *TrAC Trends Anal. Chem.* 29 (2010) 1399–1408.
- [20] V. Cerdà, L. Ferrer, J. Avivar, A. Cerdà, Flow Analysis: A practical guide, First ed, Elsevier Science Ltd, Amsterdam, The Netherlands, 2014.
- [21] J.R. Bacon, C.M. Davidson, Is there a future for sequential chemical extraction?, *Analyst* 133 (2008) 25–46.
- [22] V. Cerdà, J. Estela, R. Forteza, A. Cladera, E. Becerra, P. Altimira, P. Sitjar, Flow techniques in water analysis, *Talanta* 50 (1999) 695–705.
- [23] J. Wang, E.H. Hansen, Sequential injection lab-on-valve: the third generation of flow injection analysis, *TrAC Trends Anal. Chem.* 22 (2003) 225–231.
- [24] J. Zhang, S.M. Liu, X. Lü, W.W. Huang, Characterizing Asian wind-dust transport to the Northwest Pacific Ocean. Direct measurements of the dust flux for two years, *Tellus* 45B (1993) 335–345.
- [25] International Organization for Standardization (ISO), ISO 11929 Determination of the characteristic limits (decision threshold, detection limit and limits of the confidence interval) for measurements of ionizing radiation-fundamentals and application, Geneva, 2010.
- [26] R. Rodríguez, A. Borràs, L. Leal, V. Cerdà, L. Ferrer, MSFIA-LOV system for ^{226}Ra isolation and pre-concentration from water samples previous radiometric detection, *Anal. Chim. Acta* 911 (2016) 75–81.
- [27] M. Thompson, R. Wood, Harmonized guidelines for internal quality control in analytical chemistry laboratories (Technical Report), *Pure Appl. Chem.* 67 (1995) 649–666.
- [28] International Organization for Standardization (ISO), Proficiency testing by inter-laboratory comparisons-guidelines. ISO/IEC Guide 43-1, 1997.
- [29] M.L. Romero-González, M. Barrera Izquierdo, F. Valiño García, Evaluation of analytical intercomparison exercise of radionuclides in environmental samples 2008–2009 (phosphogypsum), Nuclear Safety Council of Spain (CSN) - Centre for Energy, Environment and Technology (CIEMAT), Madrid, Spain, 2009.



An integrated automatic system to evaluate U and Th dynamic lixiviation from solid matrices, and to extract/pre-concentrate leached analytes previous ICP-MS detection



Melisa Rodas Ceballos^{a,b}, Rafael García-Tenorio^c, José Manuel Estela^d, Víctor Cerdà^d, Laura Ferrer^{a,*}

^a Environmental Radioactivity Laboratory (LaboRA), University of the Balearic Islands, 07122 Palma de Mallorca, Spain

^b Sciware Systems, Spin-Off UIB-004, 07193 Bunyola, Spain

^c Dpto. Física Aplicada II, Universidad de Sevilla, ETSA, Avda. Reina Mercedes s/n, 41012 Seville, Spain

^d Environmental Analytical Chemistry Laboratory (LQA²), University of the Balearic Islands, 07122 Palma de Mallorca, Spain

ARTICLE INFO

Keywords:

Uranium
Thorium
Dynamic lixiviation
Environmental solid samples
Automatic flow system
ICP-MS

ABSTRACT

Leached fractions of U and Th from different environmental solid matrices were evaluated by an automatic system enabling the on-line lixiviation and extraction/pre-concentration of these two elements previous ICP-MS detection. UTEVA resin was used as selective extraction material. Ten leached fraction, using artificial rainwater (pH 5.4) as leaching agent, and a residual fraction were analyzed for each sample, allowing the study of behavior of U and Th in dynamic lixiviation conditions. Multivariate techniques have been employed for the efficient optimization of the independent variables that affect the lixiviation process. The system reached LODs of 0.1 and 0.7 ng kg⁻¹ of U and Th, respectively. The method was satisfactorily validated for three solid matrices, by the analysis of a soil reference material (IAEA-375), a certified sediment reference material (BCR- 320 R) and a phosphogypsum reference material (MatControl CSN-CIEMAT 2008). Besides, environmental samples were analyzed, showing a similar behavior, i.e. the content of radionuclides decreases with the successive extractions. In all cases, the accumulative leached fraction of U and Th for different solid matrices studied (soil, sediment and phosphogypsum) were extremely low, up to 0.05% and 0.005% of U and Th, respectively. However, a great variability was observed in terms of mass concentration released, e.g. between 44 and 13,967 ng U kg⁻¹.

1. Introduction

Uranium and thorium are naturally occurring radioactive elements, widely distributed in the Earth's crust, and both are quite useful in industries. Uranium and thorium mining, milling, and processing; phosphate fertilizer production; tin processing; phosphate rock processing; coal combustion; and industrial boilers are some of the primary anthropogenic sources of uranium and thorium released into the air, soil, and water [1,2]. Whilst the mobility of Th in soil is very low, because it will remain strongly sorbed, the mobility and bioavailability of U is ruled by oxidation state, having more solubility as U(VI) and less in the reduce state (U(IV)), by the complexation in inorganic and organic ligands, pH, interaction with organic matter and sorption by minerals including hydroxides and clays [1].

The leaching process of solid samples (e.g. soil, sediment, sludge, phosphogypsum) has consolidated importance for the potential impact of trace elements or radionuclides in the environment, causing their

transference to water of adjacent zones or rainwater [3–5]. The lixiviation to the water or rainwater is dependent of several factors as the pH, concentration of complexing anion, porosity of the medium, temperature, presence of organic and inorganic compounds, redox potential, amount of water available for the leaching, and microbial activity. It is important to know the activity concentration of U and Th in soil, sediment, waste or rock and the mobile fraction of each one, to assess the impact of the different matrices in the environment [6].

Many leaching tests have been developed in static or semi-static way, which are used to understand an environmental process that occur frequently [6–11]. Nevertheless, dynamic processes also occur, being the natural leaching conditions more difficult to be duplicated in a laboratory. An approach to the study of leaching under dynamic conditions is possible using flow analysis techniques in which the leaching flow rate is constant and reproducible. In this sense, the combination of the multisyringe flow injection analysis (MSFIA) [12] and lab-on-valve (LOV) [13] enabling the advantages of both techni-

* Corresponding author.

E-mail address: laura.ferrer@uib.es (L. Ferrer).

ques: MSFIA contributes with ruggedness, versatility and provides multi-channel operation with a precise control of reagents volume and flow rate, whilst the LOV permits the automatic regeneration of the column packing and the integration of several channels in a unique device [14]. Besides, the reduction of reagent and samples amounts together with the minimization of sample handling, increasing of the analyst security working with radioactive samples [12,15].

Because of the low concentration of U and Th in environmental samples, it is expected that the leached fraction have ultra-trace levels, for which the sensitivity of an ICP-MS as detector is mandatory. ICP-MS allows the determination of long-lived radionuclides, specifically actinides elements at low concentration, in a sensitive and fast way [16,17].

Thus, once the leached fraction has been obtained, it is passed through the microcolumn packing with a selective resin in order to make the matrix fraction clean-up and pre-concentrate both analytes of interest. UTEVA resin was chosen as selective extraction material for U and Th, allowing the simultaneous retention and elution [18].

The main objective of this work is the study of the dynamic lixiviation of U and Th in different environmental solid matrices using rainwater (pH 5.4) as leaching agent exploiting an automatic MSFIA-LOV system for lixiviation, extraction and pre-concentration previous ICP-MS detection. The proposed system was optimized by experimental design in order to assess the optimal conditions that affect the leaching process.

2. Experimental

2.1. Reagent and solutions

All the solutions were prepared with Milli-Q water (Bedford, MA, USA) and analytical grade reagents: nitric acid (HNO_3) (65%, Scharlau, Barcelona, Spain), hydrofluoric acid (HF) (48%, Panreac Barcelona, Spain), aluminum nitrate ($\text{Al}(\text{NO}_3)_3 \cdot 9\text{H}_2\text{O}$, Scharlau) and oxalic acid ($\text{H}_2\text{C}_2\text{O}_4$, Panreac). From atomic absorption standards solution of uranium (1001 mg L^{-1} in 2% HNO_3), thorium (1012 mg L^{-1} in 5.1% HNO_3) and bismuth (1000 mg L^{-1} in 0.5 mol L^{-1} HNO_3), were prepared the stock solutions (U and Th in 3 mol L^{-1} HNO_3). Bismuth was used as internal standard solution as a factor correction for ICP-MS measures.

The stock solution of artificial rainwater was prepared by precise weight of ammonium sulfate (7.67 mg L^{-1} , Probus, Barcelona, Spain), calcium chloride (4.43 mg L^{-1} , Probus), magnesium sulfate (3.55 mg L^{-1} , Probus), sodium nitrate (12.2 mg L^{-1} , Probus), sodium chloride (1.69 mg L^{-1} , Scharlau) and potassium sulfate (0.98 mg L^{-1} , Panreac) and dissolved in Milli-Q water [19].

Besides, UTEVA (Uranium and TEtraVAalent actinides) resin of 50–100 μm particle size (Triskem International, France), syringe filter units of 0.45 μm pore size (Millipore), nitrocellulose filters of 0.8 μm pore size (Millipore) and fiberglass wool for chromatography were employed.

2.2. Environmental solid samples

The proposed methodology was applied to different kind of environmental solid matrices, i.e. soil, sediment and phosphogypsum (PG).

Two soil samples were analyzed: a reference material from International Atomic Energy Agency (IAEA-375), collected on the field of the collective farm “Staryi Vishkov” Novozybkov district, Bryansk region, Russia, in July 1990 (zone affected by Chernobyl accident) [20]; and a soil reference material (MatControl CSN-CIEMAT 2016), prepared by the Laboratory for the Preparation of Quality Control Materials (MatControl) in collaboration with the Environmental Radiology Laboratory (LRA), from Analytic Chemistry Department of the University of Barcelona (Spain).

A sediment channel certified reference material (BCR-320R) from the Institute for Reference Material and Measurements (IRMM) of

Joint Research Centre from the European Commission was also analyzed for the U and Th determination.

Two PG samples from a non-active PG stack owned by Fertiberia, Huelva, Spain: a sample randomly collected from the stockpiles, and a PG reference material (MatControl CSN-CIEMAT 2008), also prepared by MatControl and LRA from the University of Barcelona (Spain). The PG is a by-product of phosphate fertilizer industry, and it is produced by wet chemical treatment with H_2SO_4 . As a result of this process the ^{238}U with its decays products are fractionated between the PG and the phosphoric acid, estimating that < 40% is remaining in the PG [7], and is categorized as Technologically Enhanced Naturally Occurring Radioactive Material (TENORM) [21–23], although in this work the PG is categorized as an environmental sample by its growing use and dissemination in agricultural soils as soil amendment [24]. Besides, the U in the PG is quite variable depending of its treatment and age. The fresh PG (just after its generation in the factory) has a bigger fraction of U due to presence of impurities of soluble phosphoric acid that was not fully separated in the production process. When the PG is disposed in the piles, the U associated to the phosphoric acid quickly is leached remaining in the PG a fraction of U that is clearly more insoluble (generally this insoluble U is associated to some undissolved phosphate rock material) [7].

2.3. Sample treatment

All samples were settled in ceramic melting pots and placed in an oven at $55 \pm 5 \text{ }^\circ\text{C}$ for drying until constant weight.

The total content of U and Th present in soil and PG samples and in their residual fractions was determined following a microwave digestion program with 10 mL of HNO_3 concentrated (increasing the temperature to $180 \text{ }^\circ\text{C}$ in 10 min and maintaining this temperature during 9.5 min with a microwave Multiwave Go, Anton Paar). After that, the HNO_3 was evaporated to dryness and residues were diluted up to 250 mL with 3 mol L^{-1} HNO_3 . For determining the total content of U and Th in sediment sample and in its residual fraction, the digestion was performed with 9 mL of HNO_3 concentrated and 2 mL of HF concentrated following the microwave digestion program described previously. In addition, after digestion, the acid mixture was evaporated to dryness and residues were diluted up to 250 mL with 3 mol L^{-1} HNO_3 .

Since the higher U and Th contents in the whole sample and in their residual fractions, an additional dilution was necessary, in all samples.

In the case of PG samples, 4 mL of the digested solution were diluted up to 25 mL with 3 mol L^{-1} HNO_3 / 0.5 mol L^{-1} $\text{Al}(\text{NO}_3)_3$. While, for the soil and sediment samples 2 mL of the digested solution were diluted up to 50 mL with 3 mol L^{-1} HNO_3 .

Finally, all solutions were filtered through a 0.45 μm syringe filter and analyzed by the proposed automatic methodology.

The leaching fractions were directly analyzed by the proposed automatic methodology.

2.4. Manifold and software

The automatic system used for the leaching and extraction/pre-concentration of U and Th is presented in Fig. 1.

The automatic MSFIA-LOV system is composed by a multisyringe burette module (BU4S, Crison Instruments, Alella, Barcelona, Spain), a monolithic device LOV (Sciware Systems, Bunyola, Spain) mounted over a multi-position selection valve (Sciware Systems). LOV was fabricated from methacrylate with 8 integrated microchannels of 1.5 mm i.d. and 16 mm length, except the column channel made of 3.2 mm i.d. MSFIA module was equipped with two syringes of 10 mL (S_1 and S_3), one syringe of 1 mL (S_2) and 1 syringe of 5 mL (S_4) (Hamilton, Switzerland). At the head of each syringe is located a three way solenoid valve, redirecting the liquid depending of its position (“on” position connects to the manifold and “off” position to the reagents reservoir).

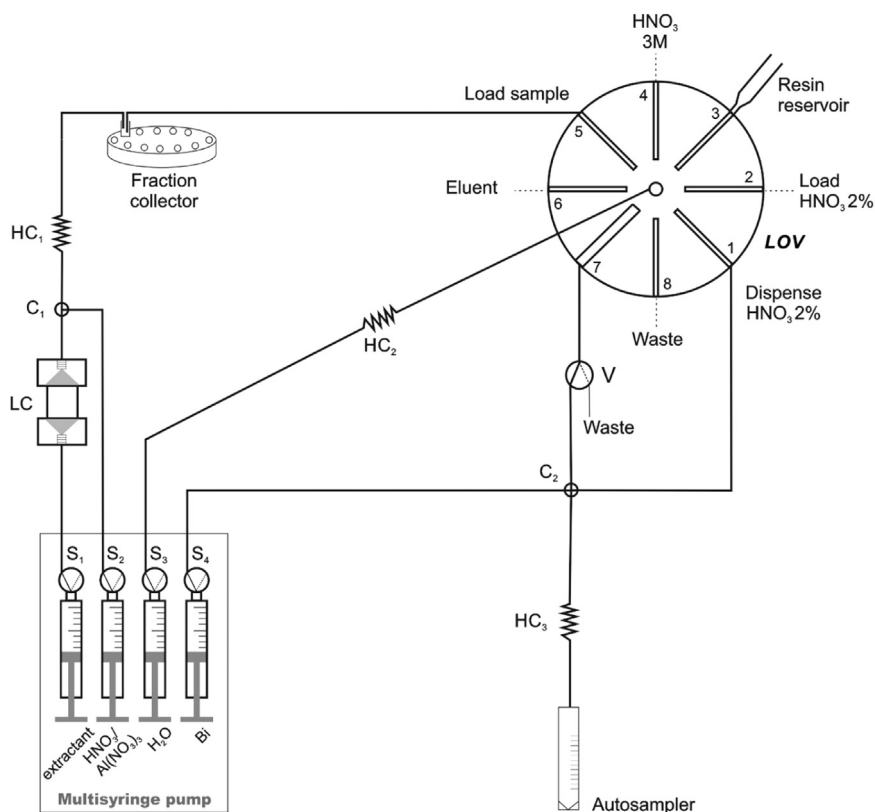


Fig. 1. Automatic MSFIA-LOV system for the dynamic leaching, extraction and pre-concentration of uranium and thorium from solid environmental samples. C: connector; HC: holding coil; LC: leaching column; LOV: Lab-on-valve; S: syringes; V: external solenoid valve.

S₁ was connected to a homemade leaching column (LC) made with methacrylate and described elsewhere [25]. The LC was connected to a three-way connector (C₁) and then to a fraction collector via a holding coil (HC₁). To the C₁ arrives the S₂, which contains 6 mol L⁻¹ HNO₃/ 1 mol L⁻¹ Al(NO₃)₃ for the PG analysis or 6 mol L⁻¹ HNO₃ for soil and sediment analyses.

S₃ is connected to the central LOV port via HC₂ and the configuration of the lateral ports are: dispense HNO₃ 2% (port 1), load HNO₃ 2% (port 2), UTEVA resin reservoir (port 3), 3 mol L⁻¹ HNO₃ (port 4), load sample (port 5), 0.05 mol L⁻¹ oxalic acid as eluent (port 6), UTEVA resin reservoir (port 7) and waste (port 8). The UTEVA resin reservoir consists in a 5 mL plastic syringe containing beads suspended in 3 mol L⁻¹ HNO₃. The microcolumn is packed with 0.04 g of UTEVA resin and fiberglass wool was putted at the end to retain the resin. The outlet of microcolumn is connected via an external solenoid valve (V, MTV-3-N ¼ UKG, Takasago, Japan) to a fraction collector.

S₄ contains Bi standard (14.6 µg L⁻¹) and port 1 of LOV (dispense HNO₃ 2%) were connected (four-way connector, C₂) to HC₃ to dispense the final solution to be analyzed in ICP-MS.

Manifold were constructed with poly(tetrafluoroethylene) (PTFE) tubing: HC₁ and HC₃ of 0.8 mm of i.d., 6 and 0.25 m long, respectively. HC₂ was made with 1.5 mm i.d. PTFE tubing and 10 m long. Connectors (C₁ and C₂) were fabricated of methacrylate. All connections were made with Teflon connectors.

Instrumental control was carrying out with the software AutoAnalysis 5.0 (Sciware Systems). An ICP-MS Elan DRC-e (Perkin Elmer) was used as detector, it was fitted with a cross flow nebulizer and Scott spray chamber (Perkin Elmer). ²³⁸U and ²³²Th were selected for measurement, since they are the more abundant natural occurring isotopes for uranium and thorium, respectively [1]. ²⁰⁹Bi was simultaneously measure in order to correct the instrumental drift.

The Statistical Statistica software package was used for the experimental design and data processing.

2.5. Analytical procedure

Firstly, approx. 0.4500 ± 0.0500 g d.w. of samples is placed into LC and 10 or 15 mL of artificial rainwater, for soil/sediment and PG samples, respectively, is passed through the LC. Then, the leached fraction is mixed through the HC₁ with 5 mL of 6 mol L⁻¹ HNO₃ for soil/sediment samples, and 7.5 mL of 6 mol L⁻¹ HNO₃/ 1 mol L⁻¹ Al(NO₃)₃ for PG samples, in order to achieve the optimal medium for U and Th retention. The leached fraction was collected in a fraction collector. When the residual fraction or the entire sample is analyzed, the analytical procedure starts from this step.

The second step is the conditioning of UTEVA resin with 1 mL of 3 mol L⁻¹ HNO₃. Then, the leached fraction or entire sample/residual fraction was dispensed through the microcolumn at 0.8 mL min⁻¹ with V in “off” position (to the waste). 0.2 mL of 3 mol L⁻¹ HNO₃ was eluted through the microcolumn to avoid interferences. After that, U and Th retained in the column were eluted with 1.4 mL of 0.05 mol L⁻¹ H₂C₂O₄ with V in “on” position to autosampler.

Finally, the internal standard of Bi (14.6 µg L⁻¹), HNO₃ 2% and the eluate were mixed in HC₃, and collected in the autosampler. The UTEVA resin was replaced when required in automatic way, discarding the old one to the waste and loading new one from the reservoir. The resin durability has been estimated in 150 injections for the simultaneous determination of both analytes with recoveries higher than 95% [17].

3. Results and discussion

3.1. Optimization of experimental conditions

The independent variables studied in order to find the best conditions for the lixiviation process from soil and sediment, were the solid sample weight into the LC and the lixiviation flow rate. A full factorial design 2² was performed. The experimental domain, the

Table 1

Variables, levels and experimental matrix of the full factorial design for lixiviation process from soil and sediment samples.

Variables		Levels			
		Low (-)	Central Point (0)	High (+)	
Sample weight (mg d.w.)		500	1000	1500	
Flow rate (mL min ⁻¹)		0.6	2.8	5.0	
Assay	Sample weight	Flow rate	Analytical response [*]		
			U	Th	D
1	-	-	1.2047	0.1164	1.00
2	+	-	0.0920	0.0112	0.04
3	-	+	0.0561	0.0092	0
4	+	+	0.0767	0.0096	0.03
5	0	0	0.0637	0.0041	0
6	0	0	0.0728	0.0053	0.01
7	0	0	0.0688	0.0048	0

* The analytical response is presented as U or Th cps/ Bi cps; D: global desirability.

analytical response (U or Th cps / Bi cps), the matrix design and the global desirability (D) of the system are shown in Table 1. With the aim to evaluate multiple responses, D is used transforming two analytical responses into one [26]. The range of variables were set considering the lowest amount of solid sample that guarantee reproducibility and the lowest flow rate that can set in the multisyringe module, whereas the maximum of both values were those that avoid overpressure, preventing the membrane filter rupture.

The results obtained within the experimental domain studied, indicate that the flow rate and sample weight are significant with negative effects, entailing that a lower flow rate and a lower sample weight increase the analytical response. This result can be attributed to a slow leaching of U and Th and particularly to the low solubility of Th in water, that tends to remain bound to the particulate matter [1,27]. Also, a D = 1 is observed in the assay with the lowest flow rate and lowest sample weight (Table 1), indicating that more contact time between the extractant and the sample is required for an efficient extraction of U and Th. A small amount of sample (30 mg) for a better effective contact surface area between the extractant and the solid sample was essential in a previous work, in which a column for soil lixiviation was employed [28]. In addition, a significant positive interaction between the two variables is observed for both radionuclides. Evaluating the marginal means, it is established that the positive interaction is due to the combination of the two lowest values of the variables (i.e. increase of the analytical signal (+) = low flow rate (-) × low sample weight (-)). Through the function D, the optimized values within the range studied were 500 mg of sample weight and 0.6 mL min⁻¹ leaching flow rate, and these values were set for the performance of future assays.

In the case of variables that affect the lixiviation process from the PG samples an univariate optimization was carried out, since preliminary results are available for this kind of sample. The experimental domain for PG sample weight was between 400 and 800 mg d.w., and leaching flow rate between 0.6 and 5 mL min⁻¹. Results indicate that optimal values were 400 mg d.w. of PG sample and 3.5 mL min⁻¹ for the leaching flow rate. The difference of these variables respect those for soil and sediment probably is due to hygroscopic nature of the PG sample.

The automatic system for extraction and pre-concentration of U and Th had been previously optimized [17]. In the case of PG, since the sample matrix has an elevated content of phosphates, the medium of retention was HNO₃/Al(NO₃)₃ because of the aluminum can avoid the interference of phosphates on the Th uptake by the UTEVA resin, following the manufacturer recommendation [18].

3.2. Validation of the automatic system

The validation of the proposed methodology was carried out for each kind of sample. Thus, three solid matrices samples, i.e. a soil

reference material (IAEA-375), a certified sediment reference material (BCR-320R) and a PG reference material (MatControl CSN-CIEMAT 2008) were analyzed. The analyses were performed by triplicate for each solid matrix (n=3), in which 10 leached fractions and a residual fraction were obtained for each one, and all of them were analyzed by the proposed automatic methodology.

The sum of the leached fractions plus the residual fraction did not show significant differences with the certified and reference values of U and Th, comparing with *t*-test at a confidence level of 95%. Although the leached percentage was extremely low (less than 0.06%) respect to the total content this together with the residual fraction, was analyzed with the developed system, considering the results satisfactory.

The results of solid matrices validation are presented in Table 2 as average of three replicates (n=3) for each solid sample ± uncertainty (k = 2), that was calculated in accordance with the Guide for the expression of uncertainty in measurements [29].

The limits of detection (LOD) and quantification (LOQ) were calculated following the IUPAC recommendations [30]. The system reached LODs of 0.1 and 0.7 ng kg⁻¹ of U and Th, respectively.

Mass calibrations curves (cps of analyte/cps of internal standard ratio versus mass in ng of U and Th) were performed for each radionuclide, obtaining $y = 6.2674x + 0.004$ ($r^2 = 0.9999$, $n = 7$) for U and $y = 5.8029x + 0.0058$ ($r^2 = 0.9986$, $n = 7$) for Th.

3.3. Dynamic lixiviation of U and Th from solid environmental samples

The developed automatic MSFIA-LOV system was applied to study the dynamic lixiviation of U and Th in three different solid environmental matrices, i.e. soil, sediment and PG. In general, the dynamic lixiviation behavior of U and Th in the analyzed samples was similar, i.e. the content of radionuclides decreases with the successive extractions (except the U content in PG samples in which the fraction 2 is higher than fraction 1), and it is maintained constant in the last five fractions. In addition, the U release was always two or three orders of magnitude higher than Th, which is in concordance with the low mobility of Th, which generally tends to remain bound to the particulate matter [1,27].

The lixiviation process for soil and sediment samples consisted of 10 fractions of 10 mL each one. In the case of U, all fractions were quantified, while only the first five fractions contained Th above the LOD. Figs. 2a and 3a show the dynamic lixiviation behavior for U and for Th in two soil samples, respectively. It can be seen that, although

Table 2

U and Th in leached fractions and residual fraction analyzed by the MSFIA-LOV system for lixiviation, extraction and pre-concentration steps previous ICP-MS detection, from reference materials.

	Uranium (mg kg ⁻¹ d.w.)		Thorium (mg kg ⁻¹ d.w.)	
	Sum of fractions (∑ _{F=1} ¹⁰ F+ residual)	Reference or certified value	Sum of fractions (∑ _{F=1} ¹⁰ F+ residual)	Reference or certified value
Soil (IAEA-375)	1.80 ± 0.18 ^a	1.99 ± 0.08 ^b	4.93 ± 0.53 ^a	5.15 ± 0.66 ^b
Sediment (BCR-320R)	1.84 ± 0.08 ^a	1.56 ± 0.20 ^a	4.88 ± 0.30 ^a	5.3 ± 0.40 ^a
PG (MatControl 2008)	5.11 ± 0.23 ^a	4.50 ± 0.82 ^c	1.23 ± 0.29 ^a	1.50 ± 0.29 ^c

Results are expressed as (a) average ± uncertainty (k = 2) (n = 3); (b) average ± uncertainty (k = 2) (n = 6); (c) average ± uncertainty (k = 2) (n = 21 and n = 18 for U and Th, respectively). Significant differences were not found at a confidence level of 95%. PG: phosphogypsum.

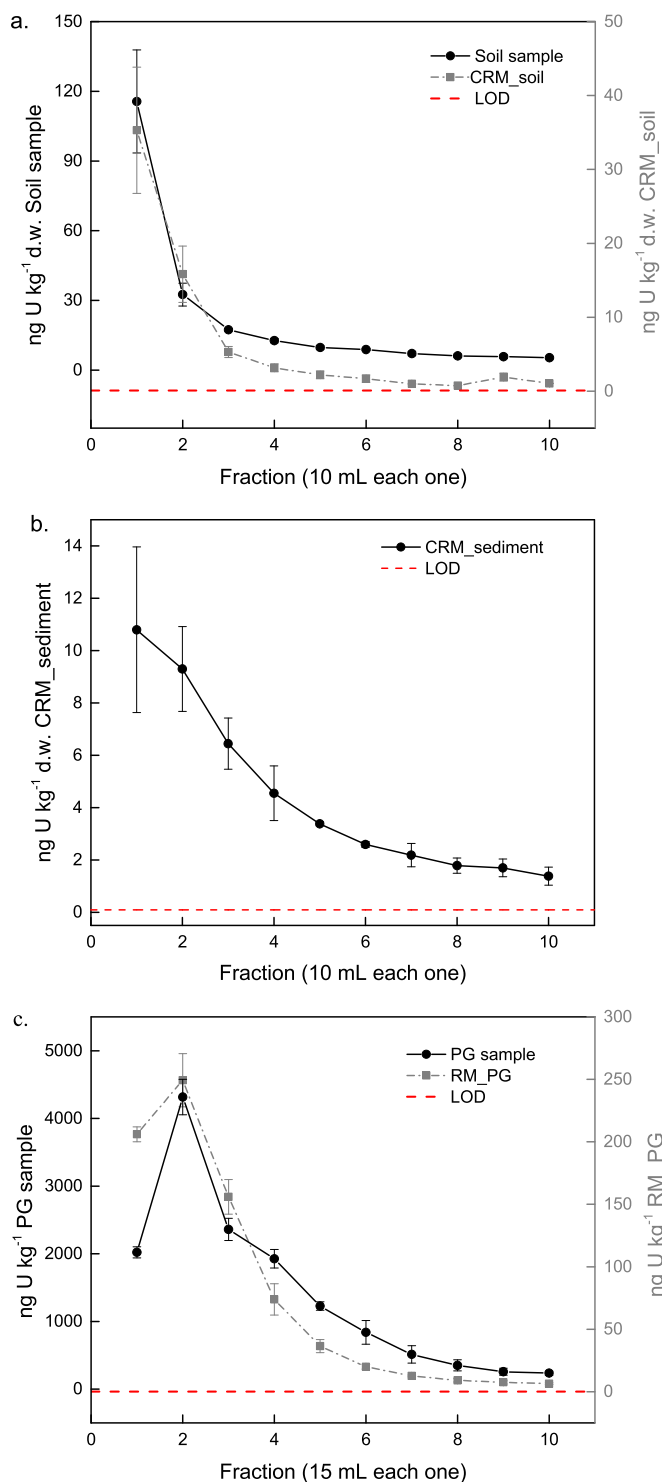


Fig. 2. Uranium dynamic lixiviation in solid environmental samples using artificial rainwater as leaching agent. The results are expressed as average \pm standard deviation ($n = 3$). a) Soil sample and soil reference material (CRM_soil); b) Sediment certified reference material (CRM_sediment); c) Phosphogypsum sample (PG sample) and phosphogypsum reference material (RM_PG).

the behavior is similar, the percentage vary, thus varying the amount of U released, e.g. between 0.004% (68 ng kg^{-1}) and 0.016% (221 ng kg^{-1}) from soil samples with a total U content of 1.77 and 1.42 mg kg^{-1} , respectively. In case of Th, a release of 0.0004% (18 ng kg^{-1}) was obtained from soil samples with 4.93 and 4.87 mg kg^{-1} Th, respectively. Fig. 2b shows the U dynamic lixiviation behavior for sediment sample, while Th was below the LOD in all the

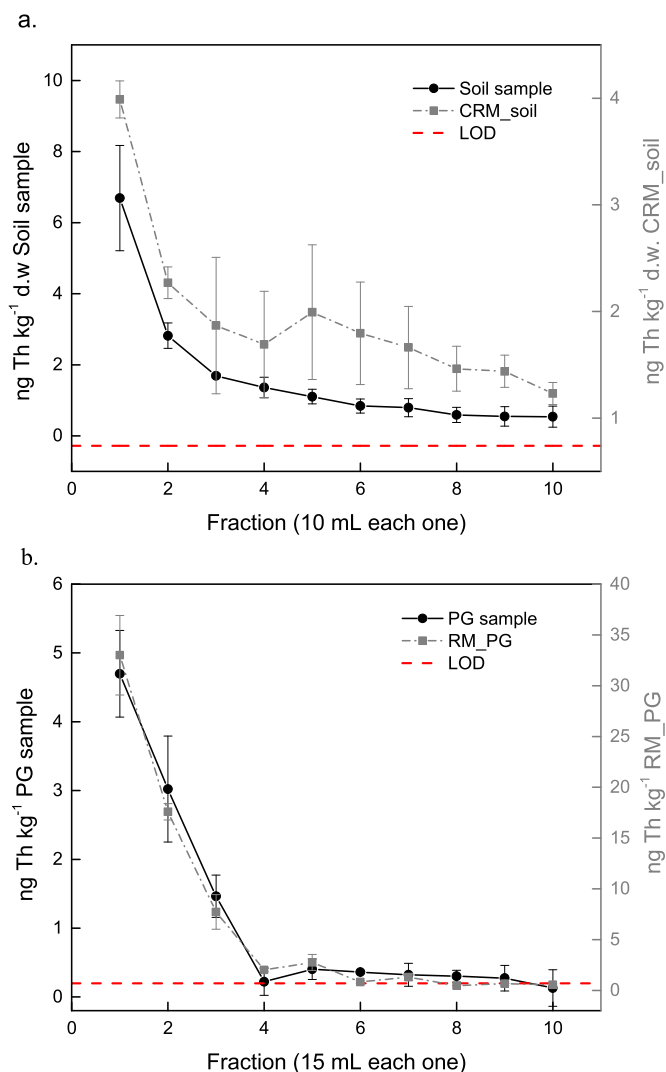


Fig. 3. Thorium dynamic lixiviation in solid environmental samples using artificial rainwater as leaching agent. The results are expressed as average \pm standard deviation ($n = 3$). a) Soil sample and soil reference material (CRM_soil); b) Phosphogypsum sample (PG sample) and phosphogypsum reference material (RM_PG).

leached fractions analyzed. The percentage of U released respect to the total content was 0.002% (44 ng kg^{-1}) from sample with 1.84 and 4.88 mg kg^{-1} of U and Th, respectively.

The lixiviation process for PG samples was performed with 10 fractions of 15 mL each one. Figs. 2c and 3b show the U and Th release behavior in PG samples, respectively. Th presents similar behavior that mentioned above, i.e. decreasing with the successive extractions, varying the leached percentage between 0.005% ($67 \text{ ng kg}^{-1} \text{ d.w.}$) and 0.0004% ($11 \text{ ng kg}^{-1} \text{ d.w.}$) from PG samples with a total content 1.23 and 3.10 mg kg^{-1} Th. The exception is the U release from PG, since the maximum appears in the second fraction. The percentage of U released respect to the total content was between 0.015% ($782 \text{ ng kg}^{-1} \text{ d.w.}$) and 0.05% ($13,967 \text{ ng kg}^{-1} \text{ d.w.}$). The total content of U in PG sample was between 5.10 and $26.71 \text{ mg kg}^{-1} \text{ d.w.}$ Also, in PG sample, it is observed that U has more mobility than Th, since in all the leached fractions U can be quantified, while Th only in the first three fractions. The U total content of PG sample agree with those reported in previous works, which were in a range of $5.89\text{--}36.53 \text{ mg kg}^{-1}$ [7,11,22]. The results obtained in a static leaching study were very different from those presented here. In static tests, using fresh and marine water as extractants, the percentage of ^{238}U release from PG samples was between 40 – 60% for periods of stirring time between 600 – 2880 min, concluding that elevated U mobilization depends on the

acidity of the leachates, i.e. by the presence of phosphoric acid in the PG [7]. Besides, the high percentage of U leached (40–60%) was in agree with the fresh PG sample used. The low U leached observed in this study corresponds to the “U washed sample” analyzed.

Other static lixiviation study carried out with PG agitated for 20 h and varying the pH among 2 – 9, indicates that the variation of the rates of leaching and the dissolved mass of PG is a function of extractant pH. Thus, the leached radionuclides appear to be associated with the elements exclusively absorbed on the solid surface, regardless of the chemical form, while those that were not leached should be absorbed in sites less soluble with structures of type CaSO_4 [2].

The mass ratios of Th/U found in the leached fractions (0.002 – 0.04 PG sample and 0.0015 – 0.0088 RM_PG) and in bulk PG (0.12 – 0.24), indicating that the PG sample collected in the stockpiles from Huelva are enriched in U in relation to Th, as well as the U release is higher than Th.

Therefore, the lixiviation process of U and Th under dynamic conditions from the environmental solid matrices analyzed, shows U and Th releases extremely low, up to 0.05% and 0.005% of U and Th, respectively, using rainwater at pH 5.4 as extractant. This behavior can probably be explained, by the direct dependence on the leaching conditions such as the composition of the leaching agent and its pH, the contact time between the sample and the extractant, the porosity of the medium and the amount of water available for the leaching [6,7,31]. A semi-static lixiviation study, in which the solid sample was placed in contact with two different extractants (distilled water and $0.1 \text{ mol L}^{-1} \text{ NaNO}_3$) by a period of 142 days, replacing the extractant each 15 days (9 times), obtained a low uranium release, up to a 0.59%. Authors propose that the processes that govern the release of mobile U are the diffusion and the surface wash-off [6].

Otherwise, at the end of the leaching process a decrease of the amount of solid samples was observed, being a $7 \pm 3\%$ for soil, $11 \pm 1\%$ for sediment and $19 \pm 1\%$ for PG. The U and Th content of this dissolved fraction are added to the leached fraction percentage. The PG solubility reported in previous works of static lixiviation were between 6 – 40% [7,31,32].

The great variability found in different environmental sample matrices, especially of U releases, e.g. between 44 ng U kg^{-1} (0.5 mBq kg^{-1}) and $13,967 \text{ ng U kg}^{-1}$ (173 mBq kg^{-1}), demonstrate the relevance of the lixiviation assays in dynamic conditions for holistic environmental impact studies.

4. Conclusion

A rapid evaluation of dynamic lixiviation of uranium and thorium from solid environmental samples was possible thanks to the hyphenation of flow analysis techniques, a dedicated sample cell and a selective resin. A multisyringe flow injection analysis (MSFIA) - lab-on-valve (LOV) system allows the on-line lixiviation, extraction and pre-concentration of U and Th in different environmental solid matrices. The automatic MSFIA-LOV system was combined with an ICP-MS enabling the detection of both radionuclides at ultra-trace levels in the leached fractions and in the residual fractions. The use of multivariate techniques allows the quick and efficient optimization of the independent variables that affect the lixiviation process.

A similar behavior of U and Th releases under dynamic lixiviation conditions, from environmental solid matrices, i.e. soil, sediment and phosphogypsum, was observed using rainwater at pH 5.4 as extractant. U and Th content decrease for successive fractions, being the mobility of both radionuclides was extremely low, obtaining up to 0.05% and 0.005% of U and Th release, respectively, remaining almost all them in the residual fraction (> 99.95%). Nevertheless, the great variability found in different environmental sample matrices analyzed, especially of U releases, highlight the importance of the dynamic lixiviation assays for holistic environmental impact studies.

Acknowledgements

Financial support from the Spanish State Agency for Research (AEI) cofinanced by European Regional Development's funds (FEDER), are gratefully acknowledged (CTM2013-42401-R, AEI/FEDER, UE). M. Rodas Ceballos acknowledges MINECO for the allowance of an Industrial PhD fellowship (DI-14-06961).

References

- [1] D.A. Atwood, *Radionuclides in the Environment*, 1st edition, Chichester, West Sussex, United Kingdom., 2010.
- [2] M. Azouazi, Y. Ouahidi, S. Fakhi, Y. Andres, J. Abbe, M. Benmansour, Natural radioactivity in phosphates, phosphogypsum and natural waters in Morocco, *J. Environ. Radioact.* 54 (2001) 231–242.
- [3] J.R. Bacon, C.M. Davidson, Is there a future for sequential chemical extraction?, *Analyst* 133 (2008) 25–46.
- [4] C.R.M. Rao, A. Sahuquillo, J.F. Lopez Sanchez, A review of the different methods applied in environmental geochemistry for single and sequential extraction of trace elements in soils and related materials, *Water Air Soil Pollut.* 189 (2008) 291–333.
- [5] G. Olszewski, A. Borylo, B. Skwarzec, The radiological impact of phosphogypsum stockpile in Wiślinka (northern Poland) on the Martwa Wisla river water, *J. Radioanal. Nucl. Chem.* 307 (2016) 653–660.
- [6] A.C. Patra, C.G. Suresh, S. Mohapatra, S.K. Sahoo, R.M. Tripathi, V.D. Puranik, Long-term leaching of uranium from different waste matrices, *J. Environ. Manag.* 92 (2011) 919–925.
- [7] J.L. Aguado, J.P. Bolívar, E.G. San Miguel, R. García-Tenorio, Ra and U isotopes determination in phosphogypsum leachates by alpha-particle spectrometry, *Radioact. Environ.* 7 (2005) 160–165.
- [8] M.B. Nisti, C.R. Saueia, L.H. Malheiro, G.H. Groppo, B.P. Mazzilli, Lixiviation of natural radionuclides and heavy metals in tropical soils amended with phosphogypsum, *J. Environ. Radioact.* 144 (2015) 120–126.
- [9] D.H. Moon, D. Dermatas, An evaluation of lead leachability from stabilized/solidified soils under modified semi-dynamic leaching conditions, *Eng. Geol.* 85 (2006) 67–74.
- [10] R.O. Abdel Rahman, A.A. Zaki, A.M. El-Kamash, Modeling the long-term leaching behavior of ^{137}Cs , ^{60}Co , and $^{152,154}\text{Eu}$ radionuclides from cement–clay matrices, *J. Hazard. Mater.* 145 (2007) 372–380.
- [11] M.J. Gázquez, J. Mantero, F. Mosqueda, J.P. Bolívar, R. García-Tenorio, Radioactive characterization of leachates and effluences in the neighbouring areas of a phosphogypsum disposal site as a preliminary step before its restoration, *J. Environ. Radioact.* 137 (2014) 79–87.
- [12] V. Cerdà, J. Estela, R. Forteza, A. Cladera, E. Becerra, P. Altimira, P. Sitjar, Flow techniques in water analysis, *Talanta* 50 (1999) 695–705.
- [13] J. Wang, E.H. Hansen, Sequential injection lab-on-valve: the third generation of flow injection analysis, *TrAC Trends Anal. Chem.* 22 (2003) 225–231.
- [14] V. Cerdà, L. Ferrer, J. Avivar, A. Cerdá, *FlowAnalysis: A Practical Guide*, 1st edition, Elsevier Science Ltd, Amsterdam, The Netherlands, 2014.
- [15] Y. Fajardo, J. Avivar, L. Ferrer, E. Gómez, V. Cerdà, M. Casas, Automation of radiochemical analysis by applying flow techniques to environmental samples, *TrAC Trends Anal. Chem.* 29 (2010) 1399–1408.
- [16] D. Larivière, V.F. Taylor, R.D. Evans, R.J. Cornett, Radionuclide determination in environmental samples by inductively coupled plasma mass spectrometry, *Spectrochim. Acta B At. Spectrosc.* 61 (2006) 877–904.
- [17] J. Avivar, L. Ferrer, M. Casas, V. Cerdà, Fully automated lab-on-valve-multisyringe flow injection analysis-ICP-MS system: an effective tool for fast, sensitive and selective determination of thorium and uranium at environmental levels exploiting solid phase extraction, *J. Anal. At. Spectrom.* 27 (2012) 327–334.
- [18] Triskem International, UTEVA resin specifications, France, n.d. (http://www.triskem-international.com/iso_album/ft_resine_uteva_en_160927.pdf).
- [19] J. Zhang, S.M. Liu, X. Lü, W.W. Huang, Characterizing Asian wind-dust transport to the Northwest Pacific Ocean. Direct measurements of the dust flux for two years, *Tellus* 45B (1993) 335–345.
- [20] J. Merešová, W. Uwe, T. Altiztzioglou, Evaluation of EC Interlaboratory Comparison on Radionuclides in Soil, Belgium, 2012.
- [21] J.P. Bolívar, R. García-Tenorio, J. Mas, Radioactivity of phosphogypsum in the South-West of Spain, *Radiat. Prot. Dosim.* 76 (1998) 185–189.
- [22] J.M. Abril, R. García-Tenorio, G. Manjón, Extensive radioactive characterization of a phosphogypsum stack in SW Spain: ^{226}Ra , ^{238}U , ^{210}Po concentrations and ^{222}Rn exhalation rate, *J. Hazard. Mater.* 164 (2009) 790–797.
- [23] EPA, Potential uses of phosphogypsum and associated risks. Background information document for 40 CFR 61 Subpart R National Standard for Radon emissions from phosphogypsum stacks, U.S. Environmental Protection Agency Office of Radiation Programs, Washington, D.C. 20460, 1992.
- [24] J.M. Abril, R. García-Tenorio, S.M. Enamorado, M.D. Hurtado, L. Andreu, A. Delgado, The cumulative effect of three decades of phosphogypsum amendments in reclaimed marsh soils from SW Spain: ^{226}Ra , ^{238}U and Cd contents in soils and tomato fruit, *Sci. Total Environ.* 403 (2008) 80–88.
- [25] M. Rodas Ceballos, A. Borràs, R. García-Tenorio, R. Rodríguez, J.M. Estela, V. Cerdà, L. Ferrer, ^{226}Ra dynamic lixiviation from phosphogypsum samples by an automatic flow-through system with integrated renewable solid-phase extraction, *Talanta* 167 (2017) 398–403.

- [26] G. Derringer, R. Suich, Simultaneous optimization of several response variables, *J. Qual. Technol.* 12 (1980) 214–219.
- [27] A.J.G. Santos, B.P. Mazzilli, D.I.T. Fávoro, P.S.C. Silva, Partitioning of radionuclides and trace elements in phosphogypsum and its source materials based on sequential extraction methods, *J. Environ. Radioact.* 87 (2006) 52–61.
- [28] M.P. Beeston, H.J. Glass, J.T. van Elteren, Z. Šlejkovec, Assessment of elemental mobility in soil using a fluidised bed approach with on-line ICP-MS analysis, *Anal. Chim. Acta* 599 (2007) 264–270.
- [29] International Organization for Standardization (ISO), Evaluation of measurement data - Guide to the expression of Uncertainty in Measurement, Geneva, Switzerland, 2008.
- [30] L.A. Currie, Detection and quantification limits: origins and historical overview, *Anal. Chim. Acta* 391 (1999) 127–134.
- [31] P.P. Haridasan, C.G. Maniyan, P.M.B. Pillai, A.H. Khan, Dissolution characteristics of ^{226}Ra from phosphogypsum, *J. Environ. Radioact.* 62 (2002) 287–294.
- [32] J.M. Rutherford, P.M. Dudas, M.J. Arocena, Radium in phosphogypsum leachates, *J. Environ. Qual.* 24 (1995) 307–314.